



This work is protected by copyright and other intellectual property rights and duplication or sale of all or part is not permitted, except that material may be duplicated by you for research, private study, criticism/review or educational purposes. Electronic or print copies are for your own personal, non-commercial use and shall not be passed to any other individual. No quotation may be published without proper acknowledgement. For any other use, or to quote extensively from the work, permission must be obtained from the copyright holder/s.

---

# **The detection of Forensic and Archaeological burials using geophysics and soil analysis**

**Henry C. Dick**

---

Submitted for the degree of Doctor of Philosophy

Keele University

December 2017

## **Abstract**

Graveyards and cemeteries around the world are increasingly being designated as full. There is growing requirements to identify burial space or to exhume and re-inter if necessary. Near-surface geophysical methods offer a potentially non-invasive target detection solution, with additional soil sampling analysis to provide ground truth information; however there has been lack of research to identify optimal detection methods. This study has collected multi-frequency (225 MHz – 900 MHz) ground penetrating radar, electrical resistivity, electromagnetic induction and magnetic susceptibility surface data over different burial scenarios (ancient, old and modern burials). Surveying ancient burial sites revealed they can be geophysically detectable even after 650+ years of burial, given optimum local soil type and depositional environment conditions. Surveying old and modern burials indicate that progressively older burials are more difficult to detect but complicated by local soil type. Different geophysical techniques were optimal in different sites, which therefore suggests a multi-technique approach should be utilised by survey practitioners. Graveyard geophysical targets included the grave soil above graves themselves, the grave contents, brick-lining (if present) and grave soil water that can be all detectable from background levels. Grave markers were also identified not to always be located where burials were positioned. Buried cadaver decomposition releases elements into the surrounding soil, which can significantly change the local site geochemistry. Resulting elevated element levels, associated with cadaver decomposition, can assist in identifying burial location(s), when compared to background levels and temporally vary. These included inorganic elements,

pH and conductivity. Potassium, sulphate, sodium and phosphate were also identified as potential grave markers, which also showed strong correlation coefficients with grave soilwater conductivity values. Background elemental concentrations were consistently low and were controlled by rainfall.



## **Acknowledgements**

This work was partially funded by Nigerian Government through Tertiary Educational Trust Fund (TETFund), an academic staff training and development scheme. I want to sincerely thank the University of Port Harcourt for the opportunity as an academic staff to benefit from this scholarship scheme.

I would also like to acknowledge the invaluable support of my supervisors Dr J. K. Pringle and Dr N. J. Cassidy. I am most delighted to have work with them and have earned so much from their wealth of knowledge in the related fields.

Keele University has always proved to be a place for high quality and innovative research, and I most appreciate the enabling environment and standard trainings it did offer me to carry out my research work. Therefore, I would like to say a very big thank you to all the management and staff of this distinguished institution. I am also grateful to John Jervis and James Hansen for the wonderful work they have done in the related topic.

To my family (Mrs Rhoda Dick, Godwin, Uzoamaka (snr), Ikedichi, Comfort, Abraham and my wonderful father, though late now, Elder Dick Okpara Udensi, who could not live to see his dream being fulfilled) for their eternal presence, love, understanding and financial support all through my research, words are not enough to express my appreciation and gratitude. It will be incomplete if I stop here without mentioning invaluable support and courage I received from my dear wife, Mrs Tessy Ogonda Dick, who beyond all odds prioritised my research work more than her pleasure and that of our children (Josephine, Joan, Jessica and Justin). My appreciation goes to the Pastors of The Redeemed Christian

Church of God, Living Water Parish, Stoke on Trent (Pastor and Pastor Mrs Chilaka), for their ever abiding support through God's words and prayers.

Finally, to God, the anchor of my faith, of whom I have obtained mercy and grace to help in time of need.

## Contents

<b>Abstract.....</b>	<b>i</b>
<b>Acknowledgements .....</b>	<b>iii</b>
<b>List of Figures.....</b>	<b>ix</b>
<b>List of Tables.....</b>	<b>xxvi</b>
<b>Chapter 1: Introduction .....</b>	<b>1</b>
1.1 Forensic geoscience.....	1
1.2 Search for forensic and archaeological burials .....	4
1.3 Soil components and analysis .....	5
1.4 Thesis aims and structure.....	6
<b>Chapter 2: The detection of forensic burials: a literature review .....</b>	<b>9</b>
2.1 Introduction.....	9
2.1.1 Contribution of geoscience to forensic searches.....	9
2.1.2 The impact of a cadaver burial on the local environment.....	10
2.2 Relevant Near-surface geophysical techniques .....	15
2.2.1 Electrical resistivity ( $\rho$ ) .....	16
2.2.2 Ground penetrating radar (GPR).....	29
2.2.3 Electromagnetic Induction (EMI) .....	43
2.2.4 Magnetic Susceptibility (MS) .....	46

2.2.5	Other geophysical techniques for grave detection.....	49
<b>2.3</b>	<b>Soil sampling and geochemical analysis .....</b>	<b>50</b>
2.4	Conclusion .....	52
 <b>CHAPTER 3: Detection and characterisation of an ancient mass burial</b>		
<b>cemetery in Central London, UK.....</b>		<b>53</b>
3.1	Introduction.....	53
3.1.1	Aim .....	56
3.2	Material and methods .....	57
3.2.1	Study site.....	57
3.2.2	Archaeological site excavations .....	63
3.2.3	Near-surface geophysical investigations.....	66
3.2.3.1	Electro-magnetic (EM) surveys.....	68
3.2.3.2	Constant Separation Traversing resistivity surveys .....	70
3.2.3.3	Ground Penetrating Radar surveys .....	72
3.2.3.4	Electrical Resistivity Imaging resistivity surveys.....	73
3.3	Results .....	75
3.3.1	EM datasets.....	75
3.3.2	Electrical resistivity CST datasets .....	79
3.3.3	GPR datasets .....	81
3.3.4	Eastern Parish Boundary .....	89

3.4	Discussion .....	92
3.5	Conclusions, study limitations and further work .....	120
<b>CHAPTER 4: Determining optimum geophysical techniques and</b>		
<b>equipment configurations in English church graveyards.....</b>		<b>123</b>
4.1	Introduction.....	123
4.1.1	Grave detection methods .....	126
4.2	Aims and Objectives .....	132
4.3	Materials and methods .....	135
4.3.1	Study sites .....	135
4.3.2	Geophysical site specifications .....	138
4.4	Determining optimal equipment/survey acquisition configurations and data.....	138
4.4.1	Optimal spacing of electrical resistivity probes.....	138
4.4.2	Survey distance from headstones.....	144
4.4.3	Geophysical data acquisition and processing .....	150
4.5	Case Study 1: St. Michael's of all Angels Church, Stockton, Norfolk, UK .....	156
4.5.1	Background .....	156
4.5.2	Case study 1: Geophysical results .....	161
4.6	Case Study 2: St. John's Church, Keele site, Newcastle under Lyme, Staffordshire, UK.....	173

4.6.1	Background .....	173
4.6.2	Case study 2: Geophysical results .....	177
4.7	Case Study 3: St. Luke's Church, Endon, Staffordshire, UK .....	192
4.7.1	Background .....	192
4.7.2	Case study 3: Geophysical results .....	197
4.8	Statistical computation of techniques detectability .....	204
4.8.1	GPR techniques .....	204
4.8.2	Electrical resistivity and magnetic susceptibility .....	205
4.9	Discussion .....	206
4.10	Limitation and further work .....	212
4.11	Conclusions.....	213

## **CHAPTER 5: Elemental analysis of an in situ animal burial decomposition fluids**

	<b>and long term graveyard soils.....</b>	<b>215</b>
5.0	Overview.....	215
5.1	Chapter aims and objectives .....	215
5.2	Introduction.....	216
5.2.1	Animal mass burial pits .....	223
5.2.2	Main factors that control leachate production, concentration and transport .....	228
5.3	18 months monitoring study of pig burial.....	232

5.3.1	Study area .....	232
5.3.2	The Lysimeter .....	234
5.3.3	Methodology .....	235
5.3.3.1	Simulated grave .....	235
5.3.3.2	Sample collection and on-site measurements .....	236
5.3.4	Climatological data collection .....	239
5.3.5	Analysis techniques .....	241
5.3.5.1	Ion Chromatography (IC) Dionex System .....	241
5.3.5.2	Inductively Coupled Plasma Optical Emission Spectroscopy (ICP-OES) .....	243
5.3.5.3	Statistical analysis of physicochemical parameters .....	244
5.3.6	Results .....	247
5.4	Detection of elevated metallic distribution in graveyard soils .....	260
5.4.1	Introduction .....	260
5.4.2	Materials and Methods .....	261
5.4.2.1	Site descriptions .....	261
5.4.2.2	Sampling and laboratory analysis .....	262
5.4.2.3	Data Analysis .....	267
5.4.3	Results .....	272
5.5	Discussion .....	278

5.6	Conclusions, study limitations and further work .....	296
<b>CHAPTER 6</b>	<b>Discussion .....</b>	<b>298</b>
6.1	The rate of detection of modern and potential ancient mass burial.....	299
6.2	Geophysical responses against age of burials.....	303
6.3	Grave soil water conductivity dependant .....	306
6.4	Graveyards contamination impact factors.....	308
6.5	Analysis of graveyard and mass grave leachate plume.....	311
6.5.1	Geophysical analysis of graveyard .....	311
6.5.2	Geochemical analysis of grave fluid.....	312
6.6	Study limitations.....	313
<b>CHAPTER 7</b>	<b>Conclusions .....</b>	<b>316</b>
7.1	Key Outcomes.....	316
7.2	Recommendations for future research .....	320
7.2.1	Clandestine grave monitoring.....	320
7.2.2	Graveyards .....	321
7.2.3	Soil sampling .....	321
7.3	Concluding remarks.....	323
<b>References</b>	<b>.....</b>	<b>324</b>



## List of Figures

<b>Figure 1.1:</b> Schematic diagram showing the relationship of forensic geoscience to some other disciplines and sub-disciplines (from Pye and Croft, 2004). .....	3
<b>Figure 2.1:</b> Examples of possible alterations to the local environment due to the presence of a clandestine grave by Jervis (2010), with further details listed (bottom panel) modified from Hunter and Cox (2005), and Harrison and Donnelly (2009). .....	12
<b>Figure 2.2:</b> Schematic model to illustrate leachate plumes generated from decomposing human remains. The presence of a leachate plume may be a marker to cadaver burial location; however it may also increase the target area (Harrison and Donnelly, 2009). .....	14
<b>Figure 2.3:</b> Current flow through, driven by potential difference across a block of material of resistivity $\rho$ (edited from Styles, 2012). .....	17
<b>Figure 2.4:</b> Approximate electrical resistivity ranges for different type of rocks (from Reynolds, 2011). .....	18
<b>Figure 2.5:</b> The flow of current from a point current source and the resulting potential distribution with homogeneous subsurface structure (Telford <i>et al.</i> , 1990). .....	19
<b>Figure 2.6:</b> Signal contribution section for the Wenner array. Contours represent the contribution of by individual elements of a homogeneous subsurface to the	

measured resistivity. Dashed lines indicate regions where the contribution to the measured resistivity is negative (modified from Barker, 1979). .....	20
<b>Figure 2.7:</b> Array types: a) standard Wenner array with equal electrode spacing, b) Schlumberger array configuration where b spacing stays constant while a increases until reading are too small, and b is then increases to start over again and finally, c) Dipole-dipole array with n as an integral multiple of a (after Styles, 2012). .....	22
<b>Figure 2.8:</b> Resistivity section showing a leachate plume migrating through a landfill site boundary (after Styles, 2012). .....	25
<b>Figure 2.9:</b> Bulk resistivity plot showing low-resistivity anomalies at the head and foot of a pig grave (rectangle) interred six weeks previously (after Jervis <i>et al.</i> , 2009a). .....	26
<b>Figure 2.10:</b> Electrical resistivity datasets from a 0.5m fixed-offset survey of a graveyard in Hackney, East London (from Hansen <i>et al.</i> , 2014). .....	28
<b>Figure 2.11:</b> A schematic diagram of a GPR system, showing the interface module, control unit, transmitter, receiver and antennas. The signal travel paths in order of arrival are; 1) direct wave, 2) direct ground wave and 3) reflection from subsurface interface (adapted from Moorman, 2001). .....	30
<b>Figure 2.12:</b> Schematic diagram showing how GPR antennae passing over a buried object at positions 1, 2 and 3 produce a detectable response and hyperbola in a 2D profile (from Dupras <i>et al.</i> , 2006). .....	32

<b>Table 2.1:</b> Typical range of dielectric characteristics of various materials measured at 100 MHz. Summarized from Cassidy (2009), Reynolds (2011) and Styles (2012).....	34
<b>Figure 2.13:</b> The polar radiation patterns for transmitted GPR waves in H- and E- planes showing both transverse electric (TE) mode and transverse magnetic (TM) mode in (a) free space and (b) the ground with a permittivity of 4 (from Milsom and Eriksen, 2011).....	38
<b>Figure 2.14:</b> A 400 MHz 2D profile across a house floor. Buried water pipes are visible as reflection hyperbolas (Conyers, 2006a). ....	39
<b>Figure 2.15:</b> Reflection profile from a cemetery with wooden coffins interred between 1898 and 1921. One metal coffin is identifiable by the alternating strong hyperbolic reflections below it (Conyers, 2006b).....	41
<b>Figure 2.16:</b> Schematic of the Electromagnetic Induction process in the air and in the Earth, showing electromagnetic field transmitted into the ground from the transmitting coil, which generates small eddy currents on the surface of a conductor, and the eddy currents in turn create a secondary electromagnetic field that is measured by the receiver coil (from Styles, 2012). ....	44
<b>Figure 2.17:</b> Example of an EM conductivity survey for a clandestine grave. The bold oval (top) shows where the body was ultimately found during subsequent excavations (from Nobes, 2000). ....	46

<b>Figure 2.18:</b> Sequential magnetic susceptibility mapview dataset at 12 months, 15 months, 18 months and 21 months. Burial simulated grave positions shown as rectangular dotted lines throughout (edited from Molina <i>et al.</i> , 2016). .....	48
<b>Figure 3.1:</b> Map of the general and survey area (with location inset) and relevant Medieval features superimposed (modified from Dick <i>et al.</i> , 2015).....	59
<b>Figure 3.2:</b> a) Mapview of Charterhouse Square showing approximate location of discovered shaft (green circle), named geophysical survey lines and site orientations, parish boundary (red dotted line), b) site photograph and c) parish boundary building plaque. Modified from Dick <i>et al.</i> (2015). .....	60
<b>Figure 3.3:</b> Approximately NW-SE orientated, 2D schematic cross-section of the study site using BGS borehole information, with sea level at zero elevation (see Table 3.1).....	61
<b>Figure 3.4:</b> Mapview of shaft discovered earth-cut graves with identified burials and confirmed <i>Yersinia pestis</i> (see keys) at (a) 2.7 m and (b) 2.3 m BGL respectively (Fig. 3.2 for location). Two graves discovered at 2.5 m not shown. Modified from Dick <i>et al.</i> (2015). .....	64
<b>Figure 3.5:</b> 2D schematic cross-section of earth-cut graves. Modified from Crossrail (2013). .....	65
<b>Figure 3.6:</b> Co-mingled human remains and carbon dating analysis of Black Death Plague victims from rural French graveyards (from Kacki <i>et al.</i> , 2011).....	66

<b>Table 3.2:</b> Summary statistics of EM, CST, GPR and ERI geophysical datasets collected during this study. See Fig. 3.2 for dataset location. ....	69
<b>Figure 3.7:</b> Photographs of near-surface geophysical equipment used. a) Geonics™ EM31-Mk2 conductivity meter; b) Geoscan™ RM-15-D mobile resistivity meter with 1m probe separation); c) GPR PulseEKKO™ 1000 225 MHz frequency antennae and associated equipment and; d) Campus TIGRE™ Electrical Resistivity Imaging system with a 32 electrode spread. ....	70
<b>Figure 3.8:</b> 2D GPR profile showing hyperbolic velocity matching where hyperbolic functions have been fitted to diffraction hyperbola from a 225-MHz GPR section acquired from Charterhouse Square, with average velocity of 0.13 m/ns. ....	73
<b>Figure 3.9:</b> Processed electro-magnetic (EM) conductivity Inphase VMD dataset with generated colour contoured digital gridded surface (see key) and annotated area of interest marked, sampling positions shown as parallel dotted points. Modified from Dick <i>et al.</i> (2015). ....	77
<b>Figure 3.10:</b> Processed electro-magnetic (EM) conductivity Quadrature VMD dataset with generated colour contoured digital gridded surface (see key) and annotated area of interest marked, sampling positions shown as parallel dotted points. Modified from Dick <i>et al.</i> (2015). ....	78
<b>Figure 3.11:</b> Processed merged CST resistivity dataset (black dots) with colour contoured digital surface generated (see key) and annotated interpretations marked. Modified from Dick <i>et al.</i> (2015). ....	80

<b>Figure 3.12:</b> Selected GPR 2D processed profile lines with marked interpreted buried objects. Red arrows represent accepted graves and black arrows represent suspected graves. Only the red arrows were used for statistical calculations (Fig. 3.2 for location).....	86
<b>Figure 3.13:</b> 3D GPR time-slice images of the survey site with colour legend denoting relatively strong reflected energy (amplitude) .....	88
<b>Figure 3.14:</b> (a) 2D GPR (L25) and (b) ERI 1 profile across the parish boundary with marked interpretations (Fig. 3.2 for location). Modified from Dick <i>et al.</i> (2015). .....	90
<b>Figure 3.15:</b> a) 2D GPR (L29) and (b) ERI 2 profile across the parish boundary with marked interpretations (Fig. 3.2 for location). .....	91
<b>Figure 3.16:</b> Summary showing geophysical interpretation, a) 2D planview map and b) Schematic 3D visualisation of the site (not to scale). Modified from Dick <i>et al.</i> (2015). .....	94
<b>Figure 3.17:</b> Depth distribution of anomalous objects identified on 20 selected 2D GPR profile lines in Charterhouse Square, Central London. ....	97
<b>Figure 4.1:</b> Generalised schematic of burial styles encountered in the three case studies discussed (modified from Hansen and Pringle, 2011).....	125
<b>Figure 4.2:</b> Historic Anglo-Saxon grave study in East Anglia, U.K. (a) magnetic susceptibility survey results and (b) excavated remains (from Pringle <i>et al.</i> , 2015a).....	129
<b>Figure 4.3:</b> 2D GPR profile example acquired in a graveyard (graves marked by arrows) in London, UK (edited from Hansen <i>et al.</i> , 2014). ....	132

<b>Figure 4.4:</b> A hypothesis showing possible expected trends of the potential geophysical response (any technique) against age of burial. ....	133
<b>Figure 4.5:</b> UK map showing the three graveyards (see key) survey site locations. ....	136
<b>Figure 4.6:</b> Examples of church graveyard above-ground memorials that were not able to be geophysically surveyed (modified from Goodwin, <i>pers. comm.</i> ). ....	137
<b>Figure 4.7:</b> Photograph of Test Line 2 and the Geoscan RM15-D electrical resistivity meter, set up with both 0.5 m and 1 m resistance data, being simultaneously collected at each sampling position at Stockton graveyard, Norfolk, UK. ....	139
<b>Figure 4.8:</b> Graph showing a comparative analysis of 0.5 m and 1.0 m resistivity electrode spacing on a test line 1 m away from known grave positions (marked) in Stockton graveyard, Norfolk, UK. ....	140
<b>Figure 4.9:</b> Photograph of test line and the Geoscan RM15-D electrical resistivity meter set up with 0.25 m, 0.5 m and 1 m resistance data being simultaneously collected at each sampling position on the 0.5 m, 1 m and 1.5 m (marked) survey lines at Keele graveyard, Staffordshire, UK. ....	141
<b>Figure 4.10:</b> Graph showing comparative analysis of 0.5 m and 1.0 m resistivity electrode spacing on a test line 1 m away from known grave positions (marked) in Keele graveyard, Staffordshire, UK. ....	142
<b>Figure 4.11:</b> (a) Mapview of graves (with burial ages noted – see Table 4.2) and subsequent repeat electrical resistivity surveys using (b) 0.25 m, (c) 0.5 m and, (d)	

1 m separated mobile electrodes on three survey lines (0.5 m, 1m and 1.5 m away from headstones) at St. Johns' Church, Keele, Staffordshire, UK.....	143
<b>Table 4.2:</b> Survey summary of test profile lines and graves at the three study sites (Fig. 4.5 for respective site locations). ....	144
<b>Figure 4.12:</b> Graph showing a comparative analysis of fixed-offset (0.5 m spaced) electrodes surveying test profiles (Fig. 4.9 for location) at 0.5 m, 1 m and 1.5 m from grave headstones with known grave positions marked (black arrows and Table 4.2), collected in Keele graveyard, Staffordshire, UK.....	145
<b>Figure 4.13:</b> 2D 450 MHz shielded GPR profile results over Keele graveyard trial lines (Fig. 4.9 and Table 4.2) at 0.5 m, 1 m and 1.5 m away from grave headstones (marked).....	147
<b>Figure 4.14:</b> Graph showing a comparative analysis of magnetic susceptibility profile results over the Endon graveyard test line at 0.5 m, 1 m and 1.5 m away from grave headstones, with known grave positions marked (black arrows – see Table 4.2).....	149
<b>Figure 4.15:</b> Photographs of near-surface geophysical techniques for the case studies showing (a) bulk ground resistivity (0.5 m and 1.0 m fixed-offset), (b) Bartington <sup>TM</sup> MS-2D susceptibility meter and (c) 225 MHz dominant frequency GPR data being collected. ....	151
<b>Figure 4.16:</b> Approximately NW-SE orientated, 2D schematic cross-section of the St. Michael's local area using BGS borehole information (see Table 4.5). ....	157



<b>Figure 4.17:</b> Schematic diagram showing the soil auger and generalised 1 D soil profile results at St. Michael’s graveyard site .....	158
<b>Figure 4.18:</b> Map view of St. Michael of all Angels church graveyard, Norfolk, UK, showing surveyed (and numbered) graves, 2D profile lines and orientations and annotated site photographs. ....	159
<b>Figure 4.19:</b> Stockton 2D survey line 1 (Fig. 4.18 for location), showing, (a) grave locations represented by headstones with year of burial inset, (b) magnetic susceptibility plot against profile distance and, (c) apparent resistivity plot against profile distance.....	162
<b>Figure 4.20:</b> Stockton 2D survey line 1 (Fig. 4.18 for location), showing, (a) grave locations represented by headstones with year of burial inset, (b) 225 MHz, (c) 450 MHz and, (d) 900 MHz frequency 2D GPR profiles with marked interpreted burial position.....	163
<b>Figure 4.21:</b> Stockton 2D survey line 2 (Fig. 4.18 for location), showing, (a) grave locations represented by headstones with year of burial inset, (b) magnetic susceptibility plot against profile distance and, (c) apparent resistivity plot against profile distance.....	165
<b>Figure 4.22:</b> Stockton 2-D survey line 2 (Fig. 4.18 for location), showing, (a) grave locations represented by headstones with year of burial inset, (b) 225 MHz, (c) 450 MHz and, (d) 900 MHz frequency 2D GPR profiles with marked interpreted burial position.....	166

<b>Figure 4.23:</b> Stockton 2D survey line 3 (Fig. 4.18 for location), showing, (a) grave locations represented by headstones with year of burial inset, (b) magnetic susceptibility plot against profile distance and, (c) apparent resistivity plot against profile distance.....	168
<b>Figure 4.24:</b> Stockton 2-D survey line 3 (Fig. 4.18 for location), showing, (a) grave locations represented by headstones with year of burial inset, (b) 225 MHz, (c) 450 MHz and, (d) 900 MHz frequency 2D GPR profiles with marked interpreted burial position.....	169
<b>Figure 4.25:</b> Combined Stockton survey line cross-plot of (a) resistivity and (b) magnetic suscep geophysical responses against age of burial (Table 4.6) respectively. ....	170
<b>Figure 4.26:</b> Stockton survey line 2 cross-plot of resistivity response against burial age (Table 4.6).....	171
<b>Figure 4.27:</b> Approximately NW-SE orientated, 2D schematic cross-section of the Keele church site using BGS borehole information (see Table 4.9 for data information). ....	174
<b>Figure 4.28:</b> Schematic diagram showing the soil auger and generalised 1 D soil profile results at St. John’s graveyard site. ....	175
<b>Figure 4.29:</b> Map view of St. John’s church graveyard, Staffordshire, UK, showing surveyed (and numbered) graves, 2D profile lines and orientations and annotated site photographs. ....	176

<b>Table 4.11:</b> Statistics of geophysical data collected from Keele graveyard, Staffs., UK. ....	178
<b>Figure 4.30:</b> Keele 2D survey line 1 (Fig. 4.29 for location), showing (a) grave locations represented by headstones with year of burial inset, (b) magnetic susceptibility plot against profile distance and, (c) apparent resistivity plot against profile distance.....	179
<b>Figure 4.31:</b> Keele 2-D survey line 1 (Fig. 4.29 for location), showing (a) grave locations represented by headstones with year of burial inset, (b) 225 MHz, (c) 450 MHz and, (d) 900 MHz frequency 2D GPR profiles with marked interpreted burial position.....	181
<b>Figure 4.32:</b> Keele 2D survey line 2 (Fig. 4.29 for location), showing, (a) grave locations represented by headstones with year of burial inset, (b) magnetic susceptibility plot against profile distance and, (c) apparent resistivity plot against profile distance.....	182
<b>Figure 4.33:</b> Keele 2-D survey line 2 (Fig. 4.29 for location), showing, (a) grave locations represented by headstones with year of burial inset, (b) 225 MHz, (c) 450 MHz and, (d) 900 MHz frequency 2D GPR profiles with marked interpreted burial position.....	183
<b>Figure 4.34:</b> Keele 2D survey line 3 (Fig. 4.29 for location), showing, (a) grave locations represented by headstones with year of burial inset, (b) magnetic susceptibility plot against profile distance and, (c) apparent resistivity plot against profile distance.....	184

<b>Figure 4.35:</b> Keele 2-D survey line 3 (Fig. 4.29 for location), showing, (a) grave locations represented by headstones with year of burial inset, (b) 225 MHz, (c) 450 MHz and, (d) 900 MHz frequency 2D GPR profiles with marked interpreted burial position.....	186
<b>Figure 4.36:</b> Keele 2D survey line 4 (Fig. 4.29 for location), showing, (a) grave locations represented by headstones with year of burial inset, (b) magnetic susceptibility plot against profile distance and, (c) apparent resistivity plot against profile distance.....	187
<b>Figure 4.37:</b> Keele 2-D survey line 4 (Fig. 4.29 for location), showing, (a) grave locations represented by headstones with year of burial inset, (b) 225 MHz, (c) 450 MHz and, (d) 900 MHz frequency 2D GPR profiles with marked interpreted burial position.....	189
<b>Figure 4.38:</b> Combined Keele survey line cross-plot of (a) magnetic susceptibility and, (b) resistivity geophysical responses against age of burial (Table 4.10) respectively. ....	190
<b>Figure 4.39:</b> Approximately NW-SE orientated, 2D schematic cross-section of the site using BGS borehole information, with sea level at zero elevation (see Table 4.13). ....	193
<b>Figure 4.40:</b> Schematic diagram showing the soil auger and generalised 1 D soil profile results at St. Luke’s graveyard Endon site. ....	194

<b>Figure 4.41:</b> Map view of St. Luke’s church graveyard Endon site, Staffordshire, UK, showing surveyed (and numbered) graves, 2D profile lines and orientations and site photographs. ....	195
<b>Table 4.15:</b> Statistics of geophysical data collected from Endon graveyard, Staffs, UK. ....	197
<b>Figure 4.42:</b> Endon 2D survey line 1 (Fig. 4.41 for location), showing, (a) grave locations represented by headstones with year of burial inset, (b) magnetic susceptibility plot against profile distance and, (c) apparent resistivity plot against profile distance.....	198
<b>Figure 4.43:</b> Endon 2D survey line 1 (Fig. 4.41 for location), showing (a) grave locations represented by headstones with year of burial inset, (b) 225 MHz, (c) 450 MHz and, (d) 900 MHz frequency 2D GPR profiles with marked interpreted burial position.....	199
<b>Figure 4.44:</b> Endon 2D survey line 2 (Fig. 4.41 for location), showing, (a) grave locations represented by headstones with year of burial inset, (b) magnetic susceptibility plot against profile distance and, (c) apparent resistivity plot against profile distance.....	200
<b>Figure 4.45:</b> Endon 2D survey line 2 (Fig. 4.41 for location), showing, (a) grave locations represented by headstones with year of burial inset, (b) 225 MHz, (c) 450 MHz and, (d) 900 MHz frequency 2D GPR profiles with marked interpreted burial position.....	201

<b>Figure 4.46:</b> Combined Endon survey line cross-plot of (a) resistivity and (b) magnetic susceptibility geophysical responses against age of burial (Table 6.14) respectively. ....	202
<b>Figure 4.47:</b> Ternary diagram showing optimum grave detection techniques and respective dominant soil types and textures. ....	211
<b>Figure 5.1:</b> Concentrated heap of solid waste near landfill, Port Harcourt, Nigeria (Ehirim <i>et al.</i> , 2009). ....	218
<b>Figure 5.2:</b> Measured pig leachate (solid line) sampled from three different pig grave environments and background (dashed line) soil-water conductivity values over the 3-years survey period (adapted from Pringle <i>et al.</i> , 2012b). ....	223
<b>Figure 5.3:</b> Map of UK 2001 FMD outbreak locations (after DEFRA, 2001). ....	225
<b>Figure 5.4:</b> Typical lined animal mass burial pit at Birkshaw Forest, Lockerbie, UK, taken in 2001 following the foot-and-mouth animal disease outbreak (Rawell, 2009). ....	226
<b>Figure 5.5:</b> Typical unlined on-farm animal mass burial pit during the UK 2001 FMD outbreak (Hickman and Hughes, 2002). ....	226
<b>Figure 5.6:</b> Composition and elemental components of a typical 70 kg human body (modified from Swann <i>et al.</i> , 2010). ....	227
<b>Figure 5.7:</b> Schematic diagram and photograph of the study site in Keele University, showing the surveyed area with pig grave (yellow dot) and control (green dot) positions approximately indicated and location map (inset). ....	233

<b>Figure 5.8:</b> Annotated diagram showing how a lysimeter should be installed in the ground (after Jervis, 2010).	235
<b>Figure 5.9:</b> Study site, (a) “pig lysimeter grave,” (b) and (c) “pig carcass,” (d) “control site with lysimeter,” and (e) soil “fluid” measurement photographs, respectively.	238
<b>Figure 5.10:</b> Screen-shot of IC separation analysis of inorganic anions in grave soilwater, showing individual anions and their respective concentration values from the test site.	242
5.3.5.2 Inductively Coupled Plasma Optical Emission Spectroscopy (ICP-OES).	243
<b>Figure 5.11:</b> ICP discharge processes on a sample (adapted from Boss and Fredeen, 1997)	244
<b>Figure 5.12:</b> Degrees of positive and negative correlation.	245
<b>Figure 5.13:</b> Graphical summary of total rainfall (bars) and average temperature (red line) data from the study site over the monitoring period.	247
<b>Figure 5.14:</b> Combined plot of concentrations of selected element parameters against Post-Burial Days (PBD) over the monitoring period. (a) grave soil (leachate) water, (b) background soil water and (c) Pure Leachate with control values deducted from leachate.	253
<b>Figure 5.15:</b> Comparative analysis of concentration of individual inorganic elements and electrical conductivity over the monitoring period (where Ca is	

Calcium, K is Potassium, Na is Sodium, Cl is Chloride, NO <sub>3</sub> is Nitrate, SO <sub>4</sub> is Sulphate, PO <sub>4</sub> is Phosphate and EC is Electrical Conductivity).....	255
<b>Figure 5.16a:</b> Map of St. Michael's of all Angels Church graveyards Stockton, Norfolk, showing soil sample locations across the site (location map inset).....	263
<b>Figure 5.16b:</b> Map of St. John's Church graveyards, Keele, Staffordshire, showing soil sample locations across the site (Location map inset).....	264
<b>Figure 5.16c:</b> Map of St. Luke's Church graveyards, Endon, Staffordshire, showing soil sample locations across the site (Location map inset).....	265
<b>Figure 5.17:</b> The enrichment factors, geo-accumulation factors and contamination factors for (a) Stockton (b) Keele and (c) Endon sites respectively. See Tables 5.17-9 for details. ....	277
<b>Figure 5.18a-e:</b> Stockton site map with element concentration levels at sampled locations a) aluminium (Al), b) calcium (Ca), c) iron (Fe), potassium (K) and magnesium (Mg). ....	288
<b>Figure 5.19a-e:</b> Keele site map with element concentration levels at sampled locations a) aluminium (Al), b) calcium (Ca), c) iron (Fe), potassium (K) and magnesium (Mg). ....	290
<b>Figure 5.20a-e:</b> Endon site map with element concentration levels at sampled locations a) aluminium (Al), b) calcium (Ca), c) iron (Fe), potassium (K) and magnesium (Mg). See Figure 15.16c for profile lines across grave locations.....	293



<b>Figure 6.1:</b> Combined Stockton graveyard survey line cross-plots showing different linear trends (youngest being statistically significant) for the three burial age divisions.....	305
---	-----

## List of Tables

<b>Table 2.1:</b> Typical range of dielectric characteristics of various materials measured at 100 MHz. Summarized from Cassidy (2009), Reynolds (2011) and Styles (2012).....	34
<b>Table 3.1:</b> List of available site investigation borehole and pertinent information derived to generate the schematic 2D cross-section shown in Fig. 3.3. ....	62
<b>Table 3.2:</b> Summary statistics of EM, CST, GPR and ERI geophysical datasets collected during this study. See Fig. 3.2 for dataset location. ....	69
<b>Table 3.3:</b> Data processing protocols used for resistivity survey in these studies .....	71
<b>Table 3.4:</b> Tabulated list of geophysical targets encountered in this study and their geophysical responses (see Fig. 3.15 for location). Modified from Dick <i>et al.</i> (2015).....	93
<b>Table 3.5:</b> Anomalies depth bgl present on 2D GPR profiles in the survey area.....	116
<b>Table 4.1:</b> Typical range of dielectric characteristics of various materials measured at 100MHz GPR antenna frequency (Daniels, 2004; Cassidy, 2009) .....	131
<b>Table 4.2:</b> Survey summary of test profile lines and graves at the three study sites (Fig. 4.5 for respective site locations). ....	144
<b>Table 4.3:</b> Summary of GPR antenna frequency specifications used for all survey sites. ....	154
<b>Table 4.4:</b> Sequential GPR data processing steps used in the study. ....	155

<b>Table 4.5:</b> List of available Stockton site investigation borehole and pertinent information to generate the schematic 2-D cross-section shown in Figure 4.16.....	157
<b>Table 4.6:</b> Details of graves surveyed for case study 1 (St. Michael’s Church graveyard) .....	160
<b>Table 4.7:</b> Statistics of geophysical data collected from Stockton graveyards, Norfolk, UK. ....	161
<b>Table 4.8:</b> Summary of GPR Stockton survey (St. Michael’s graveyard), Norfolk, UK.....	172
<b>Table 4.9:</b> List of available Keele site investigation borehole and pertinent information derived to generate the schematic 2-D cross-section shown in Figure 4.27.....	174
<b>Table 4.10:</b> Details of graves surveyed for case study 2 (St. John’s Church graveyard) .....	177
4.6.2 <i>Case study 2: Geophysical results</i> .....	177
<b>Table 4.11:</b> Statistics of geophysical data collected from Keele graveyard, Staffs., UK. ....	178
<b>Table 4.12:</b> Summary of GPR Keele survey (St. John’s graveyard) .....	191
<b>Table 4.13:</b> List of available local Endon site investigation borehole and pertinent information to generate the schematic 2-D cross-section shown in Figure 4.39.....	193
<b>Table 4.14:</b> Details of graves collected from case study 3 (St. Luke’s Church graveyard). ....	196

<b>Table 4.15:</b> Statistics of geophysical data collected from Endon graveyard, Staffs, UK. ....	197
<b>Table 4.16:</b> Summary of GPR Endon survey results (St. Luke’s graveyard).....	203
<b>Table 4.17:</b> GPR grave detection summary for the 3 case studies.....	209
<b>Table 4.18:</b> Resistivity and magnetic susceptibility grave detection summary for the 3 case studies.....	209
<b>Table 5.1:</b> Typical measured ranges of concentration of various constituents in landfill and mortality leachates against the groundwater standards.....	220
<b>Table 5.2:</b> Main factors affecting leachate formation in landfills (after El-Fadel <i>et al.</i> , 2002). ....	231
<b>Table 5.3:</b> Summary of measured monthly local average temperature and total rainfall data from the study site over the 18 months monitoring period. Stated measurements are averages with $\pm 0.1$ °C and 0.1 mm accuracy. Bgl – below ground level. ....	240
<b>Table 5.4:</b> On-site measured physicochemical parameters in leachate and background soil water samples over the monitoring period .....	249
<b>Table 5.5:</b> Summary of selected element parameters from grave soil (Leachate) sample measured during the monitoring period.....	251
<b>Table 5.6:</b> Summary of selected element parameters from background soil water sample measured during the monitoring period.....	252

<b>Table 5.7:</b> Correlation Coefficients among different grave soil (Leachate) parameters.....	256
<b>Table 5.8:</b> Correlation Coefficients among different control soil water parameters.....	256
<b>Table 5.9:</b> Regression equations between elements and conductivity in leachate samples. ....	258
<b>Table 5.10:</b> Regression equations between elements and conductivity in soil water samples. ....	259
<b>Table 5.11:</b> Classification of geo-accumulation index .....	268
<b>Table 5.12:</b> Classification of enrichment Factor .....	270
<b>Table 5.13:</b> Classes of Contamination factor ( $Cf_x$ ) and Contamination degree ( $C_{deg}$ ) (Hakanson, 1980; Loska <i>et al.</i> , 2004) .....	271
<b>Table 5.14:</b> Description of sites background soil elemental concentration levels .....	272
<b>Table 5.15:</b> Description of study sites average soil elemental concentration levels .....	272
<b>Table 5.16:</b> Summary of enrichment factors, geo-accumulation factors and contamination .....	275
<b>Table 5.17:</b> Geo-accumulation factor with respect to individual graveyard and classification .....	275
<b>Table 5.18:</b> Enrichment Factor with respect to individual graveyard and classification .....	276

**Table 5.19:** Contamination factor with respect to individual graveyard and classification.....276

**Table 6.1.** Generalised table to indicate potential of geophysical techniques and soil sampling analysis success for grave(s) location assuming optimum equipment configurations. Note this table does not differentiate between target size, burial depth/age and other important specific factors (see text). The dominant sand | clay soil end-types are detailed where appropriate for simplicity, therefore not including peat, cobbles etc. types. Modified from Pringle *et al.*, (2012b). .....310

## **Chapter 1: Introduction**

In this chapter, the research areas of forensic geoscience, forensic geophysics and search methods are introduced, and the influence of soil components in detection of clandestine graves is briefly discussed. Finally, the generic aims of this thesis and the structure of the following chapters are described.

### **1.1 Forensic geoscience**

The term ‘forensic geoscience’, may be defined as a sub-discipline of geoscience that is concerned with the application of geological and wider environmental science information and methods to investigations which may come before a court of law (Pye and Croft, 2004). Thus, going by its definition, it encompasses a number of sub-disciplines, such as forensic geology, forensic geophysics, forensic soil science, environmental forensics, forensic mapping, geomatics and remote sensing (Pringle et al. 2012a). Due to the number of sub-disciplines that made up forensic geoscience, its scientific boundaries are not clearly defined, and as such had significant overlaps with other related sub-disciplines (Pye and Croft, 2004).

Forensic geoscience is generally seen as a specialist tool that supports law enforcement investigations to help determine what happened, where, when, how and why it occurred (Donnelly, 2009). It also involves the analysis of soil and materials as trace evidence to determine if there was an association between a suspect or other object or item and a scene of crime (Pringle et al. 2012a). Aside from law enforcement investigations, the

application of forensic geoscience methods has also seen a growing interest in environmental and humanitarian search investigations which have accordingly resulted in a significant number of published articles (see, e.g. Ruffell, 2010; Pringle *et al.* 2012a; Donnelly, 2013). In recent times, other applied sciences such as geography, geostatistics, remote sensing and geographic information system (GIS), have been incorporated within the wider discipline of geoforensics (the application of geology to criminal investigations) and have found uses in criminology in the prediction of crime and thereby targeting of police resources to certain geographic areas (Hirschfield and Bowers, 2001; Ruffell and McKinley, 2005). As regards scope and applications, geoforensic and geoscience methods are not restricted to use in criminal investigations, however, they can also be applied to a wide range of civil law relating to such problems as environmental accidents, construction failure, pollution and of other serious crime such as terrorism, genocide, rape and drug smuggling (Pye and Croft, 2004). The diagrammatic representation of relationship of forensic geoscience to some other disciplines and sub-disciplines is shown in Fig. 1.1. However, there are concerns with the inconsistency of terminologies employed by different disciplines which have developed to confusing terms, this was reported by Ruffell (2010), explaining the need to standardize terms used in forensics geoscience.



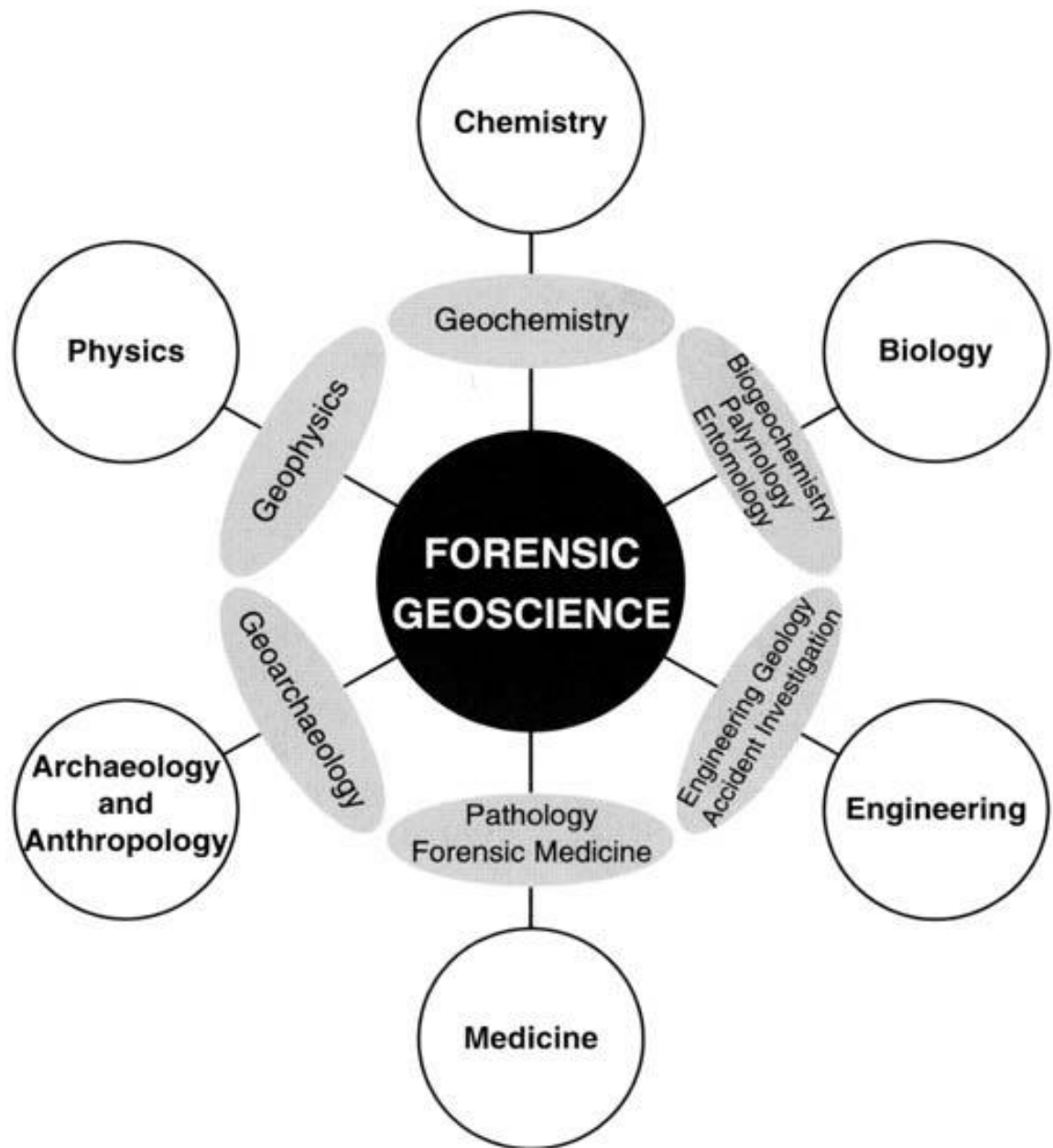


**Figure 1.1:** Schematic diagram showing the relationship of forensic geoscience to some other disciplines and sub-disciplines (from Pye and Croft, 2004).

## 1.2 Search for forensic and archaeological burials

According to best practice, a search has been defined as '*the application and management of systematic procedures, combined with appropriate equipment to locate a specific target or targets*' (Harrison and Donnelly, 2009). The fields of archaeology, anthropology, and geology clearly connect in the area of forensic field investigation, such as the search for clandestine graves or mass burials (Pringle et al. 2012a; Bergslien, 2012). Thus, forensic search cannot be a random exploration but must be systematic and well designed in order to achieve a specified goal. Generally, what is being searched for in forensic investigation of human burials are items or objects associated with the victim's body, such as; weapons used during murder, clothing containing ferrous or non-ferrous metal components like zips, studs and buckles, drugs, leachate plumes associated with decomposition and skeletonisation of human remains (Donnelly, 2009).

Different types of searches have been summarized by Harrison and Donnelly (2009) to include firstly, *scenario-based searches*, which rely on information or data gathered by investigators such as behavioural profiling, last sighting reports, and records of movement to develop a working hypothesis. Secondly, *feature-based searches*, which enables the identification of physical landmarks that be easily relocated by the culprit, such as a dark rock amongst an area of light coloured rock, as the focus here is on searching key features within the search sector relevant to the search scenario, rather than searching the whole area within the sector. Lastly, intelligence-led, which ensure that searches are based on logic and reliable intelligence during investigation of a crime, and also involve the

deployment of all geophysical and related search techniques based on a sound scientific understanding of the geology and ground conditions.

For the last two decades, methodologies have been adapted in searching for burials that combine the expertise of forensic investigators and archaeological personnel on numerous investigations (see, e.g. Renfrew and Bahn, 2000; Dupras *et al.*, 2006). Though their philosophy may be very similar, respective search specialists' final goal may differ as both disciplines use and interpret evidence in different ways.

### **1.3 Soil components and analysis**

Technically, soil can be defined as the unconsolidated material on the upper layer of earth typically consisting of a mixture of organic remains, water, air, clay and rock particles (Bergslien, 2102). Although soils mean different things to different disciplines, soil scientists view soils as being made up of different-sized mineral particles (i.e., sand, silt, and clay) and organic matter (Fitzpatrick, 2008). The potential contribution of studies of soil and its components to criminal investigations has unlocked useful information following the transferability between the scene and the criminal (see Murray, 2004; Morgan and Bull, 2007). However, in the context of this study, the purpose for soil sample analysis was not to link the scene to the culprit, rather to identify burial location following the observed changes in soil elemental concentrations between graves and background sites. Hence, soil is also considered as a material for the burial of human, animal, or plant remains in cemeteries or special kinds of landfills. The decomposition of cadavers buried in soil has received increasing attention due to pressing issues in forensic science and

possible public health hazards, as decomposition of remains introduces pulses of nutrients (i.e. C, N, P, K, Mg, Ca and Na) into the soil, which will subsequently remain in the soil even after the leachate fluid has gone (Perrault and Forbes, 2016).

Soils are the physical context within which forensic evidence is found. Thus, understanding some of the potential implications of different physical and chemical soil properties is very important. Soil properties such as the acidity or alkalinity, soil temperature, soil texture, soil elemental composition and concentration, and soil fluid conductivity play a significant role in locating a clandestine grave (Carter and Tibbett, 2006; Pringle *et al.*, 2010a; Pringle *et al.*, 2012b).

#### **1.4 Thesis aims and structure**

In this thesis, the use of multi-geophysical techniques for the detection of recent and old burials has been studied. Empirical studies have shown that as the buried human bodies deteriorate and decompose over time, they release inorganic and organic constituents into the host soil with potential for the soil being contaminated by elevated elements from cadaver decomposition. As such, comparative analysis of soil parameters can also be used to assist the detection of graves. It is thus very important to integrate both geophysical and geochemical approaches to improve the success rate in forensic grave detection. Therefore, the main aims of this research is described below, but with more specific aims detailed in the individual chapters:

- 1 To determine if non-invasive geophysical methods could both detect and characterise a potential ancient mass burial;
- 2 To determine if geophysical responses over modern burial site graves, compared to background values, will decrease as the age of burial increases;
- 3 Perform a systematic statistical analysis of parameters to determine the contributions from individual inorganic ions responsible for the variations in pig cadaver 'soil water' conductivity;
- 4 Determine the elevated metallic elements in long-term burial sites (graveyards) when compared with control values, using contamination impact factors as a potential for detecting clandestine burials.

To achieve these aims, a review of the literature was conducted so that the context of the case study chapters can be better understood. Additionally, the results are discussed in a chapter to address the thesis aims, and the thesis conclusions and limitations then presented. Thus the content of the chapters are now summarised below:

- Chapter 2 is a literature review, in which forensic search, forensic geophysical techniques and geochemical analysis of soil and 'grave soil' water as an alternative approach of locating clandestine graves are discussed. Brief background theory for relevant geophysical techniques is also provided.
- Chapter 3 details an archaeological geophysical site investigation, of the detection and characterisation of an ancient mass burial cemetery using integrated geophysical methods, which includes ground penetrating radar (GPR), electrical resistivity (ERI) and electro-magnetic induction (EMI). Discussion is also given to

determine which technique is the optimum method for such urban search scenarios.

- Chapter 4 details the results of multi-geophysical surveys of three U.K. church graveyards with contrasting soil types using GPR, EMI and MS techniques. Results showed optimal GPR antennae frequencies, optimal spacing of electrical probes and recommended survey distances from headstones, with graphical summaries of expected geophysical anomalies over different burial styles. Initial work on predicting the geophysical response trend as the burial age changes is also given.
- Chapter 5 details case studies, in which soil and 'grave soilwater' leachate analyses from various burial sites are used as an alternative approach to detect graves in rural and semi-rural depositional environments.
- Chapter 6 provides a discussion, in which the combined results of Chapters 3 – 5 are considered together and the study limitations.
- Chapter 7 presents the conclusion of the thesis, including the possible implications for search and for the future and some recommendations for further research is given.

## **Chapter 2: The detection of forensic burials: a literature review**

### **2.1 Introduction**

This chapter provides a review of the research literature with emphasis on the benefits of geoscience to forensic searches, forensic geophysical techniques frequently employed and some of the standard non-geophysical methods in the search for near-surface burials. However, more specific literature is presented at the beginning of each relevant chapter.

#### *2.1.1 Contribution of geoscience to forensic searches*

Forensic search teams are increasingly utilizing geoscientific methods to assist them in the detection and location of a variety of items, the most high profile of which are clandestine burials (Pringle *et al.*, 2012a). Although increasingly being used within this field over the past few decades, forensic geoscience has a long history of application, with it being used in the late 1800s in China and India, with tracking of the accused criminal by soil and footprints as mentioned by Ruffell and McKinley (2005). However, the first recorded application of geosciences into forensic search was reported in the 1856 issue of Scientific American (see Ruffell and McKinley, 2008; Ruffell, 2010), in which a criminal investigation centred on a barrel of silver coins on a train that had been stolen and replaced with a barrel of sand. By identifying the sand from the barrel with sand from the potential railway stations at which the theft had taken place, the culprit was then identified. Among other notable contributors to forensic search in the early development included;

Han Gross, William Nicol and Edmond Locard (Murray, 2004; Bergslien, 2012). In the early twentieth century, forensic practice saw the need to include geoscience methods as a search practice following the work of Georg Popp in 1904, who became the first scientist to present in a law court the evidence associated to the murder of Eva Disch, with soil found on the accused matching soil where the murdered victim was found (Murray and Tedrow, 1975). In 1909, Rodolphe Reiss of the University of Lausanne created the School of Forensic Science and Criminology, dedicated to the scientific analysis of crime (Chisum and Turvey; 2000; Ruffell and McKinley, 2005). Between the 1930s and 1970s, much criminal investigation was dominated by governmental establishments, such as the Federal Bureau of Investigation (USA) and the then Central Research Establishment (UK). However, since 2002, there has been an increased awareness of the potential benefits of forensic geoscience, especially in assisting the police in some aspects such as, locating missing people or graves (Donnelly, 2011). Consequently, more than 14 international meetings have been organised that covered several aspects of forensic geosciences (Donnelly, 2011).

### *2.1.2 The impact of a cadaver burial on the local environment*

A number of studies have been conducted to understand how the presence of a cadaver in the grave affects the properties of the local environment (Jones, 2008; Dalan *et al.*, 2010; Aitkenhead-Peterson *et al.*, 2012; Perrault and Forbes, 2016). This is necessary in order to assist in the selection of both optimal search method(s) and the most suitable technique(s) for the specific search scenario, since there must be sufficient measureable



contrast in the physical properties between burial cadaver and surrounding soil to be justifiable. For example, it has been shown that the odour of a decomposing cadaver is detectable by specially trained search dogs (Rebmann *et al.*, 2000; Oesterhelweg *et al.*, 2008) and therefore such trained dogs are considered as part of the search strategies used to locate a burial.

Buried human remains generally decompose approximately 8 times more slowly than when allowed to decompose on the earth's surface (Rodriguez, 1997), and during decomposition generally creates a localized gradual release of cadaveric nutrients into the surrounding soil, which can cause unusual growth effect on the local vegetation in contact with the cadaver (Perrault and Forbes, 2016). This contrasting growth in vegetation has also promoted 'visual observation' as the popular first choice of search strategy in detecting the location of a clandestine grave (Killam, 2004; Hunter and Cox, 2005; Dupras *et al.*, 2006). The act of backfilling the grave can also result in the formation of mounding in an attempt to replace all the excavated soil back into the grave, otherwise, a primary surface depression gradually formed on top of the remain, created by collapsing of body cavity(ies) and consolidation of backfilled soil, which is as a notable indicator of a clandestine grave (Killam, 2004). Accordingly, an understanding of how the presence of burial can affect the condition of the local environment is necessary for a detailed search. The main ways by which cadaver burial can alter the local environment has been shown in Figure 2.1.

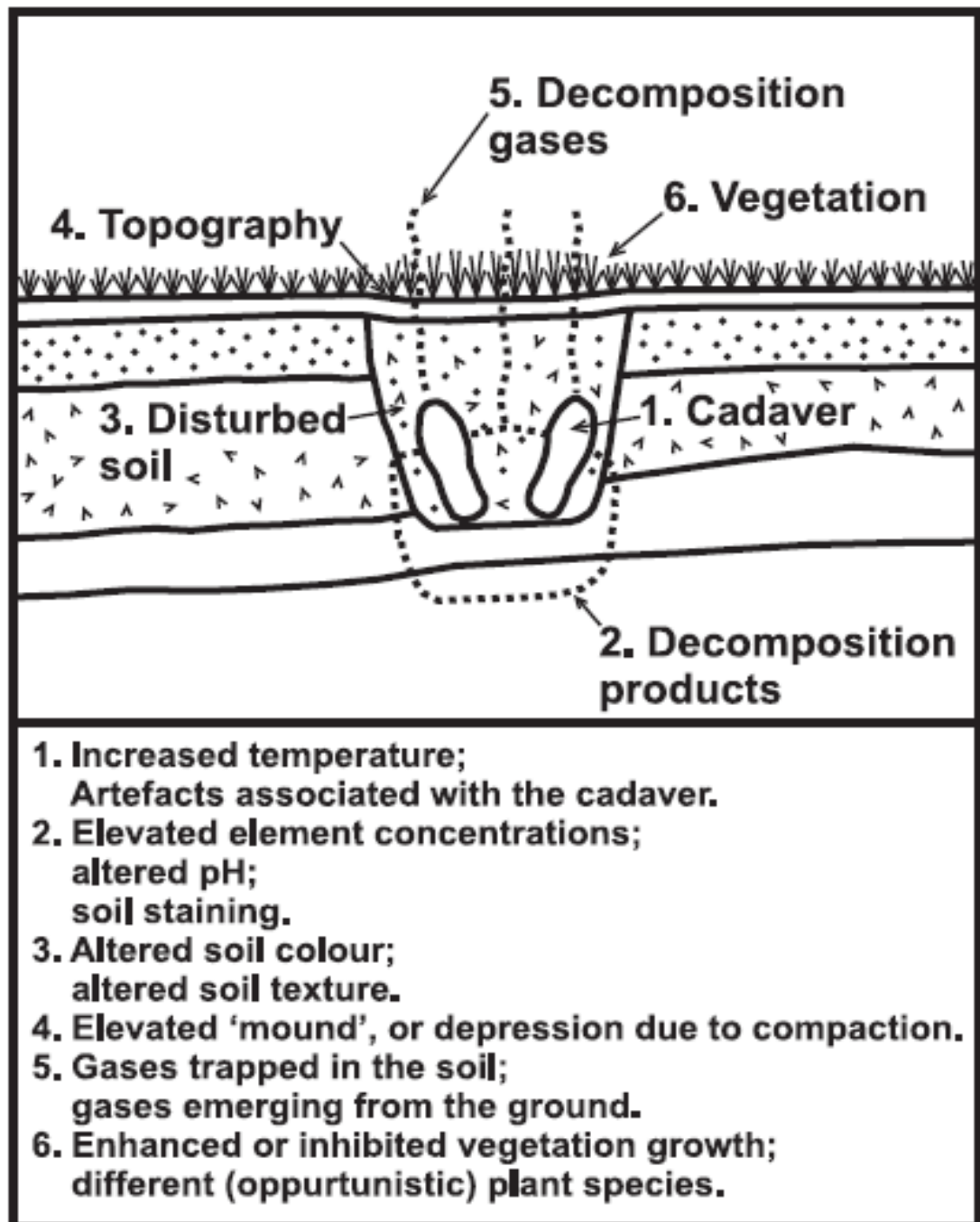


**Figure 2.1:** Examples of possible alterations to the local environment due to the presence of a clandestine grave by Jervis (2010), with further details listed (bottom panel) modified from Hunter and Cox (2005), and Harrison and Donnelly (2009).

Another useful indicator of a clandestine grave is the presence of the grave cut, due to differences in moisture retention and varying effects of weathering phenomena between the disturbed and background soil. This effect can also facilitate the chance of grave detection, firstly, by visual observation strategy and secondly when geophysical technique(s) are being applied due to electrical or magnetic properties contrasts between disturbed soil and background soil that generates different geophysical signatures (see Tibbett and Carter, 2009).

Soil colour, texture and porosity can all be effected by the presence of decomposition fluid, as soil grave collected from adjacent to a buried cadaver has been reported as “blackened, wet and odorous” (Wilson *et al.*, 2007). There is a suggestion that phosphorus from the by-products of decomposition is responsible for the blackish colouration of cadaver host soil, which also absorbs metals such as manganese to form a permanent soil staining (Dent *et al.*, 2004; Carter *et al.*, 2007). However, the chemistry behind this staining process has not clearly been understood to-date (Spennemann and Franke, 1994). Cadaver-generated fluid also contains a range of organic acids that are capable of altering the pH value of the host soil with the aid of other substances that activate bacteria metabolites (Dent *et al.*, 2004).

Cadaver decomposition, besides changing the chemistry of grave soil, can cause a serious contamination to groundwater through the release of leachate fluid, especially where the downslope movement of leachate is possible. The impact is associated with increased concentrations of intestinal flora (Calkosinski *et al.*, 2015) and organic and inorganic nutrients (Pacheco *et al.*, 1991; Yuan *et al.*, 2013; Perrault and Forbes, 2016). This has been demonstrated in a schematic diagram developed by Harrison and Donnelly (2009) in

Figure 2.2. However, the presence of metallic ions in the leachate plume may also increase the aerial footprint of geochemical and geophysical signatures and thus increase the chance of grave detection during a forensic search investigation. In the UK, the monitoring of groundwater contamination around graveyards follows the same procedure for groundwater quality monitoring conducted in landfill sites (Zychowski, 2012).

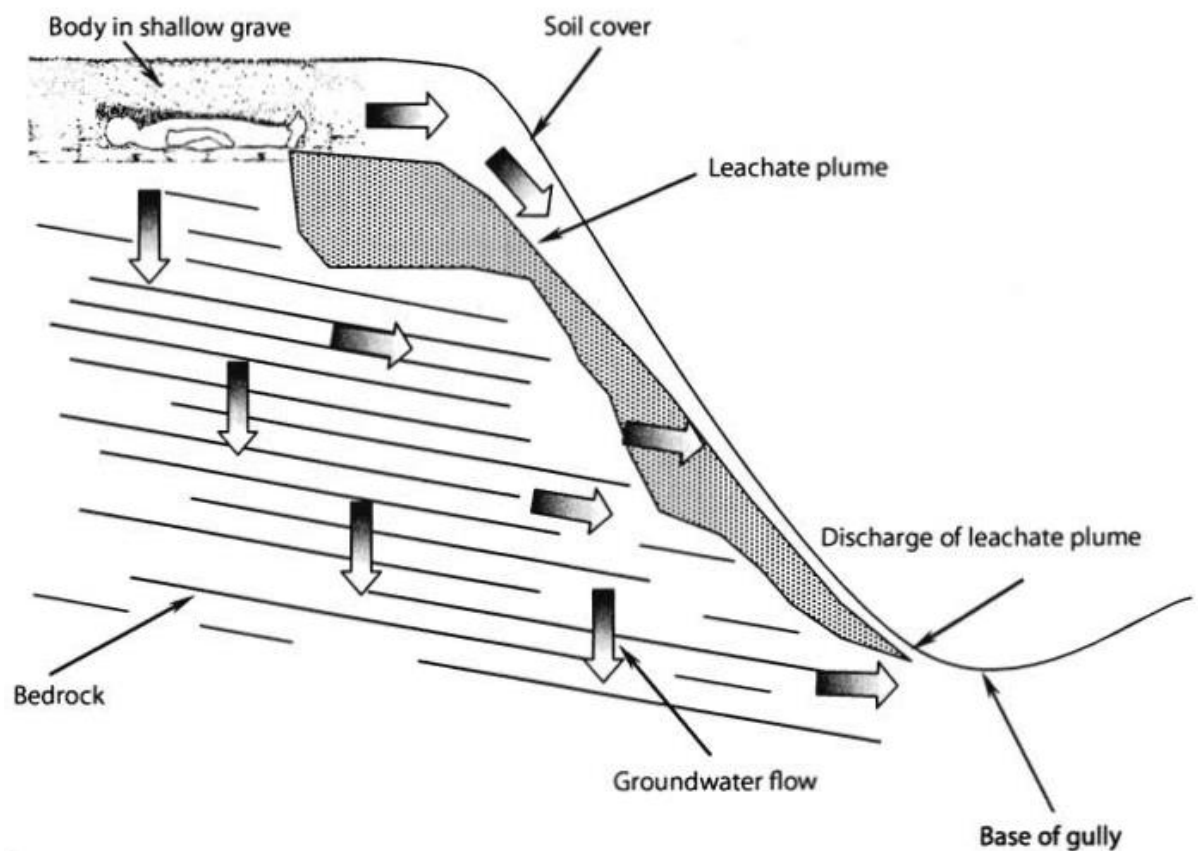


**Figure 2.2:** Schematic model to illustrate leachate plumes generated from decomposing human remains. The presence of a leachate plume may be a marker to cadaver burial location; however it may also increase the target area (Harrison and Donnelly, 2009).

## **2.2 Relevant Near-surface geophysical techniques**

Near-surface geophysical techniques depth of penetration extends up to 30 m, but has been argued to extend up to 100 m below ground level depending on the material of propagation (Reynolds, 2011). The advantages of geophysical surveys over other conventional methods have been classified in three aspects. Firstly, the methods are effectively non-invasive and this is particularly useful in certain environments such as tarmac and shallow water where reinstatement costs would otherwise be prohibitive. Secondly, fieldwork can be conducted relatively quickly with the data being able to process in the field. Thirdly, it is relatively low cost and involves less manpower resources in contrast to large-scale intrusive investigations to access the subsurface (Hunter and Cox, 2005). Geophysical techniques are being increasingly applied not just as tools for data acquisition but as means of conflict resolutions and risk managements, with the increasing demands for audit trails for liability, and risk that has to do with missing an important feature on a site may result to a large financial penalty or legal action (Reynolds, 2011).

Geophysical techniques respond to the physical properties of the subsurface media which includes; rocks, sediments, water, glacier, void etc. They can be classified into two specific types, active and passive methods. Active methods are those which transmit a signal and measure effects on the received signal, whereas passive methods measure the inherent physical properties of the ground (see Milsom and Eriksen, 2011). This section discussed specific issues of geophysics as applied in a forensics context and pursues in more detail the more relevant geophysical techniques. A more detailed scientific understanding of

individual techniques can be gained through some standard geophysical tests, such as detailed in Telford et al. (1990), Milsom and Eriksen (2011) and Reynolds (2011).

### 2.2.1 *Electrical resistivity ( $\rho$ )*

#### *Basic theory of electrical resistivity*

Electrical resistivity is a fundamental and diagnostic physical property of a material, which can be used to obtain information about the nature of the material (e.g. subsurface). For simplicity, the resistivity of a material is a measure of how well the material delays the flow of electrical current (Reynolds, 2011). Resistivity vary greatly from one material to another, and due to this variation, measuring the resistivity of an unknown material has the potential for being very useful in identifying that material. Ground resistivity is related to various geological parameters such as the mineral and fluid content, porosity and degree of water saturation in the rock (Archie, 1942). The fundamental physical law used in resistivity surveys is Ohm's law, which governs the proportional relationship between the current and voltage across a material when an electric field (E) is applied:

$$R = \frac{V}{I} \quad 2.1$$

Where, R = resistance (Ohms,  $\Omega$ ), V = voltage (Volts, V) and I = current (amps, A)

The resistance (R) is the constant of proportionality which describes the opposing force to the flow of current through a medium. However, resistivity takes into account the

amount of current flowing across parallel faces of material, which is often encountered when discussing the resistance of a material. For instance, consider an electrically uniform cube of side length ( $L$ ) and cross-sectional area ( $A$ ) of a uniform composition through which a current ( $I$ ) is passing (see Figure 2.3). Thus, the resistivity ( $\rho$ ) is defined as the material specific constant of proportionality in the expression for the total resistance of the cube.

$$\rho = \frac{RA}{L} \quad 2.2$$

Where:

$A$  = cross-sectional area of conducting material ( $\text{m}^2$ ) and  $L$  = length of conducting material (m)

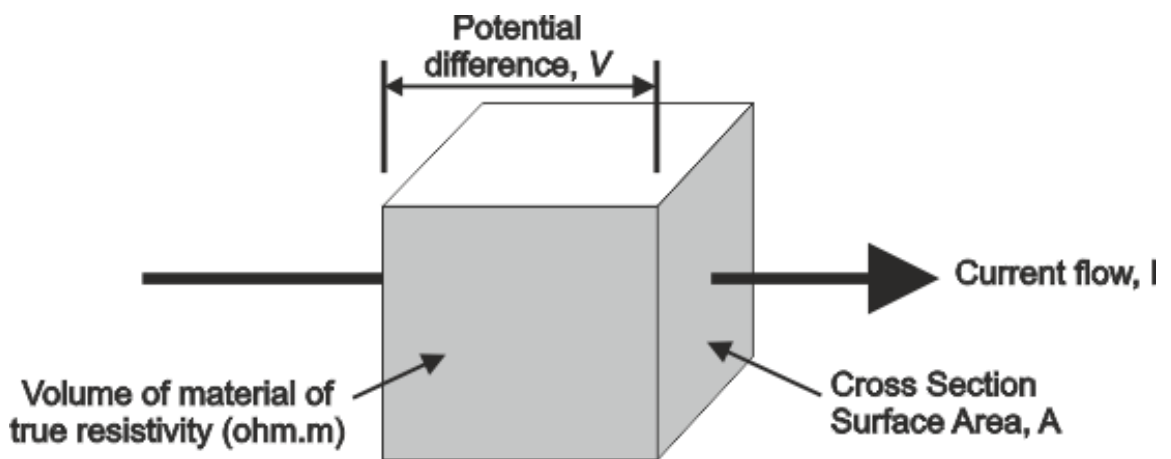


**Figure 2.3:** Current flow through, driven by potential difference across a block of material of resistivity  $\rho$  (edited from Styles, 2012).

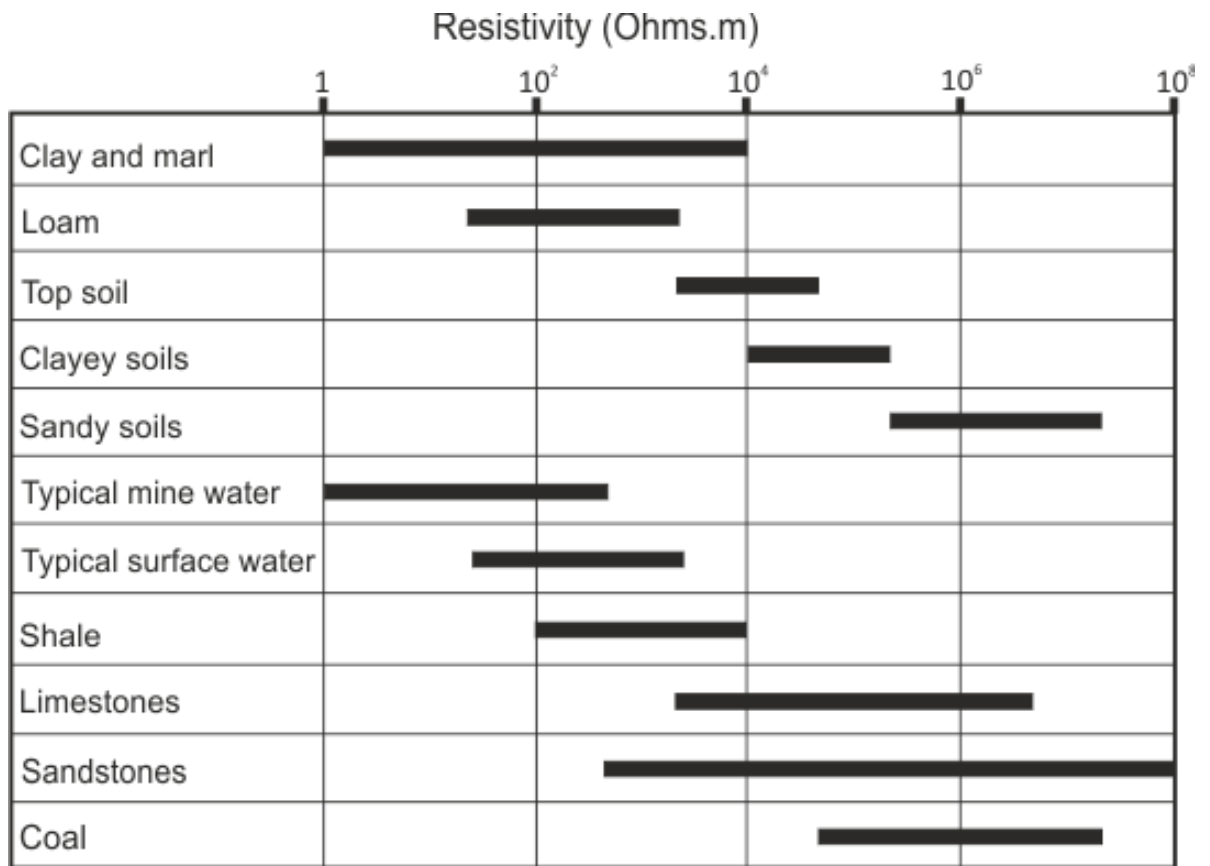


**Figure 2.4:** Approximate electrical resistivity ranges for different type of rocks (from Reynolds, 2011).

The approximate resistivity values of common rock types are shown in Figure 2.4. For a typical resistivity measurement, it can be shown that the potential difference measured using a typical four electrode array (see Fig. 2.6), at the surface of a homogeneous, isotropic half-spaced of resistivity  $\rho$  is given (Reynolds, 2011) by:

$$\nabla U = \frac{\rho I}{2\pi} \left( \frac{1}{r_{C1P1}} - \frac{1}{r_{C2P1}} - \frac{1}{r_{C1P2}} + \frac{1}{r_{C2P2}} \right) \quad 2.3$$



Where the current supplied by electrodes  $C1$  and  $C2$  is  $+I$  and  $-I$ , respectively, and  $r_{ij}$  is the distance between a current,  $C_i$ , and a potential electrode,  $P_j$ . Equation 2.10 demonstrates that measured potential difference values depend on the relative arrangement of electrodes as well as the resistivity of the ground.

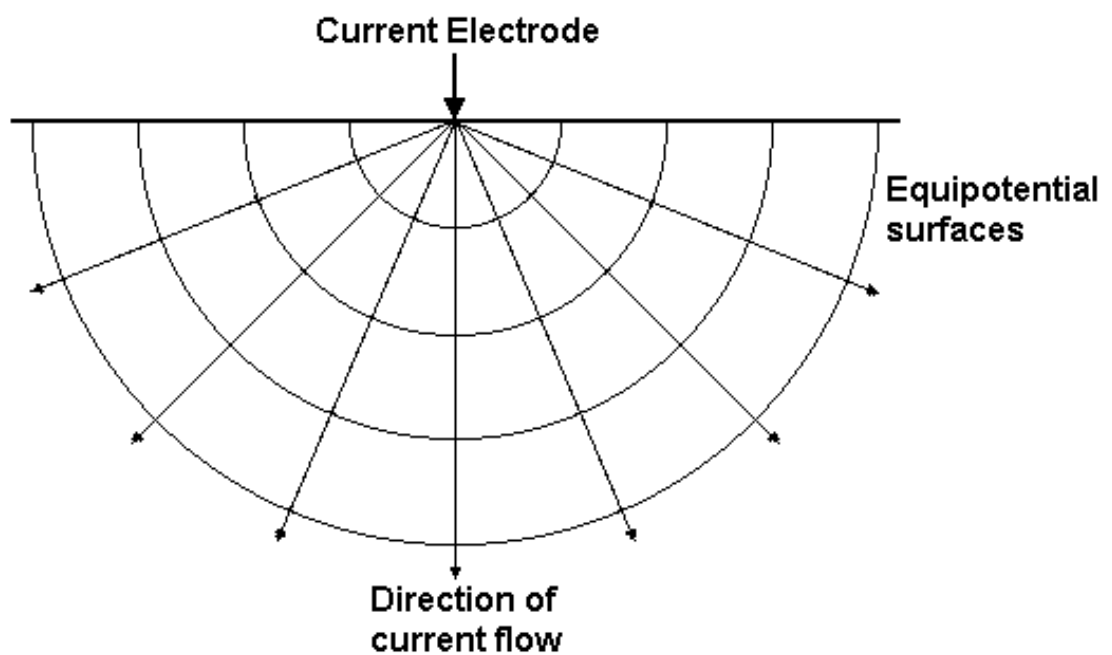


**Figure 2.5:** The flow of current from a point current source and the resulting potential distribution with homogeneous subsurface structure (Telford *et al.*, 1990).

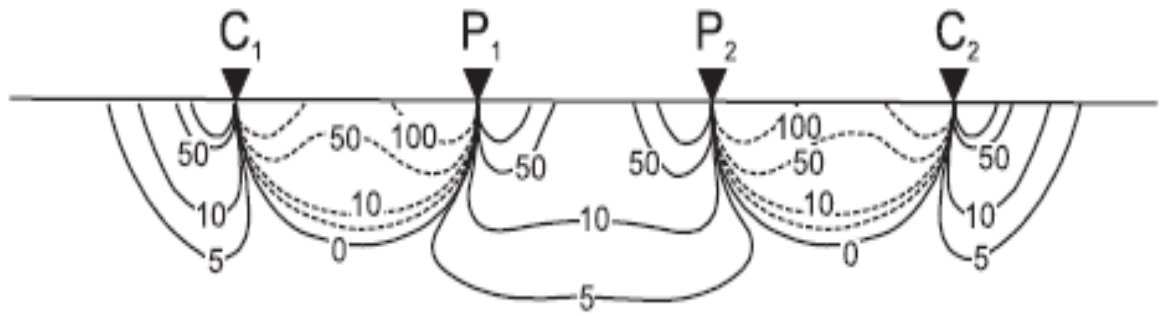


**Figure 2.6:** Signal contribution section for the Wenner array. Contours represent the contribution of by individual elements of a homogeneous subsurface to the measured resistivity. Dashed lines indicate regions where the contribution to the measured resistivity is negative (modified from Barker, 1979).

Resistivity measurements may be applied to investigate the subsurface in two possible ways; horizontal profiling (to determine the horizontal variation of resistivity) and vertical profiling (to determine the vertical variation of resistivity) (Reynolds, 2011). Horizontal profiling may be virtually interpreted, sometime without converting apparent resistivity to true resistivity especially in the case of data collected with the twin array (Styles, 2012). However, vertical profiling requires conversion of apparent resistivity to true resistivity, especially, in automated inversion based on an iterative, least square fitting method as an initial model, which is shifted vertically and the values adjusted until the root-mean-square value converged (Hautot *et al.*, 2002). Apparent resistivity values depends on the type of electrode array used, as defined by geometric factors, and currently, over 102 different surface electrode array types are recognized (Szalai and Szarka, 2008). However, the three most commonly used in forensic and archaeological studies include; Wenner, Schlumberger and dipole-dipole configurations (Styles, 2012).

Different types and patterns of electrode configuration have particular advantages, disadvantages and sensitivities. The choice of array is dependent on factors such as; the size of available space to fix the array, amount of time required for the survey, anomaly size and depth of penetration (Reynolds, 2011; Pringle *et al.*, 2012a). Wenner arrays have equal separation between all four electrodes and the wider the spacing, the deeper the depth of penetration. In Schlumberger arrays, the potential electrode spacing is temporally constant, while the current electrode spacing progressively widened until values of voltage become difficult to measure. In practice, potential electrode spacings should not more than 1/5th of the current electrode (Styles, 2012). Schematic diagrams of the three electrode configurations are shown in Figure 2.7.

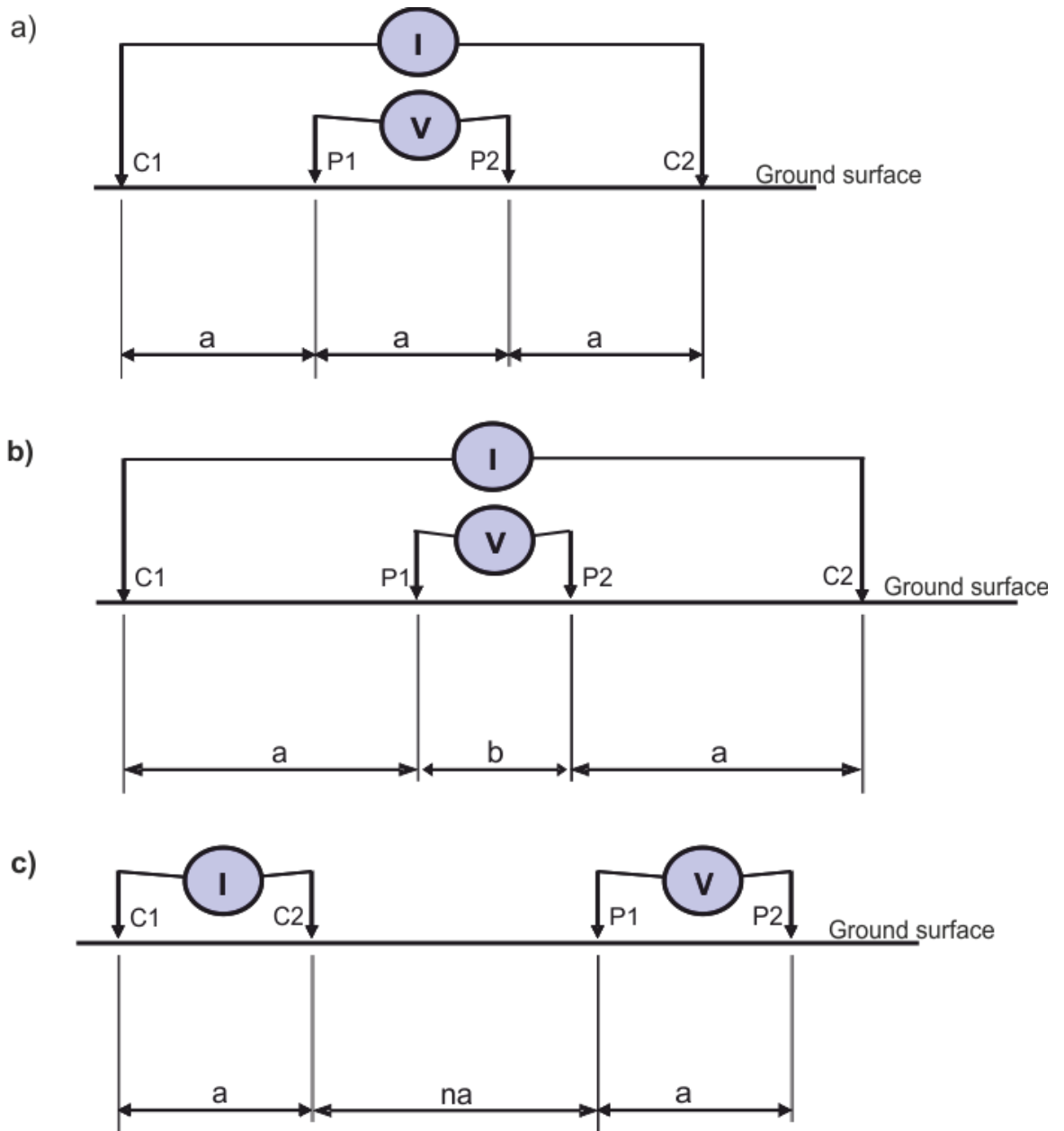


**Figure 2.7:** Array types: a) standard Wenner array with equal electrode spacing, b) Schlumberger array configuration where  $b$  spacing stays constant while  $a$  increases until readings are too small, and  $b$  is then increased to start over again and finally, c) Dipole-dipole array with  $n$  as an integral multiple of  $a$  (after Styles, 2012).

### *Applications of electrical resistivity surveys*

Resistivity surveys can be used to study the nature, distribution and flow of water in the subsurface. For example, it can be used to monitor types of groundwater pollution; to locate subsurface cavities, faults, mine shafts in geotechnical studies; mapping out the areal extent of remnants of burials and buried foundations in archaeology (Reynolds, 2011).

### *Landfill and groundwater monitoring*

Groundwater contamination from graveyards or landfills often results from leaking leachate fluid that has percolated through waste and accumulated various ions in solution (Senos Matias *et al.*, 2004; Carpenter *et al.*, 2012). In a situation where there is no protective liner, the leachates moves outwards and downwards into the surrounding and underlying aquifer and, with time, become part of the groundwater flow system as they reach the water table. Whilst hydraulic potential is the driving force for groundwater flow, electrical potential is the driving force for electrical flow. Groundwater monitoring using resistivity method is more efficient than traditional hydrogeological methods because there is no need for observation wells. This method utilizes the fact that the electrical resistivity of landfill leachate is lower than that of non-contaminated groundwater (Park *et al.*, 2016).

Electrical resistivity surveys are used to identify and map groundwater pollution. Successful leachate plume mapping depends on a resistivity contrast between the plume

and the ambient ground water, this contrast is usually in the form of a resistivity low due to an increase in dissolved solids (see, for example, Chambers *et al.*, 2006; Zume, *et al.*, 2006). In a case of hydrocarbon spillage or seepage in the soil, resistivity surveys can also be used to map such contaminated site and determine the possible boundary between polluted and unpolluted zones, with the polluted zone showing decreased soil resistivity due to abundant mobile ions associated with spilled hydrocarbon (Thabit and Khalid, 2016). The usefulness of electrical resistivity method is well recognised in contaminant leachate studies. But in some geological conditions, obtained results do not permit unambiguous identification of contaminated area due to the presence of adjoining clayey contents with contaminated layers. In order to solve such problems, Rehman *et al.* (2016) used combined electrical resistivity and induced polarization (IP) methods to successfully map groundwater contamination from a waste disposal site. Ruffell and Kulesa (2009) also successfully used a resistivity survey to identify and characterize illegal buried dump sites where clay-rich presence prevented the use of GPR.

The interpretation of the resistivity section is based on both the published electrical properties of typical subsurface materials and correlation with on-site information or observation (Styles, 2012). Resistivity surveys appeared to be gaining advantage over EM surveys of being less affected by above-ground materials (i.e. background noise) as electrodes are shallowly inserted into the ground surface. The purple and red linear features in Figure 2.8 are resistivity lows (high conductivity) in trenches that were excavated into the underlying clay and filled with industrial waste (Styles, 2012).

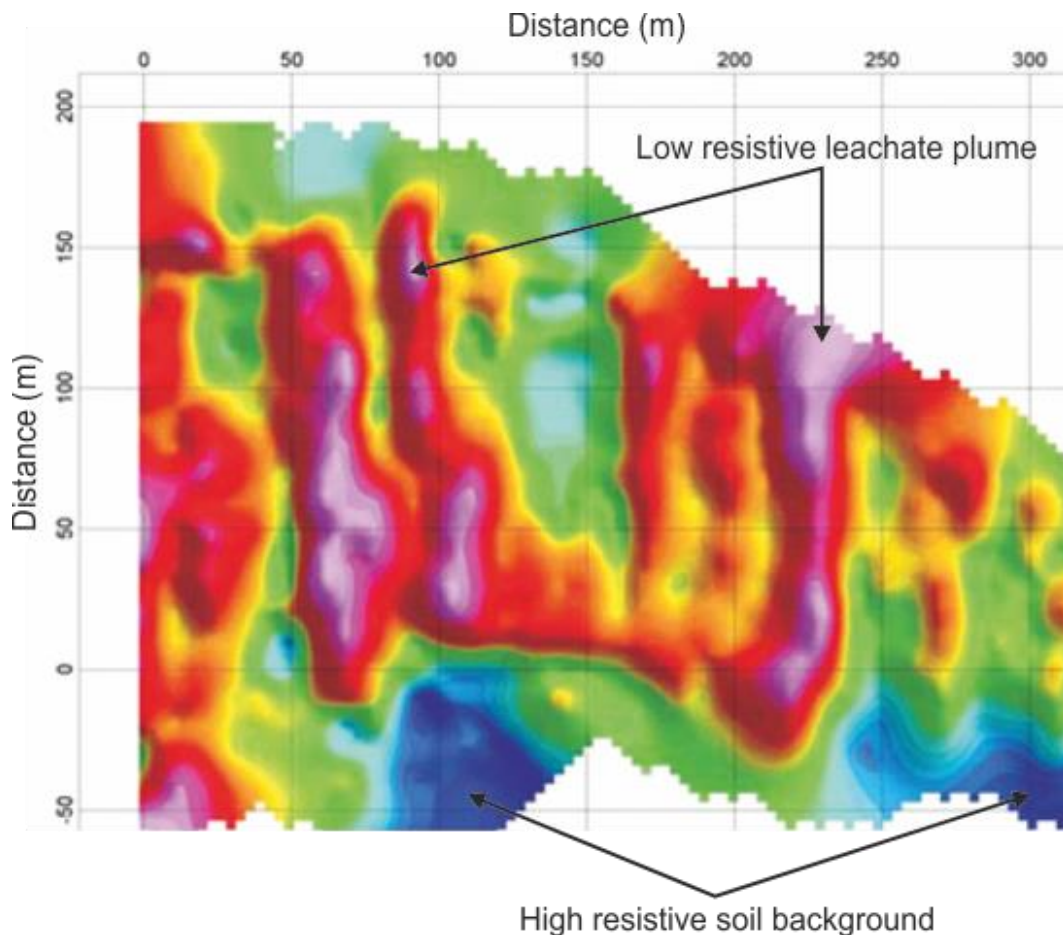


**Figure 2.8:** Resistivity section showing a leachate plume migrating through a landfill site boundary (after Styles, 2012).

#### *Resistivity survey to locate forensic and archaeological burials*

Resistivity techniques are a standard investigatory tool for environmental forensic and archaeological burials. Common application of resistivity surveys is the detection of clandestine graves, and has in recent times resulted in being increasingly used by forensic search teams to detect human remains buried within clandestine graves (Cheetham, 2005; Jervis *et al.*, 2009a; Pringle *et al.*, 2012b). A handful of studies have been undertaken on controlled studies using pig cadaver as proxy to human remain to gain a

better understanding of resistivity results in the detection of buried human remains (Pringle *et al.*, 2008; Jervis *et al.*, 2009a). With evidence that buried remains commonly appear as areas of relatively high conductivity (or low resistivity) when compared to the host background (see Fig. 2.9) (see Nobes, 2000; Pringle and Jervis, 2010; Hansen *et al.*, 2014). Potential causes can be attributed to local variations in soil moisture content due to increased porosity of backfill soil (Scott and Hunter, 2004; Jervis and Pringle, 2014) and the presence of high conductive mobile ions in leachate generated from buried cadaver (Vass *et al.*, 1992; Jervis *et al.*, 2009b).

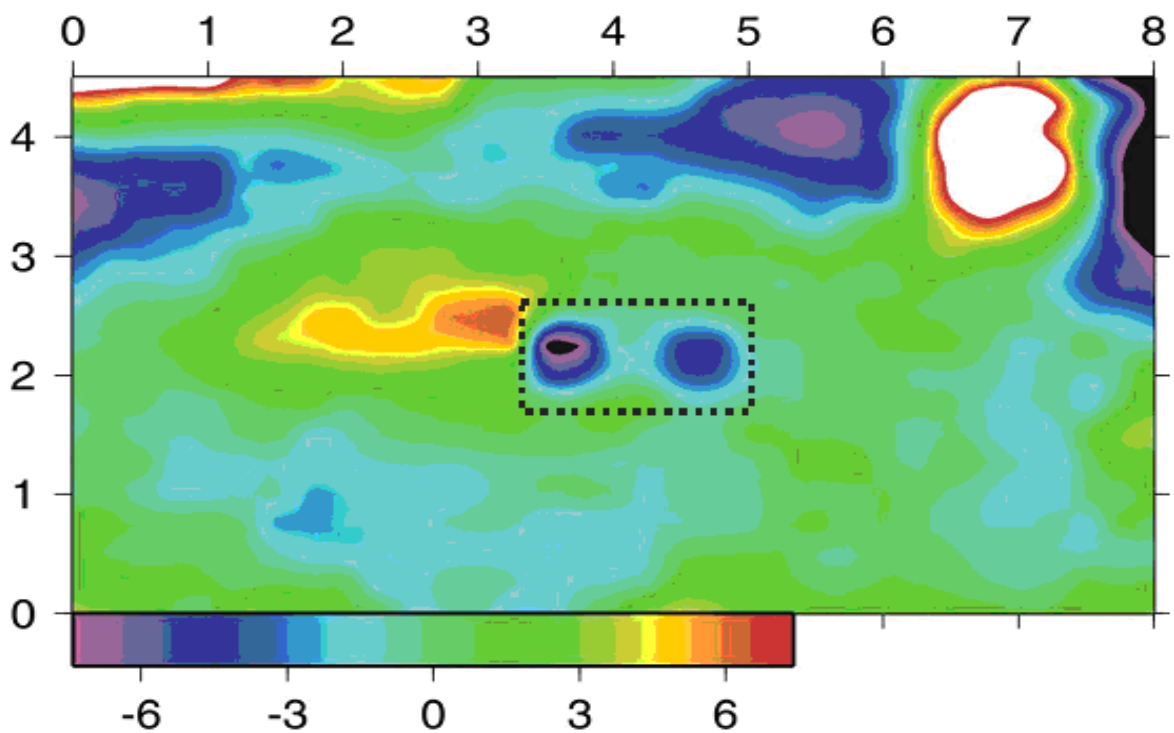


**Figure 2.9:** Bulk resistivity plot showing low-resistivity anomalies at the head and foot of a pig grave (rectangle) interred six weeks previously (after Jervis *et al.*, 2009a).



Another common application of resistivity techniques is the detection of buried archaeological remains (e.g. buried foundation and artefacts, see Fig. 2.10). In recent times (especially post 2000), there has been a growing interest in resistivity investigation for detecting and mapping buried archaeological remains and standing monuments (Tsourlos and Tsokas, 2011; Vargemezis *et al.*, 2013), discriminating areas containing hearth features and high densities of fire-cracked rocks and artefacts (Thacker *et al.*, 2002; Martinho and Dionisio, 2014), and with electrical resistivity tomography (ERT) 2D profile providing more information on the depth of buried objects (see Pringle *et al.*, 2008).

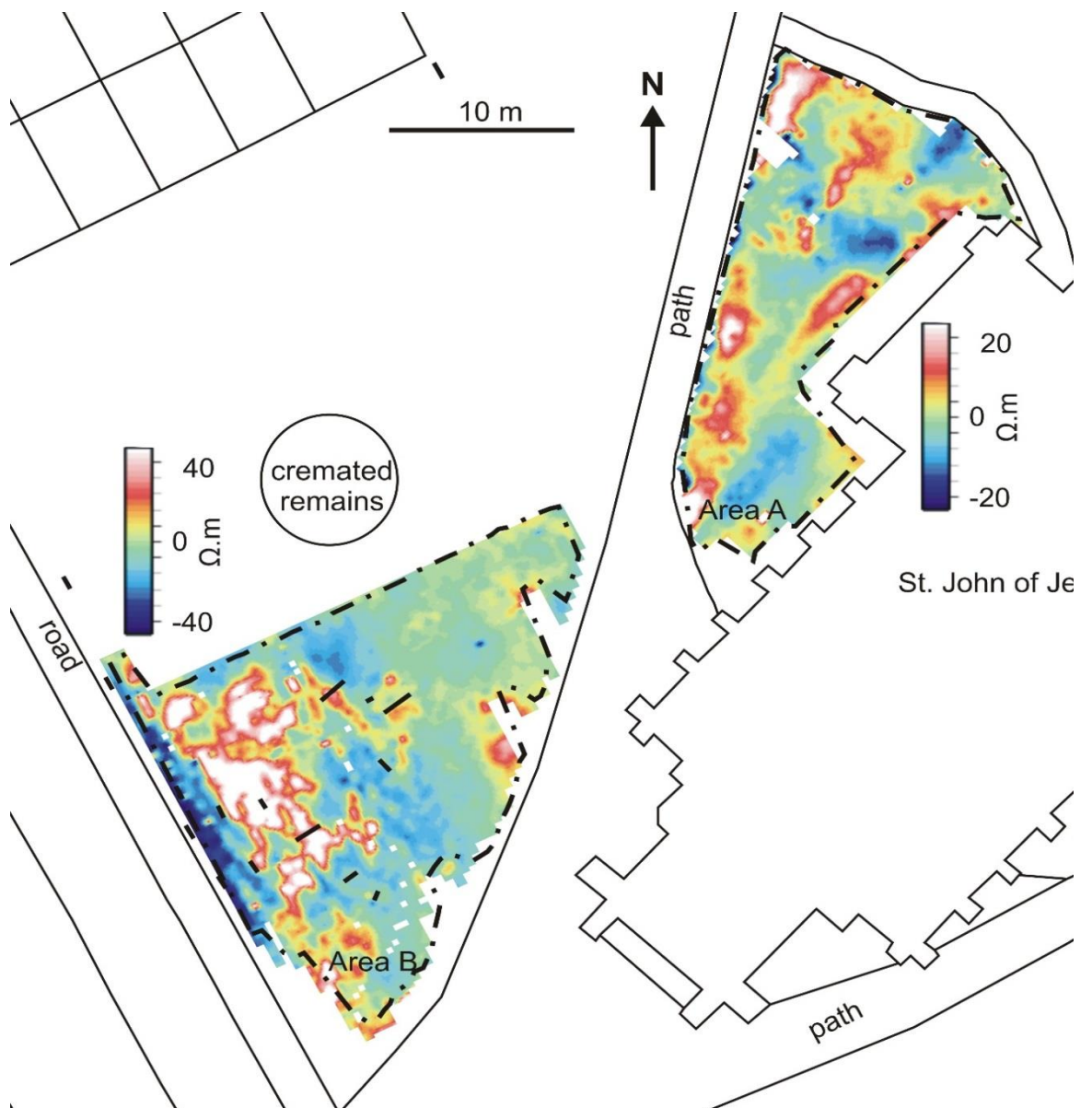


**Figure 2.10:** Electrical resistivity datasets from a 0.5m fixed-offset survey of a graveyard in Hackney, East London (from Hansen *et al.*, 2014).

### 2.2.2 Ground penetrating radar (GPR)

#### *Basic theory of ground penetrating radar*

GPR is one of the non-intrusive geophysical methods employed by near-surface geophysical investigators to study buried objects in the subsurface. It has gained popularity by some key benefits such as: high resolution (Van der Kruk *et al.*, 2012), non-destructive nature (Tsokas *et al.*, 2013), relatively low-cost and rapid acquisition (Conyers, 2006a). It has now become a well-accepted geophysical technique, particularly within the engineering and archaeological communities. It is a technique that transmits and receives electromagnetic (EM) waves to probe the subsurface (Milsom and Eriksen, 2011). The principle and application of GPR is based on the continuous transmission of a high frequency electromagnetic signal between 25 MHz and 5000 MHz that is designed primarily to investigate the shallow subsurface of the earth (Ruffell and Mckinley, 2008). For instance, as the electromagnetic wave propagates into the ground, if there is a change in electrical properties in the ground or if there is an anomaly that has different electrical properties than the surrounding media, a part of the electromagnetic wave is reflected back to the ground surface. A set of GPR equipment consist of several main components to include; antenna, radar electronics, data digitizer, computer and display unit (Figure 2.11). On the command of the control unit, the transmitter generates the electromagnetic waves that are emitted through an antenna connected to it. This transmitting antenna converts electric current to electromagnetic waves, controls and direct the radiation towards the target. As radar energy moves through various materials in the ground, at each velocity change a portion of the propagating wave will be reflected

back to the surface to be detected at a receiving antenna. The remaining energy will continue into the ground until it is absorbed and dissipated. The receiving antenna then captures the electromagnetic waves that reflected from subsurface and those coming directly from transmitting antenna, it also reciprocates the transmitting antenna by converting electromagnetic wave back to electric current. Data are collected by moving these antennas on the ground along parallel transects within grids, thereby recording reflections of those signal from significant discontinuities within the subsurface.

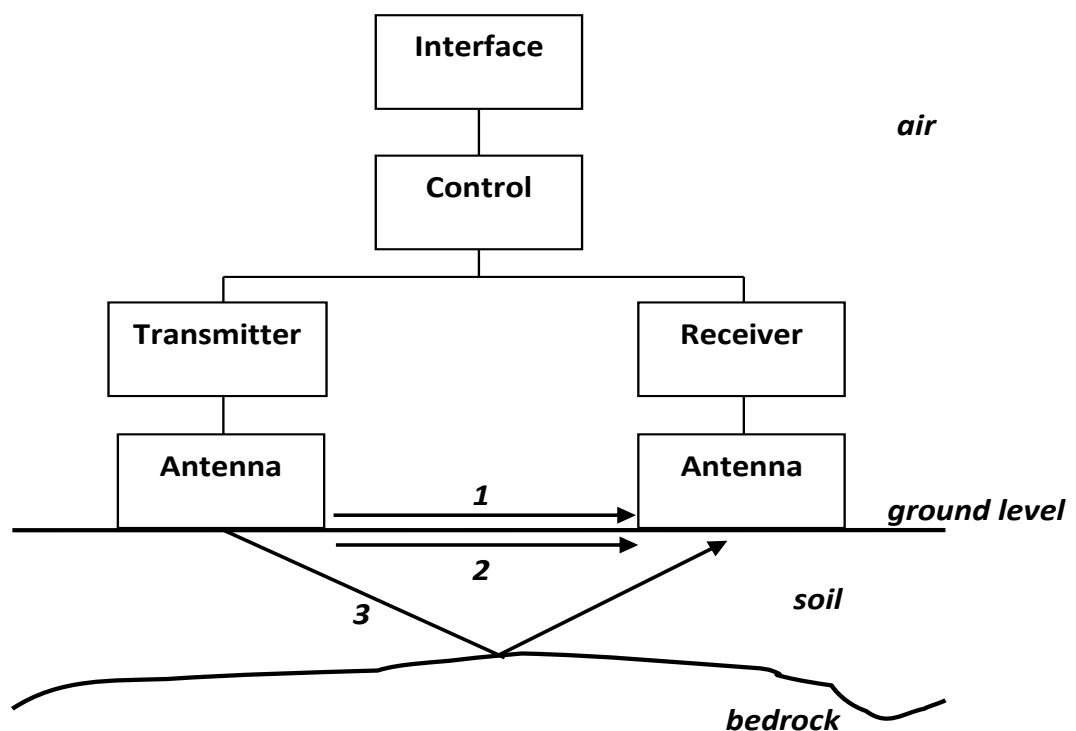


**Figure 2.11:** A schematic diagram of a GPR system, showing the interface module, control unit, transmitter, receiver and antennas. The signal travel paths in order of arrival are; 1) direct wave, 2) direct ground wave and 3) reflection from subsurface interface (adapted from Moorman, 2001).

Not all signals collected by antenna are due to subsurface reflections, however, high amplitude linear reflections and background noise (clutter) can be minimized by shielding the antenna (Conyers, 2004a) and ground coupling of antennas (Bloemenkamp and Slob, 2003), as the development of shielded radar antennae has allowed the possibility of usage both in forests and urban areas. 1D signal traces are combined to form two-dimensional profiles, which can be processed to form a three-dimensional profile of underground features (Fig. 2.12). The time it takes for the signal to penetrate the subsurface and reflect back to the ground is known as two-way travel time (TWTT) and is measured in nanoseconds. If two-way travel time is measured, the target depth can be determined if an assumed average velocity for the radar signal in the subsurface is used. The depth of investigation with GPR is generally quite shallow (typically 10 metres or less) due to the inherent attenuation of high frequency electromagnetic waves by the earth (Davenport, 2001). Greater depth penetration is obtained from lower frequency antennas while better resolution is obtained from higher frequency antennas although there is the obvious trade-off between target size and penetration depth (see Milsom and Eriksen, 2011).

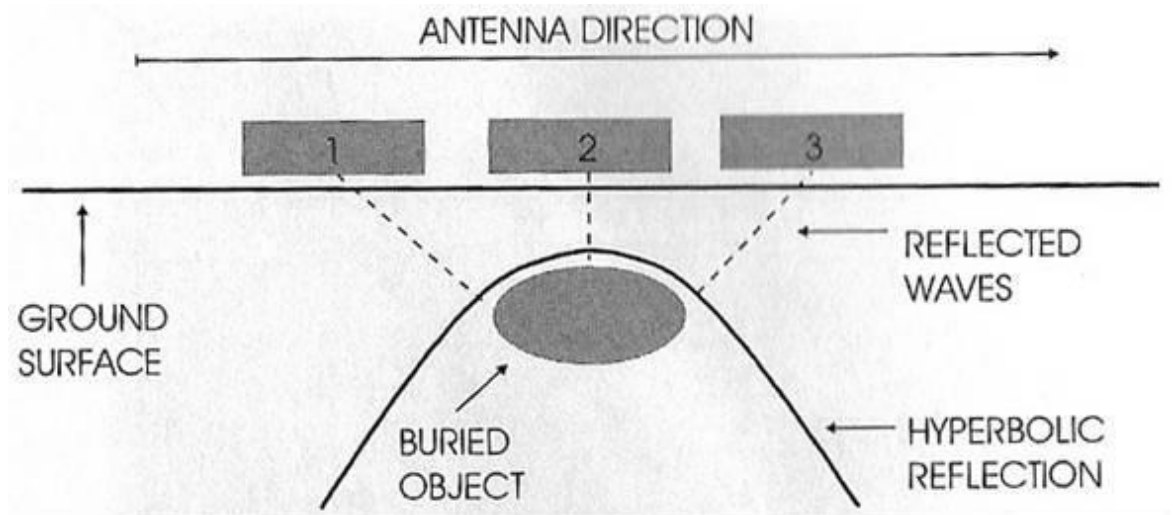


**Figure 2.12:** Schematic diagram showing how GPR antennae passing over a buried object at positions 1, 2 and 3 produce a detectable response and hyperbola in a 2D profile (from Dupras *et al.*, 2006).

According to Cassidy (2009), the term dielectric is used to describe a class of non-conducting materials that can accommodate a propagating, alternating EM field, for example, subsurface materials, of which permittivity and conductivity are loosely terms used to describe their dielectric properties. Table 2.1 shows ranges of conductivity and relative permittivity for a variety of subsurface material. The velocity of EM wave propagating in the material depends on the amount of mobile charges in it. Thus, a material with large amount of mobile charges will tend to attenuate a propagating EM wave as the charges flow, resulting in a loss of energy, therefore reducing the velocity and depth of penetration of EM wave in the material. The propagation velocity ( $V$ ) of the EM wave in a material (e.g. soil) is characterised by the dielectric permittivity ( $\epsilon$ ) and magnetic permeability ( $\mu$ ) of the medium:

$$V = \frac{1}{\sqrt{\epsilon\mu}} = \frac{1}{\sqrt{\epsilon_0\epsilon_r\mu_0\mu_r}} \quad 2.4$$

Where  $\epsilon_0 = 8.854 \times 10^{-12}$  F/m is the permittivity of free-space,  $\epsilon_r = \epsilon/\epsilon_0$  is the relative permittivity (dielectric constant) of the medium,  $\mu_0 = 4\pi \times 10^{-7}$  H/m is the free-space magnetic permeability, and  $\mu_r = \mu/\mu_0$  is the relative magnetic permeability. In most soils, magnetic properties are negligible, resulting to  $\mu = \mu_0$ , and equation 2.4 becomes:

$$V = \frac{c}{\sqrt{\epsilon_r}} \quad 2.5$$

**Table 2.1:** Typical range of dielectric characteristics of various materials measured at 100 MHz. Summarized from Cassidy (2009), Reynolds (2011) and Styles (2012).

Material	Relative permittivity, $\epsilon$	Conductivity, $\sigma$ (mS/m)	Velocity, $v$ (m/ns)	Attenuation, $\alpha$ (dB/m)
Air	1	0	0.3	0
Distilled Water	80	0.001	0.033	0.002
Fresh Water	78-88 (at 25 <sup>0</sup> C)	0.5	0.033	0.1
Sea Water	81-88	3,000	0.01	1,000
Dry Sand	3-6	0.01	0.15	0.01
Wet Sand	10-30	0.1-1	0.06	0.03-0.3
Limestone	4-8	0.5-2	0.12	0.4-1
Shale saturated	6-9	1-100	0.09	1-100
Silts saturated	22-30	1-100	0.07	1-100
Clay dry	2-20	2-1,000	0.06	1-300
Granite	5-8	0.01-1	0.13	0.01-1
Dry Salt	5-6	0.01-1	0.13	0.01-1
Ice	4-6	0.01	0.16	0.01



The main exchangeable component of GPR systems is the antenna, as they are available in a variety of different frequencies and sizes. The assigned frequency of an antenna describes the peak power of the radiated spectrum, known as the centre frequency. Low frequency antennae (10 – 120 MHz) produce a long wavelength of radar energy that can penetrate up to 50 metres in ideal conditions and are capable of resolving large subsurface features but with low resolution (Schultz, 2007). On the contrary, high frequency antennae, such as 900 MHz and above produce a short wavelength of radar energy that can penetrate up to 1 metre and are capable of resolving small features but, in addition produce high resolution image. Each time radar energy propagates through a material with a different composition or water saturation, the velocity changes and a portion of the energy is reflected back to the surface to be recorded at the receiving antenna. Then, the remaining energy continues to pass into the ground to be further reflected, until it finally diverges and dissipated with depth (Conyers, 2004b).

Penetration depth of a GPR signal is typically about 20 m, increasing to 50 m under ideal conditions and decreases to less than 2 m in high conductivity materials, although it mainly depends on the soil type and the antenna frequency. However, rough estimation for penetration depth can be obtained with rules of thumb such as;  $D_{\max} < (30/\alpha)$  and  $D_{\max} < (30/\sigma)$ , where  $D_{\max}$  is the maximum depth of penetration with considerable resolution (Bergslien, 2012). Interestingly, recommendation on frequency selection should not be established on attaining the maximum theoretical depth of penetration, rather on achieving a high enough resolution to detect the smallest sized of the feature of interest. For instance, in forensic search for clandestine burials, the depth of penetration

with quality resolution to detect the depth of cadaver is between 0.4 m and 0.6 m (Pringle *et al.*, 2008; Schultz, 2008).

Another important factor to consider when using GPR in the field is, to properly make a good contact of GPR antenna with ground surface to avoid any potential coupling effects. A situation where there is an air gap between the antenna and the ground surface that is more than 0.1 – 0.25 times the radar wavelength, tends to create an interface of high property contrast between air and ground surface (Milsom and Eriksen, 2011). Thus, a large proportion of the EM energy is lost (approx. 50% and above), thus drastically reducing the information of the deeper subsurface due to lesser amount of energy being transmitted there. This is a common challenge in undulating terrain with tiny surface troughs and crests. Another fundamental cause of energy loss is through absorption, which occurs in the process of turning the electromagnetic energy into heat (Reynolds, 2011). Therefore, the EM radiation of GPR antenna is affected by the presence of the air-earth interface and depends on the geometrical and physical characteristics of the antenna (Carcione, 1998).

Milsom and Eriksen (2011) also further explained that EM waves do not only propagate vertically beneath the source, but has a radiation pattern which expands with depth. And that the signal also has a particular geometrical profile in both magnetic (H) and electric (E) planes. Figure 2.13 shows these expressions in free space and in the ground, and indicates regions where there is zero energy. Where a feature is angled so that it is concordant with one of these null-regions, little or no energy will be reflected (Milsom and Eriksen, 2011), therefore the orientation of the antenna is an additional

consideration for small or thin targets such as pipes or reinforcement bars (rebars) in concrete, and also whether the orientation is constant throughout a survey (Cassidy *et al.*, 2011).

Data processing of GPR data can range from a basic data display and application of gain while viewing radargrams during acquisition, through to complex and sophisticated post-acquisition processing (Cassidy, 2009). It is often quite difficult in GPR processing to establish how far a user should go beyond the basic processing steps, and as such, some users always choose advanced processing steps as compulsory approaches to GPR processing, whilst others keep it simple with the basic processing steps in order to avoid possible complication of 'over processing' (Cassidy, 2009). The purpose of processing should be to enhance the quality of raw data for interpretation, and to stop at the converging point when nothing more can be gained from further manipulation (Cassidy, 2009).

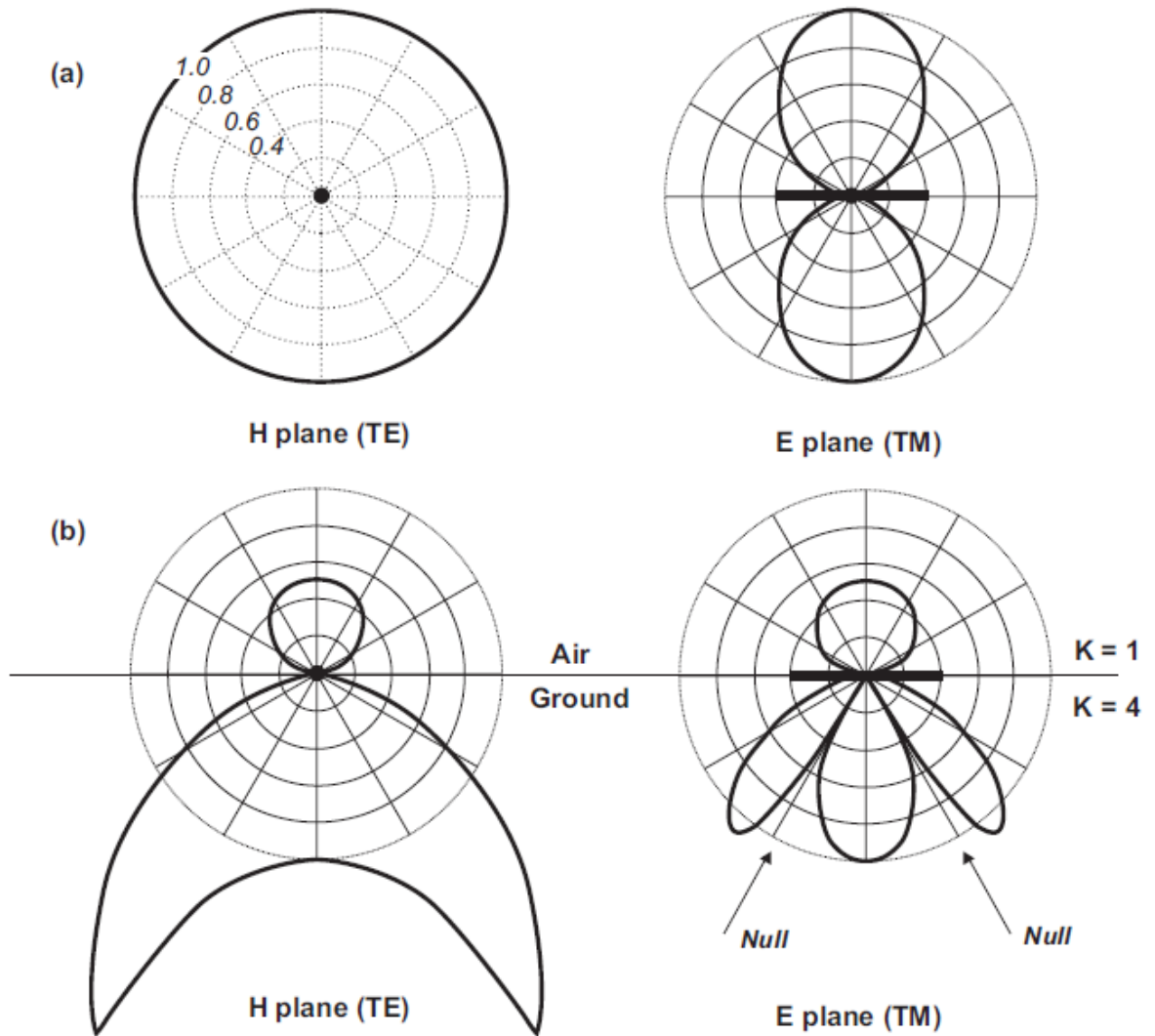


**Figure 2.13:** The polar radiation patterns for transmitted GPR waves in H- and E- planes showing both transverse electric (TE) mode and transverse magnetic (TM) mode in (a) free space and (b) the ground with a permittivity of 4 (from Milsom and Eriksen, 2011).

#### *Applications of GPR surveys*

Ground penetrating radar has been extensively used for a variety of applications (see Reynolds, 2011). GPR has demonstrated in a wide range of soil and rock conditions to be among the most suitable for geotechnical and hazard-related applications, such as

locating relict mine shafts/vents, karstic cavities and sinkholes (Batayneh *et al.*, 2002; Cassidy *et al.*, 2011). GPR applications have been promising in locating underground utilities of different cables and pipes that are commonly encountered in most excavation works in major cities of the developed world (see Fig. 2.14) as has been demonstrated by Conyers (2006a). It has been used to locate and verify locations of historic or archaeological graves (see Bevan, 1991), and has increasingly supported the discovery of huge number of forensic bodies that have been interred for differing post-mortem intervals and in varying environments (see, for example, Schultz, 2008; Pringle *et al.*, 2012a). Similarly, controlled studies using buried pig cadavers have shown that GPR is the most effective geophysical surveying tool for delineating clandestine graves (Schultz, 2008; Hansen and Pringle, 2013).

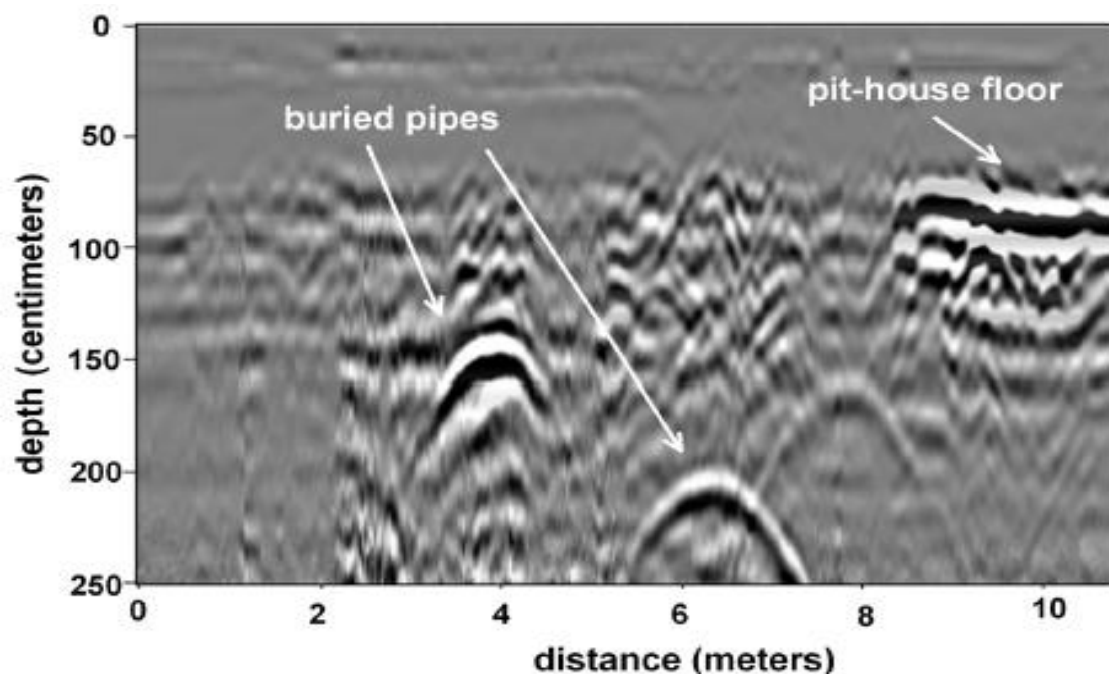


Figure 2.14: A 400 MHz 2D profile across a house floor. Buried water pipes are visible as reflection hyperbolas (Conyers, 2006a).

### *GPR survey to locate forensic and archaeological burials*

Ground penetrating radar has been considered recently as the most successful and frequently used techniques, among all the geophysical techniques adapted for forensic grave detection (Cheetham, 2005; Ruffell and McKinley, 2005; Pringle *et al.*, 2016). GPR can detect human burials in several ways. Potential detectable targets include; disturbed soil of the grave shaft and discontinuity in the natural stratigraphy, the coffin, bones, clothes and other buried metallic artefacts in the grave (Conyers, 2006b; Schultz, 2008; Pringle *et al.*, 2012c). Its strength in different site scenarios covers areas such as, detecting cadavers that are buried beneath grassed or bare ground (Mellett, 1992; Calkin *et al.*, 1995) or concrete (Bevan, 1991), graves buried in or beneath snow and ice (Davis *et al.*, 2000; Instanes *et al.*, 2004), or submerged in freshwater (Parker *et al.*, 2010).

Successful detection of unmarked burials and clandestine graves with GPR has been reported widely in archaeological searches, forensic science, and geophysical literatures, which includes the early work of Bevan (1991).

In addition to some of the early forensic published studies (e.g. Bevan, 1991; Nobes, 1999; Miller, 1996; Ivashov *et al.*, 1998; Hammon *et al.*, 2000), other papers have also established that human burial and accessories is associated with strong hyperbolic reflectors created in GPR 2D profiles as shown in Figure 2.15, thus metal coffins with relatively high permittivity were detected as strong hyperbolic reflections compared to wooden coffins. Time series data generated from investigations also showed strong hyperbolic reflectors over a pig grave compared to weaker features in an empty grave (Schultz *et al.*, 2006; Schultz, 2008; Pringle *et al.*, 2012b). Therefore, GPR can also be used

to ascertain the absence of a clandestine grave in a suspected site. For example, in the case of a survey conducted in a small portion of land located adjacent to a known cemetery grave, results showed that the suspected inhumation of a murder victim was not located in this area (Schultz *et al.* 2006). The result from the GPR survey was the basis for the decision that no further excavation process is required, thus saving both resources and time. However, precautions should be taken because if a GPR survey leads to incorrect identifications, then this could hinder criminal investigations (Mellett, 1996) and complicate burials in cemeteries that have no record of burial activities.

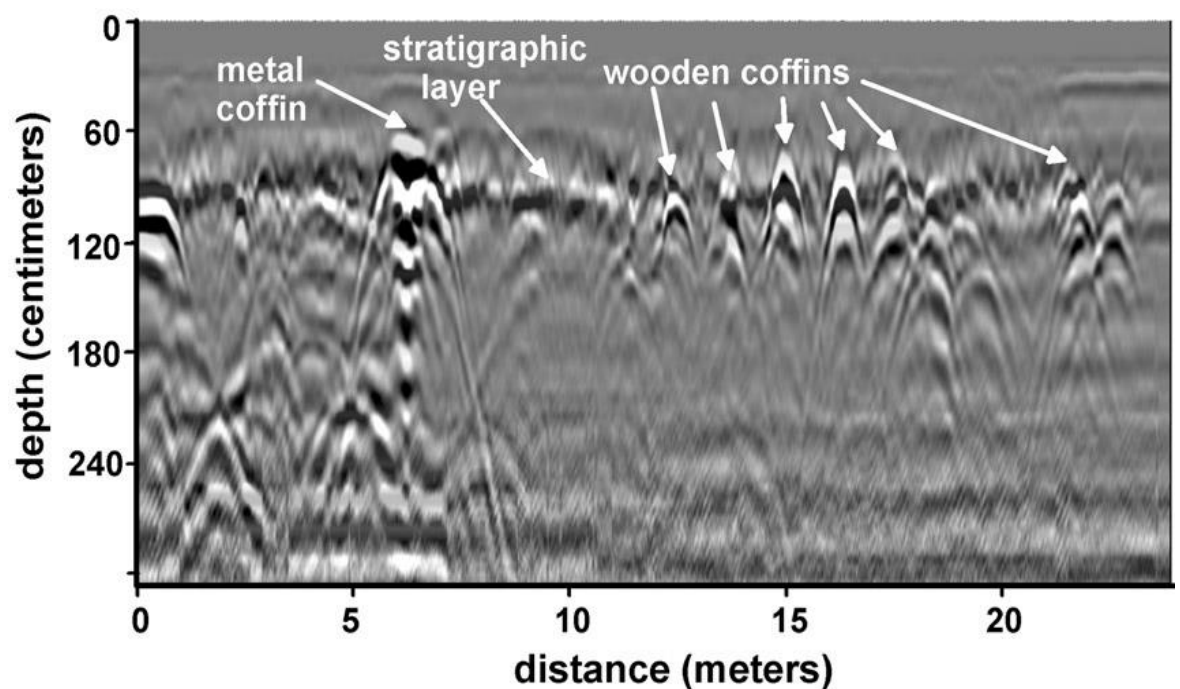


**Figure 2.15:** Reflection profile from a cemetery with wooden coffins interred between 1898 and 1921. One metal coffin is identifiable by the alternating strong hyperbolic reflections below it (Conyers, 2006b).

However, not all graves can be detected using GPR techniques. As an investigation in a marked grave in a cemetery showed no hyperbolic reflection in the generated dataset (Bevan, 1991). Known historic graves in cemeteries (Fenning and Donnelly, 2004) have shown that not all the graves produce detectable responses. It is also worth noting that geophysical data obtained from one particular grave might be influenced by the nature of the burial (Nobes, 1999). For example, factors that influence data include whether or not a coffin is used, the depth of the grave (Hammon *et al.*, 2000; Watters and Hunter, 2004), the way the body decays and releases chemical substances (Schultz, 2008) as well the length of resting time (Powell, 2004).

Whilst GPR is a very efficient method in forensic searches, survey integration with other geophysical techniques, especially in the face of complex or high conductive terrain where the signals suffer fluctuations, are recommended for better comparison and accuracy (Ruffell and Kulesa, 2009; Pringle and Jervis 2010). Many studies now integrate GPR with other geophysical techniques along the same survey lines, specifically to overcome individual limitation of acquisition in one or other methods. For example, the development of resistivity, magnetometry (Buck, 2003; Ruffell and McKinley, 2008) and recently, magnetic susceptibility (Pringle *et al.*, 2015a) has established the significance of GPR in comparison with other methods.



### 2.2.3 *Electromagnetic Induction (EMI)*

Electromagnetic Induction (EMI) uses the same principle as GPR to measure the induced electrical conductivity of the subsurface (in milliSiemens per metre - mS/m). It is related to electrical resistivity, in that it measures the electrical properties of material (Davenport, 2001), and to magnetometry, as the flow of the induced current generates a detectable magnetic field (Bergslien, 2012). The electromagnetic method is based on the induction of electric currents in the ground by the magnetic component of electromagnetic waves generated at the surface (Figure 2.16). An alternating current, of variable frequency, is passed through a coil of wire (a transmitter coil, Tx). This process generates an alternating primary magnetic field which, in turn, induces very small eddy currents in the earth, the magnitude of which is directly proportional to the ground conductivity in the vicinity of the coil. These eddy currents then generate a secondary magnetic field, a part of which is intercepted by a receiver coil (Rx).

The relationship between the primary and secondary magnetic flux is used by the receiver coil to obtain both in-phase and quadrature components of the measurement. The in-phase component is particularly useful for the detection of buried conductive structure and waste materials, while the quadrature component is linearly proportional to the apparent bulk conductivity of the subsurface. The larger the spacing between transmitter and receiver, the deeper the penetration and bigger sampling volume decreases resolution (Reynolds, 2011). Among the factors influencing conductivity measurements are; the material properties, size, shape, porosity and orientation of conductive object (Witten, 2006).

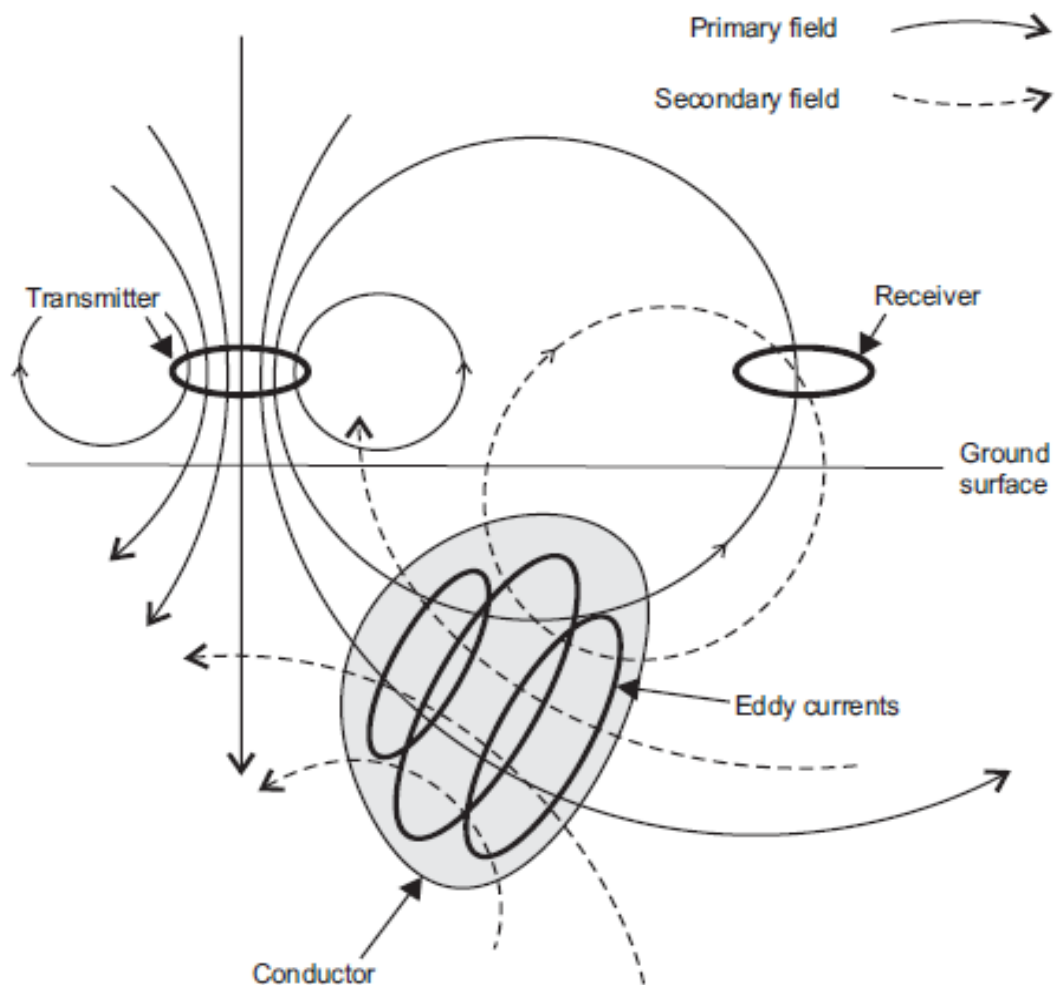


**Figure 2.16:** Schematic of the Electromagnetic Induction process in the air and in the Earth, showing electromagnetic field transmitted into the ground from the transmitting coil, which generates small eddy currents on the surface of a conductor, and the eddy currents in turn create a secondary electromagnetic field that is measured by the receiver coil (from Styles, 2012).

There are numerous models of ground-based EMI meters, the typical model used by forensic and archaeological experts is the Geonic<sup>TM</sup> EM-31 horizontal loop (or slingram) EMI meter that can be operated by a single individual and contains at one end the transmitter and the other end receiver coils mounted at two ends of a 3.7m long plastic pole. Without ground contact this provides rapid and easy data collection, which makes it suitable as reconnaissance tools to identify anomalies for further detailing (Witten *et al.*, 2003; Kvamme and Ahler, 2007). These instruments can measure a depth of approximately 10 m depending upon site conditions (Dupras *et al.*, 2006) and provide a direct readout of apparent ground conductivity, which is logged into a data recorder. The data are then downloaded to a computer for analyses and production of plan view maps of ground conductivity.

Successful application of the Geonics EM31 in forensic and archaeological sites has been reported in literature (Bevan, 1991; France *et al.*, 1992; Witten *et al.*, 2001; Bigman, 2012). These surveys evidenced that EM surveys may be used to identify pit features such as unmarked graves (Bigman, 2012), trenches (Hildebrand *et al.*, 2007; Conyers *et al.*, 2008), metallic buried structures (Dupras *et al.*, 2006), and changes in stratigraphy (Dalan, 2006; Dalan and Goodman, 2007). The combination of EMI and GPR can be used in large open areas, EMI methods can firstly be used to conduct an initial reconnaissance survey of the site to generate information on anomalous areas (Figure 2.17), where follow-up higher resolution geophysical surveys, for example, GPR surveys, may then be focused. Nobes (2000) documented EMI was first used to survey a large wooded area and then followed with GPR surveys to successfully locate a buried clandestine grave on the site.

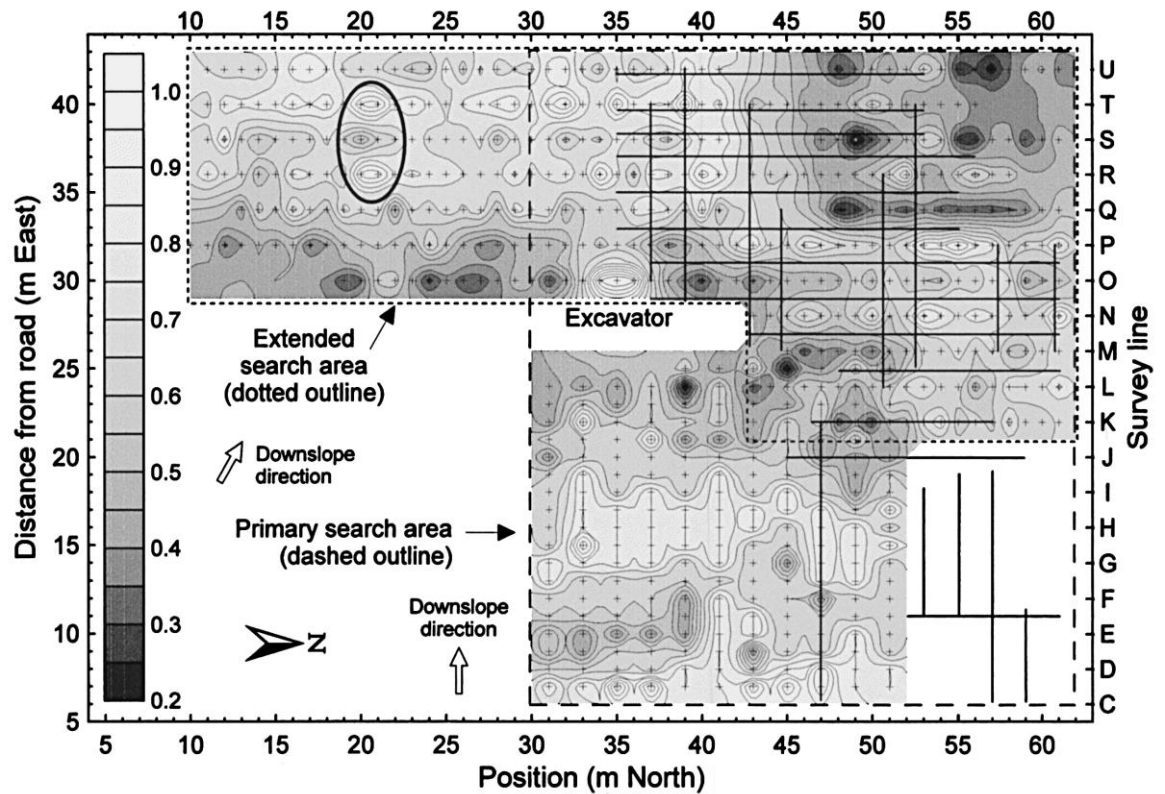


**Figure 2.17:** Example of an EM conductivity survey for a clandestine grave. The bold oval (top) shows where the body was ultimately found during subsequent excavations (from Nobes, 2000).

#### 2.2.4 Magnetic Susceptibility (MS)

All material possesses an intrinsic property of magnetism and, when a magnetic field is applied to soil and rock, the degree of magnetisation can be measured as the magnetic susceptibility in K or MS, in SI dimensionless units (Walkington, 2010). MS is an emerging technique and measures materials that are susceptible to being magnetised. In archaeological investigations, magnetic susceptibility techniques have been widely applied in detection of ferrous and metallic objects associated with burials such as metal parts of coffins, metallic homewares and other burial accessories (Jones, 2008; Bevan,

1991). It has also been shown to successfully locate areas of historic surface burning as the weakly magnetic iron oxide minerals in the soil (e.g., hematite and goethite) are converted into the highly magnetic minerals magnetite and maghemite through heating and burning (Crowther, 2003; Viberg *et al.*, 2013). Magnetic susceptibility techniques are yet to gained wider interest in forensic searches (Witten *et al.*, 2001), as most forensic targets are non-ferrous. However, in suitable soil conditions, grave backfill soil with reasonable disturbance can produce detectable variation in magnetic susceptibility.

Pringle *et al.* (2012c) suggested highly sensitive magnetometers could be reasonably successful in forensic applications. While surveying an ancient burial, the age of burial had been considered as the major factor that can potentially cause high magnetic susceptibility as proposed by Linford (2004). MS results over simulated recent clandestine burial in a variety of depositional environments have proved not to be optimal in forensic search (Juerges *et al.*, 2010). However, a controlled simulated pig graves in a rural neotropical environment in Colombia evidenced that MS can successfully image modern clandestine burials throughout the survey period of 21 months (Molina *et al.*, 2016). The result showed that targets were detected by MS as relatively low anomalies, when compared to background values (Fig. 2.18).

Other applications of MS techniques are seen on its strength to detect buried metallic targets even beneath a domestic patio versus total field and gradient methods (Reynolds, 2011). Pringle *et al.* (2008) recommended magnetic susceptibility technique for a quality control checking of magnetic gradiometry datasets: for example, assisting with the removal of magnetic data spikes.

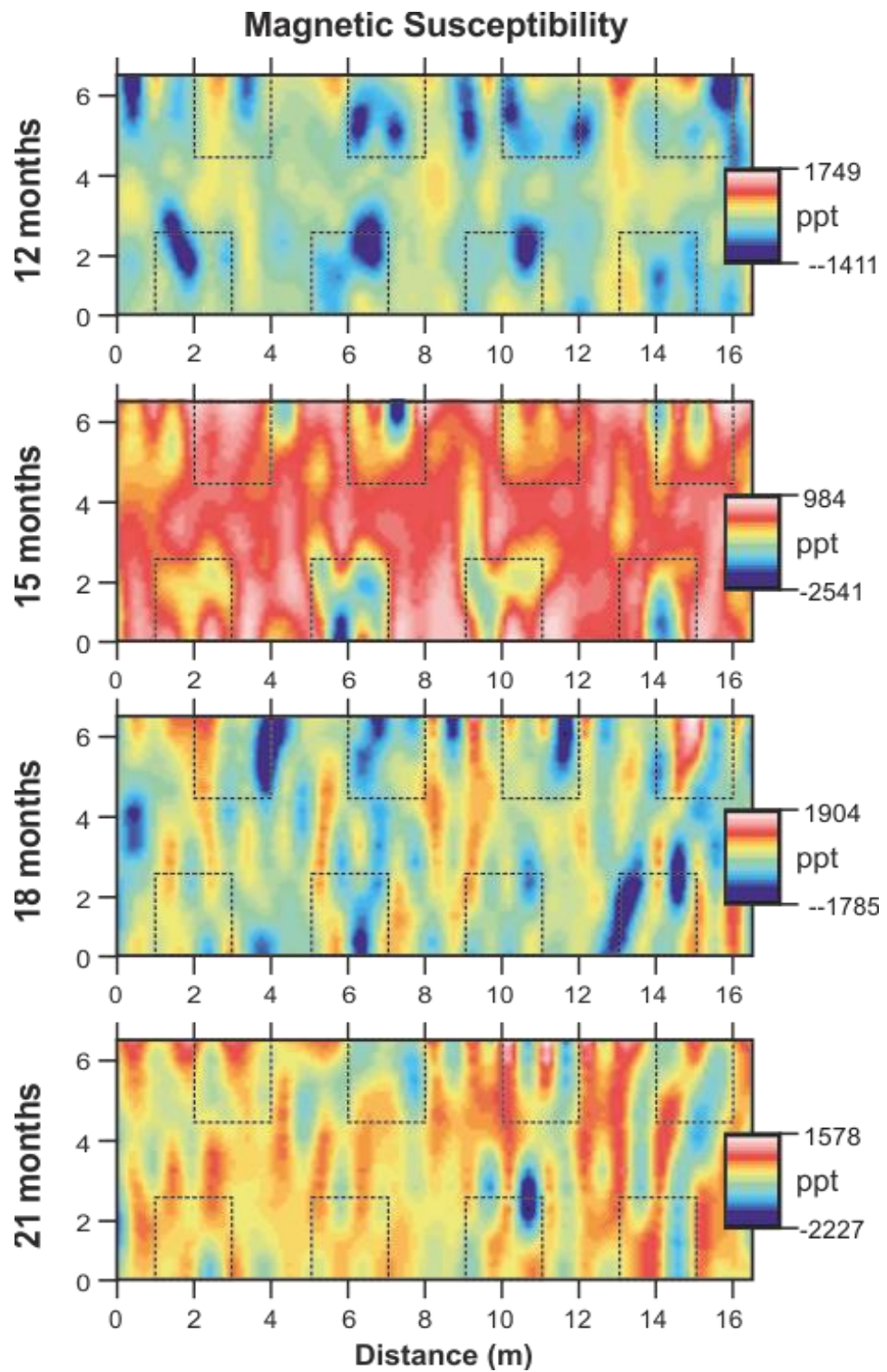


**Figure 2.18:** Sequential magnetic susceptibility mapview dataset at 12 months, 15 months, 18 months and 21 months. Burial simulated grave positions shown as rectangular dotted lines throughout (edited from Molina *et al.*, 2016).

### 2.2.5 Other geophysical techniques for grave detection

Some geophysical techniques other than those discussed in Sections 2.2.1 to 2.2.4 have also exhibited strength in detecting graves. For example, self-potential (SP), seismic and gravity methods.

Self-Potential method is used to measure differences in near-surface electrical current from their associated voltage signal and are capable of imaging near-surface fluid flow variations, as compared to background values (Reynolds, 2011). SP has proven useful for identifying buried foundations as well as ancient disturbed soils (Wynn and Sherwood, 1984), and has detected graves in controlled experiments (Lynam, 1970). However, the method has been described as an unlikely choice in detecting buried human remains in forensic situations, unless the burial is accompanied by materials capable of altering the chemical composition of the grave site (Killam, 2004; Pringle, 2012a). Factors controlling SP voltages include; recent rainfall, superficial variations in soil chemistry, and electrode polarization (Wynn and Sherwood, 1984), which can be minimized by careful field procedures and qualitative interpretations.

Seismic methods are measured by tracing vibrations in the ground. They are very popular in oil exploration due to the accuracy with which they can image underground features (Reynolds, 2011). The reflection seismic survey conducted in a controlled archaeological site over a pig burial mound at Illinois, USA, shows high resolution seismic methods can detect graves although this is not usual (Hildebrand *et al.*, 2002). Thus, it appears that seismic surveys are able to detect graves because voids, such as a burial vault or the cavity in chest of a cadaver, can reflect seismic waves (Hildebrand *et al.*, 2002). As such, it

is arguable whether seismic reflection surveys would be able to detect a clandestine grave once the chest cavity of a buried cadaver had collapsed. However, seismic methods are not usually effective technique in forensic investigations, but are normally replaced by GPR for near-surface imaging.

Gravity method measures variations in the earth's gravitational field caused by differences in the density of subsurface rocks (Reynolds, 2011). While micro-gravity surveys can resolving subtle differences in density beneath the surface, for example, it is capable of detecting cavities as small as 1 m in diameter within 5 m of the subsurface (Reynolds, 2011), but would be more difficult to identify burial site positions. It has been suggested that older graves may contain voids that could create subtle differences in density (Sarris *et al.*, 2007), but this suggestion does not yet appear to have been tested.

### **2.3 Soil sampling and geochemical analysis**

Soils are the physical context within which forensic evidence is established. Therefore, it is very crucial to understand the potential implications of any physical or chemical changes in properties of soil that occurred in the survey site. It has been shown that there are significant changes in soil properties between grave and background soil (Jonker and Oliver, 2012), due to decomposition process of cadaver that releases loads of organic matter into the host soil. Soil evidence has proved to be helpful in locating clandestine graves (Carter *et al.*, 2007). A number of studies have been conducted to understand cadaver decomposition using gravesoil or soilwater analysis (Forbes *et al.*, 2002; Pringle *et al.*, 2015a; Pringle *et al.*, 2016). Most of these reported on how cadaver decomposition



releases significant pulse of nutrient into the host soil (Hopkins *et al.*, 2000; Dent *et al.*, 2004; Perrault and Forbes, 2016). A control experiment has been conducted over a buried mammalian cadaver within which soils were sequentially collected from the grave and analysed for the presence of ninhydrin reactive nitrogen (NRN) (Carter *et al.*, 2008a; Van Belle *et al.*, 2009). The result showed that over time the concentration of NRN doubled, and as such, suggested the approach could be a useful tool for gravesoil testing before detailed traditional methods can be applied.

Forensic scientists have, over time, relied on the understanding of the mechanism of the formation of adipocere in grave soils to detect the actual location of clandestine burial (Forbes *et al.*, 2002). Adipocere formation refers to the process of conversion of body fat in a solid white substance (Forbes *et al.*, 2005). Here, soil samples were analysed using infrared spectroscopy to detect the presence of adipocere, in a situation where infrared spectroscopy proved insensitive due to minimal concentration of adipocere. Gas chromatography-mass spectrometry was found to be more suitable for the investigation of very low concentrations of adipocere (Forbes *et al.*, 2003). Soil analysis has also been used to support the estimation of post-mortem interval (PMI), thus providing vital information relating to the search and recovery of human remains (Vass *et al.*, 1992).

## 2.4 Conclusion

To date, much of the forensic and archaeological studies on the detection of clandestine burials with geophysics have focussed on the four described geophysical methods (the GPR, electrical resistivity, electromagnetic induction, and magnetic susceptibility). However, relatively small amount of studies have adopted other geophysical and non-geophysical methods for clandestine graves search. Of all the geophysical techniques trialled in the search for clandestine graves, GPR has gained the most popularity over all other techniques, and has assisted with better understanding of how human remains can be detected. However, multiple studies in different soil types have shown that GPR can be incorrectly applied under the assumption that success in one study can be replicated in another, without proper consideration for target and soil variability. For instance, GPR technique performs very poorly in a clay-rich soil environment, whereas in the same environment, resistivity or/and magnetic susceptibility techniques can be very successful. Thus, making the statement “...*there is no remote sensing method that will consistently find a body or piece of evidence*” by Davenport (2001) justified. Therefore, application of multi- techniques clearly demonstrates the optimal approach to detecting clandestine burials.

The following chapters in this thesis are, therefore, focussed on how the above described techniques can be used as complementary approach for detecting clandestine burials in contrasting environments. This will also support search practitioners in making informed decision, having gained a better understanding of the limitations of each geophysical technique.

## **CHAPTER 3: Detection and characterisation of an ancient mass burial cemetery in Central London, UK**

### **3.1 Introduction**

Mass burials of human and animals are normally the result of a natural or manmade disaster and it may be a requirement, for reasons of public health and to prevent disease spreading, that any carcass internments are not delayed (Vass *et al.* 2008; DeWitte, 2014). The non-routine nature of these events makes forward planning of a suitable or permanent site difficult, but essential if consequent environmental and local human health impact problems are to be avoided (Williams *et al.* 2009). Globally, preserving the integrity of these buried sites is receiving concern due to the emerging urban development that continues to expand quickly (Uslu *et al.* 2009).

The forensic search successful and detection for unmarked, clandestine and mass burials of human remains has also been well documented to be difficult as they are usually deliberately unmarked. However, the reported forensic search and recovery of human victims in mass burials are reported in 19th Century Irish mass burials (Ruffell *et al.* 2009), USA race riot victims in the 1920s (Witten *et al.* 2000), Spanish Civil War mass burials in the 1930s (Rios *et al.* 2010/2012; Gelonch-Sole, 2013), World War Two (WW2) mass burials (Fiedler *et al.*, 2009a; Ossowski *et al.*, 2013), post-WW2 Polish repression mass burials (Szleszkowski *et al.*, 2014), the Northern Ireland 'Troubles' in the 1960s-1980s (ICLVR website), the Cambodian Civil War in the 1970s (Kiernan, 2003), the 1990s Balkan wars mass burials (Brown, 2006; Djuric *et al.*, 2007), active civil wars with both isolated

and mass burials (SOHR, 2014), and sadly with the present global increase in active conflicts before compiling at end which has resulted to an unprecedented number of unmarked human mass burials. Forensic searches for unmarked burials in burial grounds are many and had varied successes, for example, from archaeological graves in Jordan (Frohlich and Lancaster, 1986), historic North American Indian burial grounds (Bigman, 2012), 19<sup>th</sup> century cemeteries in New Zealand (Nobes, 1999), the USA (Bevan 1991; Ellwood et al. 1994; Doolittle and Bellantoni, 2010), to early 20<sup>th</sup> century Spanish Flu victims (Davis *et al.* 2000) and graveyards (Buck, 2003; Fiedler *et al.* 2009b; Hansen *et al.* 2014).

Current forensic search methods to detect both isolated and mass human burials are highly varied and have been reviewed elsewhere (Pringle *et al.* 2012a; Parker *et al.* 2010), with best practice suggesting a phased approach, moving from large-scale remote sensing methods (Kalacska *et al.*, 2009), through to initial ground reconnaissance (Ruffell and McKinley, 2014) and control studies before full searches are initiated (Harrison and Donnelly, 2009; Larson *et al.* 2011). These full searches can involve a variety of methods, depending upon the individual case and specific site parameters, including forensic geomorphology (Ruffell and Mckinley, 2014), forensic botany (Coyle, 2005; Aquila *et al.*, 2014) and entomology (Gennard, 2012; Amendt *et al.*, 2007), scent-trained search dogs (Lasseter *et al.*, 2003; Dupras *et al.* 2006), physical probing (Killam, 2004; Ruffell, 2005a; Owsley, 1995), taphonomy (Vass *et al.*, 2008; Carter *et al.* 2008b; Dekeirsschieter *et al.*, 2009) and non-intrusive near-surface geophysics (France *et al.*, 1992; Powell, 2004; Nobes, 2000; Cheetham, 2005; Ruffell, 2005b; Schultz, 2007; Pringle and Jervis 2010;

Novo *et al.*, 2011). Important forensic search case variables to be considered include time since burial, burial style, local soil type, vegetation and climate (see France *et al.*, 1992; Strongman, 1992; Schultz *et al.*, 2006; Pringle *et al.*, 2008; Schultz, 2008; Jervis *et al.*, 2009b; Juerges *et al.*, 2010; Schultz and Martin, 2011; Pringle *et al.*, 2012b; Ruffell *et al.*, 2014).

In 2013 Europe's biggest construction project, the London underground network Crossrail extension, discovered 25 surprisingly well preserved human skeletons in Central London; subsequent carbon dating and ancient deoxyribonucleic acid (aDNA) analysis confirmed a 1348-9 AD age and presence of the *Yersinia pestis* so called "Black Death" plague strain respectively. There are generally accepted to be three plague epidemics in recorded human history, Justinian's Plague (541-542 AD) mostly within Mediterranean countries, the European Black Death plague (1345-1750 AD) and 19<sup>th</sup> Century Chinese plague which spread globally in 1894 AD (Haensch *et al.*, 2010). The Black Death was the first widespread outbreak of medieval plague in Europe, with recent historical research, using documented evidence, has estimated the Black Death killed between 30 % – 50 % of London's population between 1347 and 1351 (Sloane, 2011). Scientific advancements in dating discovered skeletal remains have allowed research into age patterns of mortality during 1348-1350 AD in London (DeWitte, 2010; DeWitte and Hughes-Morey, 2012) and subsequent health improvements after this time (DeWitte, 2014). There has also been recent discussion whether Bubonic or Pneumonic plague was the primary transmittal method (Chanteau *et al.*, 2003).

### 3.1.1 *Aim*

During construction of the London Underground Crossrail network, Europe's biggest construction project, a number of human skeletons were discovered in a shaft in central London, buried at a shallow level. The area was known to be a medieval mass burial ground (Sloane, 2011). There was an opportunity to conduct a time-limited forensic geophysical search of the adjacent Charterhouse Square.

The aims of the near-surface geophysical survey were:

- i) to determine if non-invasive geophysical methods could both detect and characterise a potential ancient mass burial site;
- ii) to detect further unmarked burials and if there were any particular areas of burial concentrations and/or specific orientations, etc.;
- iii) to delineate the spatial extent of the burial site and, if possible, estimate the depths below ground level of buried targets;
- iv) to compare different geophysical techniques and equipment configurations to determine the optimum method for such an urban search scenario and finally;
- v) to compare this study to other mass burial search studies.

## **3.2 Material and methods**

### *3.2.1 Study site*

The study site is at Charterhouse Square near St. Bartholomew's Hospital in Central London, UK, situated approximately 1 km north of the Thames River and approximately 15 m above sea level (Fig. 3.1). Charterhouse Square is a 4 acre urban grassed park containing isolated mature deciduous trees, surrounded by roads and buildings, with Charterhouse hospital itself to the north-west (Fig. 3.2). Available British Geological Survey (BGS) boreholes detail organic-rich silty topsoil succeeded by a succession of unconsolidated fluvial sands, gravels and alluvium from previous courses of the River Thames. These sediments overlie Eocene London Clay and Cretaceous Chalk bedrock types at approximately 30 m and 50 m below ground level (bgl) respectively (Fig. 3.3 and Table 3.1).

Historical records show that a 13 Acre area was leased by Sir Walter de Mauny in 1349 AD from St. Bartholomew's priory, as an emergency cemetery burial site for The Black Death plague victims with a chapel also built on site (Hope, 1925). In 1371 AD de Mauny also sponsored the construction of a Carthusian priory and enlarged the site by 4 Acres to the east, the boundary between those areas being a parish boundary that still remains today (Porter, 2009), with an additional chapel built in 1481 AD (Temple, 2010). The priory was then dissolved in 1538 AD, and the two chapels demolished in 1545 AD and 1615-16 AD respectively (Barber and Thomas, 2002). During this period land was released for housing, some of which remains today as the Charterhouse Hospital and the Square itself

(Fig. 3.2). The construction of the London Metropolitan Railway and a new street built in the 1860s and early 1870s AD encroached upon the southern part of the site (Porter, 2009). As part of London's WW2 air-raid precautions, in 1939 AD six underground emergency water tanks were installed in the square. An exploratory site excavation was undertaken in 1997-8 AD with an isolated skeleton discovered in the north-east of the site (Fig. 3.2) (MoLAS, 1998).



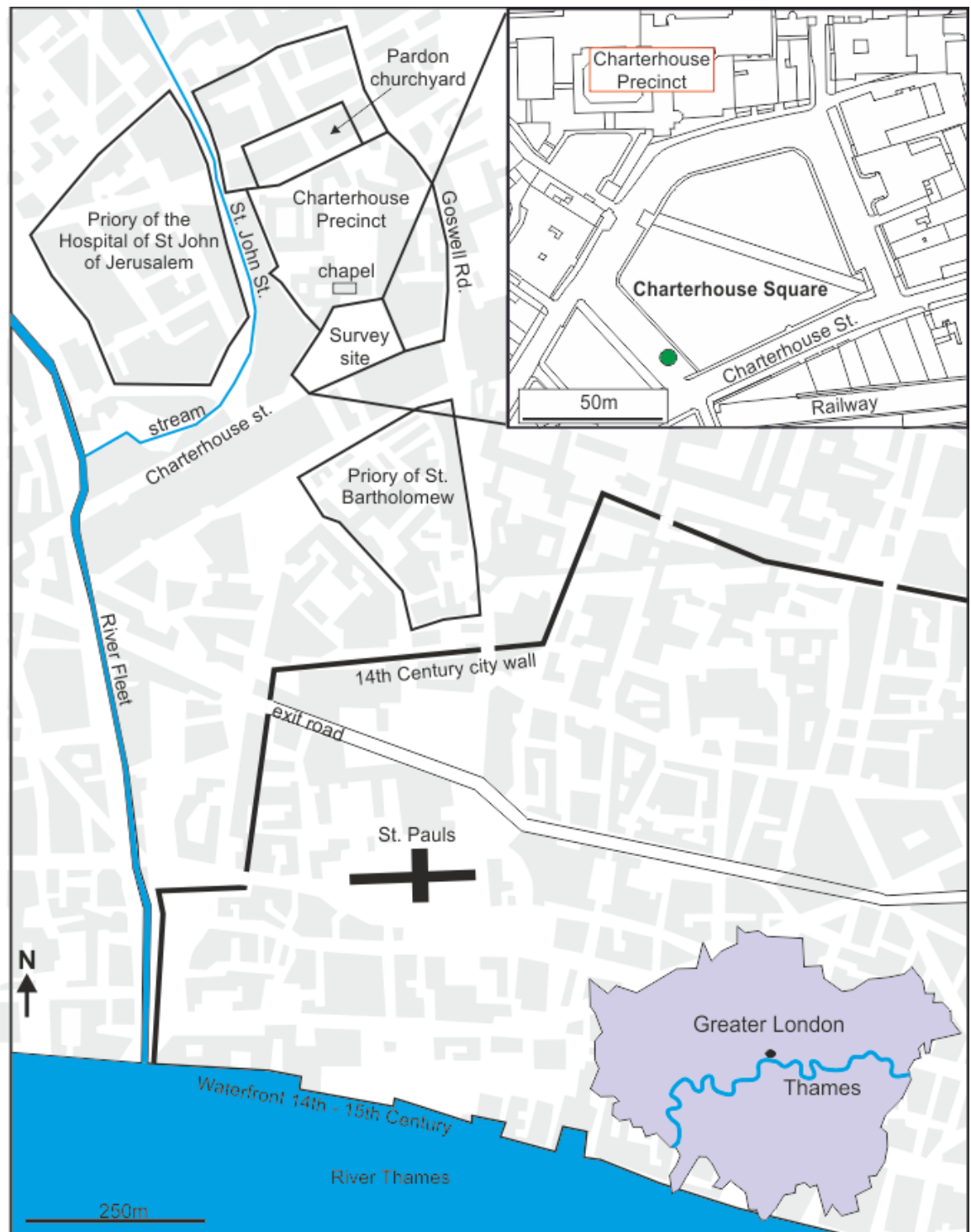


**Figure 3.1:** Map of the general and survey area (with location inset) and relevant Medieval features superimposed (modified from Dick *et al.*, 2015).

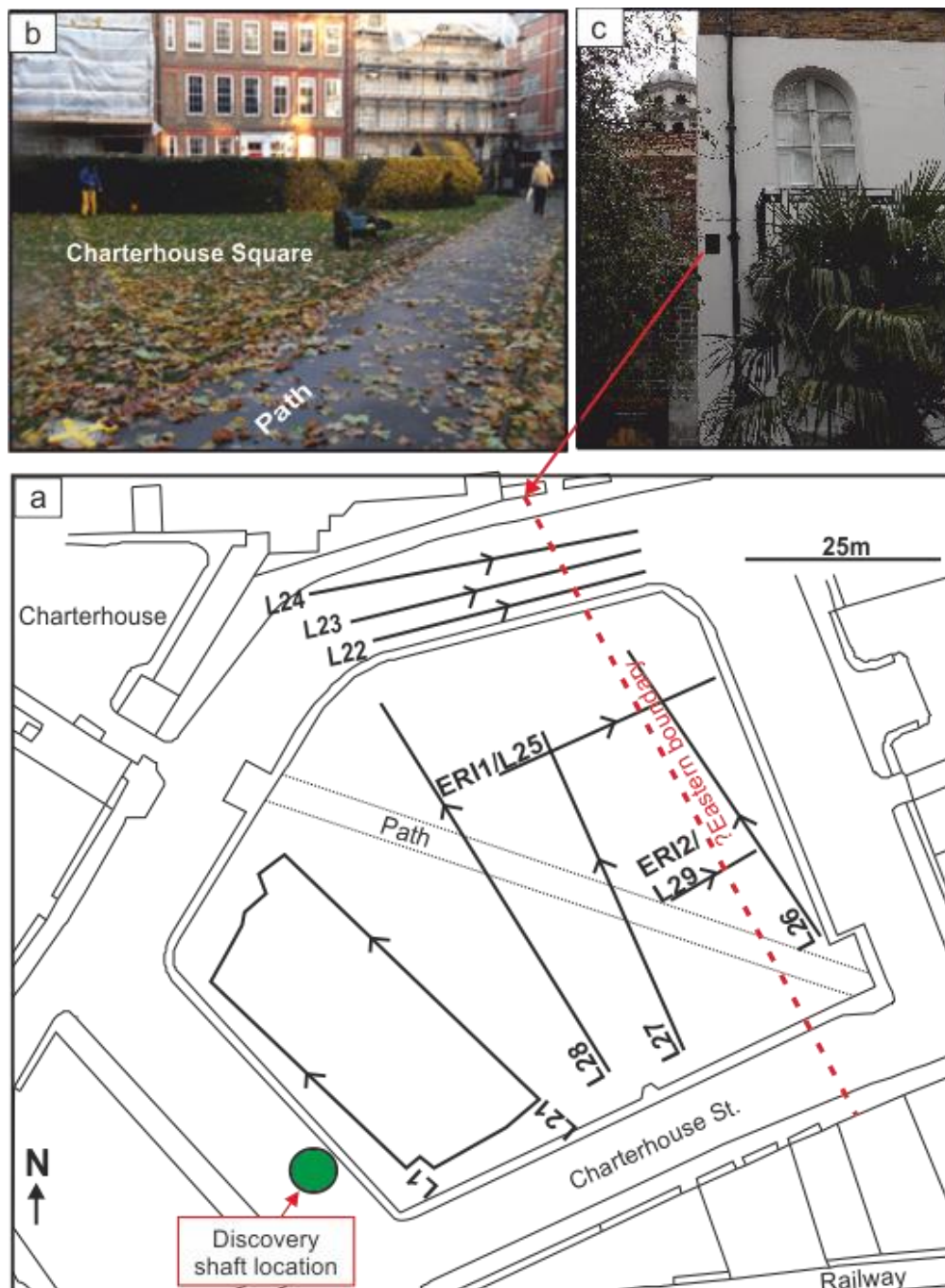


**Figure 3.2:** a) Mapview of Charterhouse Square showing approximate location of discovered shaft (green circle), named geophysical survey lines and site orientations, parish boundary (red dotted line), b) site photograph and c) parish boundary building plaque. Modified from Dick *et al.* (2015).

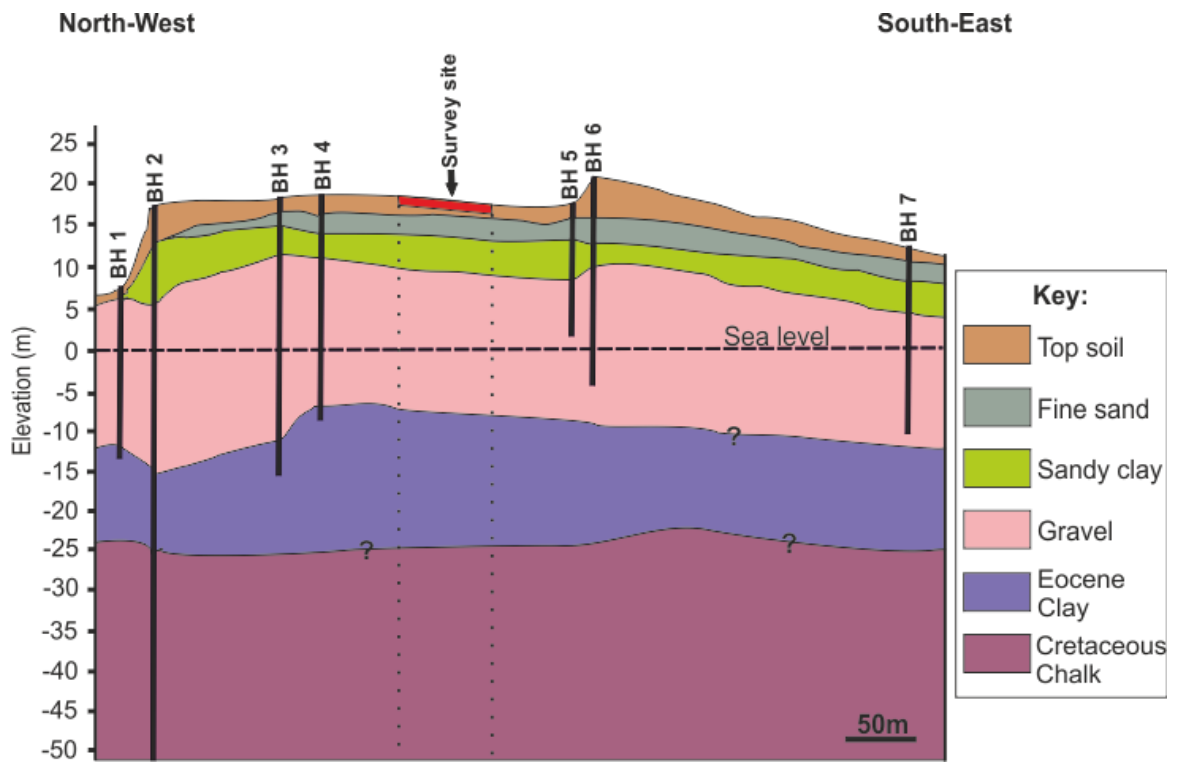


**Figure 3.3:** Approximately NW-SE orientated, 2D schematic cross-section of the study site using BGS borehole information, with sea level at zero elevation (see Table 3.1).

**Table 3.1:** List of available site investigation borehole and pertinent information derived to generate the schematic 2D cross-section shown in Fig. 3.3.

S/N	Borehole Number	Borehole Name	OSGB X (m)	OSGB Y (m)	Drilled Date	Drilled Depth (m)	Height above Sea Level (m)
1	BH1	TQ38SW5217	531615	181815	1986	20	7.3
2	BH2	TQ38SW3700	531650	182150	2002	130	16.5
3	BH3	TQ38SW4774	531780	182160	1999	33	18
4	BH4	TQ38SW4775	531810	182150	1999	26	18
5	BH5	TQ38SW3035	532064	181702	1986	15	17
6	BH6	TQ38SW3008	532090	181840	1983	20	18
7	BH7	TQ38SW1203	532440	181640	1970	21.5	12

(Data courtesy of British Geological Survey)

### 3.2.2 *Archaeological site excavations*

In 2013 as part of London's Cross Rail underground network extension, a 4.5 m diameter vertical shaft was dug on the road to the south-west of the Square (shown in Fig. 3.2). At 2.3 m bgl below approximately 0.4 m of vertically compacted clay, eight isolated earth-cut graves containing eleven relatively well preserved human skeletal remains were encountered that were aligned approximately northeast-southwest (Figs. 3.4 and 3.5 ). These remains did not show any signs of trauma although further disarticulated human remains were also recovered from two of the grave fills. At 2.5 m bgl two further isolated earth-cut graves containing two relatively well preserved incomplete human remains were encountered, again aligned northeast-southwest. At 2.7 m bgl, a further nine isolated earth-cut graves and one double-grave, containing 11 well preserved predominantly adult human remains were encountered, nine aligned northeast-southwest and two aligned north-south. Two isolated graves had multiple human burials, one with remains on top of the first and the other had them side by side. Recovered pottery shards allowed a burial date of estimate 1270-1350 AD (Crossrail, 2013).

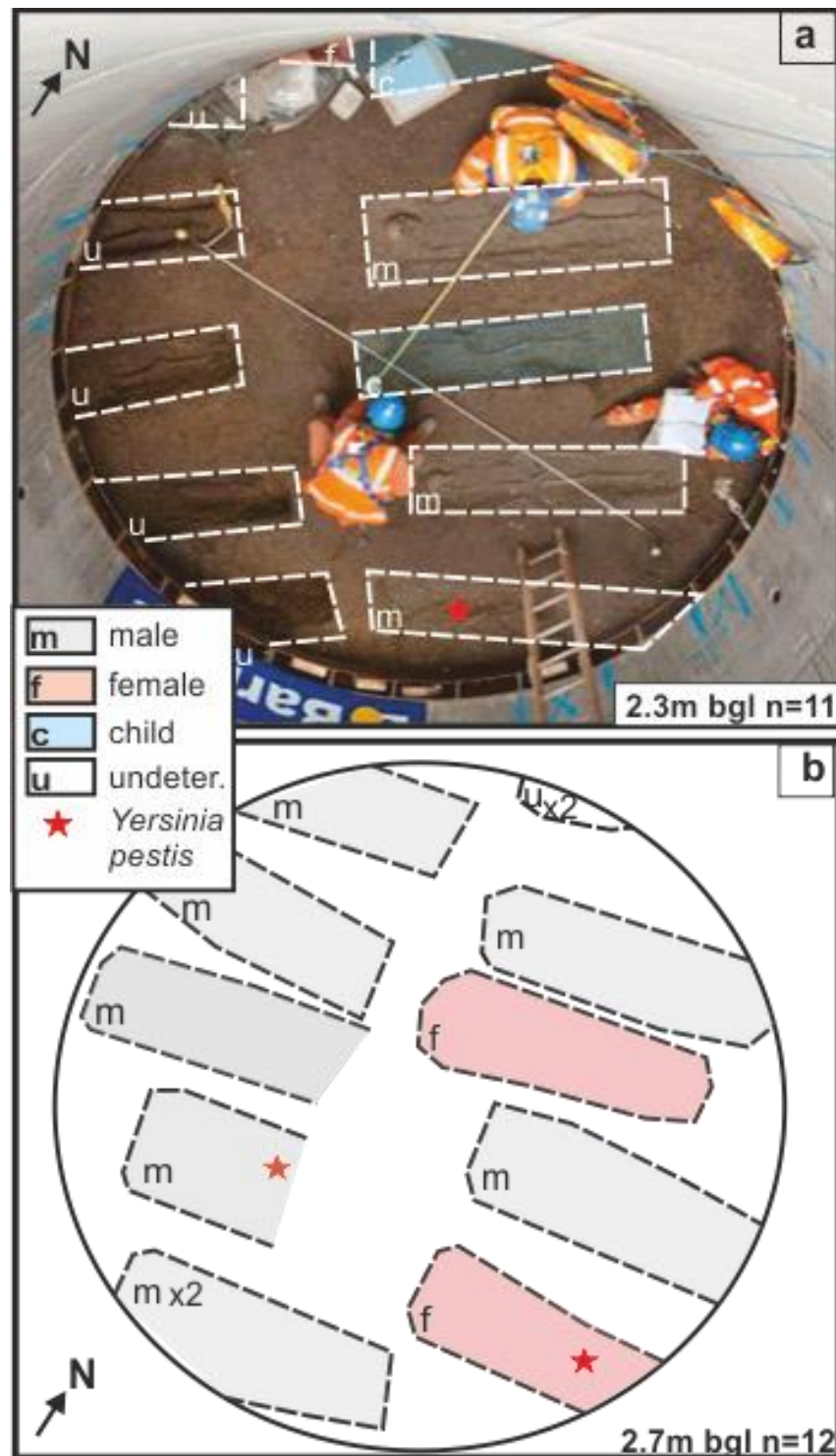


**Figure 3.4:** Mapview of shaft discovered earth-cut graves with identified burials and confirmed *Yersinia pestis* (see keys) at (a) 2.7 m and (b) 2.3 m BGL respectively (Fig. 3.2 for location). Two graves discovered at 2.5 m not shown. Modified from Dick *et al.* (2015).

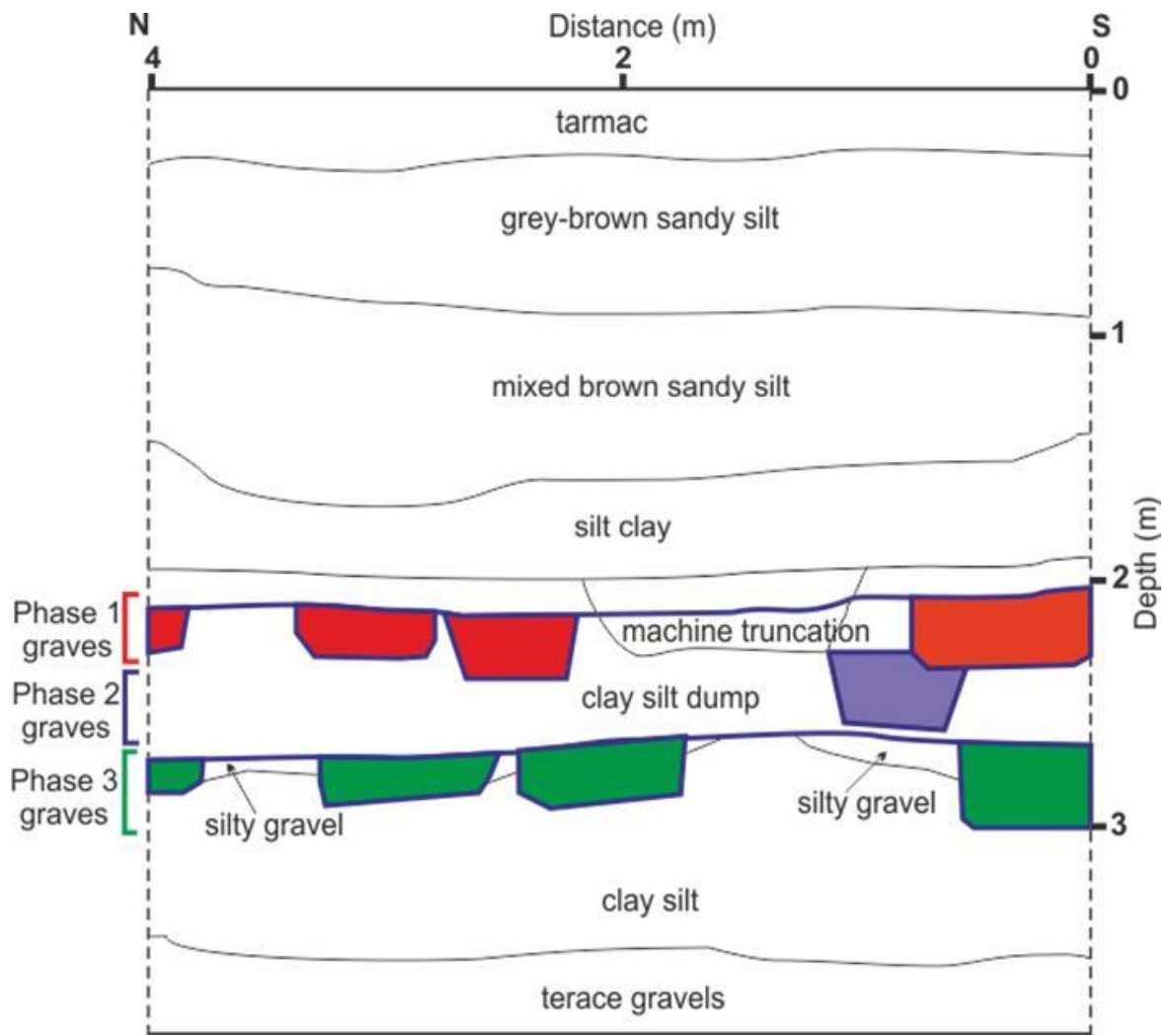


**Figure 3.5:** 2D schematic cross-section of earth-cut graves. Modified from Crossrail (2013).

Subsequent radio-carbon dating and rapid aDNA analysis of similar recovered human remains (see Fig. 3.6 for example) gave a date of 1349-1350 AD and confirmation that the skeletons contained the *Yersinia pestis* Black Death plague strain (Kacki *et al.*, 2011). This rapid diagnostic test for *Yersinia pestis* F1 antigen reveals (Fig. 3.6) from left to right, the positive results of the spongy bone samples from the multiple graves (SLC 1013, SLC 1014,



SLC 1083 and SLC 1084) and from the sample graves (SLC 116, SLC 158, SLC 148 and SLC 320) respectively.

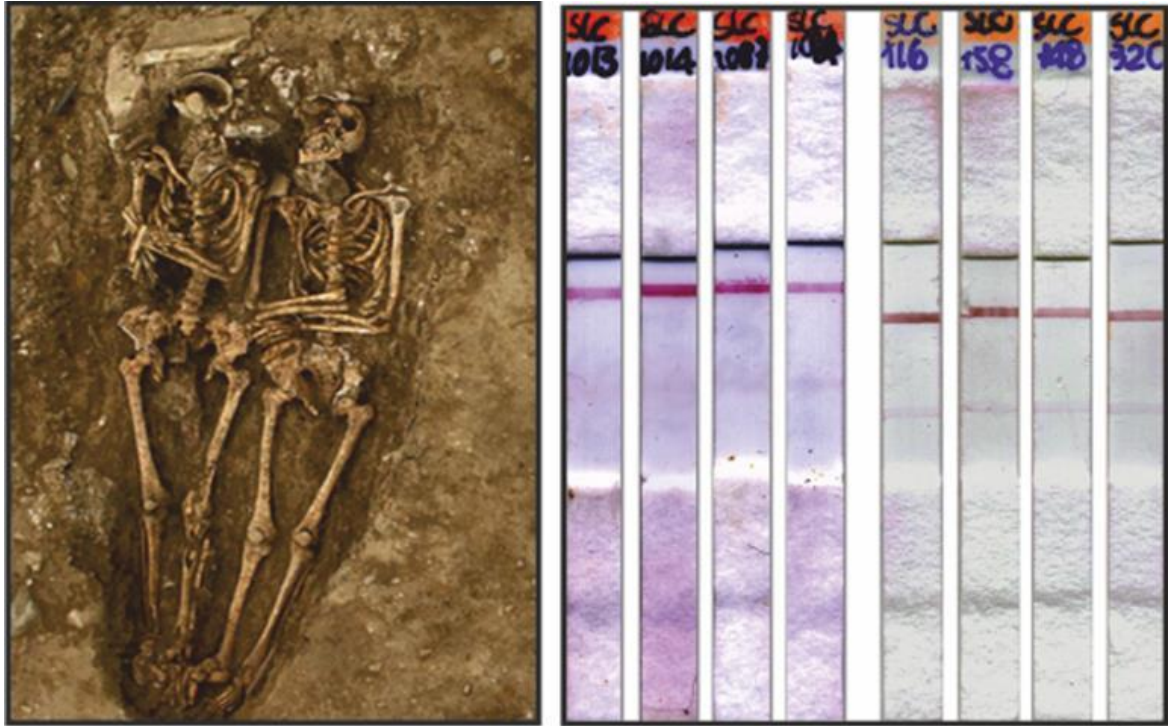


**Figure 3.6:** Co-mingled human remains and carbon dating analysis of Black Death Plague victims from rural French graveyards (from Kacki *et al.*, 2011).

### 3.2.3 Near-surface geophysical investigations

Traditional site investigation techniques such as soil sampling, trial pits and core drilling are invasive, often time consuming and expensive, and give a limited image of the subsurface. However non-invasive geophysical techniques such as ground penetrating radar (GPR), electrical resistivity imaging (ERI) and electro-magnetic induction (EMI) can provide good site coverage and commonly are used for characterising subsurface site



properties and structures if present (see Reynolds, 1997). Geophysical techniques can also be used to recognise anomalous areas that consist of localised and measurable contrasting site properties. Complications can occur where there are other materials present such as metallic debris, large deciduous tree roots, underground utilities and clay-rich soil on site which can mask any potential anomaly (Rezos *et al.*, 2010). Above-ground sources or interference are also common in urban sites such as fencing, buildings, etc., these may generate a false interpretation of the site. However, collection of multiple integrated geophysical techniques and careful data collection methodologies should boost and validate the geophysical survey and resulting interpretations.

As best practice suggests (see Reynolds, 2011; Larson *et al.*, 2011; Pringle *et al.*, 2012a) initial near-surface geophysical trial surveys in Charterhouse square showed detectable anomalies and measureable geophysical contrasts across the square, after which, a full two day survey was undertaken. Survey 2D profile positions were all surveyed using a Leica™ 1200 total station theodolite and reflector prism with 0.005 m average measured position accuracy before being merged with the digital sitemap in ArcGIS™ ArcMap v.10 software.

### *3.2.3.1 Electro-magnetic (EM) surveys*

A bulk ground conductivity survey was undertaken over the study site using a Geonics™ EM31-Mark2 conductivity meter at approximately 2m spaced lines (Fig. 3.7a), in order to characterise the site and to determine if the burial area margins could be delineated. This instrument images bulk changes in the near-surface, typically down to approximately 10m below ground level (bgl) in ideal conditions (see Milsom and Eriksen, 2011). However, the maximum depth of investigation depends on several factors, mostly associated with the instrumental parameters (frequency and inter-coil separation); the acquisition procedure (vertical or horizontal core orientation); and finally the electromagnetic contrast between the target and the host environment. The instrument was initially calibrated by choosing a small area outside the designated research grid known to be without burials or metals at the northeast side of the square following standard operative procedures (Milsom and Eriksen, 2011), which was determined to be relatively geophysically homogeneous from the trial surveys. Due to the potential cultural interference from above-ground conductive objects, the EM dataset was collected with the meter in vertical magnetic dipole (VMD) orientation which has been evidenced to reduce its sensitivity to above surface conductive objects (see Milsom and Eriksen, 2011) and changes at a greater depth (Reynolds, 1997). Both inphase and quadrature data types were collected in a one-way orientation at approximately 1 s increments by the operator keeping a relatively constant walking pace and were recorded on a handheld data logger. A Garmin™ Global Positioning System (GPS) instrument was also incorporated and was used by Trackmaker31™ v.1.21 personal computer software to allocate a positional location to conductivity readings in real-world co-ordinates. Standard post-survey data processing

was undertaken in Microsoft Excel software, including data de-spiking to remove anomalous data points and de-trending to remove long wavelength site trends from the data according to standard practice (see Milsom and Eriksen, 2011) before the dataset was imported into ARCGIS ArcMAP™ v.10 software. A Digital, 2D colour pseudo-sections of both inphase (InP) and quadrature (Qd) components were generated by interpolating the respective processed datasets result using a minimum curvature gridding algorithm. See the summary statistics of geophysical surveys in Table 3.2 for further information.

**Table 3.2:** Summary statistics of EM, CST, GPR and ERI geophysical datasets collected during this study. See Fig. 3.2 for dataset location.

<b>2D Profile Line</b>	<b>Survey type</b>	<b>Station total</b>	<b>Station spacing (m)</b>	<b>Station reading duration</b>	<b>Maximum approximate depth of penetration bgl (m)</b>
N/A	EM	1,240	~ 1 x ~2	1 s	~10
1-8	CST	3,120	0.1	~6 s	2
1-31	GPR	13,070	0.1	8s	3
1	ERI	32	1	~1½ h	~4.5
2	ERI	16	0.5	~¾ h	~2.5



**Figure 3.7:** Photographs of near-surface geophysical equipment used. a) Geonics™ EM31-Mk2 conductivity meter; b) Geoscan™ RM-15-D mobile resistivity meter with 1m probe separation); c) GPR PulseEKKO™ 1000 225 MHz frequency antennae and associated equipment and; d) Campus TIGRE™ Electrical Resistivity Imaging system with a 32 electrode spread.

### 3.2.3.2 Constant Separation Traversing resistivity surveys

A Geoscan™ RM15-D bulk ground electrical resistivity equipment with a 1 m fixed-offset dipole-dipole electrode probe configuration (Fig. 3.7b) was used to collect eight, 1 m spaced, approximately 38 m long, Constant Separation Traverse (CST) 2D profiles (L1-4),

located adjacent to the crossrail discovered burials (Fig. 3.2 for location). The instrument has a stated measurement accuracy of 0.1  $\Omega$ . Measurement positions were surveyed at 0.1 m sample spacing with the remote probes set at least 10 m from sample positions following best practise guidance (see Milsom and Eriksen, 2011). Whilst 0.5 m fixed-offset probe configurations are more commonly used for such search investigations (see Pringle and Jervis, 2010; Hansen *et al.*, 2014), a 1 m probe separation was deemed necessary to allow the instrument to penetrate to the depths of the discovered archaeological graves (Fig. 3.5). After digital data download, the raw data were converted from x, y, z format to grid (i.e.  $z = f(x,y)$ ) format using a continuous curvature surface gridding algorithm (Smith and Wessel, 1990). Then standard data processing were undertaken, including; (i) conversion of measured resistance ( $\Omega$ ) values to apparent resistivity ( $\Omega.m$ ) to account for probe spacing configuration; (ii) data de-spiking to remove anomalous data points and; (iii) dataset de-trending to remove long wavelength site trends from the data (see Milsom and Eriksen, 2011) for background (Table 3.3). The dataset was then imported into ARCGIS ArcMAP™ v.10 software and a digital, colour contoured surface was generated from the dataset using a minimum curvature gridding algorithm.

**Table 3.3:** Data processing protocols used for resistivity survey in these studies

Step	Process	Justification
1	Conversion	Spatially-corrected data to XYZ in GMT (where applicable)
2	Gridding	Minimum curvature gridding algorithm interpolates data to a cell size of 0.025 m by 0.025 m to create smooth image
3	De-trending	Removal of long-wavelength trends from measured data by fitting a cubic surface to grid and then subtracting from surface data, allows small-wavelength features to be better distinguished
4	Normalisation	Dividing dataset by its SD Z value created grid with mean Z of ~ 0 and SD of ~ 1 allowing dataset comparison.

### 3.2.3.3 Ground Penetrating Radar surveys

After the initial trials to determine the optimal set frequency radar antennae, Ground Penetrating Radar (GPR) PulseEKKO™ 1000 equipment was utilised with 225 MHz frequency antennae (Fig. 3.7c) to collect a series of 2D profiles that were variably spaced and orientated due to the limited time available onsite (Fig. 3.2 for location). This relatively low frequency, fixed-offset antennae should penetrate to approximately 3 m bgl depths at which the presumed undiscovered graves may be located (see Hansen *et al.*, 2014) judging by the discovered burials (Section 3.2.2). Radar trace spacings were 0.1m along all 2D profiles using a 32 v transmitter antennae, 90 ns time window and constant 32 repeat stacks. A dense grid of 2D profiles were acquired adjacent to the discovered archaeological graves (L1-L21), three (L22-L24) were acquired on the road to the north of the square, two (L30-L31) were acquired at the garden approximately 100 m away from north of the square, two (L25, L29) orientated at right angles to the parish boundary, one (L26) outside the parish boundary and two final profiles (L28-L27) mid-way across the square (see Fig. 3.2 for location). Standard data processing steps were undertaken for all 2D profiles in REFLEX-Win™ v.3.0 data processing software in order to obtain good quality interpretations (Cassidy, 2009). These included; (i) subtracting the mean from traces; (ii) picking first arrivals; (iii) applying static correction and moved trace start times to a constant 10 ns; (iv) time-cut to remove blank data at base of profiles and; (v) manual gain 1D filter to boost deeper radar trace relative amplitudes whilst retaining shallow radar amplitudes. Average velocity of approximately 0.13 m/ns for all depths was used to convert 2D profiles from two-way travel-time (TWT) to depth (m), based on analysis of hyperbolae in 2D profiles (Fig. 3.8)

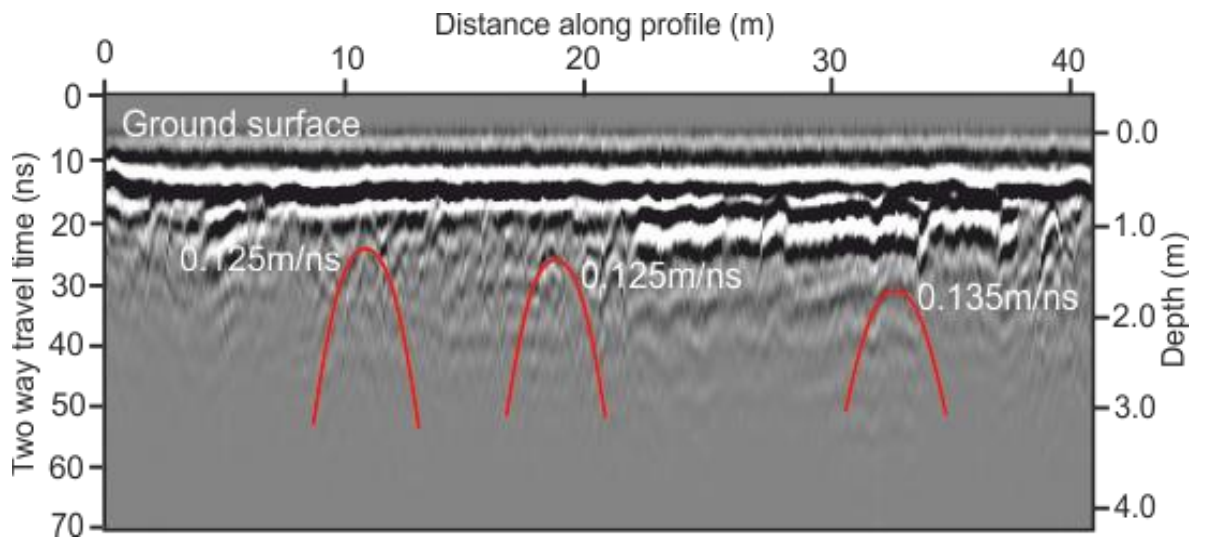


**Figure 3.8:** 2D GPR profile showing hyperbolic velocity matching where hyperbolic functions have been fitted to diffraction hyperbola from a 225-MHz GPR section acquired from Charterhouse Square, with average velocity of 0.13 m/ns.

#### 3.2.3.4 Electrical Resistivity Imaging resistivity surveys

Two 2D Electrical Resistivity Imaging (ERI) profiles (ERI 1 and ERI 2), orientated at right angles to the known parish boundary marked by plaques on square margin buildings, were also collected by a CAMPUS™ TIGRE system (see Fig 3.2 for location). Both ERI profiles used 32 steel electrodes connected to the TIGRE using multi-core cabling, inserted into the ground along each profile (Fig. 3.2) with ERI 1 and ERI 2 using 1 m and 0.5 m probe spacing respectively due to site constraints (Fig. 3.2). These probe spacings were a good compromise between depth penetration and satisfactory spatial resolution. Each measurement was also acquired 3 times and averaged which optimized good quality data. The adopted Wenner array and central positions across the presumed burial boundary chosen was relatively sensitive to vertical resistivity changes below the centre

of the array (Milsom and Eriksen, 2011). ImagerPro™ 2000 data acquisition software used a Wenner configuration and 10 'n' levels, which should detect bulk resistivity changes down to approximately 5 m bgl, has been deemed optimal by other researchers (Brown, 2006; Pringle *et al.*, 2012b). The ERI images were obtained using a least-squares inversion method. The data acquisition process selects a starting resistivity model of the subsoil; a model parameter change vector is then calculated at each iteration and the resistivity model then modified in order to minimize the sum of square differences between the model response and the observed data. Geotomo™ Res2Dinv v.355 software was then used for data processing in accordance with standard ERI surveying recommendations (Milsom and Eriksen, 2011). Optional half-cell spacing was also utilized during the data inversion process to remove potential data edge effects and reduce any near-surface electrical resistivity variations respectively. Electrical resistivity variations are commonly encountered in heterogeneous ground (e.g. Banham and Pringle, 2011). Finalised 2D models of true resistivity sections were lastly created with a relatively small RMS mis-fit of 2.3 % (ERI 1) and 4.1 % (ERI 2) between the respective calculated models and observed dataset gave confidence in data quality.



### 3.3 Results

#### 3.3.1 EM datasets

Careful data processing was undertaken following standard practice to produce optimised dataset images. Colour contoured, gridded digital surfaces generated from the processed EM Inphase (InP) and Quadrature (Qd) datasets are displayed in Figures 3.9 and 3.10 respectively. Both EM datasets (InP and Qd) were somewhat similar, except that the anomalies in the Qd component were of sufficient size and clearly delineated. However, the EM InP component does detect the parish boundary compared to the EM Qd component in the south-east of the square. This observation also confirmed the importance of measuring both EM components. The published literature does suggest that Qd response should be more sensitive to the apparent bulk conductivity of the subsurface, whilst the EM InP response should be better related to magnetic properties of buried structures and waste materials (see Reynolds, 2011 for more information).

Both EM datasets showed a relatively highly conductive  $8 \text{ m}^2$  (InP) and  $18 \text{ m}^2$  (Qd) areas, respectively, to the north-west of the square, compared to background values, although there were not many data points present (Figs. 3.9 and 3.10). The high conductivity values both in the InPhase and Qd components suggest that the anomaly is made up of ferrous material that provides an increase in electrical conductivity. This also explains the low resistivity values in CST data (between  $2.5\text{-}22.8 \text{ } \Omega\cdot\text{m}$ ) and corresponding high amplitude reflection signal shown in GPR data in this location (Figs. 3.11 and 3.12). There was also

an  $\sim 6 \text{ m}^2$  (InP) and  $\sim 20 \text{ m}^2$  (Qd) area anomaly respectively with variable relative high/low anomaly values, with respect to background value in the central area (Figs. 3.9 and 3.10). The relative high EM conductivity values at the southern side of the square were most likely due to above-ground geophysical interference (e.g. metal fence) and cultural noise in this urban environment. Generally, there was little measureable difference in EM properties across the presumed parish boundary, although the InPhase component does show a slight change (*cf.* Fig. 3.9).

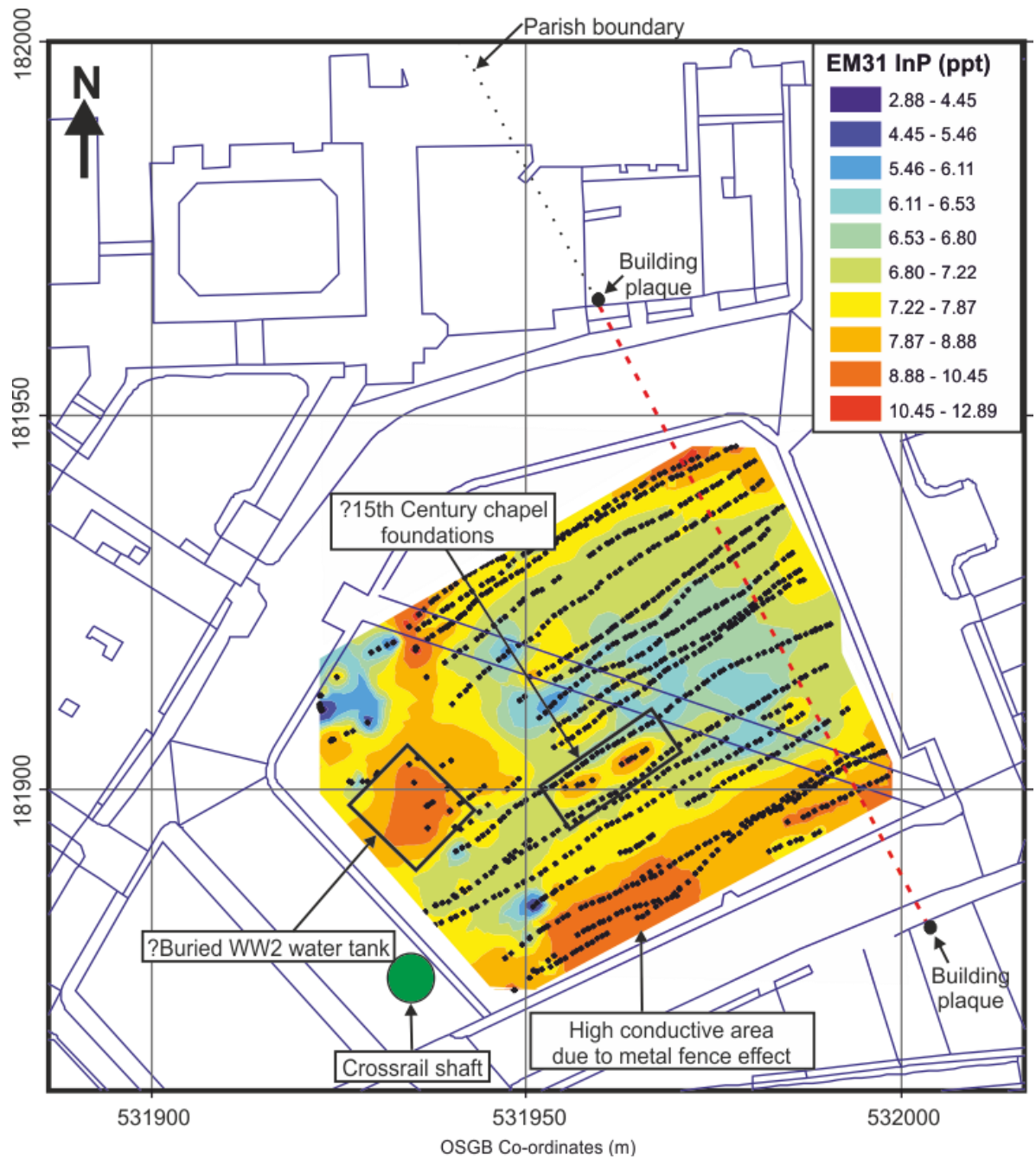


**Figure 3.9:** Processed electro-magnetic (EM) conductivity Inphase VMD dataset with generated colour contoured digital gridded surface (see key) and annotated area of interest marked, sampling positions shown as parallel dotted points. Modified from Dick *et al.* (2015).

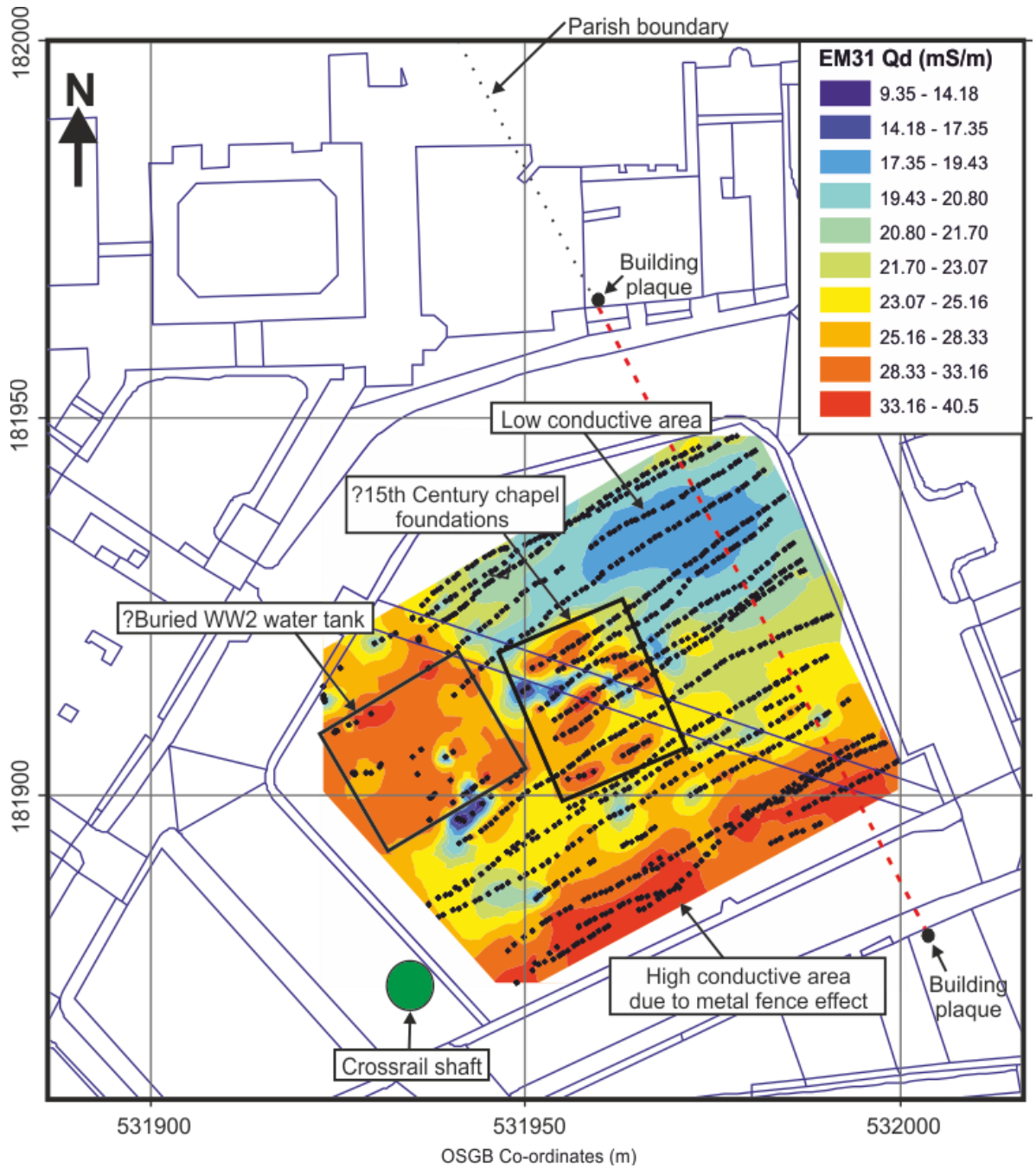


**Figure 3.10:** Processed electro-magnetic (EM) conductivity Quadrature VMD dataset with generated colour contoured digital gridded surface (see key) and annotated area of interest marked, sampling positions shown as parallel dotted points. Modified from Dick *et al.* (2015).

### 3.3.2 *Electrical resistivity CST datasets*

The processed electrical resistivity CST fixed-off-set (1 m) surveys collected over the first 8 profile lines in the south-west area of the square, adjacent to the discovered skeletons, were merged to generate a coloured contoured, gridded digital surface (Figure 3.11). This dataset showed a trend from relatively very high resistivity values in the south to very low resistivity values to the north respectively. However, individual resistivity 2D profile lines, when plotted separately, were very uniform and followed a similar trend with a large resistivity gradient approximately halfway along the profile lines (Fig. 3.11), an indication of a clear boundary between background and a possible conductive buried object to the North-West of the Square. The background resistivity of the survey site was relatively high compared to typical soil values of ranges between 30 and 215 (Reynolds, 2011) and may be due to the coarse soil type associated with River Thames deposits (river terrace unconsolidated gravels) as noted by the Crossrail (2013) interim report. The resistivity dataset therefore agrees with the high conductivity values in the EM dataset at this location. However, relative isolated anomalies compared to background values, which may be expected from individual graves containing human remains, were not observed in this resistivity dataset.

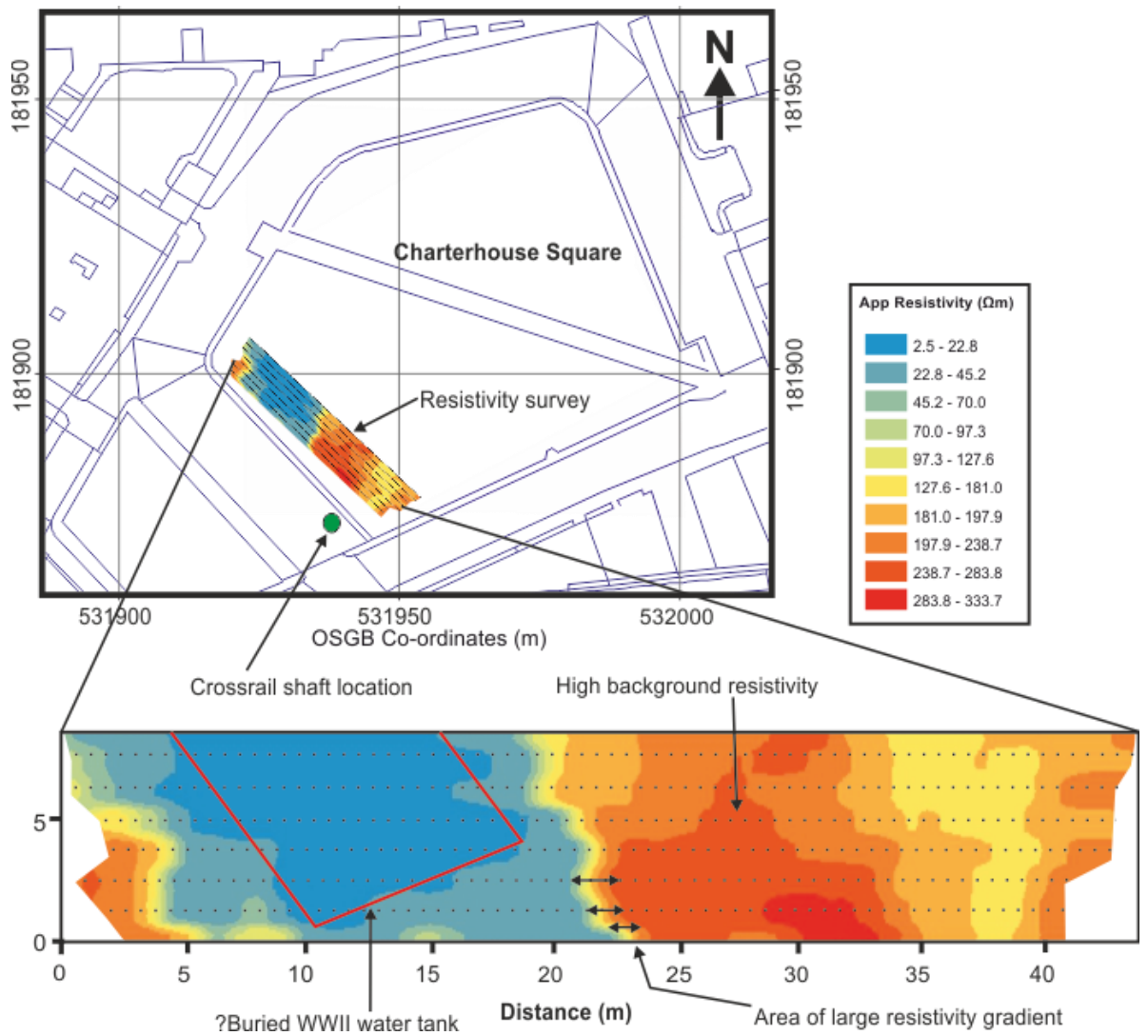
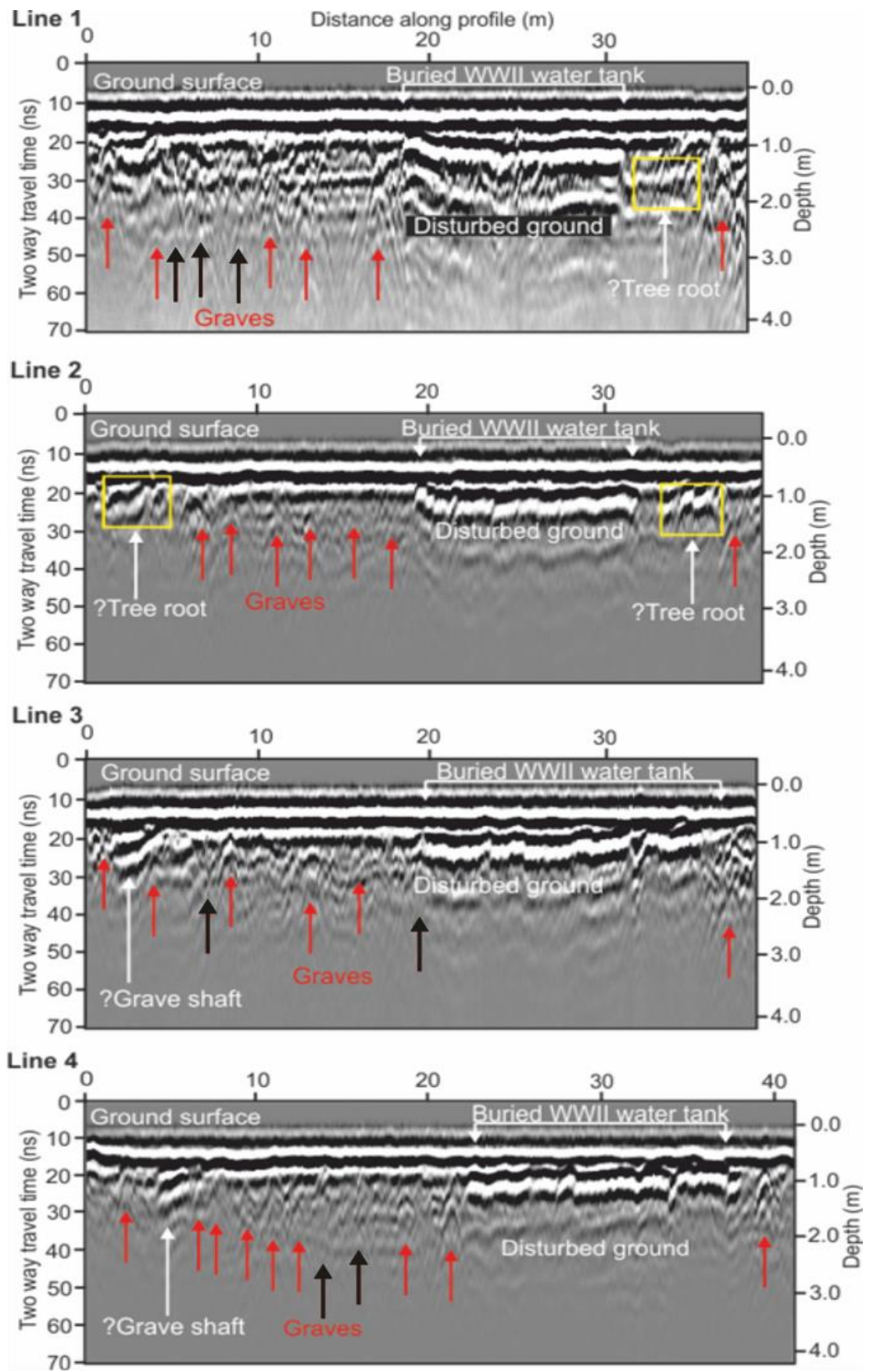


**Figure 3.11:** Processed merged CST resistivity dataset (black dots) with colour contoured digital surface generated (see key) and annotated interpretations marked. Modified from Dick *et al.* (2015).

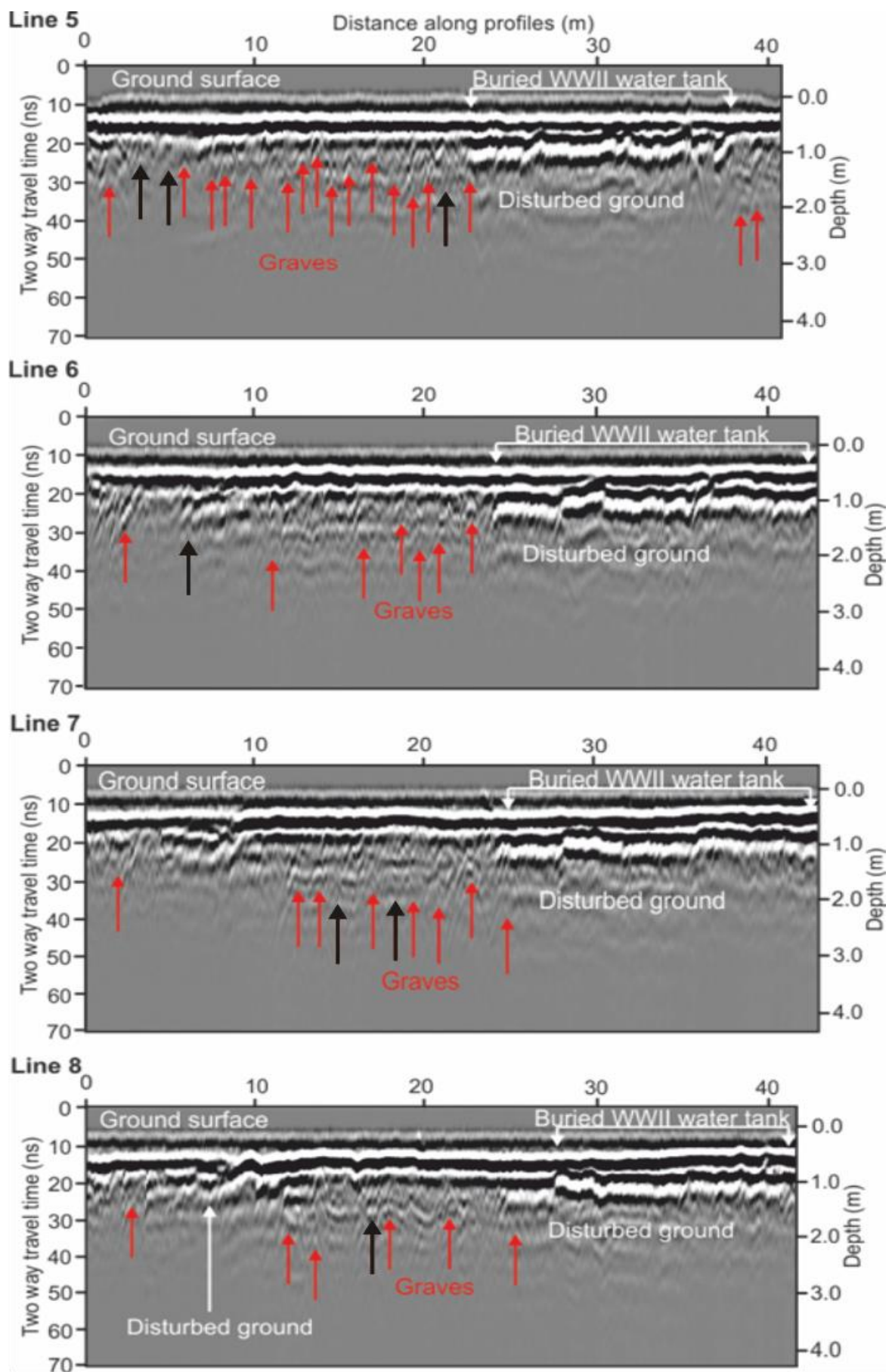
### 3.3.3 GPR datasets

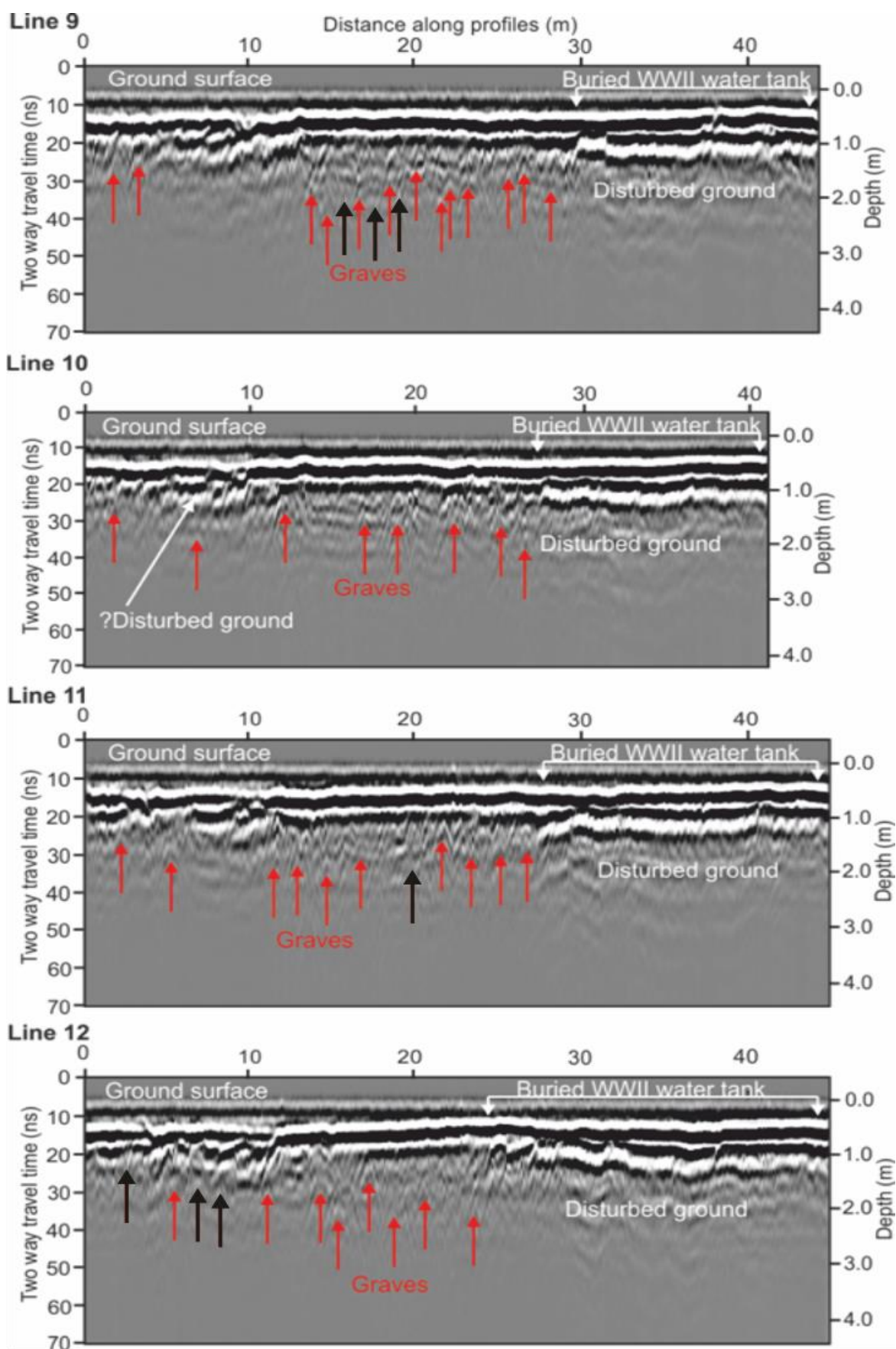
The processed 2D GPR profiles (L1-L21) consistently imaged isolated, evenly-spaced and similar-sized  $\frac{1}{2}$  hyperbolic reflection events, produced from buried objects in the southern half of all profiles (Fig. 3.12). These objects were generally buried between approximately 1.2 m and 2.7 m below ground level (bgl) that were of similar depths to the discovered historic isolated graves (Figs. 3.4 and 3.5) and have been observed in other mass burials (e.g. Ruffell *et al.*, 2009). Smaller and shallower  $\frac{1}{2}$  hyperbolic reflection events at either end of 2D profiles were most likely due to the presence of shallow tree roots from the mature deciduous trees present on the square margins (Fig. 3.12). Consistent, very strong horizontal reflections of approximately 14 m – 18 m wide, were also present at the northern end on these 2D profiles (Fig. 3.12); it could be argued that both a top at  $\sim 0.6$  m bgl and bottom  $\sim 2$  m bgl reflector of this buried object could be observed (*cf.* Fig. 3.12). This significant-sized object could be correlated to the high conductivity/low resistivity anomaly present in both the EM and electrical resistivity datasets respectively. The other long 2D profile (L28) across the park (Fig. 3.2 for location) also showed a similar pattern, in that there were multiple isolated  $\frac{1}{2}$  hyperbolic reflection events present in the southern side of the square, with few present in the north, although there was no strong horizontal reflector present in this profile (Fig. 3.12). The three 2D profiles (L22-L24) on the north road of the square (Fig. 3.2) did not image any similar isolated buried objects, except for locations beside observed surface manhole covers, or indeed where they crossed the parish boundary. The 2D profile (L26) that was located east of the parish boundary position within the square showed only two isolated  $\frac{1}{2}$  hyperbolic reflection events in the north part of the profile (Fig. 3.12).

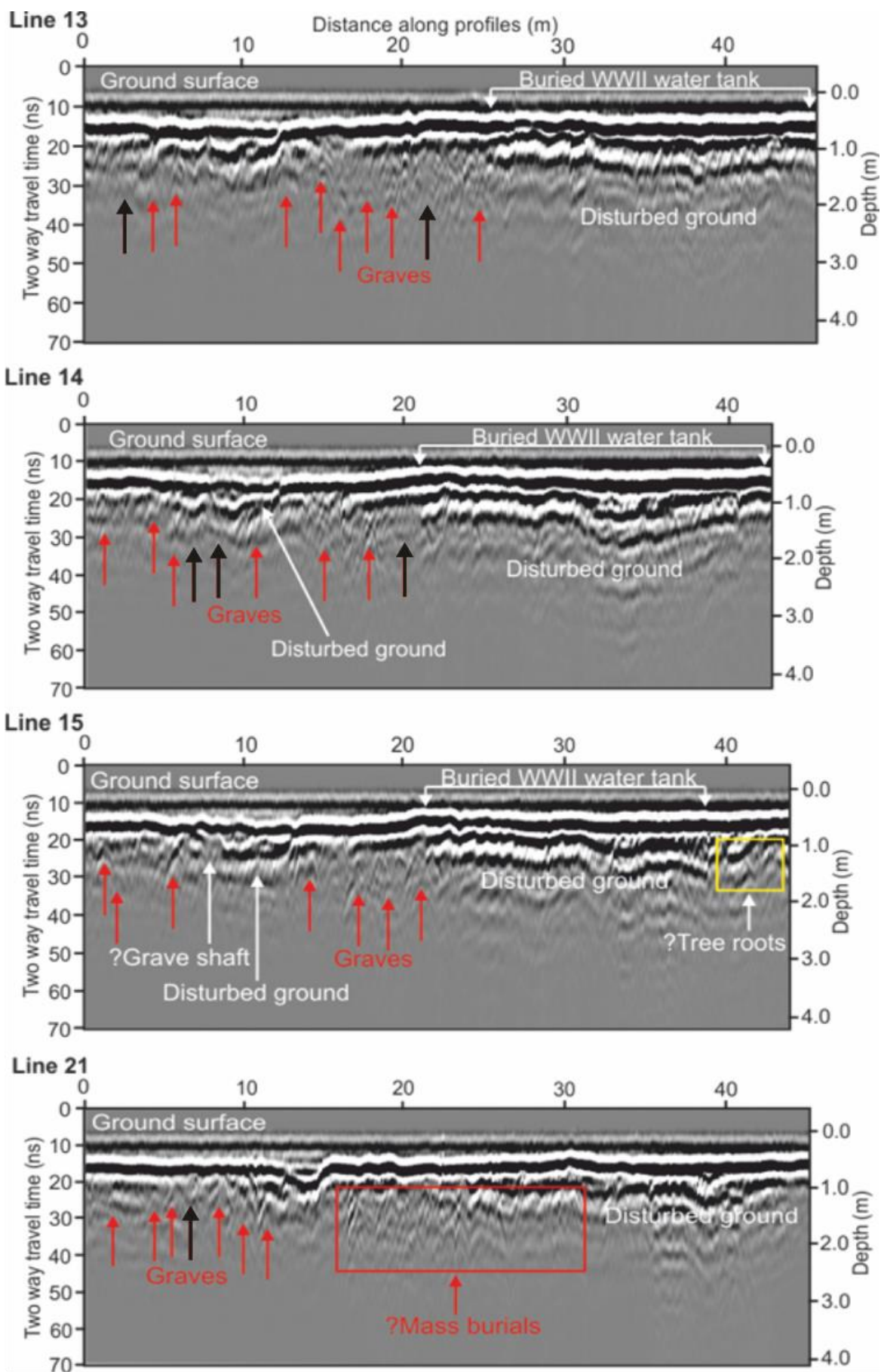














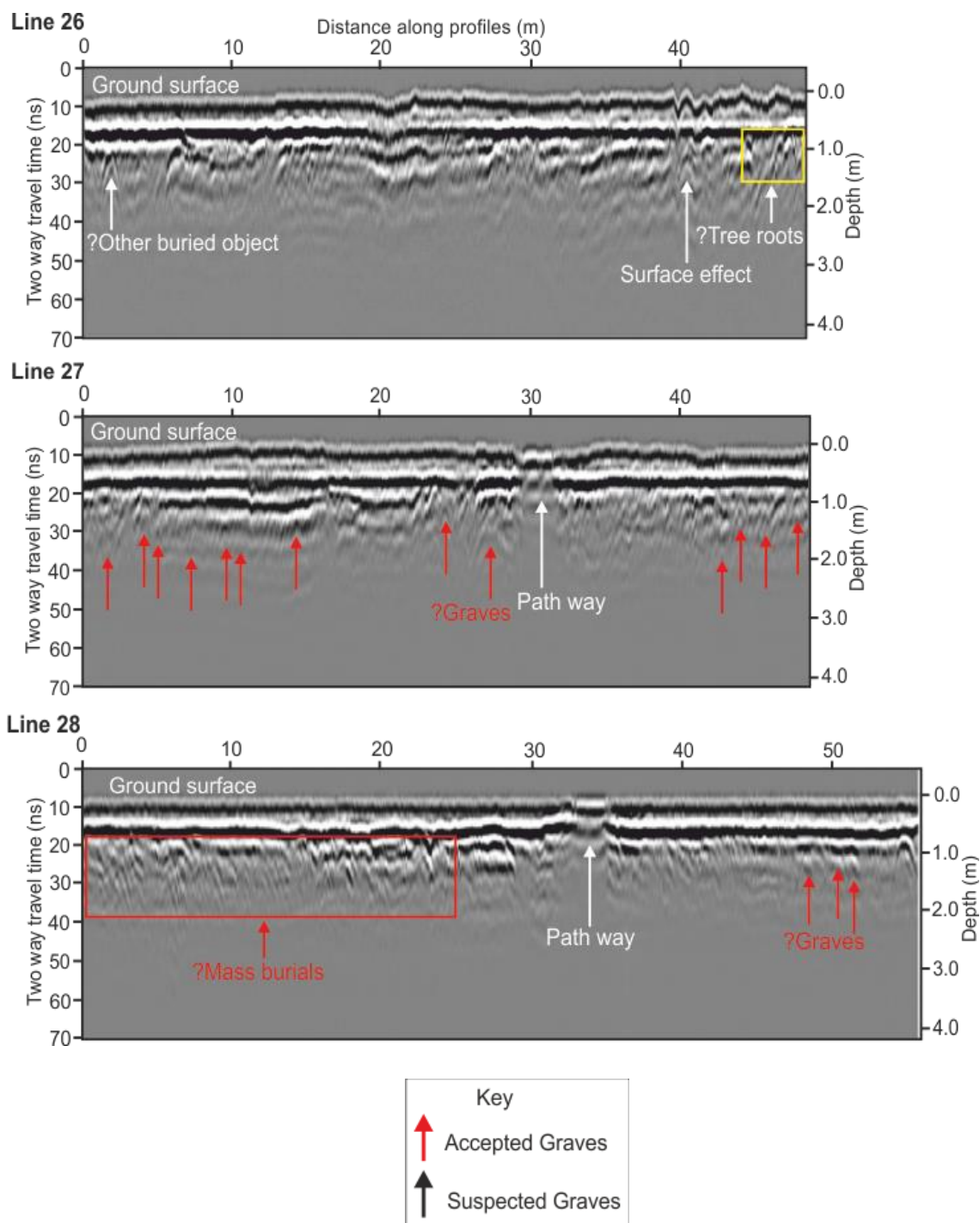


**Figure 3.12:** Selected GPR 2D processed profile lines with marked interpreted buried objects. Red arrows represent accepted graves and black arrows represent suspected graves. Only the red arrows were used for statistical calculations (Fig. 3.2 for location).

Further detailed processing was also carried out to better develop a merged image (grid plot) of the GPR surveyed area (L1-L21) by creating time slices, although it took significantly more processing time to generate. However, producing a full grid time slices of the data may sometimes reveal more subtle defects within the data as others have noted (e.g. see Linford, 2014). Once GPR 2D profiles had their correct spatial positions incorporated into their respective header files, and f-k migration undertaken using the 0.13 m/ns average site velocity measured from diffraction hyperbolas (Fig.3.8), the GPR dataset were then horizontally dissected as slices in one way time at 10 ns, 15 ns, 20 ns and 25 ns, with the origin at the ground surface. These time slices correspond to depth bgl of approximately 0.5 m, 1.0 m, 1.5 m and 2.0 m respectively. Generated by re-sampling all reflection amplitudes in all profiles within the grid and then averaging the amplitudes in slices of a given thickness. Reflection amplitudes are then gridded and interpolated to provide a uniform placement of radar reflection strengths throughout the mapped area (Sutton and Conyers, 2013).

The reason for generating radar time slices is firstly, to allow the spatial extent of any radar amplitude anomalies to be seen and therefore be identified much more effectively, and second, they should make possible the identification of subtle radar anomalies and patterns that would otherwise not be made possible when identified only in individual 2D GPR profiles. The result of the time-slices showed that majority of the burials were located within 1.0 m to 1.5 m depth bgl, represented in red, with an area of disturbed ground represented by purple, with yellow being the background (Fig. 3.13).

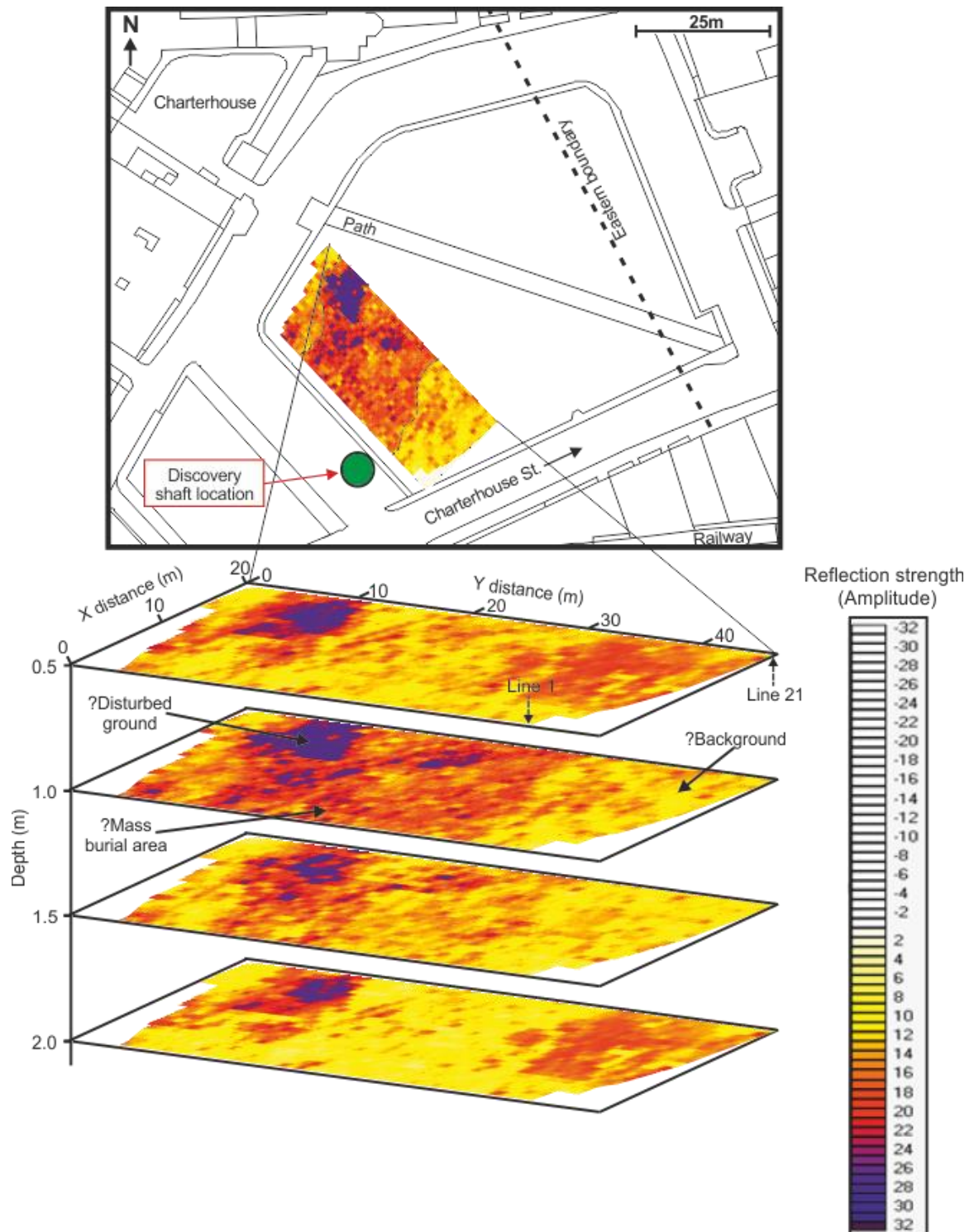


**Figure 3.13:** 3D GPR time-slice images of the survey site with colour legend denoting relatively strong reflected energy (amplitude)

#### 3.3.4 Eastern Parish Boundary

Whilst EMI, GPR and CST responses were limited to a depth of few metres bgl, the 2D ERI profiles were able to investigate deeper into the ground, although the intrinsic spatial resolution tended to degrade with depth. Both 2D ERI inverted models acquired over the parish boundary (Fig. 3.2) showed a clear change in resistivity properties across the boundary, with relative higher resistivity values to the east of boundary, high resistivity top soil (Fig. 3.14 and 3.15) and lower values to the west). There were significant heterogeneities present in both profiles, as would be expected in such urban environments, variable moisture content may also be a factor as others have found (Pringle *et al.*, 2012c), especially in parklands (Jones *et al.*, 2009).

The 2D GPR profiles (L25 and L29) acquired at right angles to the parish boundary at this same location showed few  $\frac{1}{2}$  hyperbolic reflection events, although, at the boundary position itself, a U-shaped depression and a widely-spaced  $\frac{1}{2}$  hyperbolic reflection event on the east site were both observed at both locations (see Figs. 3.14 and 3.15).

Line 25/ERI 1

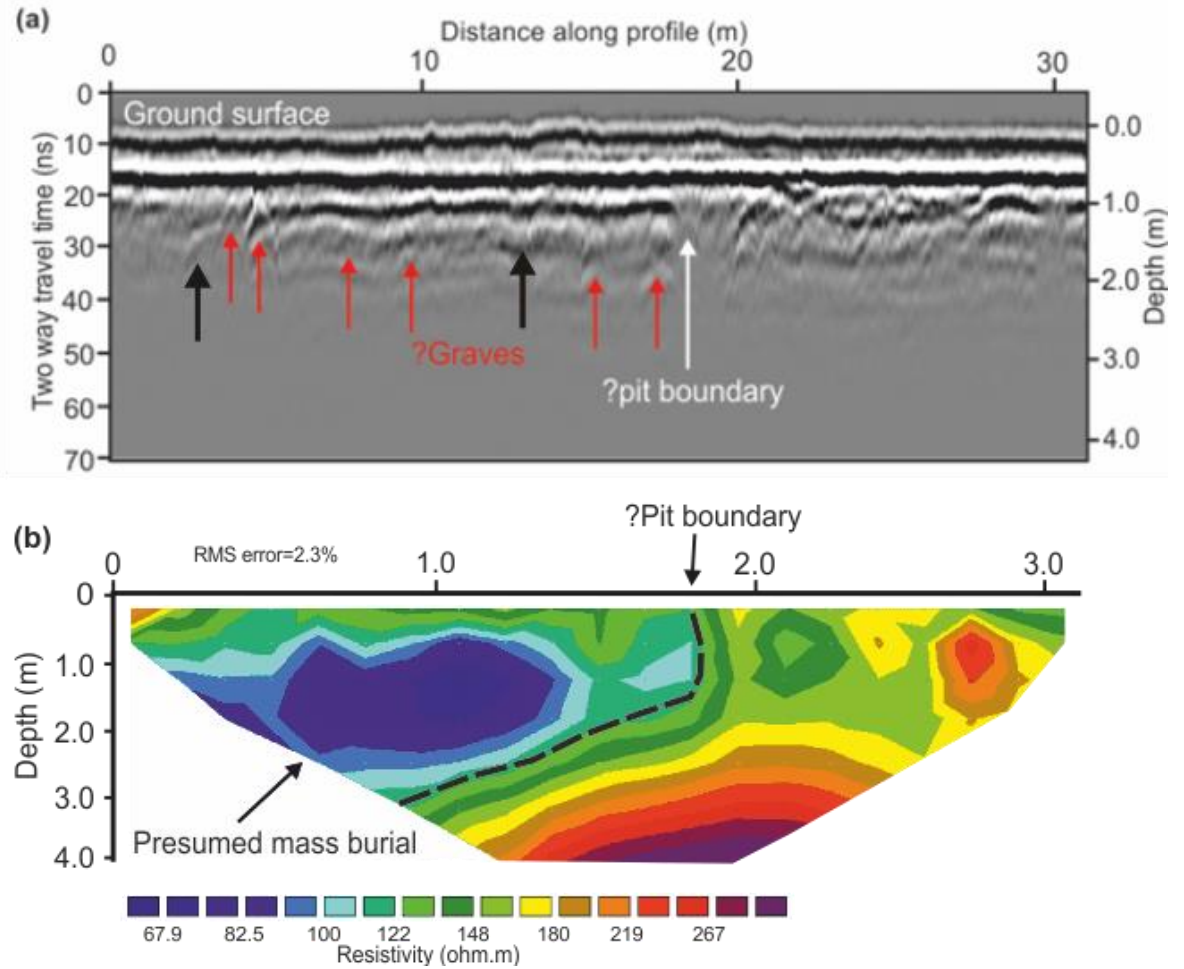


**Figure 3.14:** (a) 2D GPR (L25) and (b) ERI 1 profile across the parish boundary with marked interpretations (Fig. 3.2 for location). Modified from Dick *et al.* (2015).



### Line 29/ERI 2

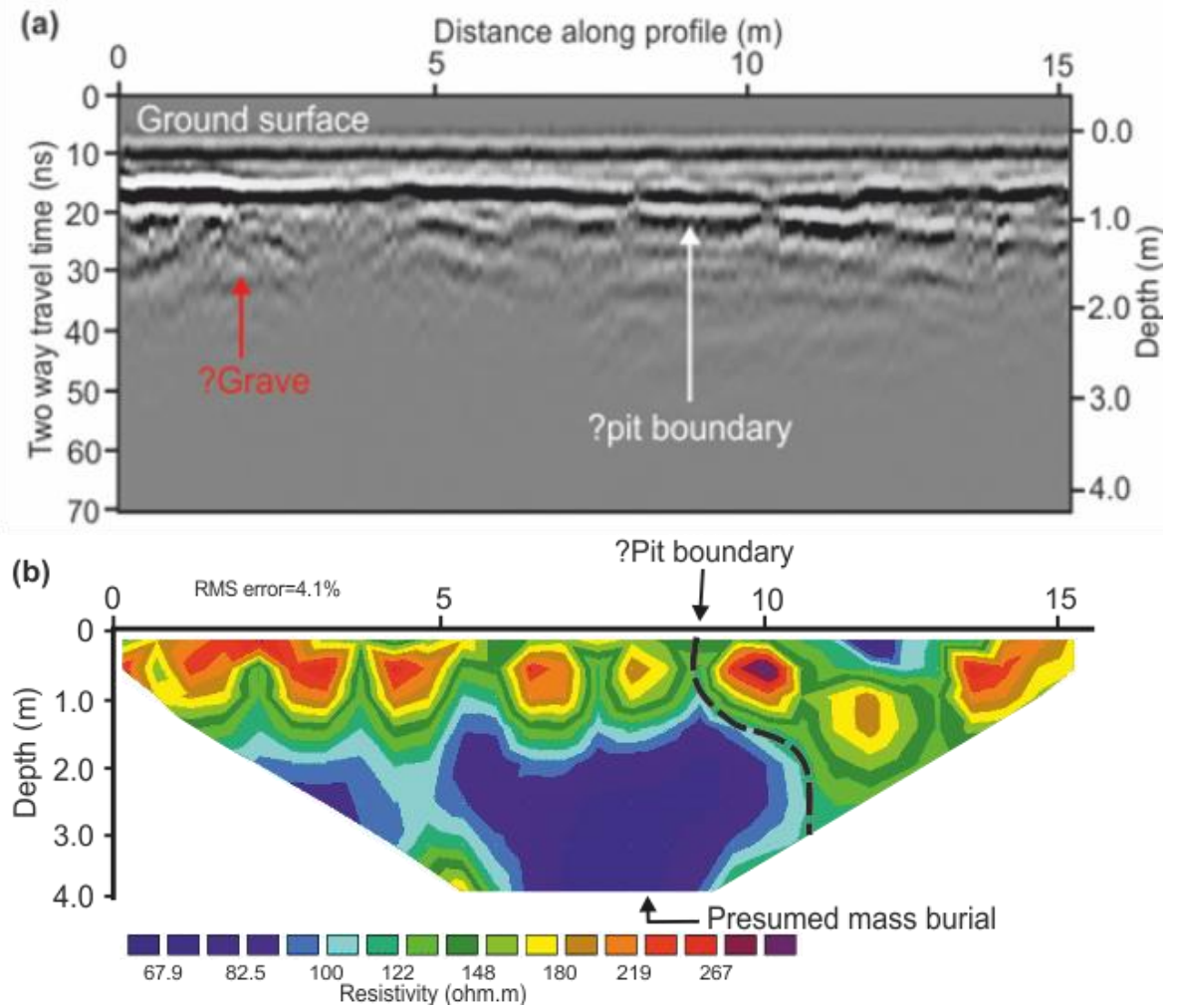


**Figure 3.15:** a) 2D GPR (L29) and (b) ERI 2 profile across the parish boundary with marked interpretations (Fig. 3.2 for location).

### 3.4 Discussion

The first aim of this study was “*to determine if non-invasive geophysical methods could both detect and characterise a potential ancient mass burial site*”. Clearly the non-invasive near-surface geophysical surveys have done this, identifying specific characteristics of the site, namely confirming that the eastern boundary of the emergency burial ground is the marked parish boundary, a square anomaly in the centre of the Square that may be buried foundations of a long-demolished but unidentified chapel, the still-remaining WW2 buried water tanks in the north-west of the site and lastly, but probably most importantly, a concentration of isolated buried objects in the south-west of the site that were probably isolated graves. Combining different geophysical techniques to gain extra information is also recommended as other authors have detailed (e.g. Milsom and Eriksen, 2011; Pringle *et al.*, 2012a), in this study it has allowed not only the identification of the eastern boundary with electrical resistivity (ERI), but also perhaps further identifying its character, being a central ditch and eastern bank that matched historical accounts (Porter, 2009). The WW2 water tanks in the north-west of the site were also identified by three techniques (EM, CST electrical resistivity and GPR). Table 3.4 and Figure 3.16 summarised the study findings. It was interesting that several of these targets were still geophysically detectable even after 660+ years of burial, thus evidencing that forensic geophysical surveys should still be undertaken to detect and characterise potential mass burial sites, even when significant periods of time have elapsed. Note that other sites may not have such optimum ground conditions, as other studies have evidenced the importance of soil type and local depositional environments on target detection (e.g. Brown, 2006; Ruffell *et al.*, 2009; Pringle *et al.*, 2012c).

**Table 3.4:** Tabulated list of geophysical targets encountered in this study and their geophysical responses (see Fig. 3.15 for location). Modified from Dick *et al.* (2015).

Site targets identified	Details	Geophysical responses
Mass burial eastern boundary	Historical records suggested bordered by ditch and bank	Not observed by EM, located by ERI and ditch & bank interpreted from 2D GPR profiles.
Mass burials	Historical records suggested buried in mass pits	Not observed by EM or electrical resistivity CST, 225 MHz GPR observed isolated burials present in south-west area.
Demolished building foundations	Two chapels known to have been onsite	Variable EM anomalies present in ~20 m <sup>2</sup> area in central part of Square, some GPR reflection events but masked by path,
WW2 fire-fighting water tanks	Records known to be present but perhaps removed	~18 m <sup>2</sup> object present in north-west of square, EM high conductive, electrical resistivity CST low resistance and strong horizontal radar reflectors that may have imaged top and base.

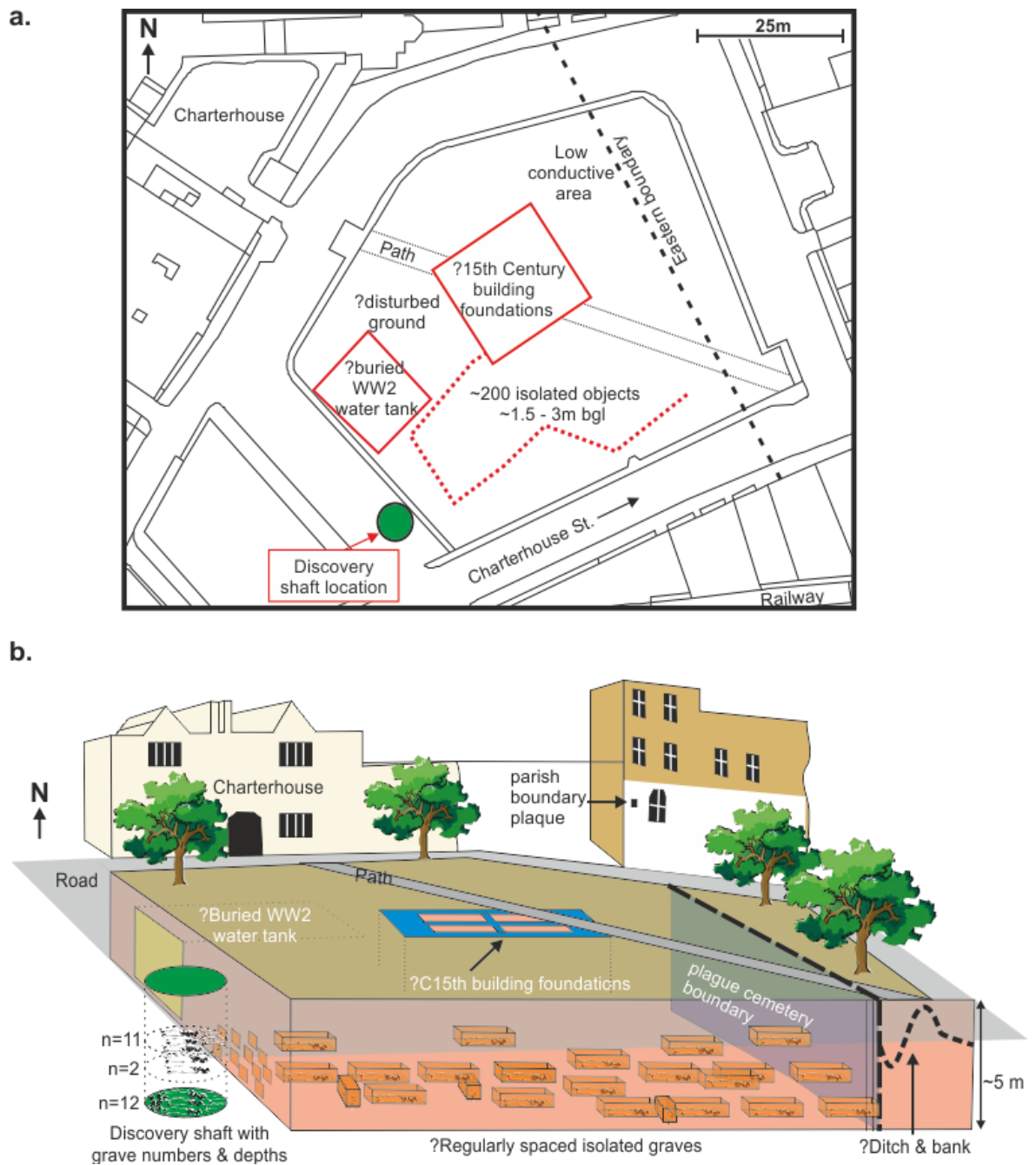


**Figure 3.16:** Summary showing geophysical interpretation, a) 2D planview map and b) Schematic 3D visualisation of the site (not to scale). Modified from Dick et al. (2015).

The second aim of this study was *“to detect further unmarked burials and if there were any particular areas of burial concentrations, and/or specific orientations, etc.”* The south-west area of the site clearly showed multiple, isolated, evenly-spaced and shallow buried objects which are most likely further graves containing archaeological remains (Fig. 3.16). Simply identifying separate isolated objects in 2D GPR profiles gave a conservative estimate of approximately 200 individuals; there may be more due to co-mingled remains present in graves as both this study (in the Cross rail shaft) and others, e.g. Kacki et al. (2011) study of contemporary remains in French cemeteries, have evidenced (see Fig. 3.6). Indeed historical records suggest that there may be several thousand individuals buried in this area (see Sloane, 2011), but it was unknown what burial style they may be, and if they had been removed or indeed built over subsequently. The isolated nature of individual burials was surprising, it was commonly thought that burials at the height of the Black Death plague epidemic were buried in mass burial pits, it was recorded at the time that *“so great a multitude eventually died that all the cemeteries of the aforesaid city were insufficient for the burial of the dead. For this reason, many were compelled to bury their dead in places unseemly, not hallowed or blessed; some, it was said, cast the corpses into the river”* (Sloane, 2011). The discovered burials in the Crossrail shaft had three different burial phases with clay-rich soil being deposited between each, perhaps in an attempt to prevent the spread of the disease (Fig. 3.16). Burial orientations looked to be similar to the discovered graves, namely approximately northeast-southwest but there could have been other orientations as north-south ones were observed in the shaft, it was difficult to further discern specific orientations of all remains with the datasets acquired. There do not seem to be many graves remaining in the north of the square and indeed outside the parish boundary; this

boundary looked to be the emergency burial boundary which matched historical records (Porter, 2009; Sloane, 2011).

The third aim of this study was *“to delineate the spatial extent of the burial site and, if possible, estimate quantitatively the depths below ground level of the target anomalies”*.

From the results of the geophysical survey, the lateral extent of the burial site (or emergency cemetery) is presumed to extend beyond the Charterhouse Square (survey site), although it was difficult to ascertain due to several fixed structures surrounding the site, preventing further data collection. The GPR 2D profiles acquired on the concrete surfaced road adjacent to the square on the north-west part of the area (Fig. 3.2) suffered serious radar signal attenuation and could not image the subsurface clearly. However, the initial site excavation by Crossrail revealed that several human remains (skeletons) were discovered outside Charterhouse square, overlain by the concrete road adjacent south-west part of the square (Fig. 3.2). On the other hand, both GPR and ERI 2D profiles (Figs. 3.13 and 3.14) have revealed the possible presence of the burial site boundary at the east part of the Square which confirms historical records of the boundary having a ditch and bank (Sloane, 2011). This boundary position also agrees with the parish boundary suggested by historical records (Fig. 3.16). During the initial Crossrail site excavation; there were three different depths to the discovered human remains ranging from approximately 2 m to 3 m below ground level. This range of depths corresponded with the GPR dataset and time-slice interpretation showing approximately 200 isolated objects present in the surveyed site of depths between 1.2 and 2.7 m (Table 3.5 and Fig. 3.17). The slight variation in depth between Crossrail site excavation and GPR dataset values

was based on their topographies, due to the presence of road surface tarmac of approximately 0.3 m thickness covering the top of excavation site which could be reconciled by adding 0.3 m to each GPR dataset depth value acquired at the Square. The GPR datasets confirmed that the target anomalies have an average depth of approximately 1.7 m bgl and standard deviation of 0.31 (Fig. 3.17). Statistically, ~46% of the anomalies were buried between 1.5 m and 2.0 m, approximately ~42% were buried between 1.0 m and 1.5 m, ~10% were buried between 2.0 m and 2.5 m, ~2% were buried between 2.5 m and 3.0 m and no anomaly was discovered above 1.0 m and below 3.0 m bgl (see Fig. 3.17).

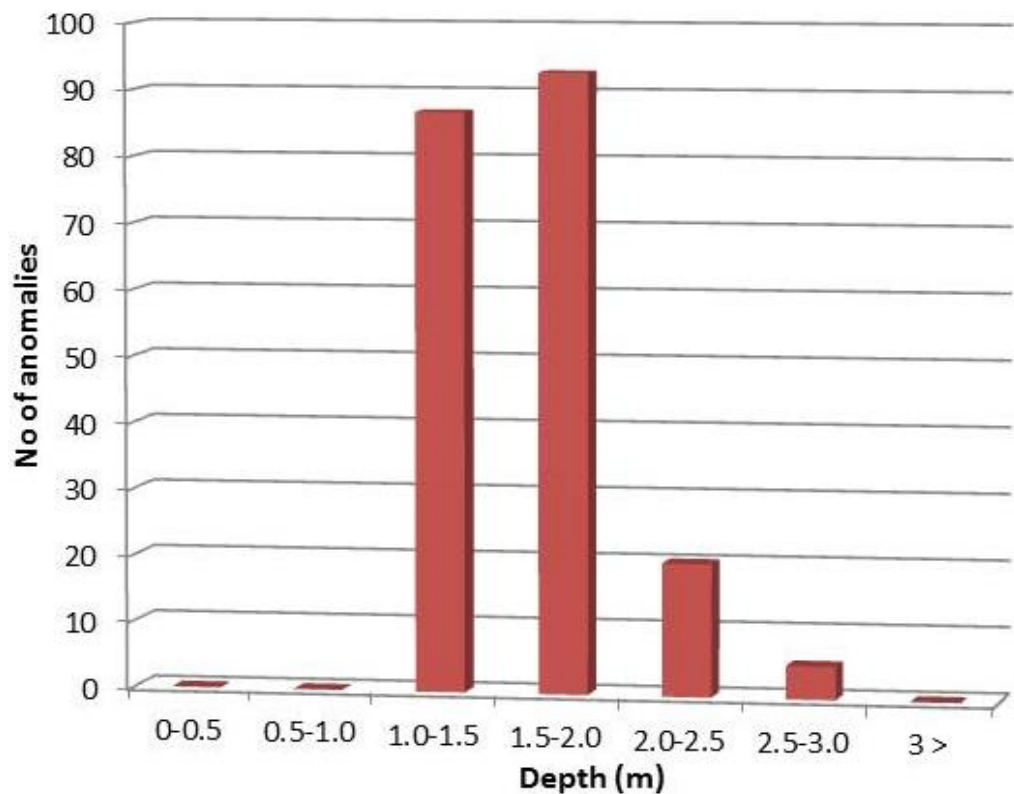


**Figure 3.17:** Depth distribution of anomalous objects identified on 20 selected 2D GPR profile lines in Charterhouse Square, Central London.

**Table 3.5:** Anomalies depth bgl present on 2D GPR profiles in the survey area.

Profile no.	Buried depth (m)																			
	G1	G2	G3	G4	G5	G6	G7	G8	G9	G10	G11	G12	G13	G14	G15	G16	G17	G18	G19	G20
1	2.0	2.7	2.7	2.7	2.7	2.5	2.7	2.1	2.1											
2	1.5	1.5	1.7	1.7	1.6	1.8	1.8													
3	1.3	1.6	1.8	1.4	1.9	1.7	2.3	2.2												
4	1.4	1.5	1.5	1.7	1.3	1.9	2.2	2.0	2.0	1.7	1.9									
5	1.6	1.4	1.4	1.4	1.5	1.2	1.5	1.5	1.2	1.2	1.6	1.3	1.2	1.6	1.5	1.7	1.5	1.5	2.1	2.1
6	1.5	1.6	1.9	1.7	1.2	1.8	1.8	1.4												
7	1.3	1.8	1.8	2.0	1.8	2.0	2.0	2.1	1.6	2.1										
8	1.5	1.8	2.1	1.8	1.6	1.6	1.8													
9	1.4	1.4	1.9	2.3	2.1	2.1	2.2	1.3	2.0	1.4	2.0	1.7	1.5	1.5	1.5	1.8				
10	1.4	1.9	1.5	1.5	1.5	1.5	1.5	2.1												
11	1.4	1.7	1.7	1.7	2.0	1.7	1.8	1.3	1.5	1.7	1.7									
12	1.3	1.5	1.5	1.7	1.7	1.8	2.2	1.5	2.2	1.8	2.0									
13	1.9	1.9	1.6	1.5	1.5	2.1	1.8	2.0	2.0	2.0										
14	1.5	1.3	1.7	1.7	1.7	1.7	1.8	1.7	1.7											
15	1.3	1.7	1.4	1.7	1.8	1.8	1.7													
21	1.4	1.4	1.3	1.4	1.3	1.5	1.5	1.4	1.3	1.4	1.4	2.0	2.0	2.1	1.5	1.4	1.5	1.8		
25	1.8	1.4	1.4	1.7	1.7	1.7	1.8	1.8												
27	1.7	1.5	1.7	1.9	1.7	1.7	1.5	1.3	1.7	1.8	1.4	1.5	1.3							
28	1.5	1.4	1.4	1.2	1.4	1.3	1.3	1.2	1.4	1.6	1.3	1.6	1.5							
29	1.5																			



The depth to the top of the buried WW2 water tank was estimated to be approximately 0.6 m below ground surface from the GPR datasets (Fig. 3.12); however, its bottom depth was not detected by GPR due to either signal attenuation or the antenna frequency depth limit.

The fourth aim of this study was *“to compare different geophysical techniques and equipment configuration to determine the optimum method for such an urban search scenario”*. From the results of this study, to detect a mass burial, a multi-phased approach using different geophysical techniques should be undertaken as best practise has detailed (Harrison & Donnelly, 2009; Larson *et al.*, 2011; Pringle *et al.*, 2012a). After the desk study, historical records and remote sensing methods should identify the potential burial site(s), then during the site reconnaissance stage, as well as the soil and bedrock type should be determined, trial surveys using available near-surface geophysical equipment should be undertaken. In this case study electro-magnetic, electrical resistivity and GPR methods were all trialled to initially determine if the potential target was geophysically detectable, i.e. measureable from background value. EM datasets were rapidly acquired over the potential mass burial site and the bulk ground changes detected before follow-up, higher resolution geophysical datasets were collected and this approach is to be recommended for other ancient mass burial detection surveys. Trial surveys could also be used to decide upon optimal geophysical equipment configurations. For example, multi-frequency GPR antennae were trialled on 2D profile lines, with the 225 MHz frequency antennae judged to have the best results. This mid-range frequency has been shown by others to be optimal to detect buried forensic objects at least 1 m depth bgl (e.g. Ruffell *et al.*, 2009; Ruffell and Kulesa, 2009; Pringle *et al.*, 2009) and not

high frequency (700MHz and above) which some search teams operate with the idea that it gives the best resolution. Electrical resistivity CST datasets were not promising in this study, even with 1 m fixed-offset probe spacings that other studies have been successful with (e.g. Hansen *et al.*, 2014), it did not successfully identify locations of suspected grave positions. It could be that this equipment was still not penetrating to the required depths bgl but, more likely, the heterogeneous nature of the site effectively masked the target burials with this technique. ERI 2D profiles were judged very useful for delineating mass burial area geometries, as others have shown (e.g. Brown, 2006), especially as they penetrate much further bgl than other techniques, up to 50 m bgl in ideal conditions (see Milsom and Eriksen, 2011). It should be noted, however, that the GPR data on the same 2D profile lines had better resolution of the mass burial boundary, on what was now known, to be the emergency cemetery boundary.

The fifth and final aim of this study was “*to compare this study to other mass burial search studies*”. There are hardly any geophysical detection of mass burial studies in the published academic literature, Ruffell *et al.* (2009) did use a combination of geographic and GPR techniques to successfully locate and characterise a 19<sup>th</sup> Century Irish mass burial, Witten *et al.* (2001) detail a multi-geophysical approach using electrical resistivity and magnetics to locate a 1920s race riot mass burial site in the US and Brown (2006) lists ERI as a potential technique to locate a 1990s mass burial site in Bosnia. From the data in this study it is suggested to use EM techniques to identify the potential mass burial location, ERI 2D profiles to characterise the burial margins and mid-frequency radar 2D profiles to characterise its content. Indeed Ruffell and Kulesa (2009) used a similar

process, using ERI and low frequency GPR to characterise modern animal mass burial sites in Ireland.

### **3.5 Conclusions, study limitations and further work**

A discovery of human remains in central London occurred in 2013 with subsequent radiocarbon dating and aDNA analysis finding individuals were victims of The Black Death plague strain in 1348-9 AD. A multi-technique and integrated forensic geophysical survey was subsequently undertaken of the adjacent Charterhouse Square. Although such historic graves are often challenging to locate with near-surface geophysics, because they are both small targets and leave little in the way of a geophysical anomaly to measure geophysically, and despite the significant time from interment to survey (approximately 660 years of burial), the surprisingly isolated graves and the mass burial boundary were still geophysically detectable.

An EM, ERI and GPR survey characterised the site, finding an eastern boundary with suspected ditch and bank that matched historical records, concentrations of isolated burials in the south-west of the site and subsequent relict building foundations and WW2 water tanks remaining. This study shows the potential of geophysical techniques to both detect and characterise historic and modern mass burials. Although geophysical techniques are crucial in the successful detection of targets in forensic and archaeological searches, many ground contamination investigations also rely on the application of geophysical techniques, especially to determine potential sources and impacts of pollutants in soils. There was no detectable pollution plume in the emergency cemetery site as would be expected for recent mass burials, presumably due to the time since

burial which therefore did not necessitate further geochemical analysis of soil/groundwater samples from the surveyed site as was initially intended.

While this study, like others (e.g. Pringle *et al.*, 2010a; Marchetti and Settimi, 2011; Reynolds, 2011), has focused on field trials, there is need to mention limitations surrounding this data acquisition. This is important in order to effectively evaluate the relevance of trends observed for the mass burial graves and the parish boundaries in the surveyed area. Not much surveying was conducted outside the Square to gain more background values and identify north, south and west boundaries of the emergency cemetery due to site constraints such as building structures and other fixed infrastructures. Another shortcoming was not being able to collect soil samples from the survey site due to restrictions which would have aided to providing ground-truth within the Square and thereby identify and validate effectively the causative anomalies. The intrinsic lack of depth resolution in using 225 MHz GPR antenna system provides a main sensitivity to the near surface features, perhaps this may have suffered signal attenuation after detecting shallow anomalies which could prevent further detection of deeper anomalies vertically below shallow ones and others within 3 m bgl and above. Whilst the initial report on archaeological site excavation reveals two different orientations (NE-SW and N-S) for the encountered human skeletal remains, the GPR dataset could not provide any further information about the orientation and alignment of the buried anomalies in the surveyed site. Lastly, due to the limited time assigned for this geophysical data acquisition, GPR survey was not covered over the entire Charterhouse Square.

This experimental methodology should be repeated in forensic searches for more recent mass burials, perhaps in animal mass burial sites and also concentrating on the geological and hydrological properties of these burial sites. In order to appropriately provide empirical evidences as to whether the selected mass burials have caused any kind of contamination or pose human health hazards to the local human population, soil/groundwater samples should also be collected both from within and around selected mass burial sites for laboratory analyses. This combination of integrated geophysical techniques and geochemical surveys is a better approach and leads to accurate characterisation of soil spatial variability as others have evidenced (e.g. Fontoura *et al.*, 2011), and may provide an improved standard workflow and protocol to scientifically investigate potential contaminated site associated with animal/human mass burials. In addition, information from this survey may be used to model the expected response of mass burial sites provided the target and background site properties are known.

## **CHAPTER 4: Determining optimum geophysical techniques and equipment configurations in English church graveyards.**

### **4.1 Introduction**

Graveyards and cemeteries are suffering from a lack of burial space, for example in the UK there are less than ¼ of burial grounds that have room to accept new burials (London Planning Advisory Committee, 1997; Hansen *et al.*, 2014) with the need to accommodate ~140,000 burials every year (Environment Agency, 2004). According to the Environmental Agency (2004), approximately 70% of graveyards in the UK are owned by the Church of England. Re-use of existing graveyards and cemeteries is one solution, for example, burial regulation relaxations have been in force in London since 2005 (Ministry of Justice, 2006). However, burial ground records, if they are available, rarely indicate burial positions, and even grave headstones are not always reliable burial position indicators (Fiedler *et al.*, 2009a; Hansen *et al.*, 2014). It is also currently unlawful to disturb or exhume human remains in the UK unless with substantial and compelling reasons to do so, unlike in some other European countries (e.g., France and Germany) where human remains can be exhumed after a specified number of years to give space for new internments (Aries, 1982).

As shown in Figure 4.1, multiple burials in a single grave, usually by family members, have been used due to burial space shortages and cost implications (Castex and Reveillas, 2007; Duday, 2007). However, this has resulted in grave maintenance issues such as;

collapse grave walls, displaced grave headstones or footstones and can be problematic with re-using brick-built vaults. Single graves with multiple burials can also be more difficult to identify, following the possible displacement or misalignment of their headstones after previous internment in the grave (see Fiedler *et al.*, 2009a)



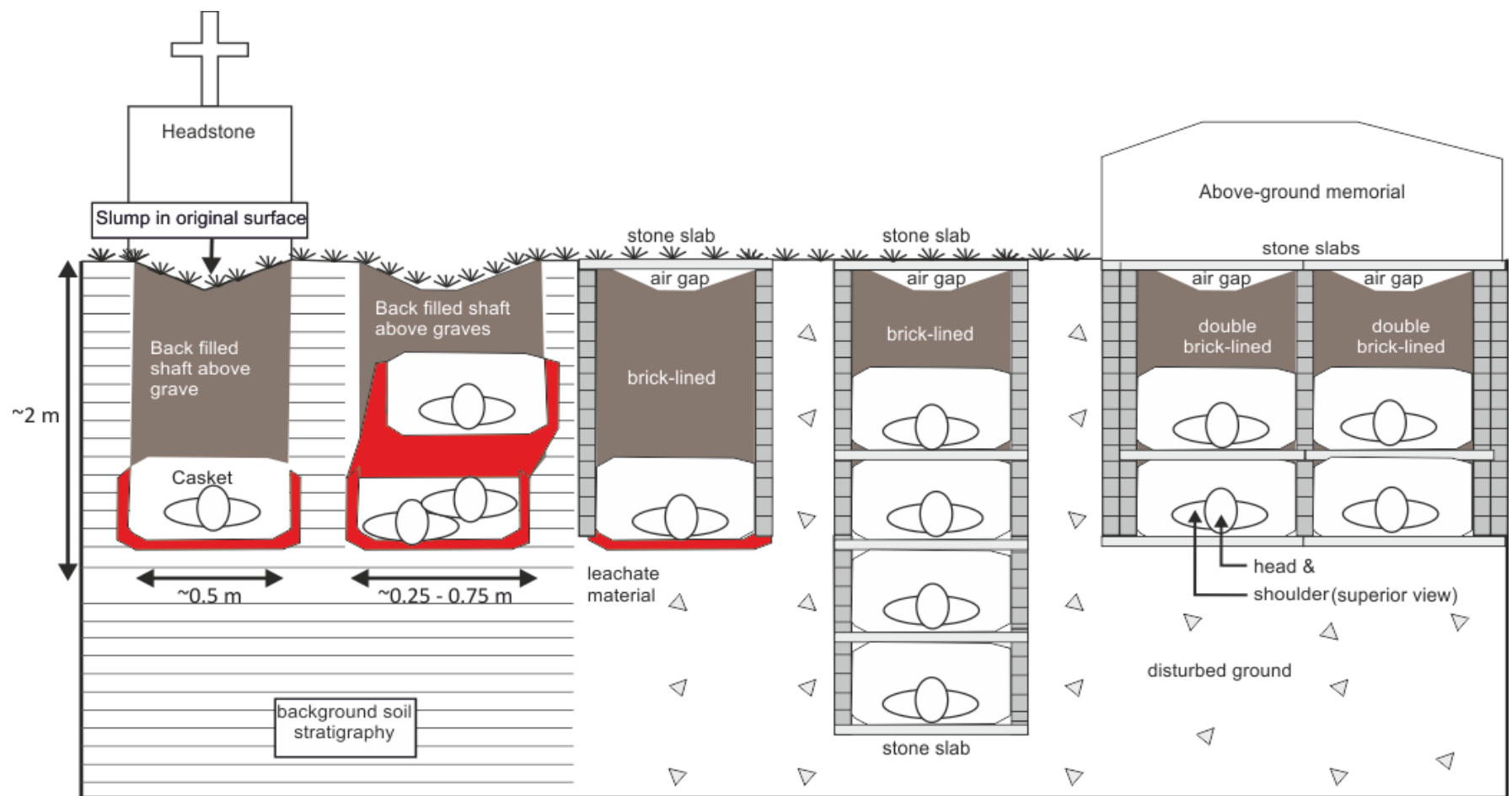


**Figure 4.1:** Generalised schematic of burial styles encountered in the three case studies discussed (modified from Hansen and Pringle, 2011).

#### 4.1.1 Grave detection methods

Researchers have used remote sensing methods to identify unmarked burials in graveyards (e.g. see Brilis *et al.*, 2000a,b). Ruffell *et al.* (2009) successfully identified historic (150-160 years old) unmarked graves using aerial photographs and confirmed positions by subsequent non-invasive geophysical surveying. Forensic surface geomorphology methods have also been utilised for successful detection of burial positions (see Ruffell and McKinley, 2014). Localised vegetation growth may also have different characteristics to background areas, for example, different species and with more or stunted growth (Dupras *et al.*, 2006) that Larson *et al.* (2011) suggests may be due to localised pH soil changes and differing ground characteristics of the burial compared to surrounding areas. Pringle *et al.* (2012a) give a comprehensive overview of current relevant search methods and case study examples.

A ground-based, non-invasive detection technique that has been utilised to effectively detect graves is near-surface geophysics. Commonly-used methods include electrical resistivity, bulk ground conductivity, magnetic and ground penetrating radar methods (see Reynolds, 2011; Milsom and Eriksen, 2011; Pringle *et al.*, 2012a).

Electrical resistivity surveys have been successfully used to locate unmarked burials in cemeteries (e.g. see Senos Matias *et al.*, 2004) and graveyards (e.g. Figure 2.10 and Hansen *et al.*, 2014), control studies on modern burials evidencing that decompositional fluids may be the dominant factor in graves that are detected electrically (see Jervis *et al.*,

2009a; Pringle *et al.*, 2012b), and may be retained in grave soil for considerable periods of time post-burial (see Pringle *et al.*, 2015a). However, for older burials (100 years and older), there is a decreasing likelihood of detection, some authors attributing this due to bone and organic degradation over time, thus reducing the contrast between the grave, its contents and undisturbed background areas (Damiata *et al.*, 2013). However, this is variable with geophysical surveys of historic burials sometimes having success (see, for example, Pringle *et al.*, 2015b; Dick *et al.*, 2015). It has also been found that local variations in soil type and moisture content, particularly when surveying in dry conditions in heterogeneous ground, affect surveys by masking target locations (e.g. see Hansen *et al.*, 2014). Resistivity surveys respond to differences in the electrical conductivity of soils and is, thus, strongly dependent on contrasts in soil moisture and porosity (see Jervis *et al.*, 2009b). Dry soil or gravel, whose pore space lacks water, or where soil are saline, all typically record relatively high resistivities (Reynolds, 2011). However, most soils record medium or low resistivity, compared to typical values, especially if clay minerals are present. All these factors make resistivity datasets difficult to interpret, but its advantage over other techniques still lies on being free of interference of nearby buildings and above-ground effects (Reynolds, 2011).

Electro-magnetic (EM) surveys in graveyards have shown variable detection success, being affected by the relatively small targets and by above-ground sources in urban areas (see Nobes, 1999; Pringle *et al.*, 2012a), they therefore have not been considered in this study.

Magnetic surveys for ancient archaeological graves have been successful, but for modern burials have had varied detection success for graves (see Stanger and Roe, 2007; Juerges *et al.*, 2010; Pringle *et al.*, 2015a and Figure 4.2). Magnetic susceptibility measurements rely on the magnetic property of soil, which depends on the presence of mainly a combination of dia-, para-, and ferro/ferri-magnetic minerals (Reynolds, 2011). These minerals were either originated from the parent rocks or due to anthropogenic activities (Linford, 2004). There are wide variations in measured magnetic susceptibility reported between different soil and rock types (Dearing *et al.*, 1996). In soils, the presence of the ferromagnetic mineral maghemite ( $\text{Fe}_2\text{O}_3$ ,  $\gamma\text{-Fe}_2\text{O}_3$ ) has a dominant effect on the magnetic susceptibility; therefore, any soil with ferromagnetic mineral tends to show high magnetic susceptibility when compared to other soils (Reynolds, 2011). Another factor that affects the magnetic susceptibility of soil is fire. Weakly magnetic iron oxides in clay and silt particles are transformed into highly magnetic oxides through burning, and when the organic matter in a soil burns at  $\sim 600^\circ\text{C} - 700^\circ\text{C}$ , it produces effects that can significantly change the overall soil magnetic susceptibility (Crowther and Barker, 1995).

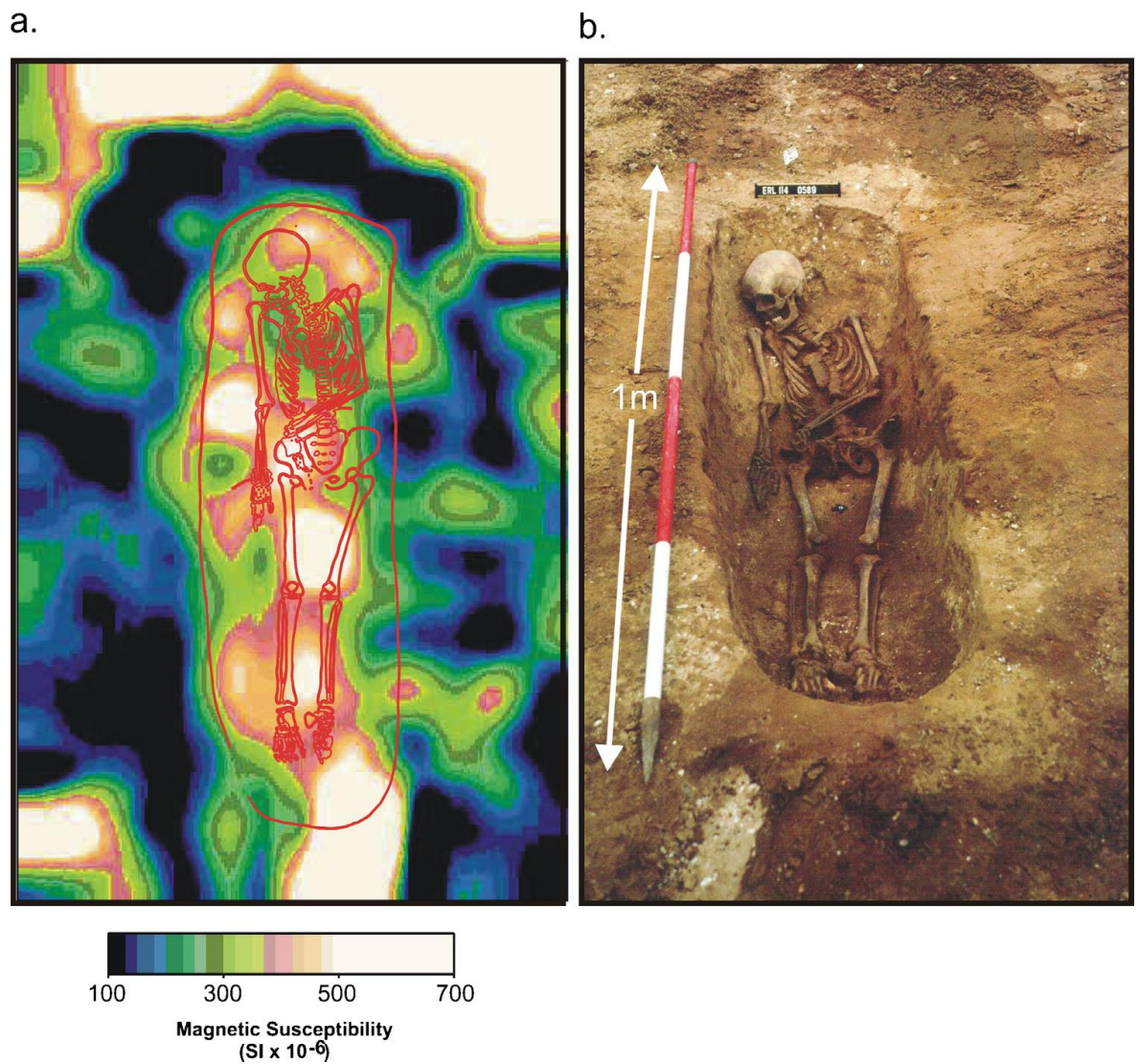


**Figure 4.2:** Historic Anglo-Saxon grave study in East Anglia, U.K. (a) magnetic susceptibility survey results and (b) excavated remains (from Pringle *et al.*, 2015a).

The depth of investigation of GPR is generally quite shallow (typically 10 m bgl or less) due to the inherent attenuation of high frequency electromagnetic waves by the relative permittivity of soil material. In natural soil, dielectric permittivity might have a larger influence than electric conductivity and magnetic permeability (Takahashi *et al.*, 2011).

According to Cassidy (2009), relative permittivity is a dimensionless constant that describes a materials capacity to store and release electromagnetic energy in the form of an electrical charge. It also varies with the amount of free and bound water. Relative permittivity ranges from 1 for air to between 78 and 88 for water (Cassidy, 2009). Small increments in water moisture can result in substantial increases in the relative permittivity of soils (Daniels, 2004). The use of 100 MHz GPR antenna by Daniels (2004) shows relative permittivity between 2 and 10 for most dry soil material and between 10 and 30 for most wet soil, while the relative permittivity of saturated peat deposits ranged between 43 and 69 (Ulriksen, 1982). The dielectric permittivities of various common materials are shown in Table 4.1. Typically GPR data is collected in a 2D profile by sequential 1D traces by fixed-offset transmitter/receiver antennae (Milsom and Eriksen, 2011). The amount of energy reflected back to the receiver antenna is a function of the dielectric permittivity gradient that exists across a soil interface or boundary (Reynolds, 2011). The greater and more abrupt the contrast in the dielectric properties of adjoining soil materials, the greater the amount of energy is reflected back to the antenna, and the more intense and conspicuous the amplitude of the reflected signal appearing on radar records (Ruffell and McKinley, 2005). Soil horizons, layers and features that have similar relative permittivity, are relatively poor reflectors of electromagnetic energy and are difficult to identify on radar records. However, the main pitfall of GPR is the lack of penetration in certain mineralogical clays and other highly conductive materials.

**Table 4.1:** Typical range of dielectric characteristics of various materials measured at 100MHz GPR antenna frequency (Daniels, 2004; Cassidy, 2009)

Materials	Relative permittivity	Conductivity (S/m)	Attenuation constant (dB/m)
Air	1	0	0
Freshwater	81	$10^{-6}$ - $10^{-2}$	0.01
Clay, dry	2-6	$10^{-3}$ - $10^{-1}$	10 - 50
Clay, wet	5-40	$10^{-1}$ - $10^{-1}$	12 - 100
Sand, dry	2-6	$10^{-7}$ - $10^{-3}$	0.01 - 1
Sand, wet	13-30	$10^{-3}$ - $10^{-2}$	0.5 - 5

GPR has been used to locate unmarked grave burials in graveyards and cemeteries with varying degrees of success (e.g. Nobes 1999; Fiedler *et al.*, 2009a; Hansen *et al.*, 2014 and Figure 4.3), and indeed of a suspected clandestine burial of a murder victim within a graveyard (Ruffell and McKinley, 2005). Suggestions by researchers (e.g. Schultz, 2008; Ruffell *et al.*, 2009; Hansen *et al.*, 2014) suggest optimum 200 MHz – 400 MHz frequency antennae to detect unmarked burials but this varies depending on a host of specific site factors. GPR has wide applications in many different sediment and soil types, the best energy penetration and subsurface resolution occurs when the ground is electrically resistive (Conyers, 2006a). GPR is a geophysical technique that is most effective at burial sites where remains are located within 1-3 m of the surface (Conyers, 2006a).

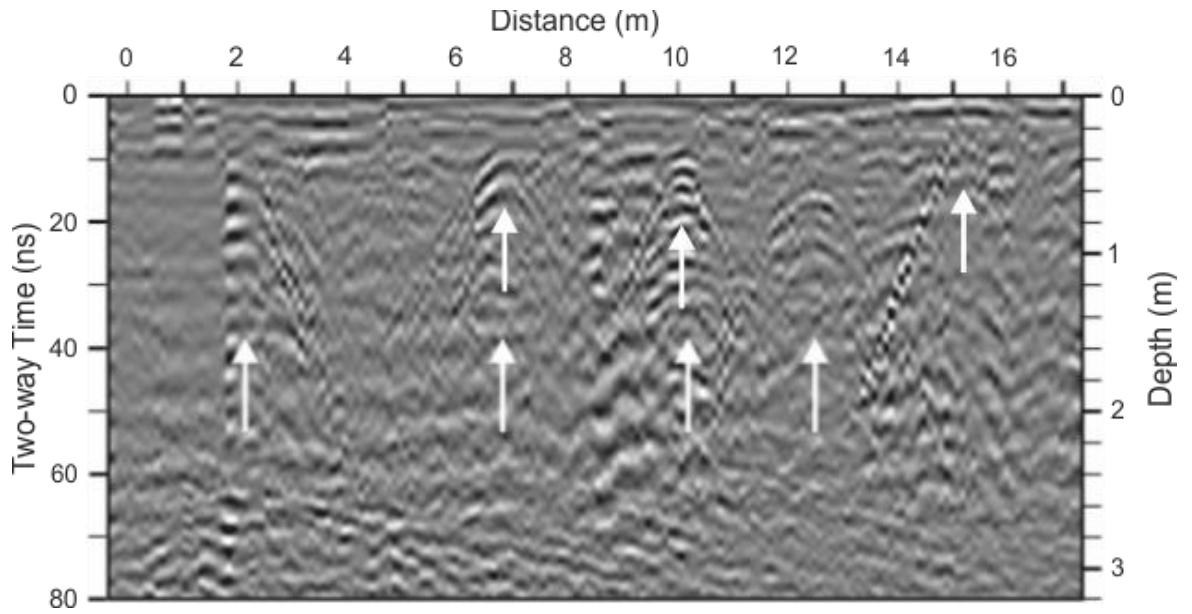


**Figure 4.3:** 2D GPR profile example acquired in a graveyard (graves marked by arrows) in London, UK (edited from Hansen *et al.*, 2014).

## 4.2 Aims and Objectives

The age or time since grave burial is defined here as *‘the time taken between grave internment in the burial site and when a geophysical survey was acquired’*. Assuming that other variables remain constant (see section 4.1.1), it is expected that geophysical responses over burial site graves, compared to background values, will decrease as the age of burial increases. This is primarily due to the gradual reduction in target size of organic matter (Schultz, 2008), ‘grave soil’ fluid conductivity (Pringle *et al.*, 2015b) and soil porosity to background levels (Jervis *et al.*, 2009a). A schematic representation of the possible expected trends (1 – 4) are shown in Figure 4.4. A control study has been undertaken by Pringle *et al.*, (2016) to investigate this, however, was limited to a 6 year



period and thus did not account for older burials; it also excluded magnetic susceptibility as a detection technique.



**Figure 4.4:** A hypothesis showing possible expected trends of the potential geophysical response (any technique) against age of burial.

Apart from burial style (detailed in Section 4.1), another important variable to be considered is the study site soil type(s), which will comprise of a unique mixture of both natural (sand, clay and silt) and anthropogenic materials. Soil behaviour can sometimes be difficult to predict due to high spatial variability that often make it almost impossible to estimate. The successful application of geophysical techniques largely depend on the physical properties of soil; there needs to be a significant and detectable contrast between the burials and the different constituents in the subsurface, such as density, velocity, electrical resistivity, conductivity, magnetic susceptibility, etc. (Hillel, 2004).

Therefore, the geophysical response of a grave will depend on the site soil and on the nature of the burials (Nobes, 1999).

This chapter therefore seeks to assist with the application of geophysical techniques to support forensic and archaeological searches, in the identification and prediction of time since burial of clandestine graves and to locate available burial spaces in burial grounds.

This study aims are to: *firstly* determine if the hypothesis given in Figure 4.5 is true, *secondly* determine the optimal geophysical detection method(s) and equipment configuration(s) of different aged burials and *thirdly* gain knowledge of the effect of different soil types on burial grave detection.

Therefore, the study objectives to achieve these aims are;

- i) Acquire data from multi-geophysical surveys at different burial sites of marked graves with known burial ages;
- ii) Create a database of the relationship between geophysical responses and the time since burial, and their effects on detectability using different geophysical techniques;
- iii) Determine the optimum geophysical techniques for predicting age since burial in the different survey sites;
- iv) Determine burial occupancies in surveyed graves to quantify this variable;
- v) Quantify the soil type(s) in study sites.

### **4.3 Materials and methods**

#### *4.3.1 Study sites*

Three study sites “Church of England graveyards” were selected, St. Michael’s, Stockton, Norfolk, St. John’s, Keele, Staffordshire and St. Luke’s, Endon, Staffordshire, see Figure 4.5 for locations. Each graveyard had statistically significant (10+) known grave positions with known contents on headstones and with burial ages ranging from the 19<sup>th</sup> Century to the present day. Importantly; permission to undertake the surveys and indeed project were also granted by the respective church vicars and their congregations. The surveyed graveyards also had contrasting soil types as this is an important variable as mentioned, St. Michael’s was clay-rich and silt, St. John’s was sandy clay and St. Luke’s was pebbles and sand.



**Figure 4.5:** UK map showing the three graveyards (see key) survey site locations.

The number of surveyed graves in the three sites also varied, depending on both the range of burial ages and their spatial positions within the respective graveyards. Some potentially suitably-aged graves were not selected to be surveyed due to site constraints, proximity to objects that may potentially cause anomalous results (e.g. trees, walls etc.) or had surface obstructions (e.g. above-ground memorials) that were popular in the inter-war period (1918-1939), see Figure 4.6.

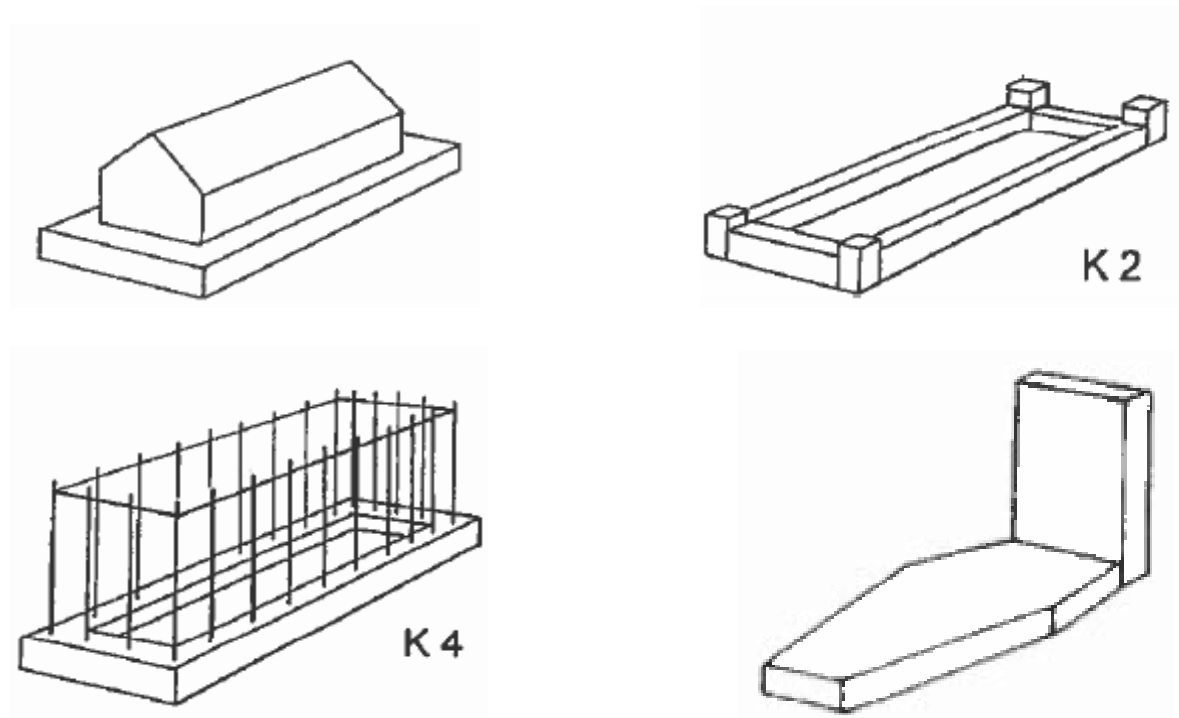


**Figure 4.6:** Examples of church graveyard above-ground memorials that were not able to be geophysically surveyed (modified from Goodwin, *pers. comm.*).

#### 4.3.2 *Geophysical site specifications*

Following standard geophysical survey protocols (see Milsom and Eriksen, 2011; Reynolds, 2011), desk studies were initially performed on all three sites to determine soil and bedrock types, site maps, etc. (see later). Reconnaissance surveys were then undertaken to collect 1D soil augers to determine soil types on site, as well as selecting graves to be surveyed, optimal survey line orientations and collecting trial data to determine optimum equipment configurations according to best practice advice (see Reynolds, 2011; Larson *et al.*, 2011; Pringle *et al.*, 2012a).

### **4.4 Determining optimal equipment/survey acquisition configurations and data processing**

#### 4.4.1 *Optimal spacing of electrical resistivity probes*

A profile line 13.6 m long over 9 known graves and ages (see details of test profile lines in Table 4.2) was created and used at St Michael's Church graveyard Stockton, Norfolk (Fig. 4.5 for location), to determine the optimum resistivity electrode probe spacing for detecting known grave positions (Fig. 4.7).



**Figure 4.7:** Photograph of Test Line 2 and the Geoscan RM15-D electrical resistivity meter, set up with both 0.5 m and 1 m resistance data, being simultaneously collected at each sampling position at Stockton graveyard, Norfolk, UK.

From looking at the results (Fig. 4.8), the 0.5 m electrode spacing showed significant variation of results (15  $\Omega\cdot\text{m}$  - 40  $\Omega\cdot\text{m}$ ) when compared to the 1 m electrode spacing (11  $\Omega\cdot\text{m}$  - 18  $\Omega\cdot\text{m}$ ); the 0.5 m spaced data also had anomalies that could be correlated to known grave positions. This is an interesting result as 0.5 m spaced data should not be able to penetrate to the typical grave depth of 1.8 m bgl, whereas the 1m probe spacing should (penetration depths being typically 1-2 x electrode spacing, see Milsom and Eriksen, 2011); it is theorised that either the resolution is not good enough when using 1

m spaced probe and/or the 0.5m probe is picking up grave soil rather than the grave (Hansen *et al.*, 2014).

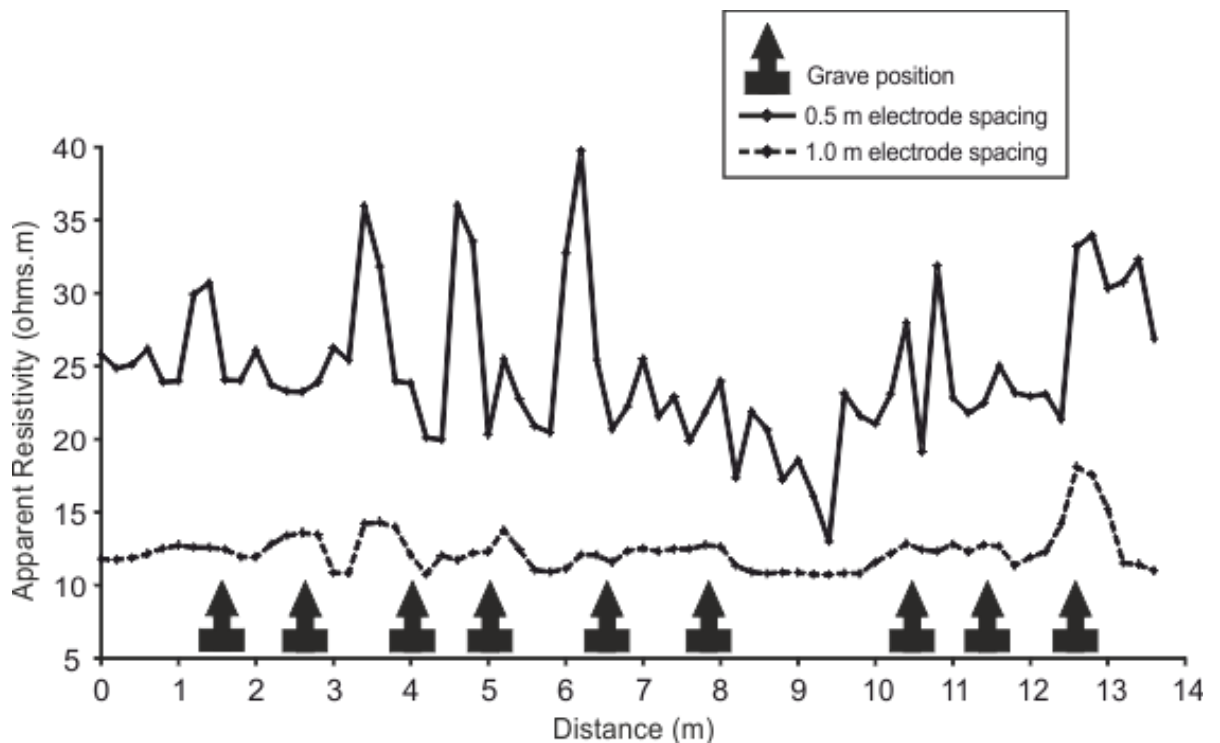


**Figure 4.8:** Graph showing a comparative analysis of 0.5 m and 1.0 m resistivity electrode spacing on a test line 1 m away from known grave positions (marked) in Stockton graveyard, Norfolk, UK.

The same procedure was also undertaken at a second graveyard site, St. John's Church, Keele, Staffordshire, UK (Fig. 4.6 for location). A test profile line over 7 known graves (see Table 4.2) was used here. The reconnaissance survey this time used 0.25 m, 0.5 m and 1.0 m fixed off-set electrode probe spacing (Fig. 4.9).





**Figure 4.9:** Photograph of test line and the Geoscan RM15-D electrical resistivity meter set up with 0.25 m, 0.5 m and 1 m resistance data being simultaneously collected at each sampling position on the 0.5 m, 1 m and 1.5 m (marked) survey lines at Keele graveyard, Staffordshire, UK.

From looking at the results (Fig. 4.10), the 0.5 m electrode spacing showed significant variation of results (164  $\Omega\cdot\text{m}$  - 194  $\Omega\cdot\text{m}$ ) when compared to the 1 m electrode spacing (65  $\Omega\cdot\text{m}$  - 75  $\Omega\cdot\text{m}$ ); also with evidence of anomalies that could be correlated to burial positions. Both the 0.25 m and 1 m spaced data showed less sensitivity with less or no anomalies present over grave positions. The three survey lines (Fig. 4.9) also allowed data to be contoured and map-view results shown (Fig. 4.11). Based on the test results, the 0.5 m fixed-offset electrode spacing was selected for full surveys in the three investigated sites.

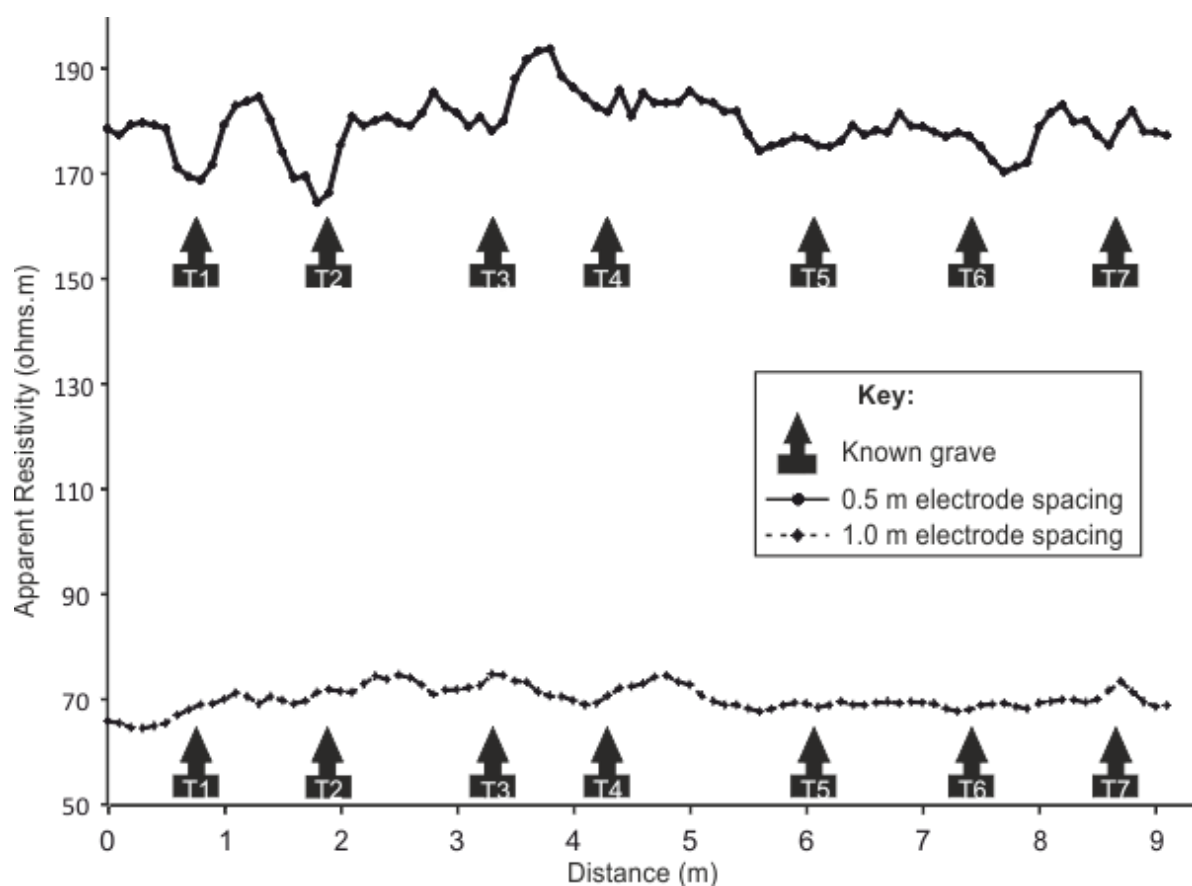


**Figure 4.10:** Graph showing comparative analysis of 0.5 m and 1.0 m resistivity electrode spacing on a test line 1 m away from known grave positions (marked) in Keele graveyard, Staffordshire, UK.

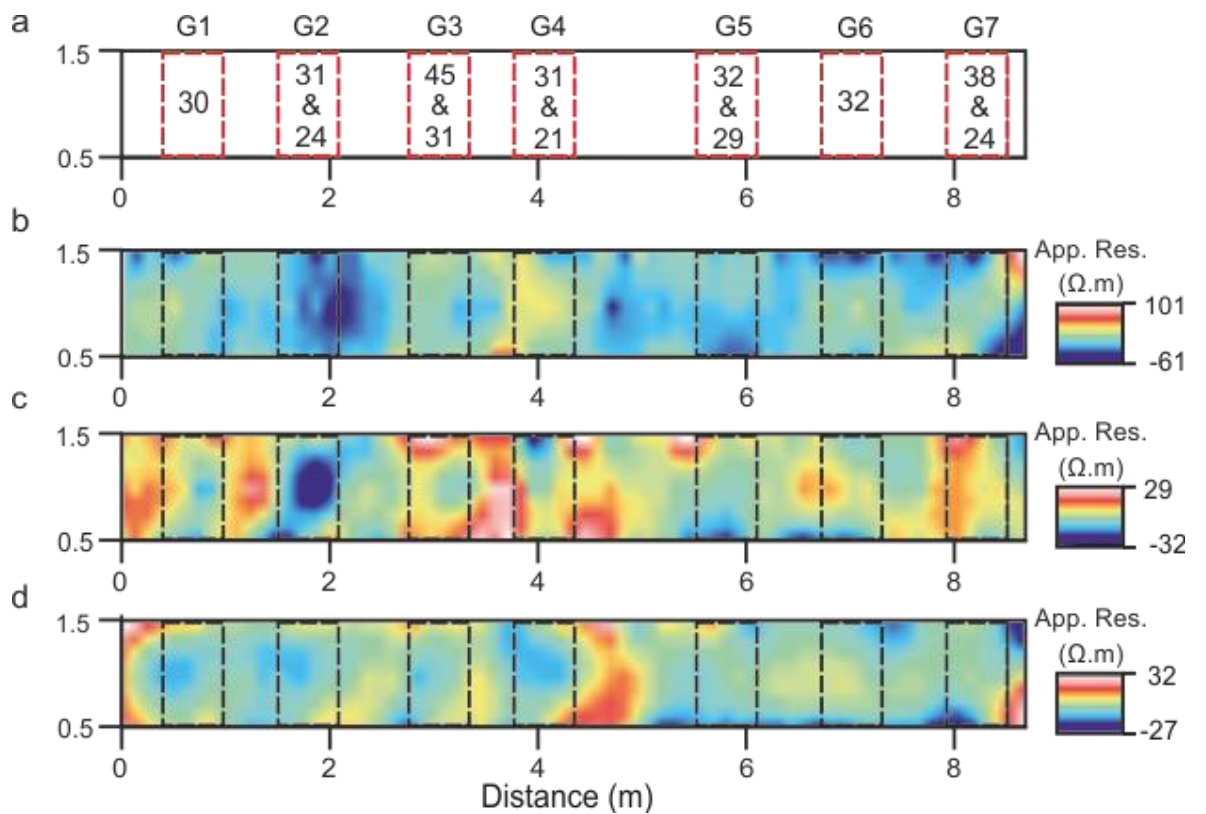


**Figure 4.11:** (a) Mapview of graves (with burial ages noted – see Table 4.2) and subsequent repeat electrical resistivity surveys using (b) 0.25 m, (c) 0.5 m and, (d) 1 m separated mobile electrodes on three survey lines (0.5 m, 1m and 1.5 m away from headstones) at St. Johns' Church, Keele, Staffordshire, UK.

**Table 4.2:** Survey summary of test profile lines and graves at the three study sites (Fig. 4.5 for respective site locations).

Survey site	Line no	Grave no	Mid-point distance (m)	Age of last burial (year)	Occupancy	Dominant soil type
St. Michael's	1	T1	1.7	30	1	Silty clay
		T2	2.6	26	2	
		T3	4.2	14	1	
		T4	5.2	16	1	
		T5	6.8	29	1	
		T6	7.8	28	1	
		T7	10.2	24	1	
		T8	11.7	19	2	
		T9	12.5	4	2	
St. John's	1	T1	0.8	30	1	Sandy clay
		T2	1.9	24	2	
		T3	3.4	31	2	
		T4	4.3	21	2	
		T5	6.3	29	2	
		T6	7.3	32	1	
		T7	8.8	24	2	
	2	T1	1.2	28	2	
		T2	2.1	15	1	
		T3	3.9	17	1	
		T4	5.4	12	1	
St. Luke's	1	T1	0.8	1	2	Pebbles and sandy loam
		T2	2.1	17	2	
		T3	3.3	7	3	
		T4	4.4	1	2	
		T5	5.5	25	1	
		T6	6.7	19	1	

#### 4.4.2 Survey distance from headstones

For this study it is also important to decide upon the optimal distance away from respective grave headstones that survey lines should be placed for full surveys; too close and they may just pick up the headstone itself rather than the grave, too far away and they may miss the grave positions. From analysing data obtained from test graves at 0.5

m, 1 m and 1.5 m away from the respective headstones (see Fig. 4.12 and Table 4.2 for grave details), line 2 (1 m from headstone) was judged optimal to best resolve burials.

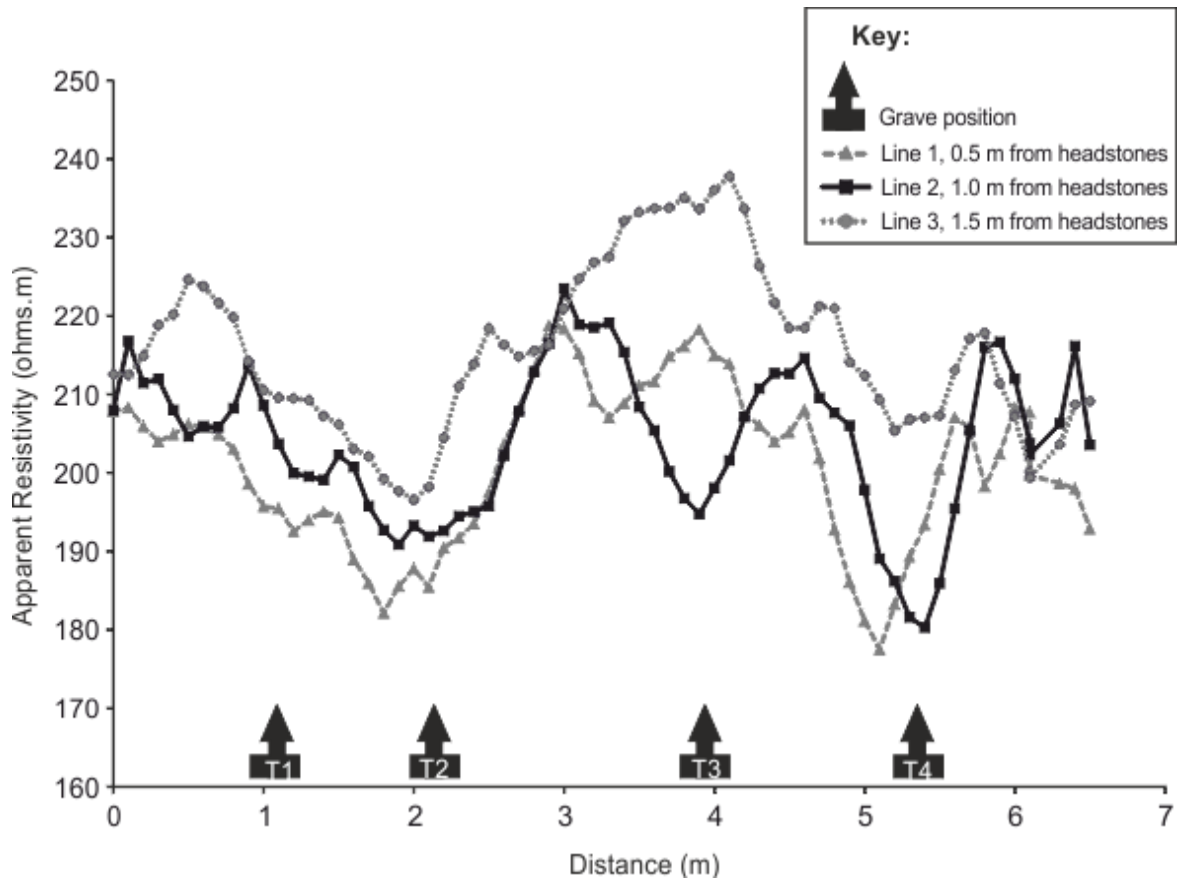


**Figure 4.12:** Graph showing a comparative analysis of fixed-offset (0.5 m spaced) electrodes surveying test profiles (Fig. 4.9 for location) at 0.5 m, 1 m and 1.5 m from grave headstones with known grave positions marked (black arrows and Table 4.2), collected in Keele graveyard, Staffordshire, UK.

GPR 450 MHz antenna frequency 2D profiles were also collected at the same distances away from headstones in order to check for radar responses as a function of distance from headstones, with results shown in Figure 4.13.

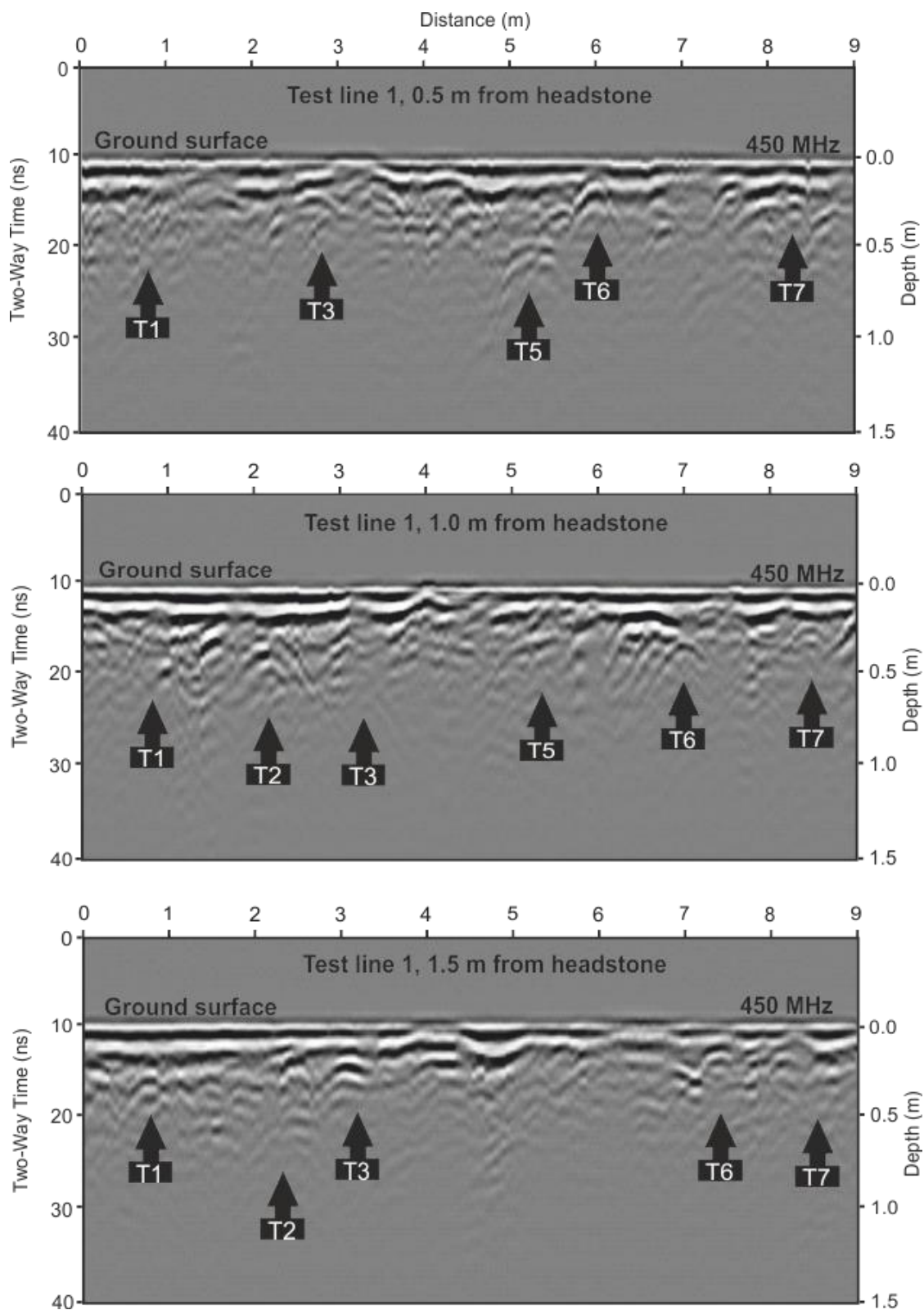


**Figure 4.13:** 2D 450 MHz shielded GPR profile results over Keele graveyard trial lines (Fig. 4.9 and Table 4.2) at 0.5 m, 1 m and 1.5 m away from grave headstones (marked).

All three GPR test profiles (0.5 m, 1.0 m and 1.5 m from headstones) successfully detected burials, however, profile 1.0 m away from headstones detected 6 out of 7 known burials, while profiles 0.5 m and 1.5 m only detected 5 burials each (Fig. 4.13). Advantages of profile 1.0 m from headstone is also that there it is less likely that surveys will pick up the headstone rather than the burial (even with shielded antennae), and the observed wider and more conspicuous hyperbolic reflections that are associated with larger body mass (in the abdominal region) of the burial cadaver or remains (Damiata *et al.*, 2013).

Finally surface magnetic susceptibility data were also collected on test lines to observe responses as a function of distance away from headstones. Results demonstrated different results (Fig. 4.14), especially over grave positions (Table 4.2), however, it was again observed that profiles situated 1 m away from headstones were optimal.

Having survey lines situated 1 m away from grave headstones was logical as, using the length of an adult human grave as a reference, the 0.5 m profile would be assumed to pass across the neck region, the 1 m profile is assumed to pass across the abdominal region and the 1.5 m profile would be assumed to pass across the feet region. This would also negate any issues of headstones not being in exactly the correct position as Fiedler *et al.* (2009a) documents; 1.0 m away from headstones had also been suggested as the optimal in a recent GPR case study by Damiata *et al.* (2013).



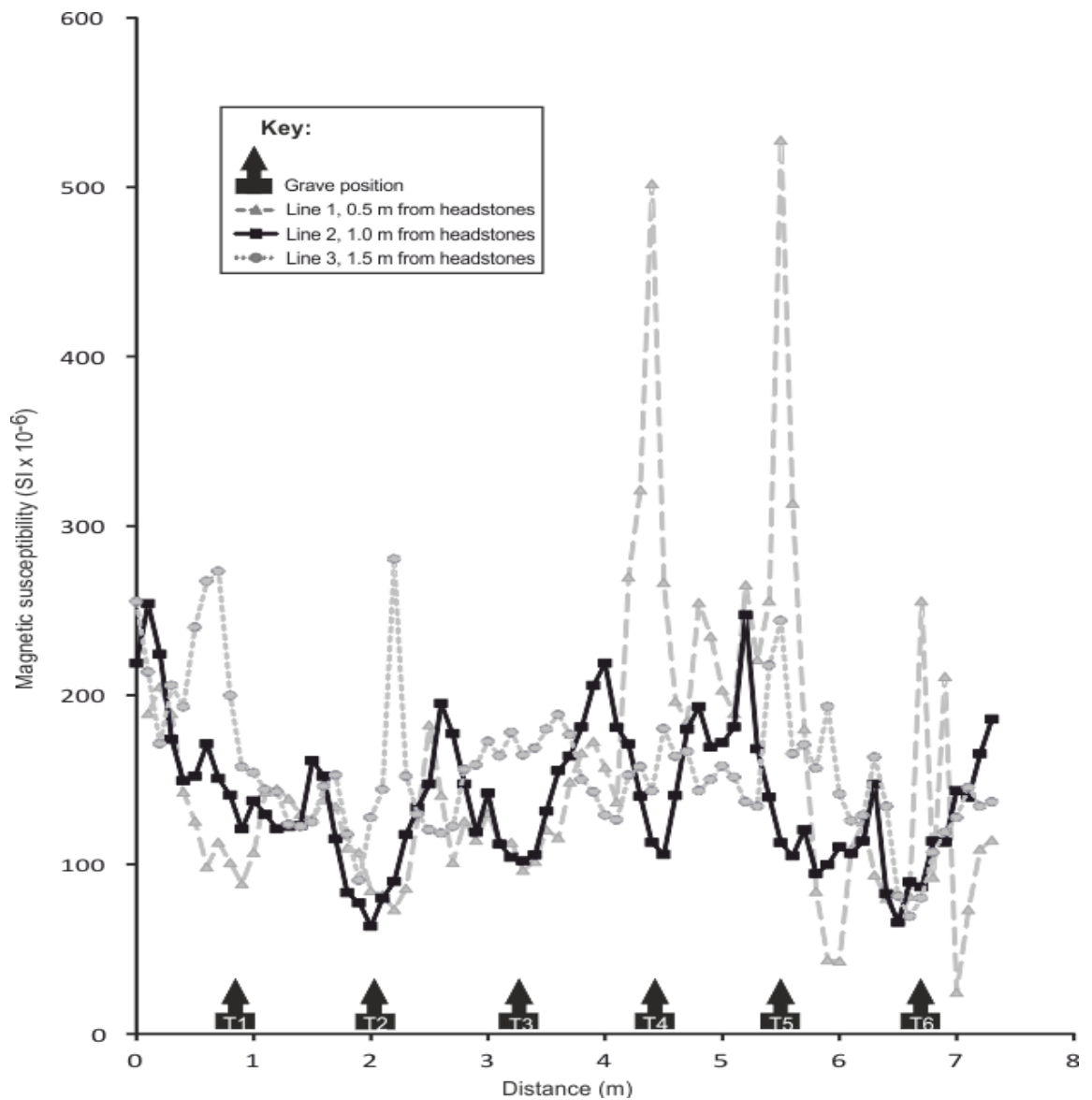


**Figure 4.14:** Graph showing a comparative analysis of magnetic susceptibility profile results over the Endon graveyard test line at 0.5 m, 1 m and 1.5 m away from grave headstones, with known grave positions marked (black arrows – see Table 4.2).

#### 4.4.3 Geophysical data acquisition and processing

Following the initial reconnaissance surveys, geophysical measurements were collected over the three case study sites at selected locations (see respective sections). The recent papers by Hansen *et al.* (2014) and Pringle *et al.* (2015a) suggest the integration of GPR, magnetic susceptibility and bulk ground resistivity as a promising approach to the detection of unknown burials in graveyards. Therefore, similar multi-techniques have been used to acquire data over the selected profile lines to account for different ages of burials and with burial ages known. The start and end of each survey line were permanently marked with plastic pegs, to ensure that the positions of the survey lines remained consistent for the three different techniques, and to guide as reference for possible re-surveying if need be.

A Geoscan<sup>TM</sup> RM15-D bulk ground electrical resistivity equipment (Fig. 4.15a) has been successfully used by forensic scientists and archaeologists to locate unknown graves (Cheetham, 2005; Pringle and Jervis, 2010; Hansen *et al.*, 2014). RM15-D equipment, with a 0.5 m fixed-offset dipole-dipole electrode probe configuration, was therefore used to collect data following the trials detailed in sections 4.41-2. The mobile 0.1 m long stainless steel electrodes were constantly separated by 0.5 m, whilst the remote probes were placed  $\sim 0.75$  m apart at a distance approximately 15 m from the survey position following best practice procedures (see Milsom and Eriksen, 2011). Measurements were taken at 0.1 m intervals along the profile lines, as was the recommended sample spacing (Cheetham, 2005, Milsom and Eriksen, 2011). The data logger automatically collected and recorded resistance measurements at each sampled position.



**Figure 4.15:** Photographs of near-surface geophysical techniques for the case studies showing (a) bulk ground resistivity (0.5 m and 1.0 m fixed-offset), (b) Bartington<sup>TM</sup> MS-2D susceptibility meter and (c) 225 MHz dominant frequency GPR data being collected.

The resistivity data was downloaded from the resistivity data logger, converted into x, y, z format data and spatially repositioned, where appropriate, before standard data processing were undertaken, including; (i) conversion of measured Resistance ( $\Omega$ ) values to apparent resistivity ( $\Omega.m$ ) to account for probe spacing configuration; (ii) data de-spiking to remove anomalous data points and; (iii) dataset de-trending to remove long wavelength site trends from the measured data to allow smaller, grave-sized features which were of interest to be more easily identified and interpreted (see Telford et al., 1990; Milsom and Eriksen, 2011). The processed dataset were then plotted graphically by profile line using Excel Microsoft package and transferred into CorelDRAW<sup>TM</sup> v.15 graphical software to develop graphical sketches which were matched with other techniques (e.g., MS and GPR) for comparison.

The magnetic susceptibility data was collected using a Bartington<sup>TM</sup> MS-2D field coil susceptibility meter, connected to a laptop which contained Bartsoft<sup>TM</sup> v.4 data acquisition software (see Fig. 4.15b). The instrument is most commonly used for field measurements of volume specific magnetic susceptibility; it consists of a 0.2 m diameter surface probe which generates a sample measurement (set a 1 s throughout), when placed on the ground surface at each sampling point, to collect data and repeated three times, with a sampling interval of 0.1 m along profile lines. After every 5 consecutive sampling points, the probe was raised and aimed upwards to calibrate the instrument (zeroed) and to measure equipment drift during data acquisition. This data acquisition protocol has successfully been used in related studies to identify unmarked burials

(Pringle *et al.*, 2015b) and to demonstrate a significant geophysical contrast between grave soil and the surrounding soil (Dalan *et al.*, 2010).

Magnetic susceptibility data was downloaded and converted into x, y, z format and spatially repositioned, where appropriate, before standard data processing were undertaken, including; (i) data de-spiking to remove anomalous data points, (ii) dataset de-trending to remove long wavelength site trends from the measured data to allow smaller, grave-sized features which were of interest to be more easily identified and interpreted (Telford *et al.*, 1990; Milsom and Eriksen, 2011).

Three dominant GPR antenna frequencies 225, 450 and 900 MHz were trialled in the sites, following previous studies that suggest multi-frequency antenna should be assessed to pick the most suitable antenna frequency for individual sites (Schultz, 2008; Pringle *et al.*, 2012b; Hansen *et al.*, 2014). These three antenna central frequencies were selected, based on velocity and attenuation of the soil and their resolution and penetration depth trade-offs. Both 110 MHz and 1.2 GHz antennae would be deemed inappropriate for the surveys due to the expected size and depth of target objects respectively (Milsom and Eriksen, 2011), as well as the antennae size (110 MHz) and small trace spacing (1,200 MHz) of the respective antennae. Data were collected throughout using PulseEKKO™ 1000 equipment (Fig. 4.15c) using the specifications detailed in Table 4.3.

**Table 4.3:** Summary of GPR antenna frequency specifications used for all survey sites.

Central frequency (MHz)	Time window (ns)	Constant signal stacks	Step size (m)	Velocity (nm/s)
225	100	32	0.1	~ 0.07
450	80	32	0.05	~ 0.085
900	60	32	0.025	~ 0.1

Once the 2D GPR profiles for each dominant frequency antenna were acquired, they were downloaded and imported into REFLEX-Win<sup>TM</sup> v.3.0 processing software (Sandmeier Scientific Software, Karlsruhe, Germany). The standard data processing steps used throughout were; (i) removal of blank data, (ii) first arrival digitally picked and shifted to 0 ns to ensure consistent arrival times, (ii) dewow filter applied, (iv) AGC gain filter, (v) time-cut to clip blank data at base of profiles, (vi) 1D filtering and finally, (vii) time-depth conversion (see Table 4.4). It was deemed important not to ‘over-process’ which may have increased the likelihood of introducing false data into profiles (Cassidy, 2009).

**Table 4.4:** Sequential GPR data processing steps used in the study.

Processing step	Process	Basic description
1	Editing	Removal and correction of bad/poor data and sorting of data files
2	Time-zero correction	Adjustment of start time to match with surface position by ensuring that first arrival is at ground level: 0 ns here. This allowed all features of uniform depth below-level to appear uniform in GPR profiles.
3	De-wow filter	Subtract the very low frequencies form the data
4	AGC (automatic gain control)	Aided in bringing out weaker reflections to the same amplitude as stronger reflections within a certain time window
5	Time-cut	Used to clip data after a subjectively identified two-way travel time beyond which noise exceeded signal
6	1 D filtering	Improved signal to noise ratio and visual quality
7	Time-depth conversion	The software by command automatically converts TWT (two-way time) into depth by hyperbolic velocity analysis using mathematical equation: $\{Depth = \frac{TWT}{2 \times velocity}\}$

## **4.5 Case Study 1: St. Michael's of all Angels Church, Stockton, Norfolk, UK**

### *4.5.1 Background*

The Church of St. Michael of all Angels is a small Anglican church which lies in rural South Norfolk, United Kingdom (Fig. 4.5). The exact date in which it was built is unknown but burials are thought to be from at least the 15<sup>th</sup> century, following a Latin inscription inside the church building dated 1615 AD. The graveyard around the church contains many grave headstones and few footstones, ranging in age from the late 18<sup>th</sup> century to present, although whether these in fact are in place or have been moved is unknown as there are limited parish records available.

The local geology comprises glacial till and clay soil that overlies Norwich Crag (that contains variations of sand, mud and shingle (NCP, 2011), below which is Cretaceous Chalk bedrock (British Geological Survey (BGS), 2013). Available local site investigation (SI) boreholes were also downloaded from the British Geological Survey online resource (Table 4.5) and integrated to generate a schematic 2-D geological cross-section of the local area (Fig. 4.16).



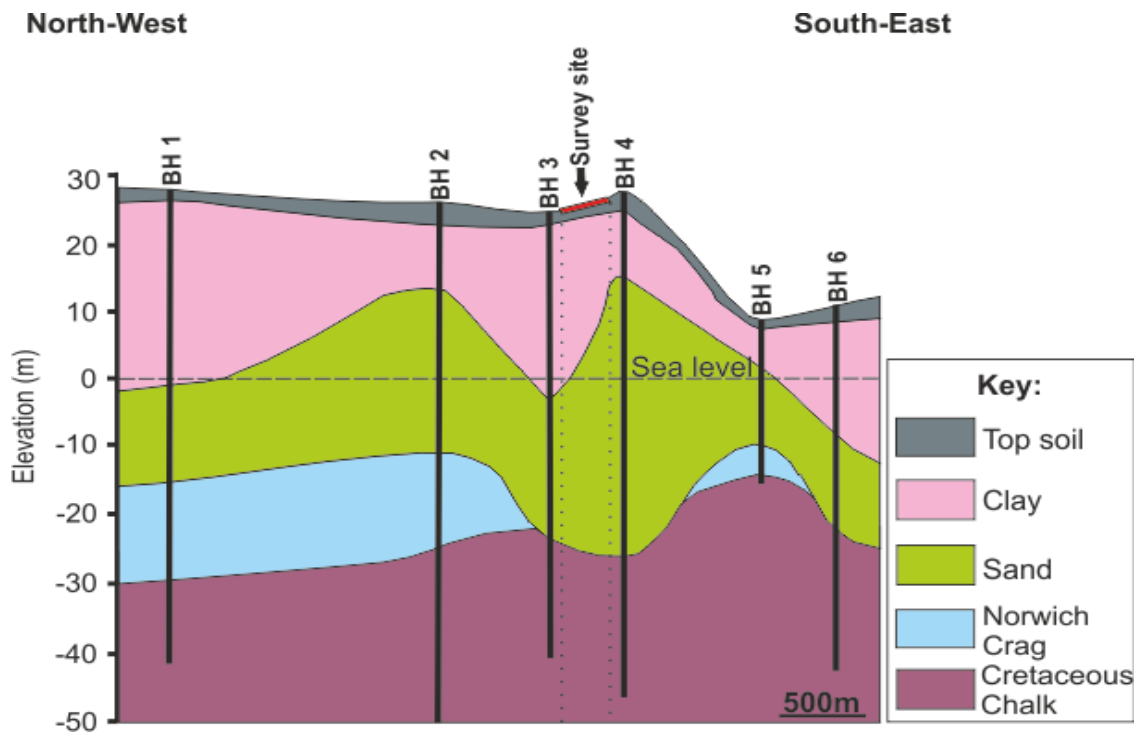


**Figure 4.16:** Approximately NW-SE orientated, 2D schematic cross-section of the St. Michael's local area using BGS borehole information (see Table 4.5).

**Table 4.5:** List of available Stockton site investigation borehole and pertinent information to generate the schematic 2-D cross-section shown in Figure 4.16.

S/N	Borehole No.	Borehole Name	X (m)	Y (m)	Drilled Date	Drilled Depth (m)	Depth to sea level (m)
1	BH 1	TQ38SW1447	534680	184650	1997	11.3	16.9
2	BH 2	TQ38SE4658	535020	184330	1995	15	3.75
3	BH 3	TQ38SE184	535620	184750	1911	91	12.2
4	BH 4	TQ38SE4384	535800	184860	N/A	12.19	13.74
5	BH 5	TQ38SE5314	536222	183939	2011	100	12
6	BH 6	TQ38SE4429	536379	183932	1992	34.5	13.12

Three soil samples from the site were also collected in a 0.7 m stainless steel hand auger and then interpreted using Chapman (2005) to have a very dark greyish brown (Munsell colour: 2.5Y/3/2) colour at depth approximately 0.1 m below the ground level, from 0.1 m to 0.45 m depth is a light olive brown (Munsell colour: 2.5Y/5/4) colour, while a pale yellow (Munsell colour: 2.5Y/8/4) colour containing white chalk fragments and flint is located below 0.45 m depth below ground level (Fig. 4.17). Sample positions are shown in Fig. 4.18.

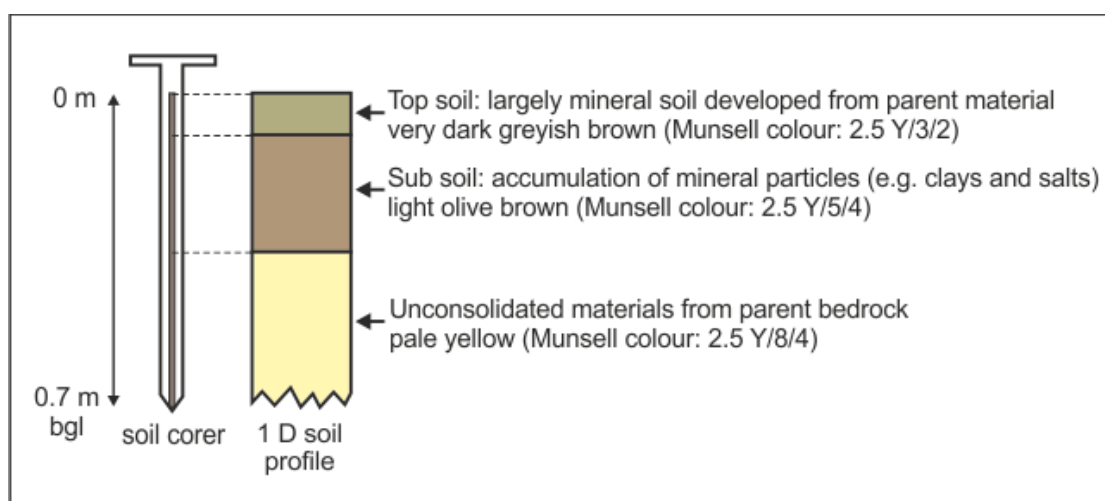


**Figure 4.17:** Schematic diagram showing the soil auger and generalised 1 D soil profile results at St. Michael’s graveyard site.

The graveyard was approximately 80 m by 60 m with the church building situated right at the centre of the site (Fig. 4.18), with three geophysical survey profiles chosen for access and varied burial ages (see Table 4.6). See Section 4.3.2.2 for geophysical data acquisition and processing steps utilised.

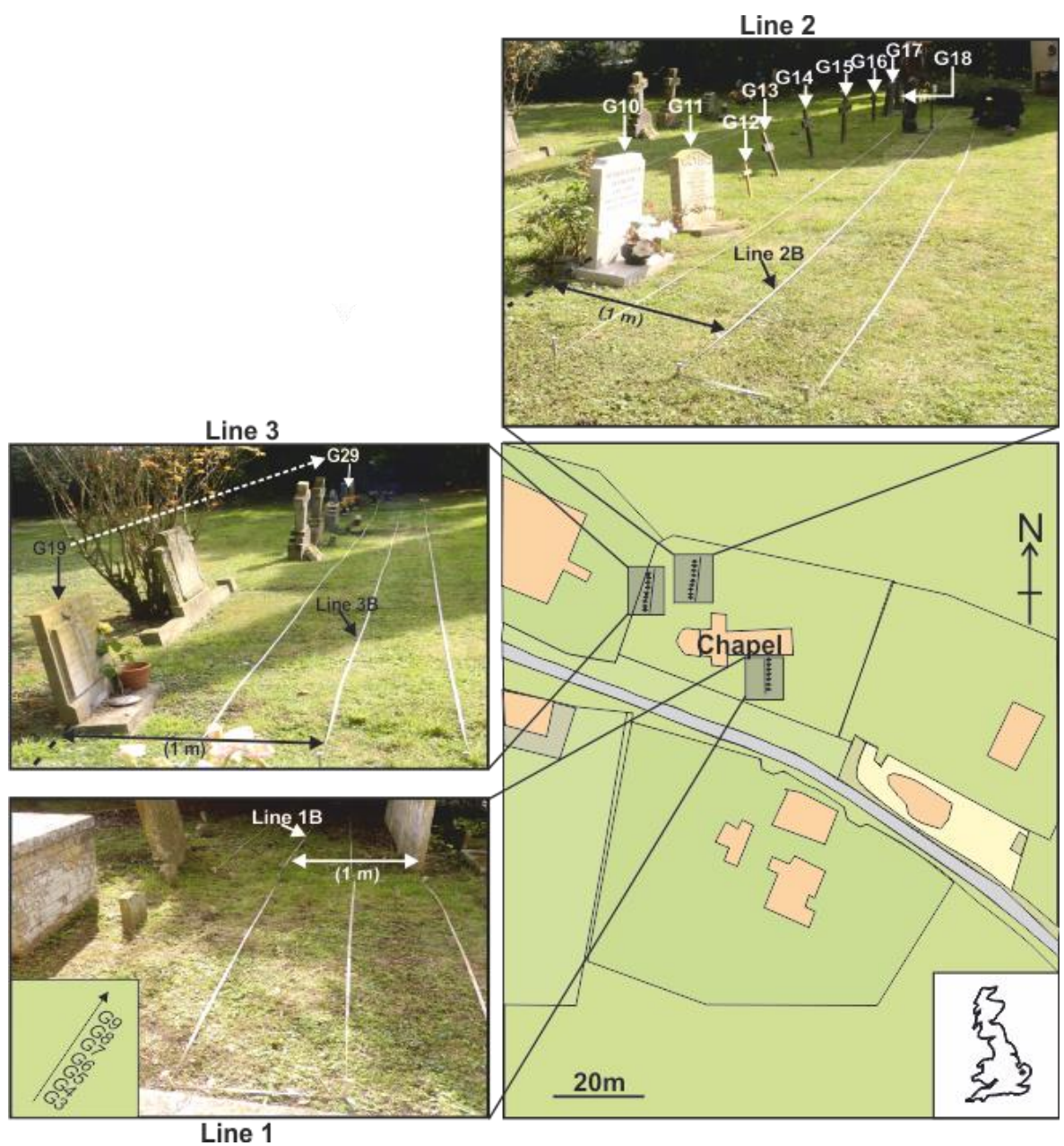


**Figure 4.18:** Map view of St. Michael of all Angels church graveyard, Norfolk, UK, showing surveyed (and numbered) graves, 2D profile lines and orientations and annotated site photographs.

**Table 4.6:** Details of graves surveyed for case study 1 (St. Michael's Church graveyard)

Survey Lines	Grave no	Mid-point distance (m)	Age of last burial (yrs)	Occupancy	Dominant soil type
1	G3	0.5	200	2	Silty clay
	G4	2.6	165	1	
	G5	3.7	214	1	
	G6	4.6	202	1	
	G7	5.6	191	1	
	G8	6.8	187	1	
	G9	8.1	176	1	
2	G10	1.7	30	1	
	G11	2.6	26	2	
	G12	4.2	14	1	
	G13	5.2	16	1	
	G14	6.8	29	1	
	G15	7.8	28	1	
	G16	10.2	24	1	
	G17	11.7	19	2	
	G18	12.5	4	2	
3	G19	0.6	30	2	
	G20	2.2	98	1	
	G21	4	72	1	
	G22	5.8	100	1	
	G23	6.9	102	1	
	G24	8.6	110	1	
	G25	10	123	1	
	G26	11.4	13	1	
	G27	12.4	12	1	
	G28	13.9	2	2	
	G29	15.2	20	2	

#### 4.5.2 Case study 1: Geophysical results

Magnetic susceptibility survey data acquired over Profile Line 1 did not detect any graves (Fig. 4.19). These were, however, the oldest graves surveyed (Table 4.6) and were very close to the church building (see Fig. 4.18). Resistivity surveys over the same profile only detected 2 graves (G5 and G7) as relatively low resistance anomalies compared to background values (see Table 4.7).

**Table 4.7:** Statistics of geophysical data collected from Stockton graveyards, Norfolk, UK.

Case study	Line no.	App. Res Min./Av/Max, SD ( $\Omega\cdot\text{m}$ )	Magnetic Susceptibility Min./Av/Max, SD ( $\times 10^{-6}$ )
Stockton	1	19.6/22.7/26.9, 1.71	141/267/711, 0.96
Stockton	2	32.1/37.8/45.0, 2.67	35.6/101.6/280, 47
Stockton	3	18/25/45.2, 5.68	82.7/420/1554, 368
Stockton	All	28.4 $\Omega\cdot\text{m}$	263

GPR 225 MHz dominant frequency 2-D profile line 1 identified only 1 grave (G9), the 450 MHz dominant frequency 2 identified 3 graves (G7, G8 and G9) and perhaps an unknown burial (?G), with the 900 MHz dominant frequency 2-D profile identified 5 graves (G3, G4, G7, G8 and G9) and the unknown burial (see Figure 4.20) as hyperbolic reflection events.

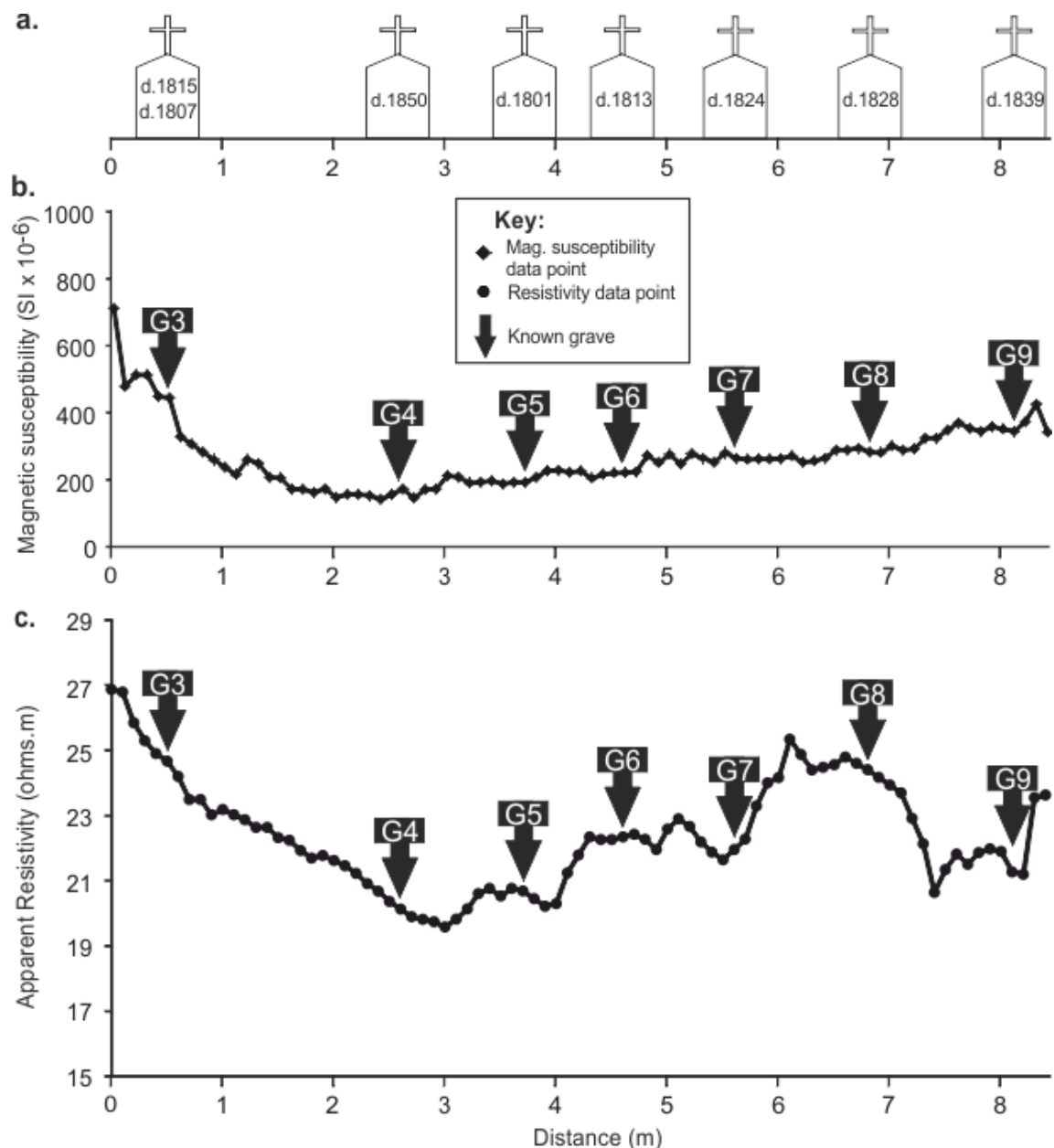


**Figure 4.19:** Stockton 2D survey line 1 (Fig. 4.18 for location), showing, (a) grave locations represented by headstones with year of burial inset, (b) magnetic susceptibility plot against profile distance and, (c) apparent resistivity plot against profile distance.

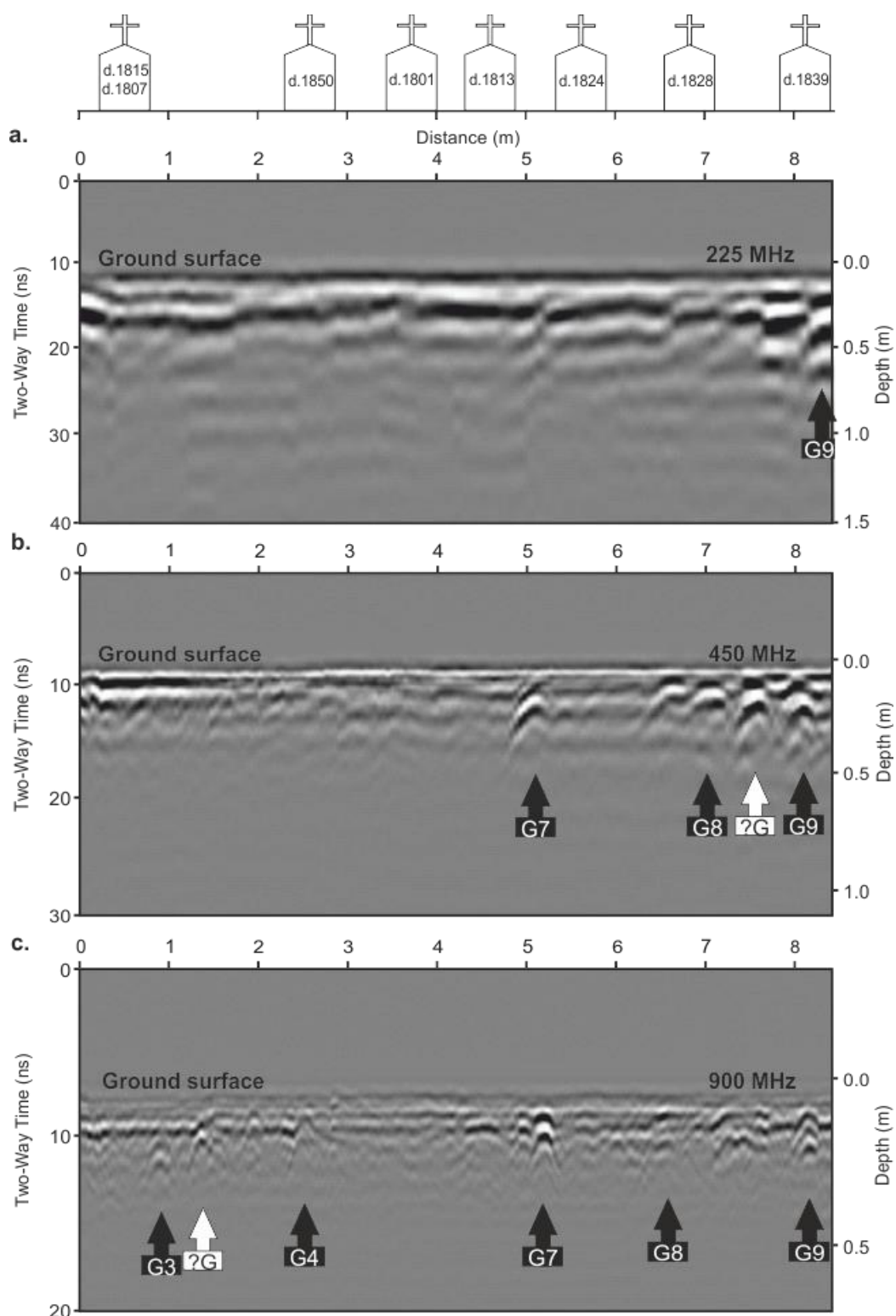


**Figure 4.20:** Stockton 2D survey line 1 (Fig. 4.18 for location), showing, (a) grave locations represented by headstones with year of burial inset, (b) 225 MHz, (c) 450 MHz and, (d) 900 MHz frequency 2D GPR profiles with marked interpreted burial position.

Magnetic susceptibility survey data acquired over profile line 2 was successful, clearly detecting all 9 known young graves (Table 4.6) including 2 unknown burials (2 ?G) as relatively high magnetic anomalies when compared to background values (Fig. 4.21b). Resistivity surveys over the same profile were also successful with 8 of 9 burials detected as areas of low resistivity response (Fig. 4.21c). However, in contrast the locations of the two unknown burials had high resistivity response when compared to background values.

GPR 225 MHz dominant frequency 2-D profile line 2 identified only 1 (G18) out of 9 graves, the 450 MHz dominant frequency detected 8 out of 9 graves, and the 900 MHz dominant frequency detected all 9 and indeed the 2 unmarked graves as hyperbolic reflection events (Fig. 4.22).



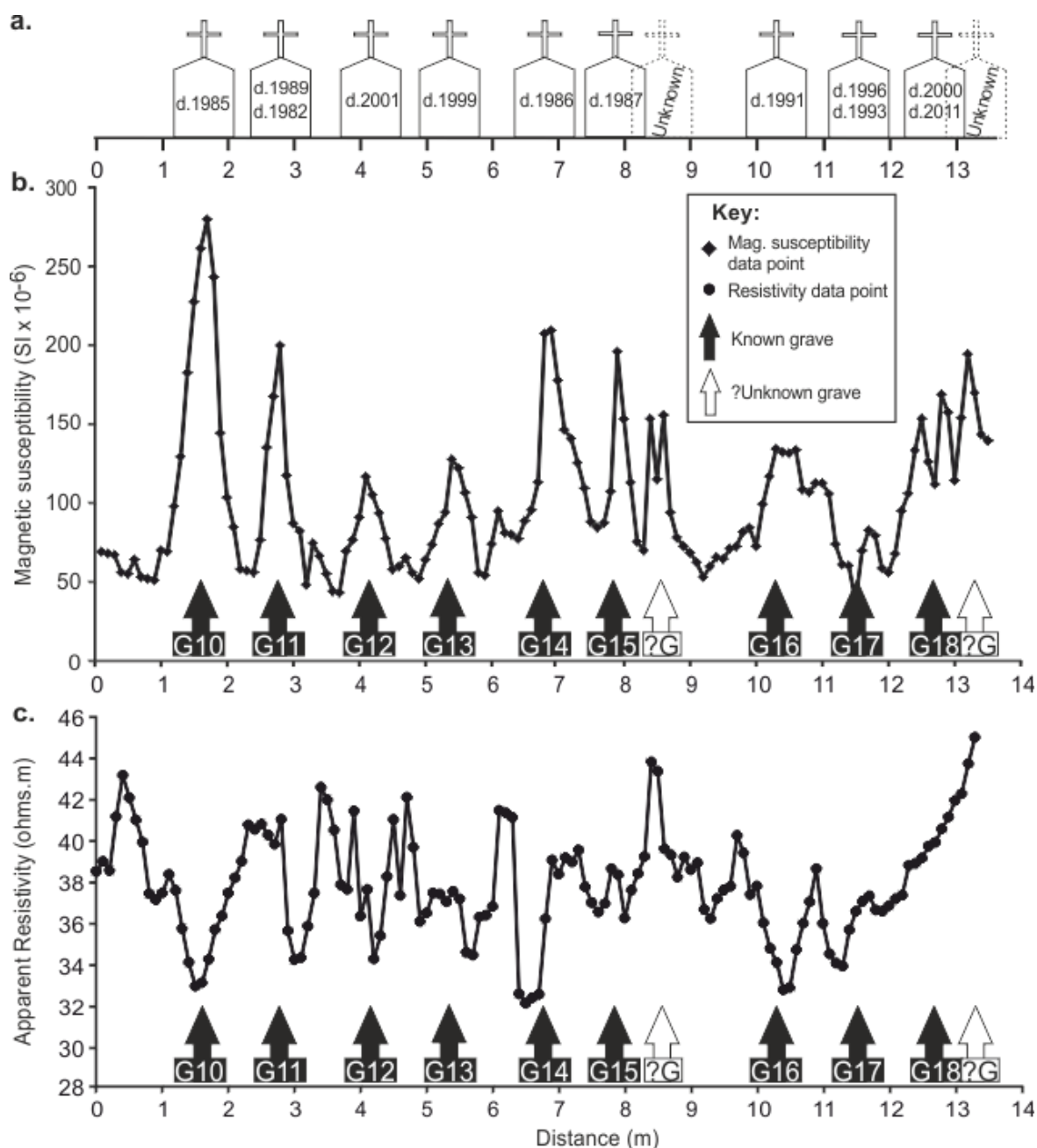


**Figure 4.21:** Stockton 2D survey line 2 (Fig. 4.18 for location), showing, (a) grave locations represented by headstones with year of burial inset, (b) magnetic susceptibility plot against profile distance and, (c) apparent resistivity plot against profile distance.

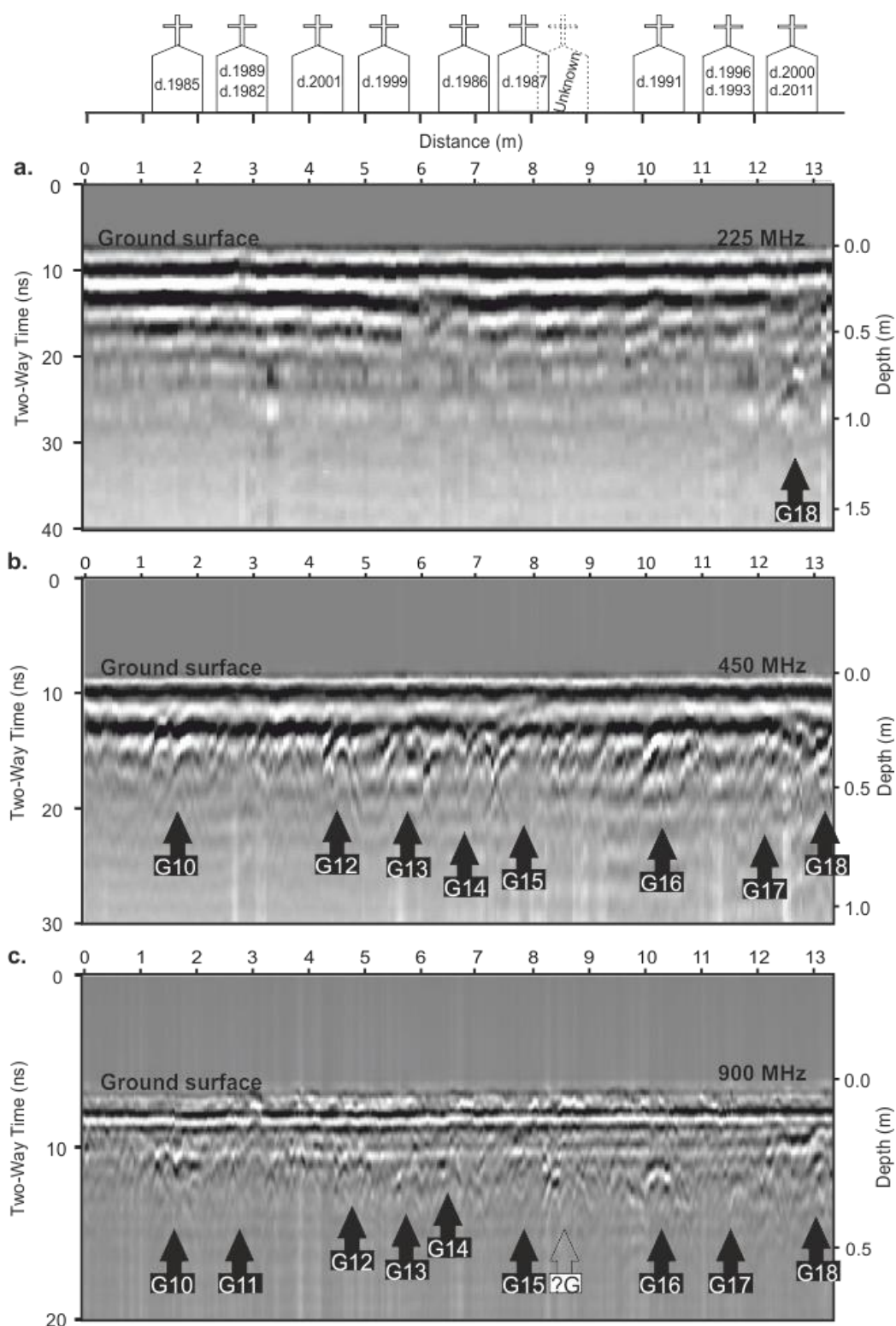


**Figure 4.22:** Stockton 2-D survey line 2 (Fig. 4.18 for location), showing, (a) grave locations represented by headstones with year of burial inset, (b) 225 MHz, (c) 450 MHz and, (d) 900 MHz frequency 2D GPR profiles with marked interpreted burial position.

Magnetic susceptibility survey data acquired over profile line 3 was reasonably successful, detecting 7 of 11 known graves (Table 4.6), with the majority (younger burials) shown as relatively high magnetic anomalies when compared to background values and two (G20 and G21) that were ~100 years old were low anomalies (Fig. 4.23b). Resistivity surveys over the same profile were not successful (Fig. 4.23c).

GPR 225 MHz dominant frequency 2-D profile line 3 identified 3 (G19, G21 & G26) out of the 11 graves, the 450 MHz dominant frequency detected 8 and the 900 MHz dominant frequency detected 7 and indeed the 2 unmarked graves as hyperbolic reflection events (Fig. 4.24). A strong horizontal reflection event was also observed between two graves (Fig. 4.24b/c). The summary of GPR detectability in Stockton graveyard is shown in Table 4.8.

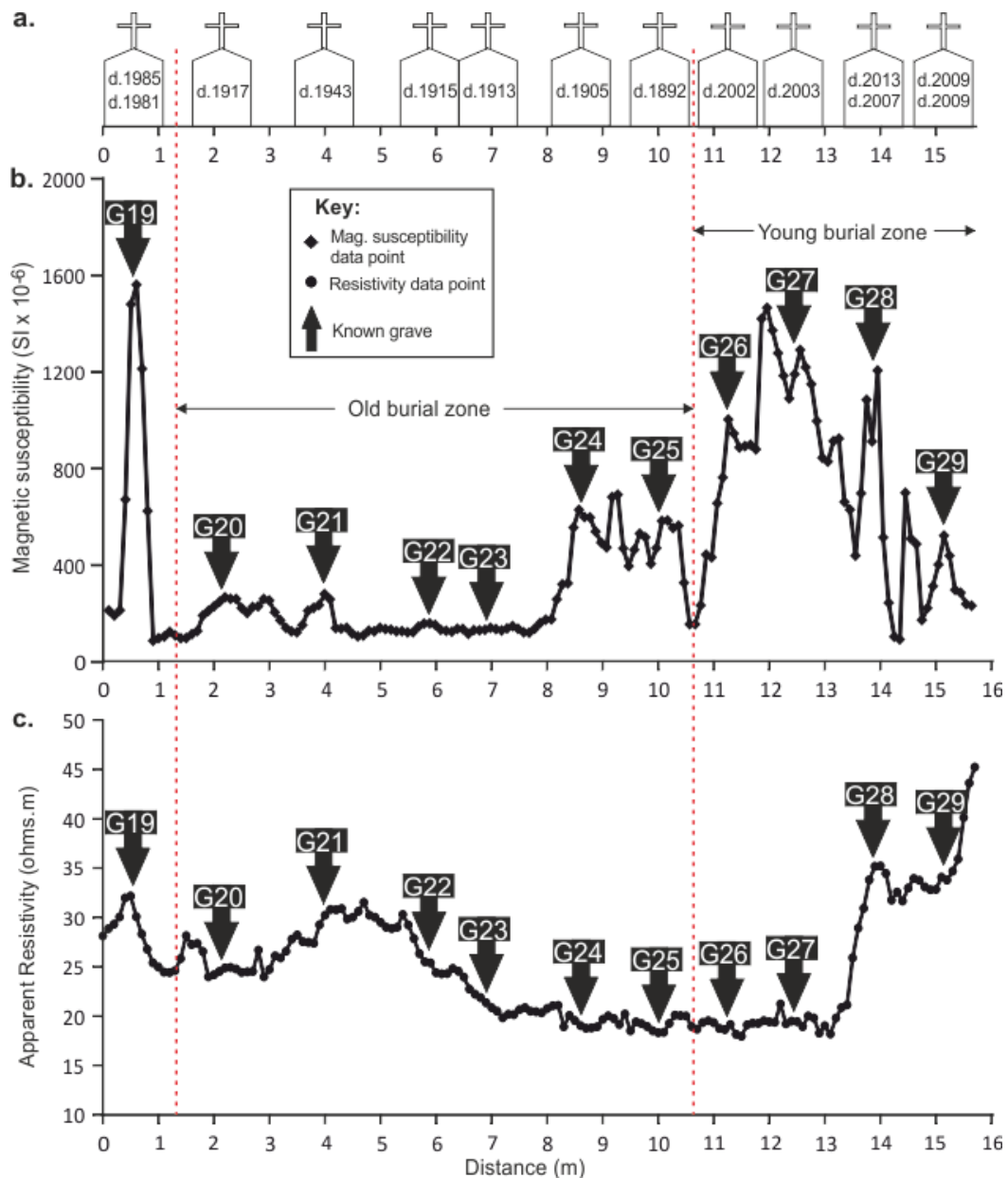


**Figure 4.23:** Stockton 2D survey line 3 (Fig. 4.18 for location), showing, (a) grave locations represented by headstones with year of burial inset, (b) magnetic susceptibility plot against profile distance and, (c) apparent resistivity plot against profile distance.

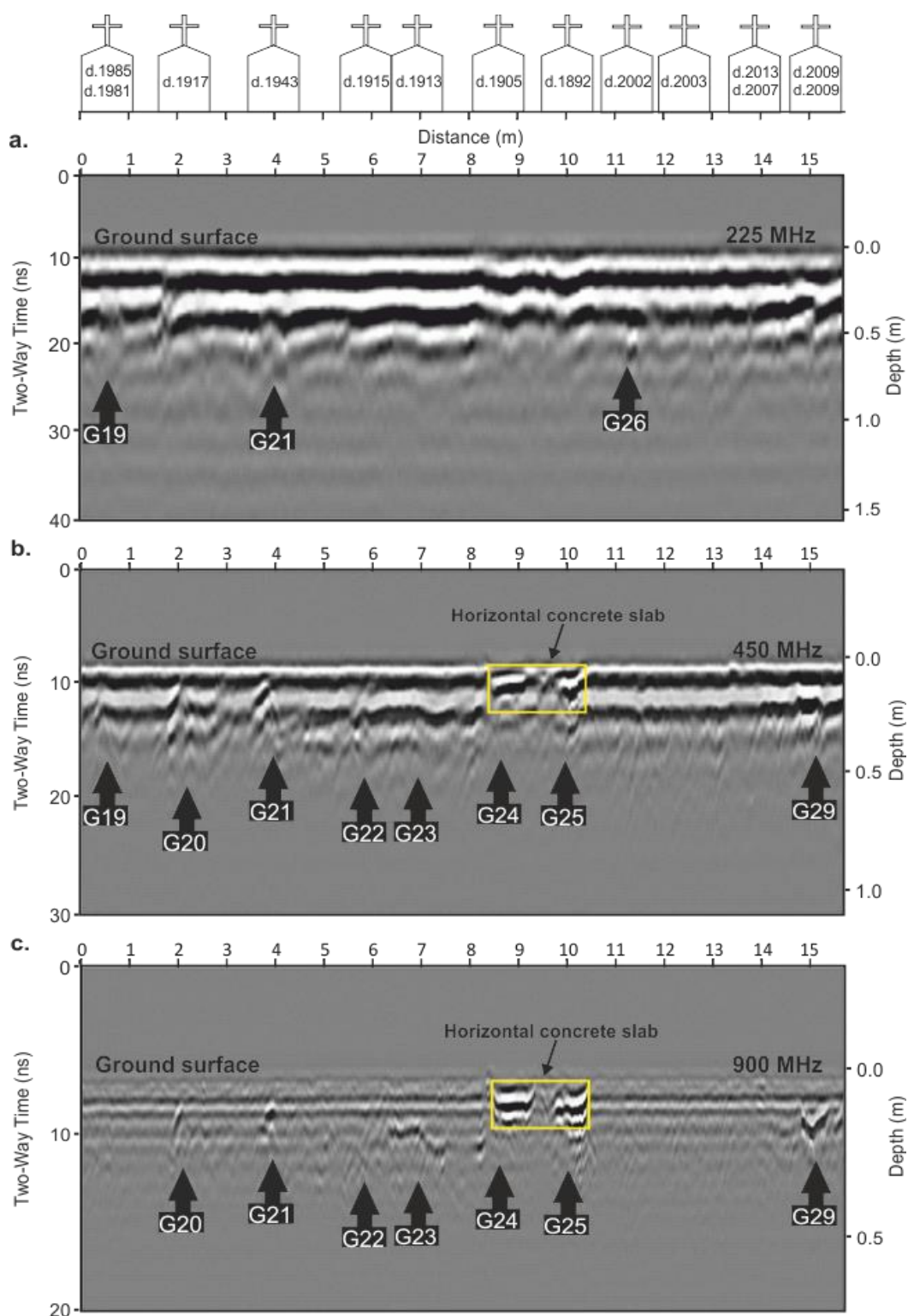


**Figure 4.24:** Stockton 2-D survey line 3 (Fig. 4.18 for location), showing, (a) grave locations represented by headstones with year of burial inset, (b) 225 MHz, (c) 450 MHz and, (d) 900 MHz frequency 2D GPR profiles with marked interpreted burial position.

The combined survey line cross-plots of resistivity and magnetic susceptibility data against burial age are shown in Figure 4.25. Whilst both show a general decrease of response against increasing burial age, it is not significant. However, plotting resistivity against younger burials does result in a statistical correlation (Figure 4.26). The values of geophysical response for each grave as used for the plotting in the three graveyards were generated by averaging the three consecutive values over the detected anomalies.

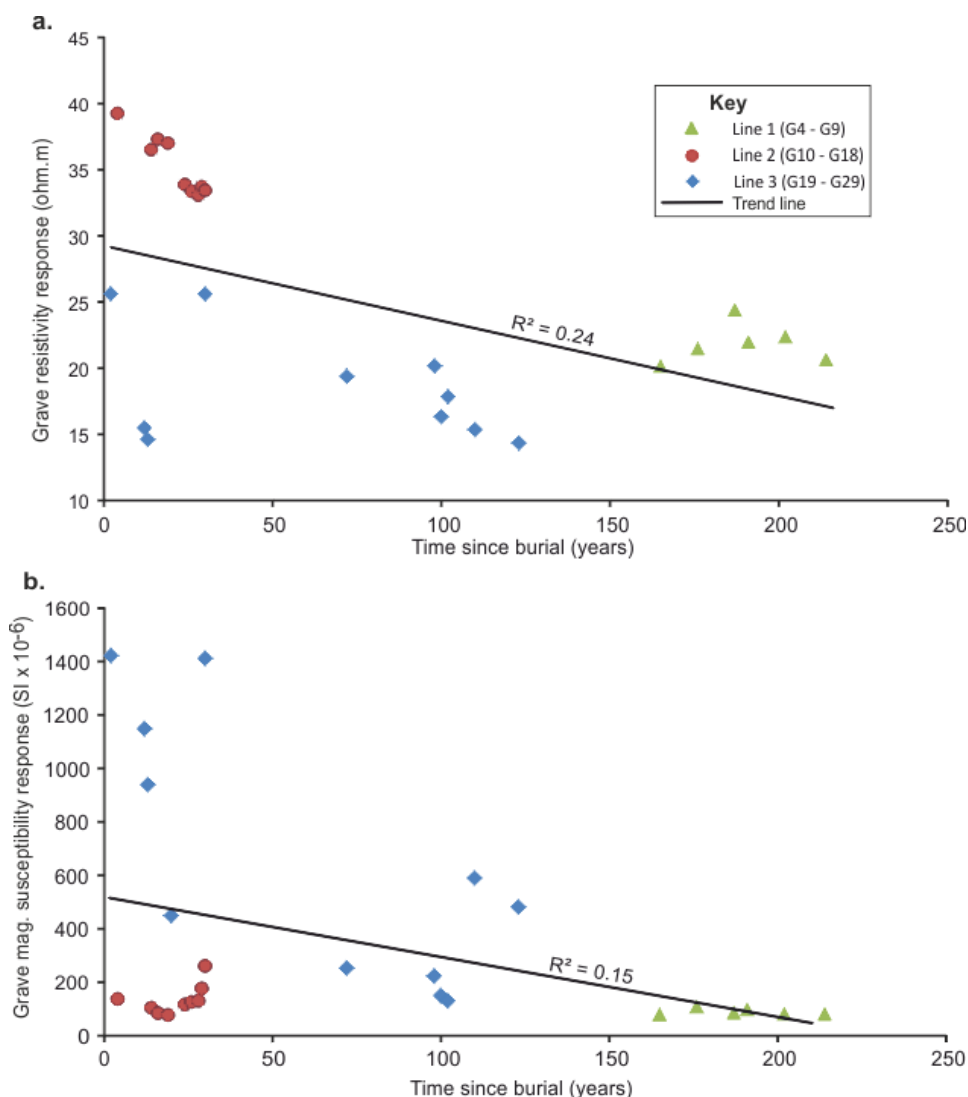


**Figure 4.25:** Combined Stockton survey line cross-plot of (a) resistivity and (b) magnetic suscep geophysical responses against age of burial (Table 4.6) respectively.

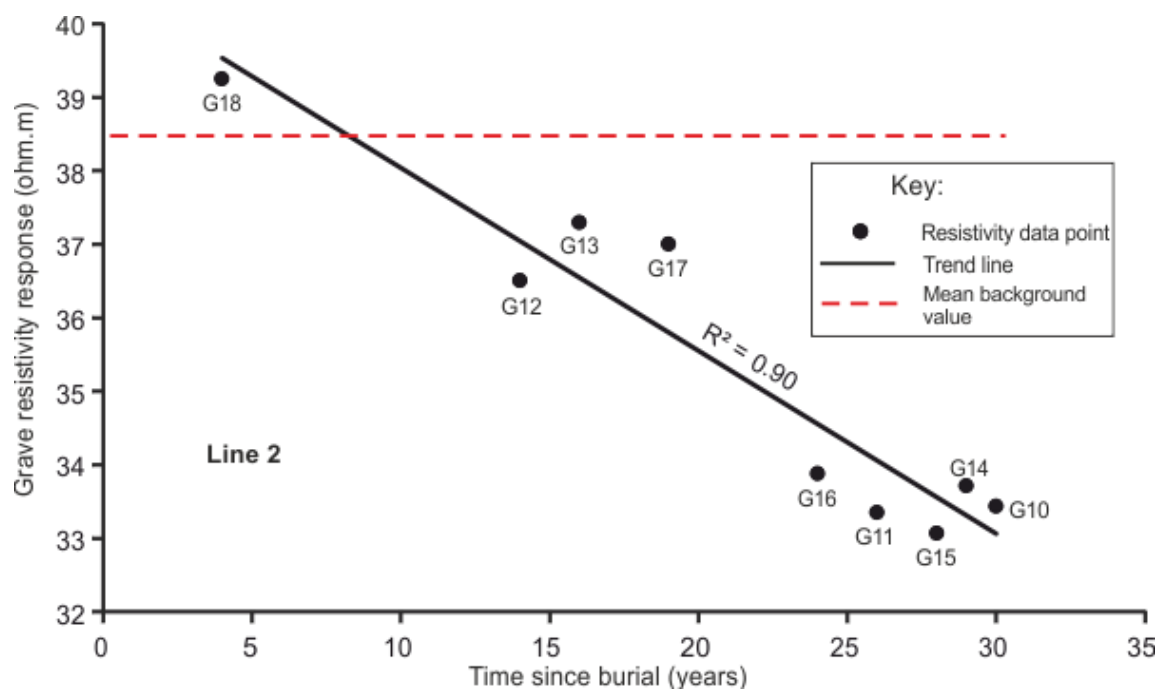


**Figure 4.26:** Stockton survey line 2 cross-plot of resistivity response against burial age (Table 4.6).

**Table 4.8:** Summary of GPR Stockton survey (St. Michael's graveyard), Norfolk, UK.

Stockton Survey lines	Grave no.	Antenna central frequency (MHz)			Occupancy
		225	450	900	
1	G3	No detection	No detection	Good	2
	G4	No detection	No detection	Good	1
	G5	No detection	No detection	No detection	1
	G6	No detection	No detection	No detection	1
	G7	Poor	Good	Excellent	1
	G8	No detection	Poor	Poor	1
	G9	Good	Good	Excellent	1
2	G10	No detection	Poor	Poor	1
	G11	No detection	No detection	Poor	2
	G12	No detection	Good	Poor	1
	G13	No detection	Poor	Poor	1
	G14	No detection	Poor	Poor	1
	G15	No detection	Poor	Poor	1
	G16	No detection	Poor	Excellent	1
	G17	No detection	Poor	Poor	2
	G18	Poor	Poor	Good	2
3	G19	Poor	Poor	No detection	2
	G20	No detection	Poor	Good	1
	G21	Poor	Good	Good	1
	G22	No detection	Poor	Poor	1
	G23	No detection	Poor	Poor	1
	G24	No detection	Good	Good	1
	G25	No detection	Poor	Good	1
	G26	Poor	No detection	No detection	1
	G27	No detection	No detection	No detection	1
	G28	No detection	No detection	No detection	2
	G29	No detection	Poor	Good	2
Maximum strength (%)	detection	9	28	43	



## **4.6 Case Study 2: St. John's Church, Keele site, Newcastle under Lyme, Staffordshire, UK**

### *4.6.1 Background*

The St. John's Church graveyard, located adjacent Keele University campus, ~200 m above sea level, is situated close to the town of Newcastle-under-Lyme in Staffordshire, UK (Fig. 4.5). According to church records, St. John's Church building was constructed between 1868 and 1870 and since then burials have been conducted at the graveyard designated area (St. John's Church News, 2015). The graveyard is large and contained hundreds of graves dispersed dominantly within the south-west area of the church land. Most graves contained grave headstones but a handful of older graves had footstones, it had variable age of burials that distinguished it as a useful site for the study.

The local geology comprises predominantly of natural sandy clay overlying mudstone bedrock (British Geological Survey 2013 downloaded data). Available local site investigation (SI) boreholes were also downloaded from BGS online resource (Table 4.6) and integrated to generate a schematic 2-D geological cross-section of the area (Fig. 4.27).

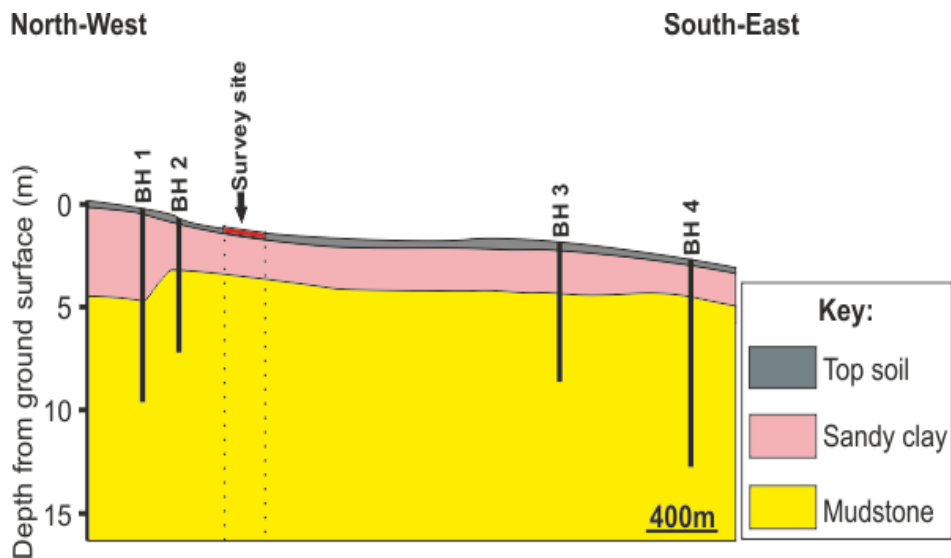


**Figure 4:27:** Approximately NW-SE orientated, 2D schematic cross-section of the Keele church site using BGS borehole information (see Table 4.9 for data information).

**Table 4.9:** List of available Keele site investigation borehole and pertinent information derived to generate the schematic 2-D cross-section shown in Figure 4.27.

S/N	Borehole No.	Borehole Name	X (m)	Y (m)	Drilled Date	Drilled Depth (m)	Depth to sea level (m)
1	BH 1	SJ84NW178	380590	345770	1987	9.5	Unknown
2	BH 2	SJ84NW496	380740	345350	1995	6.0	Unknown
3	BH 3	SJ84SW322	382340	343602	1911	7.4	Unknown
4	BH 4	SJ84SW34	382888	344512	N/A	11	Unknown

Three soil samples from the site were also collected in a 0.7 m stainless steel hand auger and then interpreted using Chapman (2005) to have a reddish grey (Munsell colour: 2.5Y/5/2) colour at depth approximately 0.08 m below the ground level, from 0.08 m to 0.5 m depth is a dark olive brown (Munsell colour: 5Y/4/3) colour, while a dark reddish

brown (Munsell Colour: 2.5 Y 8/4) colour containing coal and sandstone fragments is located below 0.5 m depth below ground level (Fig. 4.28).

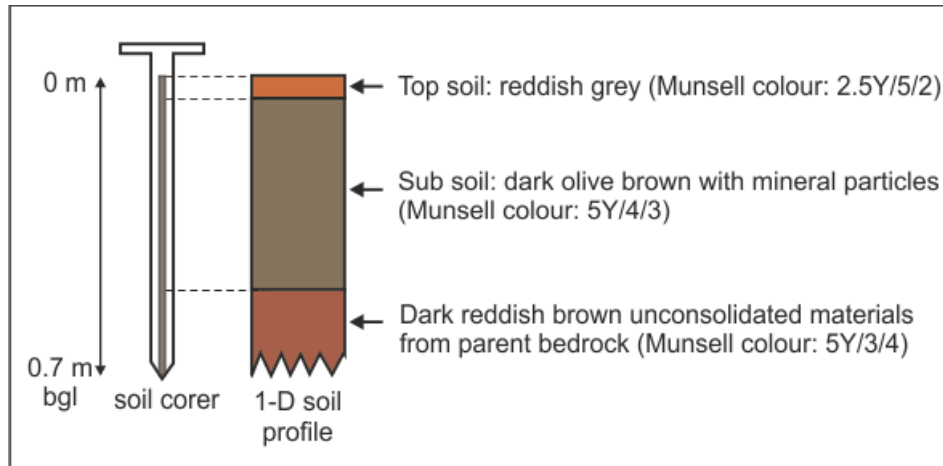


**Figure 4.28:** Schematic diagram showing the soil auger and generalised 1 D soil profile results at St. John’s graveyard site.

The graveyard was approximately 100 m by 200 m, with the church building located north-east portion of the site (Fig. 4.29) with four geophysical survey profiles chosen for access and varied burial ages (see Table 4.10). See Section 4.3.2.2 for geophysical data acquisition and processing steps utilised.

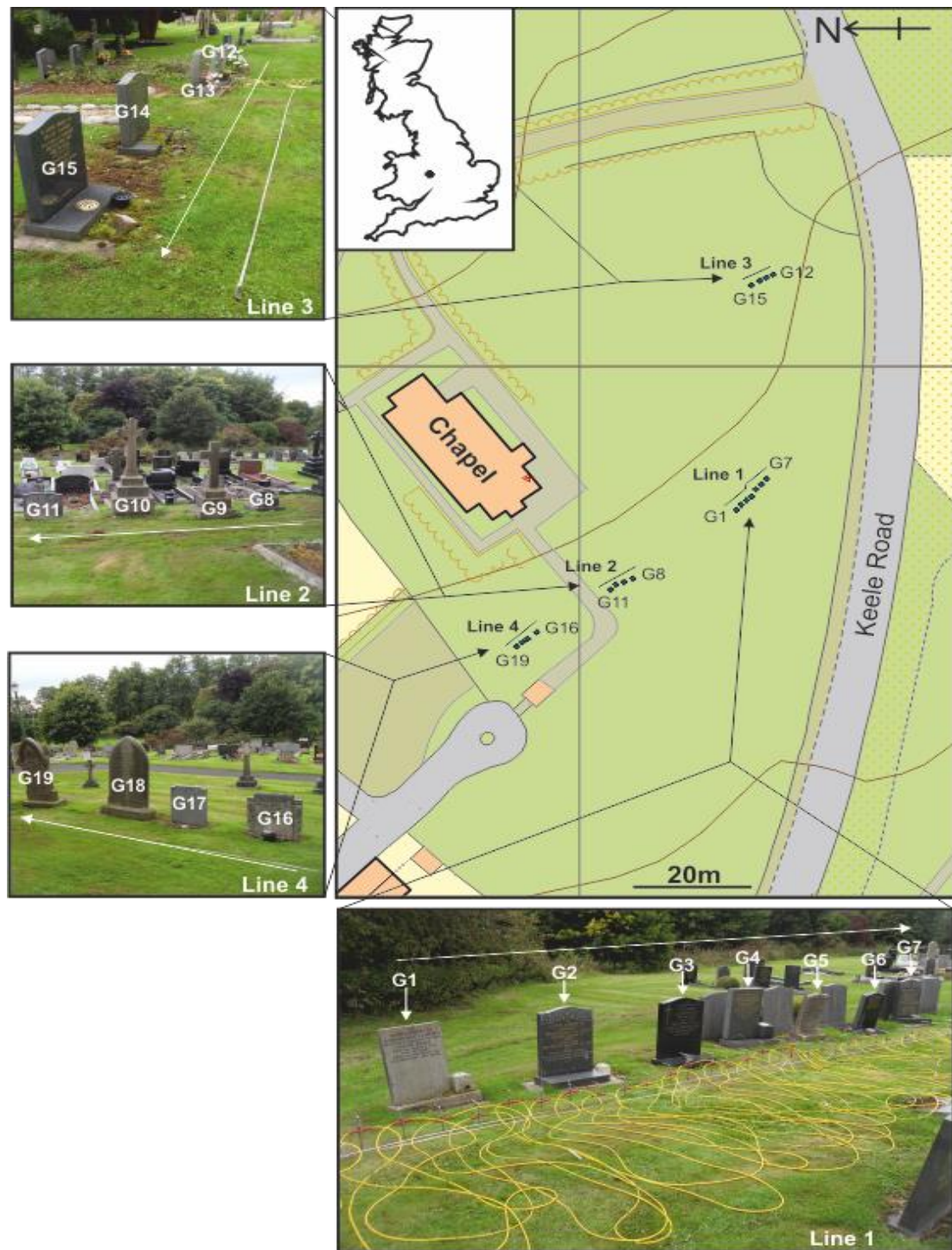


**Figure 4.29:** Map view of St. John's church graveyard, Staffordshire, UK, showing surveyed (and numbered) graves, 2D profile lines and orientations and annotated site photographs.

**Table 4.10:** Details of graves surveyed for case study 2 (St. John's Church graveyard)

Survey Lines	Grave no	Mid-point distance (m)	Age of last burial (year)	Occupancy	Soil type
1	G1	0.8	30	1	Sandy clay
	G2	1.9	24	2	
	G3	3.4	31	2	
	G4	4.3	21	2	
	G5	6.3	29	2	
	G6	7.3	32	1	
	G7	8.8	24	2	
2	G8	1	47	3	
	G9	2.7	100	3	
	G10	4	100	2	
	G11	5.4	93	2	
3	G12	1.2	13	2	
	G13	2.1	24	1	
	G14	3.2	20	1	
	G15	4.9	15	2	
4	G16	0.5	33	4	
	G17	2.4	34	2	
	G18	3.5	99	3	
	G19	4.8	23	2	

#### 4.6.2 Case study 2: Geophysical results

Magnetic susceptibility survey data acquired over profile line 1 detected 5 of the 7 young aged graves, although there may be some headstone positional errors (Fig. 4.30). Resistivity surveys over the same profile only detected 2 graves (G1 and G2) as relatively low resistance anomalies, when compared to background values (see Table 4.11).

**Table 4.11:** Statistics of geophysical data collected from Keele graveyard, Staffs., UK.

Case study	Line no.	App. Res Min./Av/Max, SD ( $\Omega$ .m)	Magnetic Susceptibility Min./Av/Max, SD ( $\times 10^{-6}$ )
Keele	1	164.5/179.1/193.7, 5.34	118.3/247.4/700.3, 128.02
Keele	2	145.2/173.6/227.0, 21.8	31.0/106.8/206.1, 38.9
Keele	3	228.7/254.1/283.9, 17.5	115.0/382.9/1004.5, 206
Keele	4	219.1/247.9/328.3, 29.4	35.3/114.0/330.0, 60.0
Keele	All	213.7	212.8

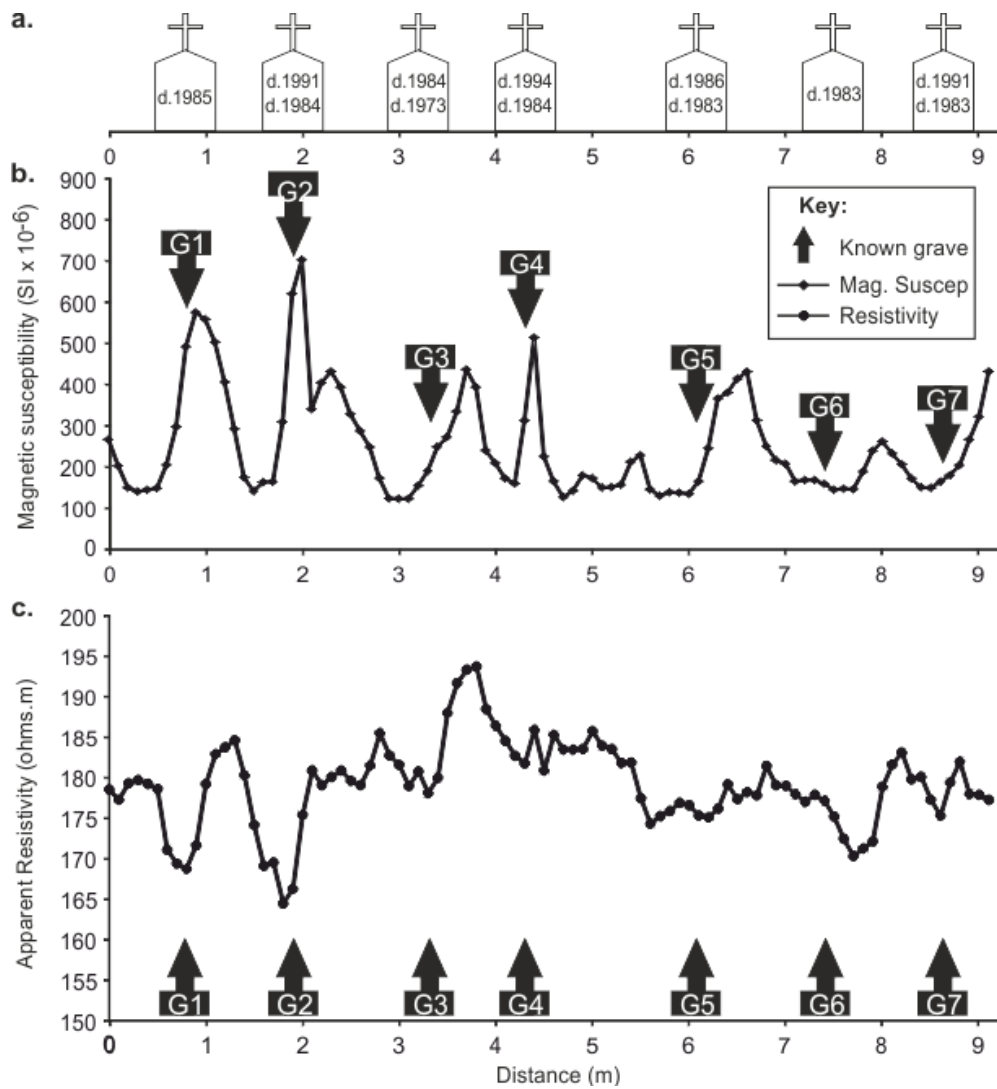


**Figure 4.30:** Keele 2D survey line 1 (Fig. 4.29 for location), showing (a) grave locations represented by headstones with year of burial inset, (b) magnetic susceptibility plot against profile distance and, (c) apparent resistivity plot against profile distance.

GPR 225 MHz dominant frequency 2-D profile line 1 identified 3 out of the 7 graves, the 450 MHz dominant frequency detected 6 and the 900 MHz dominant frequency detected all 7 and indeed 1 unmarked grave as separate, isolated hyperbolic reflection events (Fig. 4.31).

Magnetic susceptibility survey data acquired over profile line 2 detected all 4 old graves and indeed 1 unmarked burial (Fig. 4.32). In contrast, the resistivity surveys over the same profile did not detect any burials compared to background values (see Table 4.11).

GPR 225 MHz dominant frequency 2-D profile line 2 only identified 1 out of the 4 graves, with both the 450 MHz dominant frequency and the 900 MHz dominant frequency detected all 4 and 1 unmarked grave as hyperbolic reflection events (Fig. 4.33).



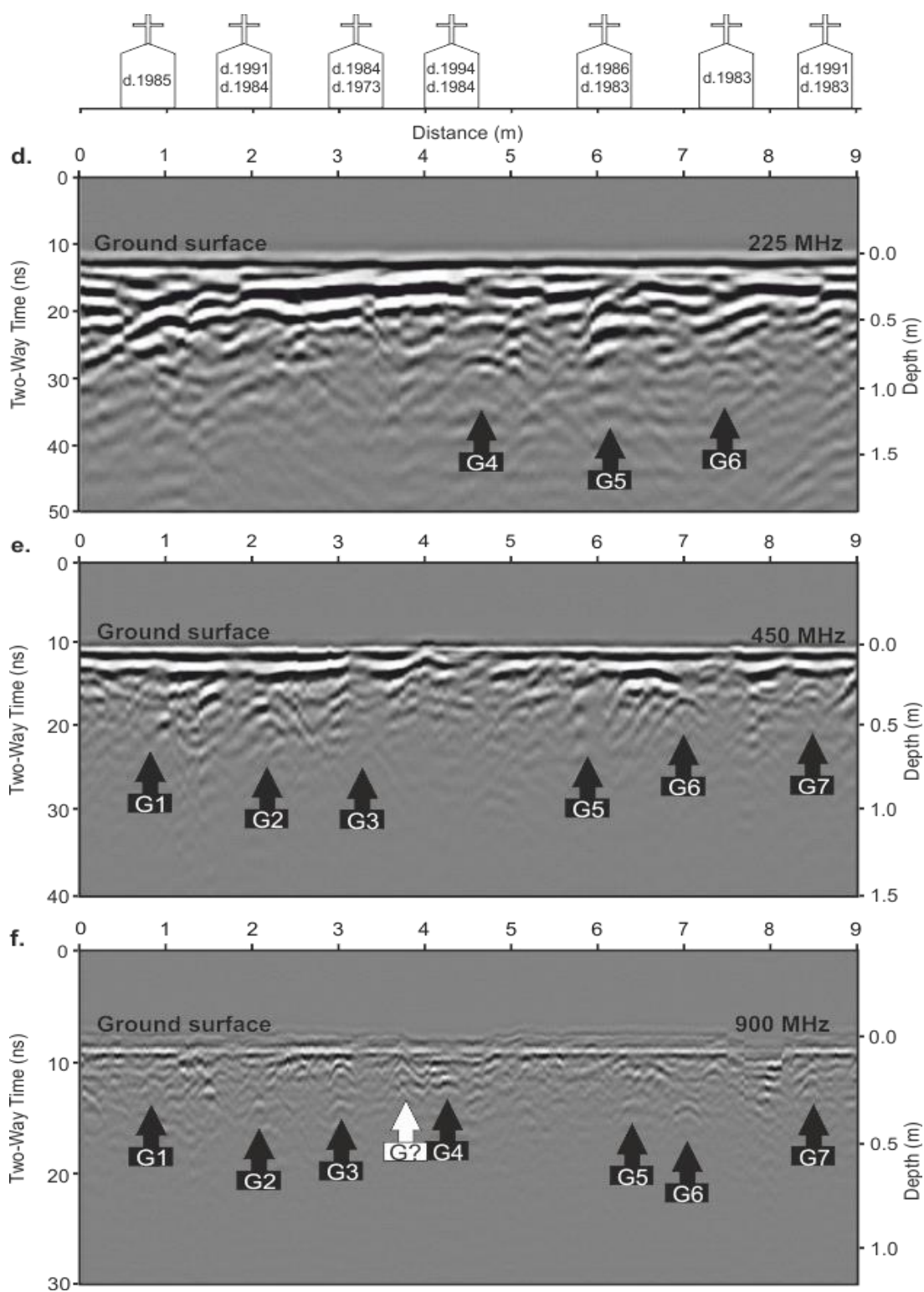


**Figure 4.31:** Keele 2-D survey line 1 (Fig. 4.29 for location), showing (a) grave locations represented by headstones with year of burial inset, (b) 225 MHz, (c) 450 MHz and, (d) 900 MHz frequency 2D GPR profiles with marked interpreted burial position.

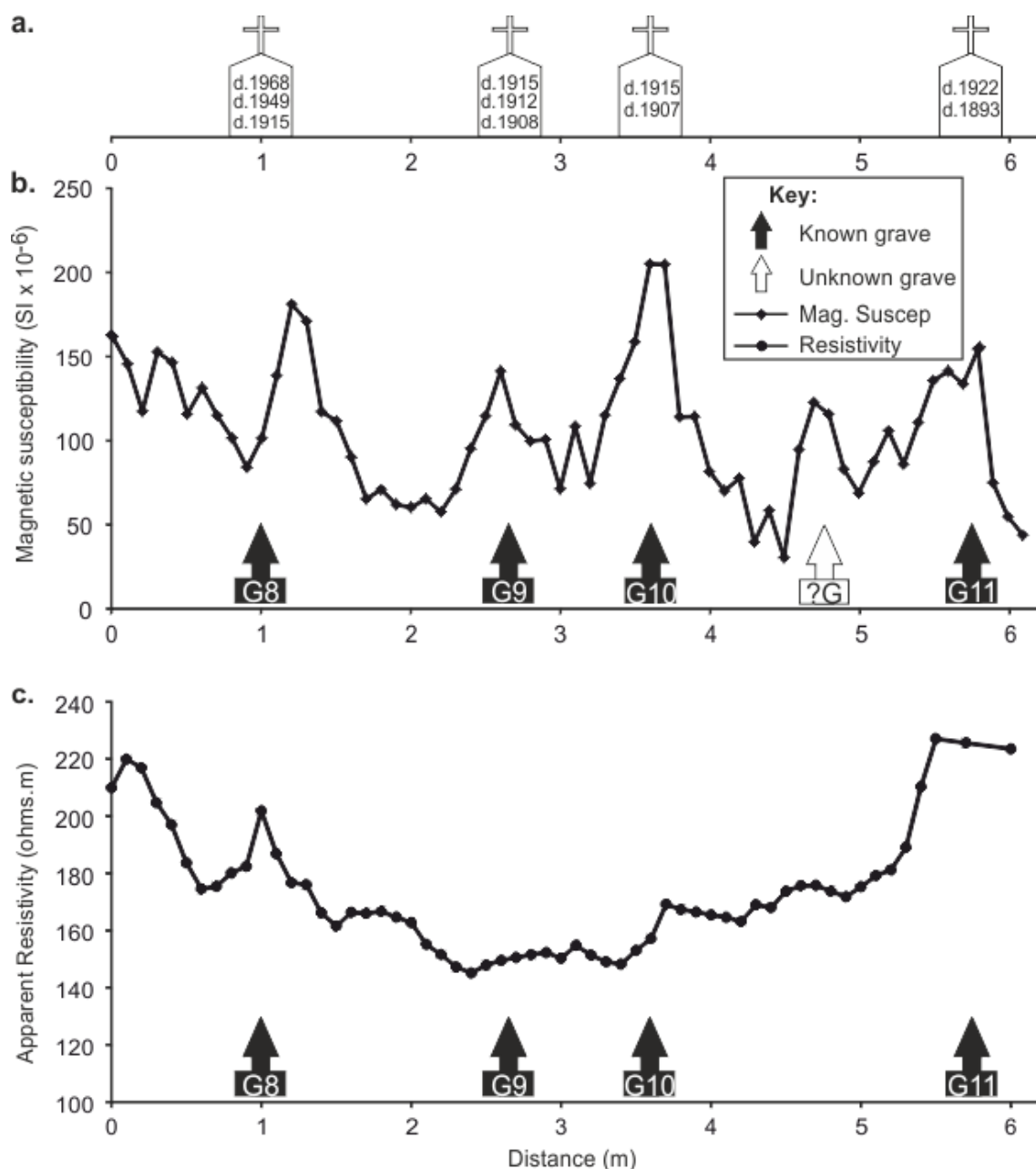


**Figure 4.32:** Keele 2D survey line 2 (Fig. 4.29 for location), showing, (a) grave locations represented by headstones with year of burial inset, (b) magnetic susceptibility plot against profile distance and, (c) apparent resistivity plot against profile distance.

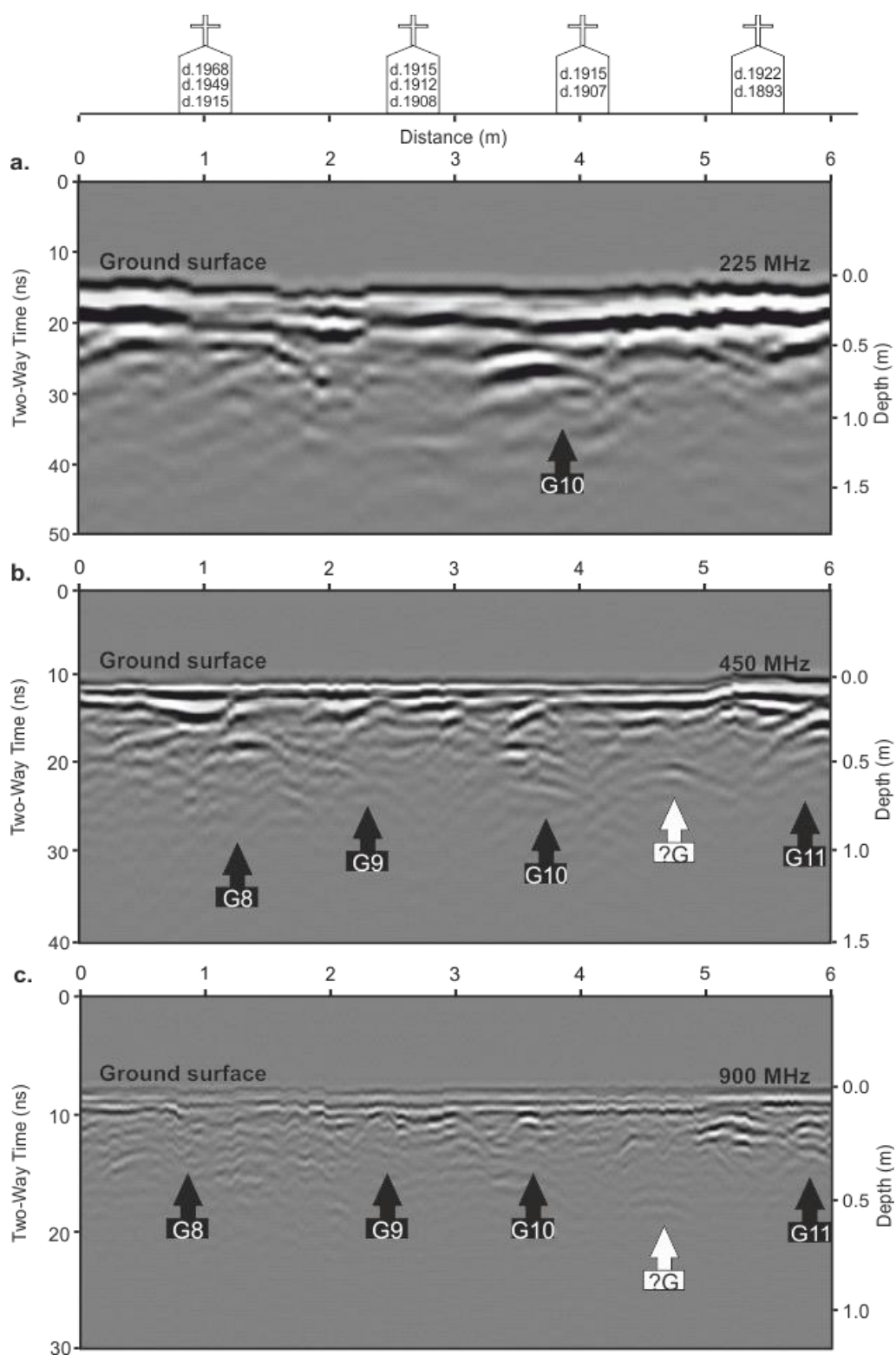


**Figure 4.33:** Keele 2-D survey line 2 (Fig. 4.29 for location), showing, (a) grave locations represented by headstones with year of burial inset, (b) 225 MHz, (c) 450 MHz and, (d) 900 MHz frequency 2D GPR profiles with marked interpreted burial position.

Magnetic susceptibility survey data acquired over profile line 3 only detected 1 of the 4 young graves and indeed 1 unmarked burial (Fig. 4.34). The resistivity surveys over the same profile did not detect any burials compared to background values (see Table 4.11).

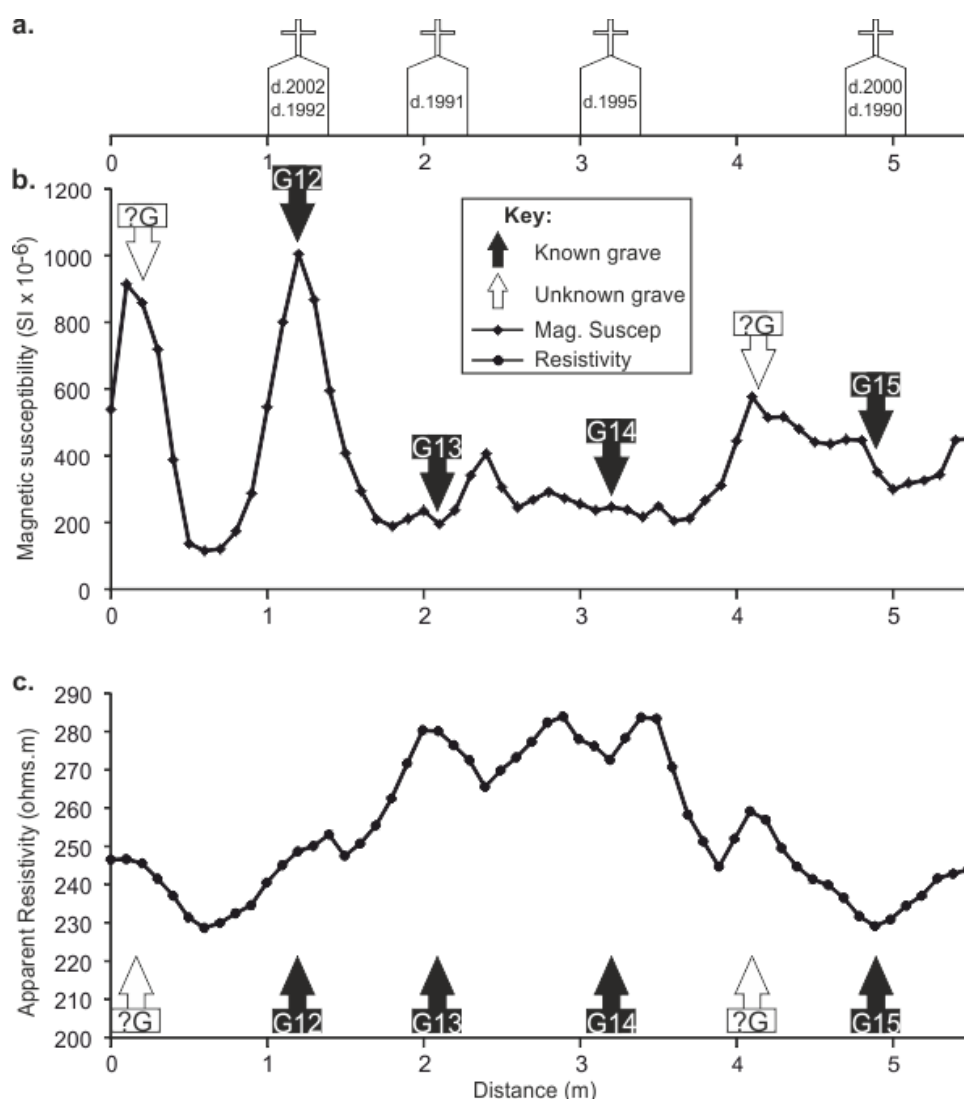


**Figure 4.34:** Keele 2D survey line 3 (Fig. 4.29 for location), showing, (a) grave locations represented by headstones with year of burial inset, (b) magnetic susceptibility plot against profile distance and, (c) apparent resistivity plot against profile distance.

GPR 225 MHz dominant frequency 2-D profile line 3 identified all 4 graves and an unmarked grave, with both the 450 MHz dominant frequency and 900 MHz dominant frequency detecting 3 and 1 unmarked grave as hyperbolic reflection events (Fig. 4.35).

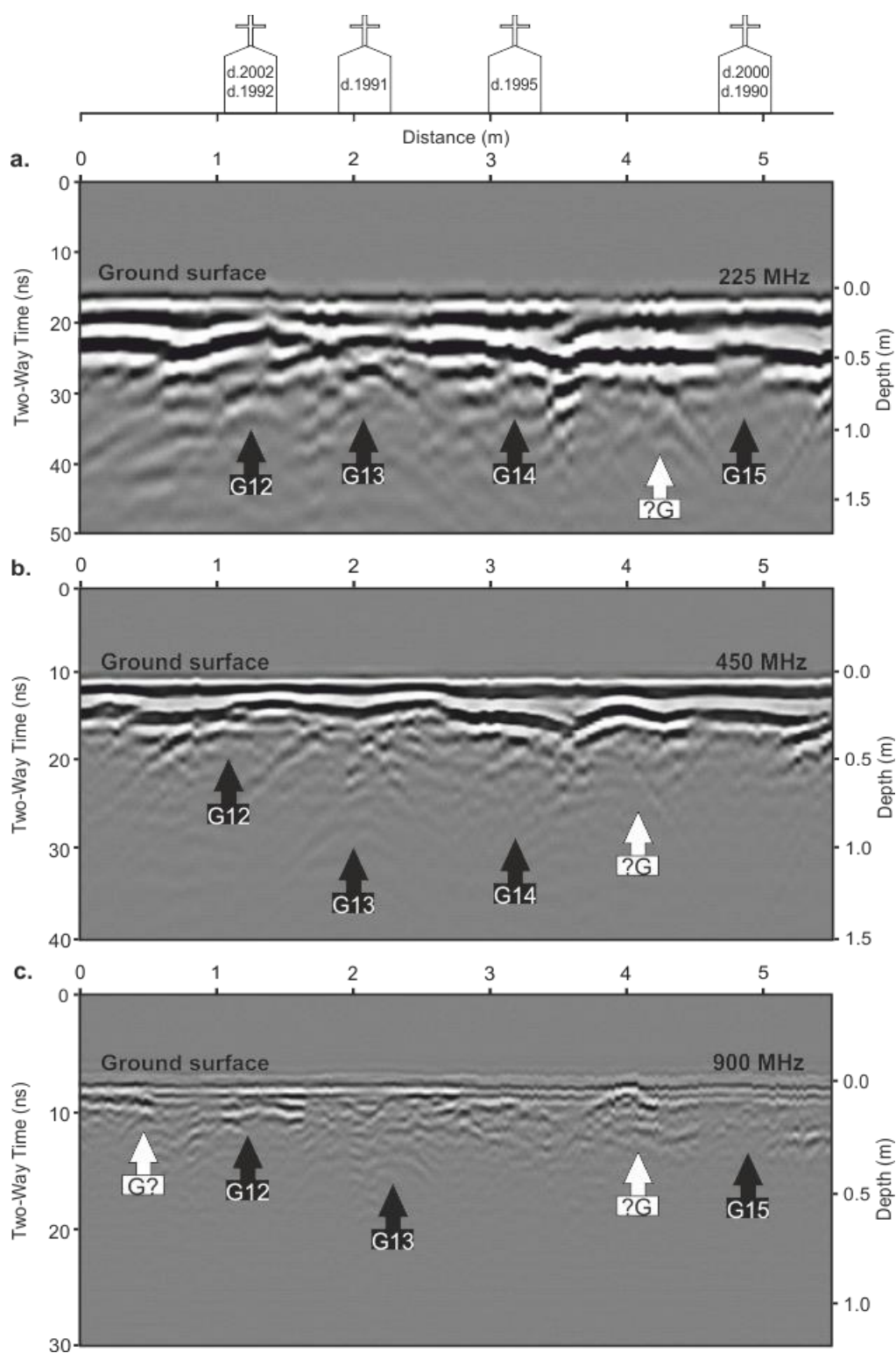


**Figure 4.35:** Keele 2-D survey line 3 (Fig. 4.29 for location), showing, (a) grave locations represented by headstones with year of burial inset, (b) 225 MHz, (c) 450 MHz and, (d) 900 MHz frequency 2D GPR profiles with marked interpreted burial position.

Magnetic susceptibility survey data acquired over profile line 4 did not detect the variable-aged graves (Fig. 4.36). The resistivity surveys over the same profile also did not detect any burials compared to background values (see Table 4.11).

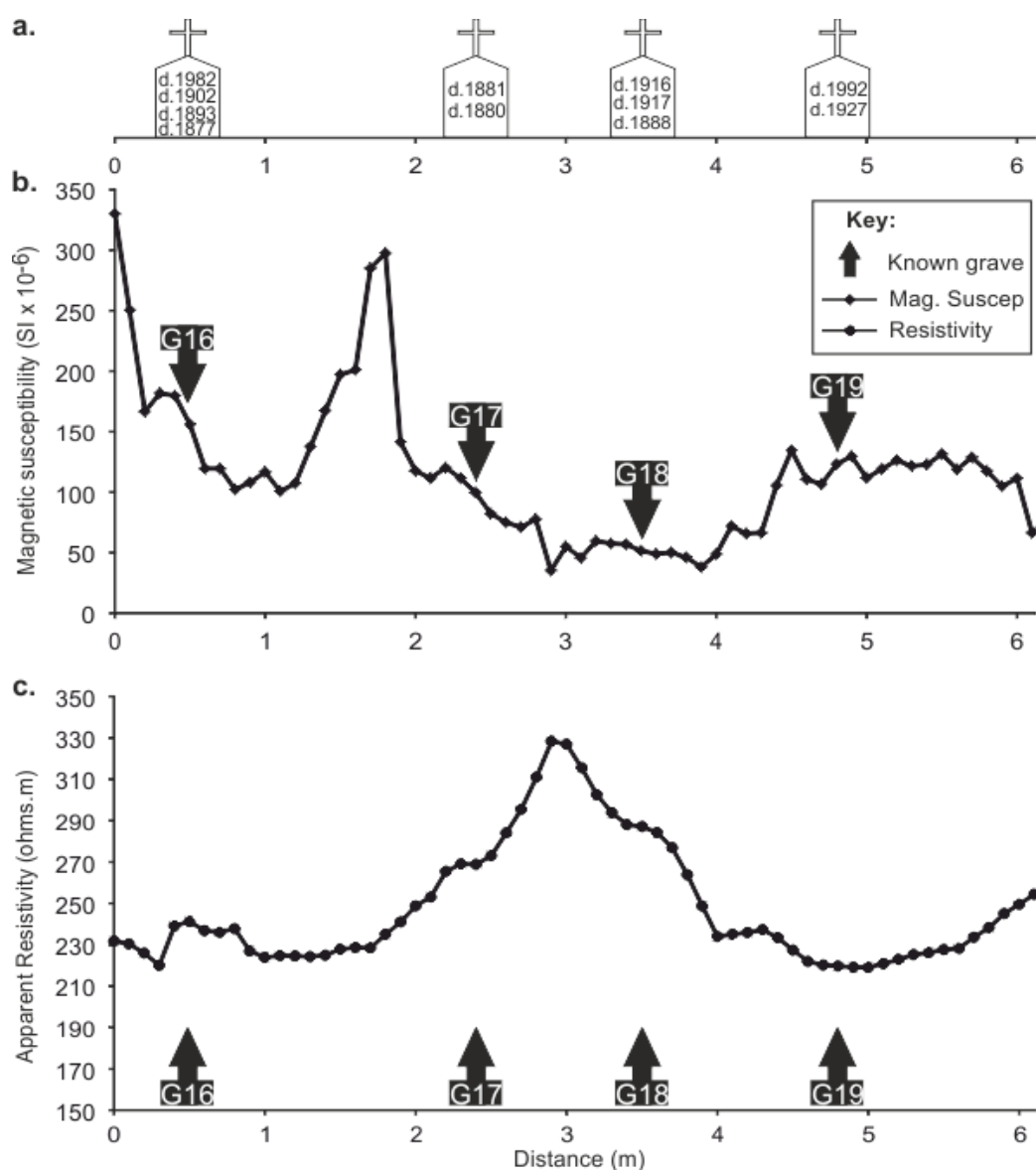


**Figure 4.36:** Keele 2D survey line 4 (Fig. 4.29 for location), showing, (a) grave locations represented by headstones with year of burial inset, (b) magnetic susceptibility plot against profile distance and, (c) apparent resistivity plot against profile distance.

All three GPR 225 MHz, 450 MHz and 900 MHz dominant frequency 2-D profiles on line 4 identified 2 of the 4 graves as hyperbolic reflection events (Fig. 4.37). Interestingly the double burial in G19 showed there were not positioned vertically (Fig. 4.37a/b). The summary of GPR detectability in Keele graveyard is shown in Table 4.12.



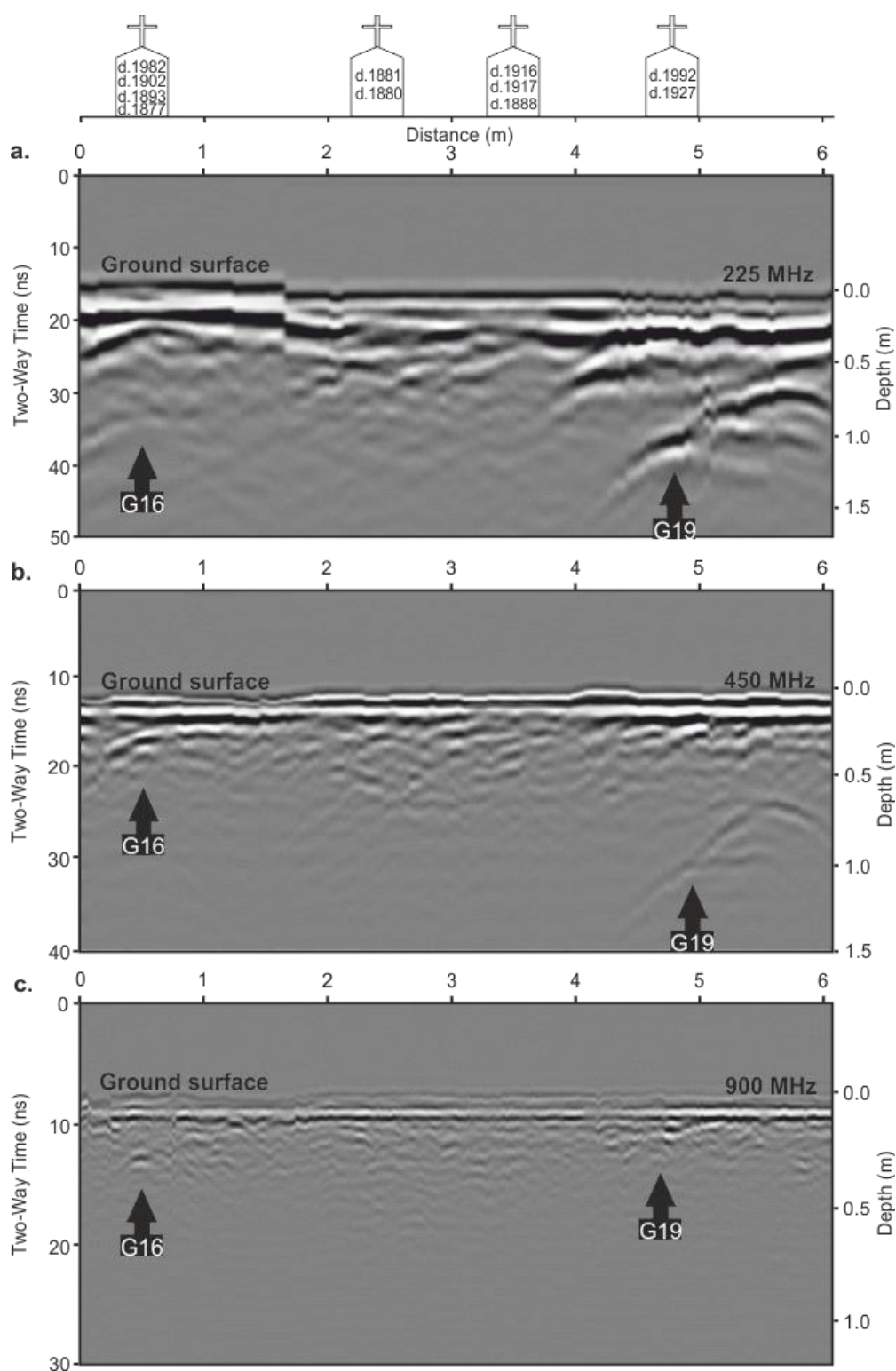


**Figure 4.37:** Keele 2-D survey line 4 (Fig. 4.29 for location), showing, (a) grave locations represented by headstones with year of burial inset, (b) 225 MHz, (c) 450 MHz and, (d) 900 MHz frequency 2D GPR profiles with marked interpreted burial position.

The combined survey line cross-plots of resistivity and magnetic susceptibility data against burial age are shown in Figure 4.38. Both show a general decrease of response against increasing burial age, however it is not significant.

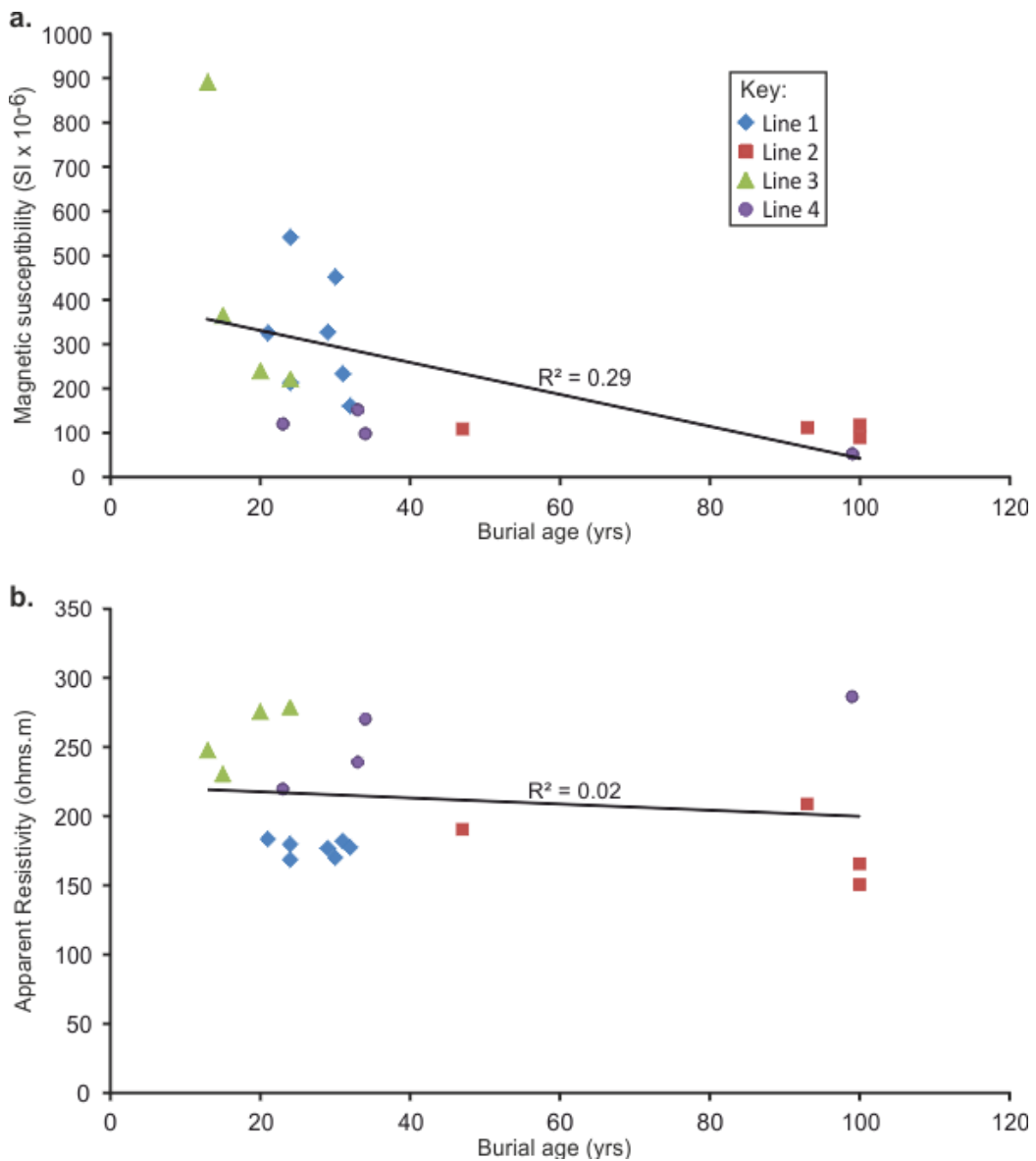


**Figure 4.38:** Combined Keele survey line cross-plot of (a) magnetic susceptibility and, (b) resistivity geophysical responses against age of burial (Table 4.10) respectively.

**Table 4.12:** Summary of GPR Keele survey (St. John's graveyard)

Keele Survey lines	Grave no. (burial age)	Antenna central frequency (MHz)			Occupancy
		225	450	900	
1	G1 (30)	No detection	Poor	Poor	1
	G2 (24)	No detection	Good	Poor	2
	G3 (31)	No detection	Poor	Excellent	2
	G4 (21)	Good	No detection	Poor	2
	G5 (29)	Poor	Poor	Poor	2
	G6 (32)	Poor	Good	Good	1
	G7 (24)	No detection	Good	Excellent	2
2	G8 (47)	No detection	Poor	Poor	3
	G9 (100)	No detection	No detection	Poor	3
	G10 (100)	Poor	Poor	Good	2
	G11 (93)	No detection	Good	Excellent	2
3	G12 (13)	Good	Good	Good	2
	G13 (24)	Poor	Poor	Poor	1
	G14 (20)	Poor	Poor	Poor	1
	G15 (15)	Poor	No detection	Poor	2
4	G16 (33)	Poor	Poor	Good	4
	G17 (34)	No detection	No detection	No detection	2
	G18 (99)	No detection	No detection	No detection	3
	G19 (23)	Good	Good	Poor	2
Maximum detection strength (%)		23	35	47	

## **4.7 Case Study 3: St. Luke's Church, Endon, Staffordshire, UK**

### *4.7.1 Background*

St. Luke's Anglican Church in Endon village is located ~10 km north-east of the city of Stoke-on-Trent, Staffordshire and ~190 m above sea level. According to the report by Tringham (1996), the chapel was first constructed by the Audley family in the 13<sup>th</sup> century, although Speake (1974) also affirmed Tringham's report, but however stated that the precise location of the then chapel is unknown, whether it fell into disuse cannot be accounted for. Meanwhile, the existing information about the church showed that the present chapel was established between 1719 and 1721, with repeated modifications in 1830, 1870, 1970 and 1981 (Speake, 1974). The first recorded burial was conducted in March 1731 (Speake, 1974), and since then burials have been conducted at the graveyard designated areas till present.

The local geology comprises of a coarse sandy soil containing predominantly sandstone pebbles overlay the Triassic Hawkesmoor Formation sandstones and conglomerate bedrock (British Geological Survey, 2013). Available local site investigation (SI) boreholes were also downloaded from the BGS (Table 4.13) and integrated to generate a schematic 2-D geological cross-section of the local area (Fig. 4.39).

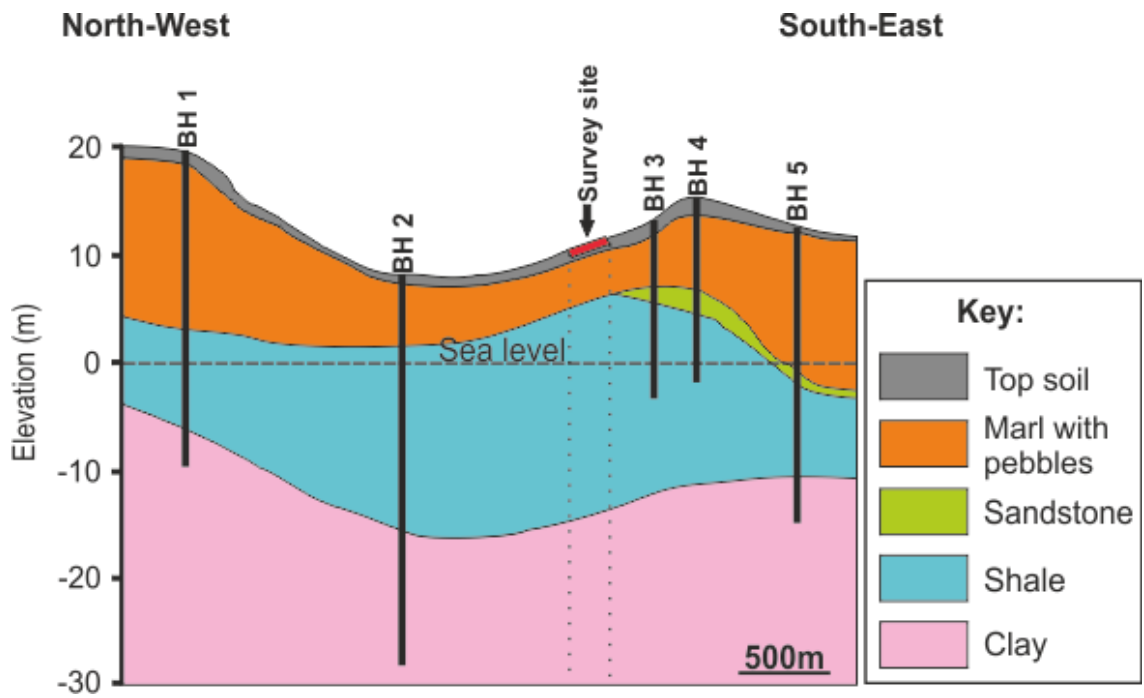


**Figure 4.39:** Approximately NW-SE orientated, 2D schematic cross-section of the site using BGS borehole information, with sea level at zero elevation (see Table 4.13).

**Table 4.13:** List of available local Endon site investigation borehole and pertinent information to generate the schematic 2-D cross-section shown in Figure 4.39.

S/N	Borehole No.	Borehole Name	X (m)	Y (m)	Drilled Date	Drilled Depth (m)	Depth to sea level (m)
1	BH 1	SJ85SE19	389900	354820	1957	30.5	20.4
2	BH 2	SJ95NW9	391440	355040	1964	37.8	8.5
3	BH 3	SJ95SW198	393290	353580	1977	16.2	12.8
4	BH 4	SJ95SW12	393600	353580	1965	17.1	15.2
5	BH 5	SJ95SW15	394320	352930	1965	28.3	13.1

Three soil samples from the site were also collected in a 0.7 m stainless steel hand corer and then interpreted using Chapman (2005) to have a yellowish red top-soil with sandstone pebbles (Munsell Colour: 5Y/5/6) at depth ~0.11 m below the ground level, from ~0.11 m to ~0.44 m depth is a reddish yellow sub-soil with sandstone pebbles (Munsell Colour: 5Y/6/6), while a dark reddish brown soil with sandstone pebbles is located below 0.44 m depth below the ground level (Fig. 4.40).

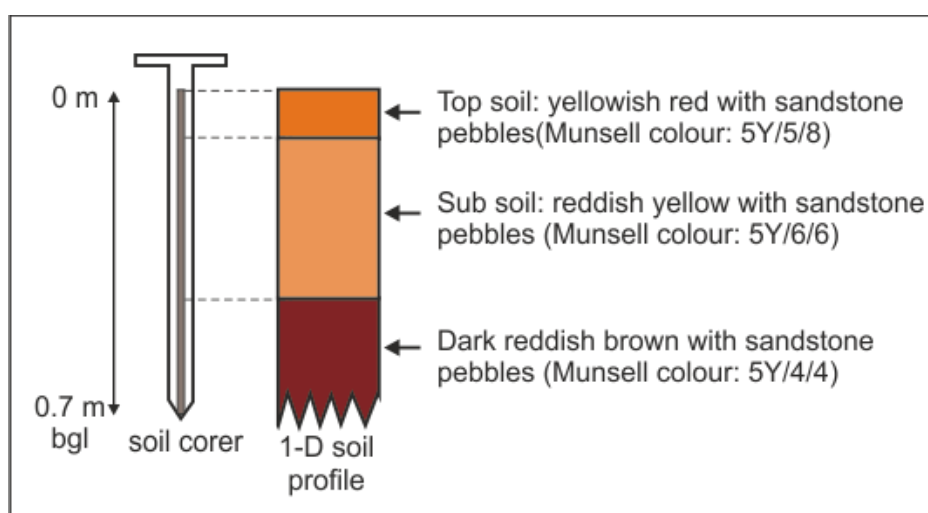


**Figure 4.40:** Schematic diagram showing the soil auger and generalised 1 D soil profile results at St. Luke’s graveyard Endon site.

The graveyard was approximately 200 m by 300 m which contained a few hundred burials dispersed over the churchyard, with the chapel building located at the eastern portion of the site and close to the main entrance gate (Fig. 4.41). Two geophysical survey profiles were chosen for access and varied burial ages (see Table 4.14). See Section 4.3.2.2 for geophysical data acquisition and processing steps utilised.



**Figure 4.41:** Map view of St. Luke's church graveyard Endon site, Staffordshire, UK, showing surveyed (and numbered) graves, 2D profile lines and orientations and site photographs.

**Table 4.14:** Details of graves collected from case study 3 (St. Luke's Church graveyard).

Survey Lines	Grave no	Mid-point distance (m)	Age of last burial (year)	Occupancy	Soil type
1	G1	0.8	39	2	Pebbles and sandy loam
	G2	2.5	25	2	
	G3	3.5	17	2	
	G4	4.8	41	1	
	G5	6.3	33	2	
	G6	7.3	15	2	
	G7	9.6	34	2	
	G8	10.9	17	2	
	G9	12.1	20	2	
	G10	13.3	40	2	
	G11	15.7	39	2	
	G12	16.9	25	2	
	G13	18.2	7	3	
	G14	19.5	18	2	
	G15	20.7	8	3	
	G16	21.9	34	3	
	G17	23.2	41	2	
	G18	24.2	42	3	
2	G19	1	16	2	
	G20	2.3	15	2	
	G21	3.7	22	1	
	G22	4.8	14	2	
	G23	6.3	25	2	
	G24	7.4	24	2	
	G25	8.5	Unknown	2	
	G26	9.6	1	2	
	G27	11	9	2	
	G28	12.3	30	2	
	G29	13.4	32	1	
	G30	14.5	29	2	
	G31	15.4	32	2	
	G32	16.8	9	2	
	G33	18	9	2	
	G34	19.7	9	2	
	G35	20.7	26	2	
	G36	21.8	17	2	
	G37	22.9	35	1	
	G38	23.9	6	2	



#### 4.7.2 Case study 3: Geophysical results

Magnetic susceptibility survey data acquired over profile line 1 detected 15 of the 19 young graves, although these were relatively low compared to background values in contrast to the first two case studies (Fig. 4.42). Resistivity surveys over the same profile detected 13 of the 18 graves and one unknown grave as relatively low resistance anomalies compared to background values (see Fig. 4.42 and Table 4.15).

**Table 4.15:** Statistics of geophysical data collected from Endon graveyard, Staffs, UK.

Case study	Line no.	App. Res Min./Av/Max, SD ( $\Omega.m$ )	Magnetic Susceptibility Min./Av/Max, SD ( $\times 10^{-6}$ )
Endon	1	116.3/156.9/199.8, 18.2	159/402/978, 155
Endon	2	117.4/161.3/215.9, 21.2	131/420/1460, 250
Endon	All	159.1	411.2

GPR 225 MHz dominant frequency 2-D profile line 2 identified 15 out of the 19 graves, with the 450 MHz dominant frequency detecting 10 and the 900 MHz dominant frequency detecting 9 and 1 unmarked grave as discrete hyperbolic reflections (Fig. 4.43).

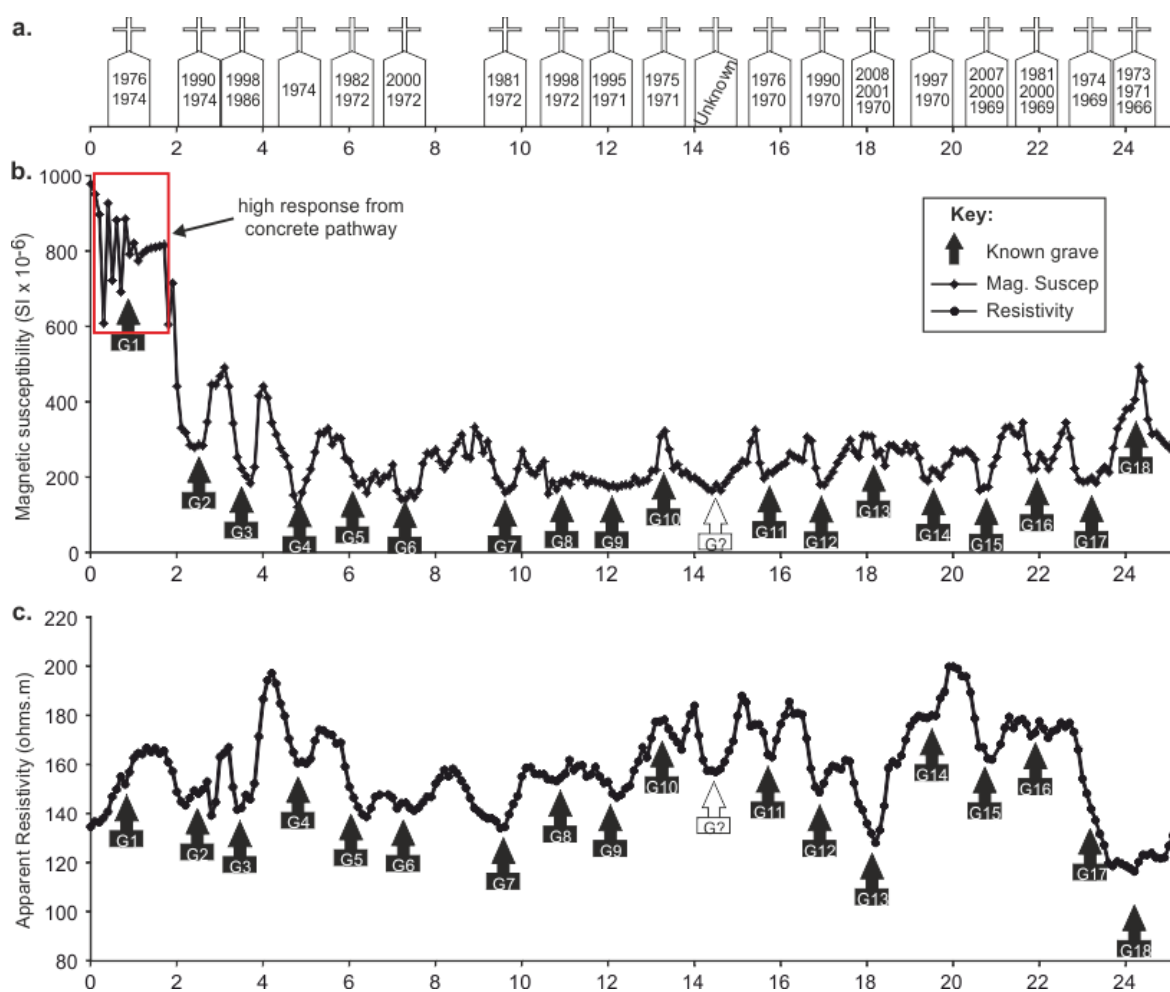


**Figure 4.42:** Endon 2D survey line 1 (Fig. 4.41 for location), showing, (a) grave locations represented by headstones with year of burial inset, (b) magnetic susceptibility plot against profile distance and, (c) apparent resistivity plot against profile distance.

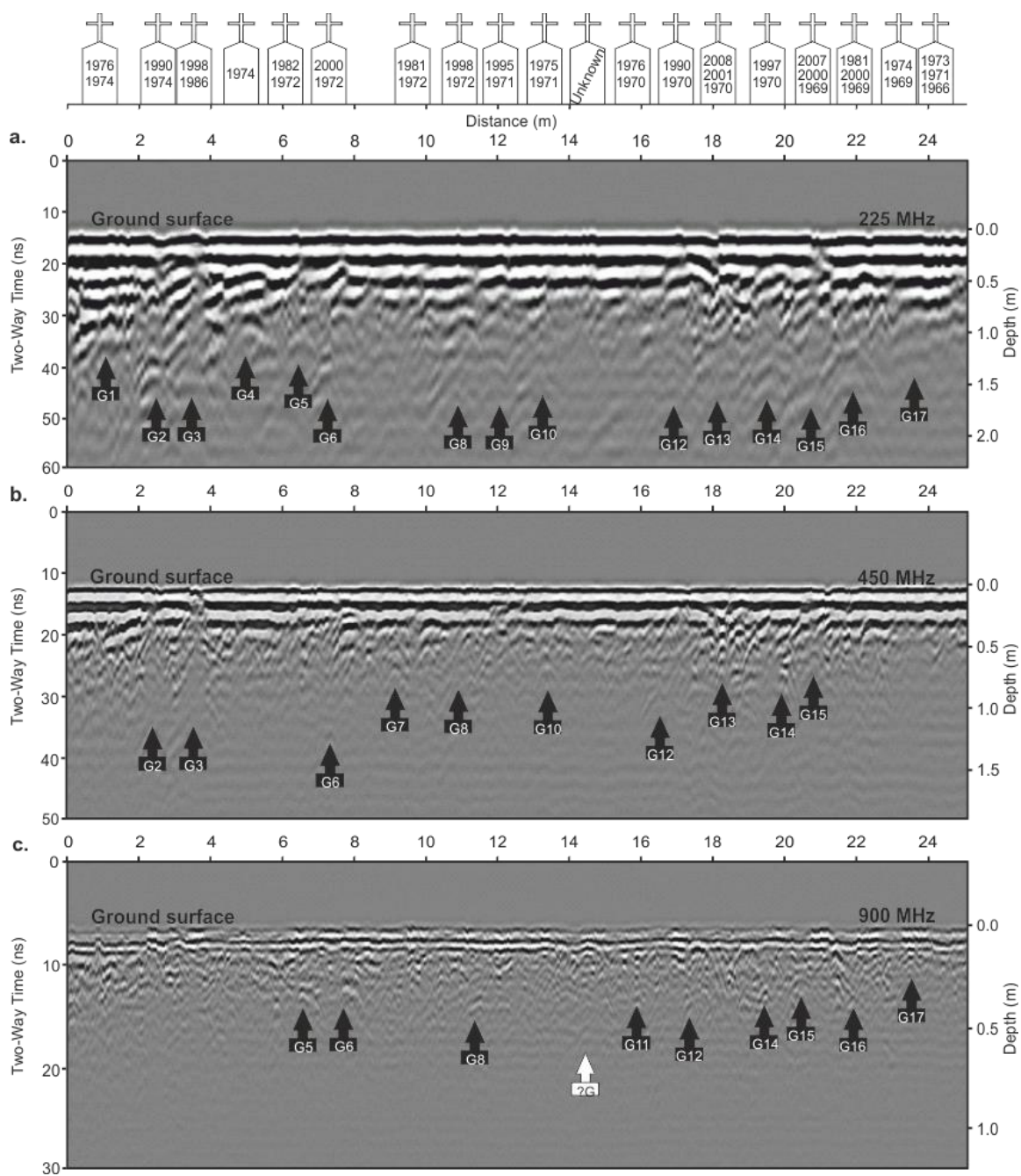


**Figure 4.43:** Endon 2D survey line 1 (Fig. 4.41 for location), showing (a) grave locations represented by headstones with year of burial inset, (b) 225 MHz, (c) 450 MHz and, (d) 900 MHz frequency 2D GPR profiles with marked interpreted burial position.

Magnetic susceptibility survey data acquired over profile line 2 detected 19 of the 20 young graves with them being relatively low compared to background values (Fig. 4.44). Resistivity surveys over the same profile detected all graves but were again relatively low resistance anomalies compared to background values (see Fig. 4.44 and Table 4.15).

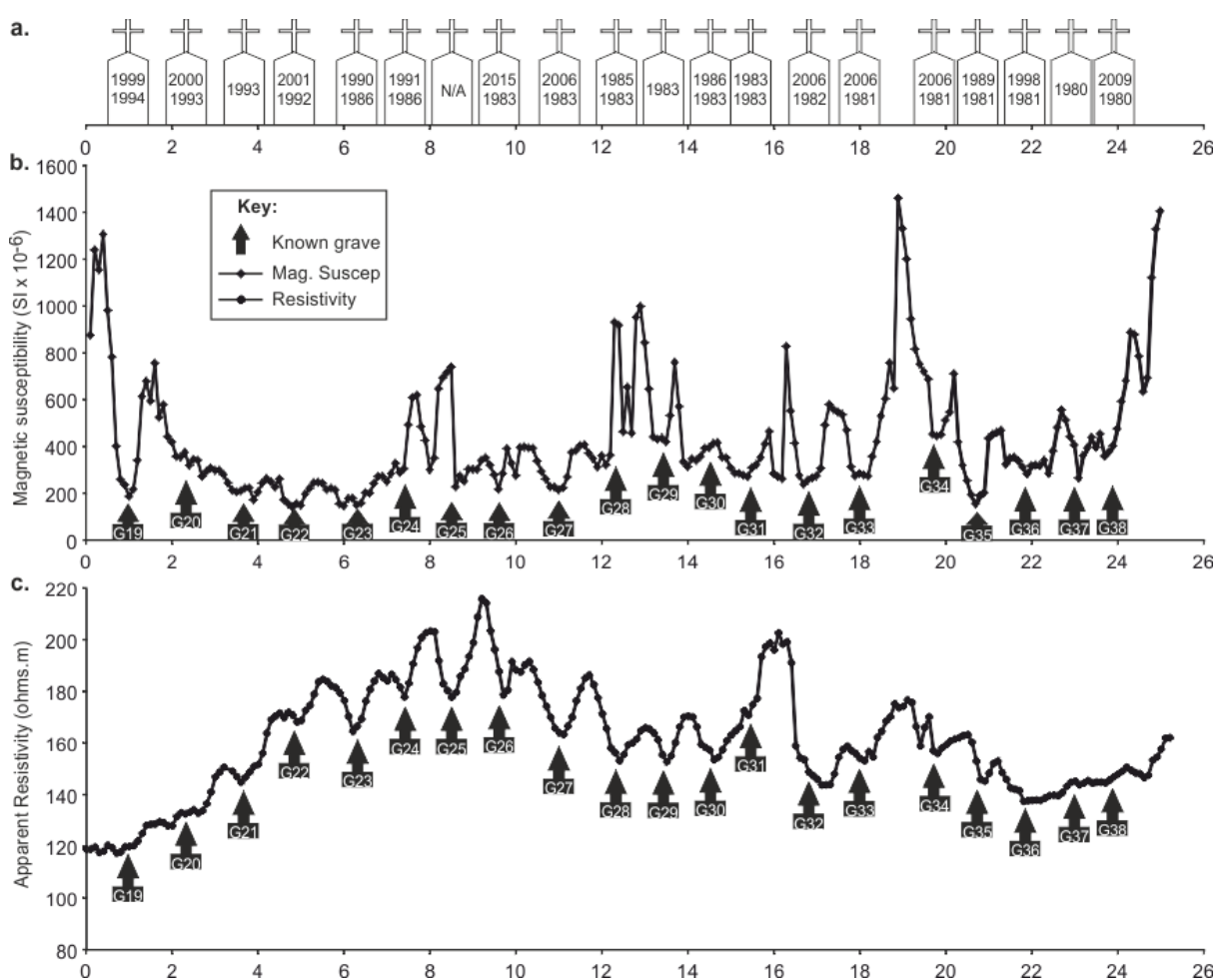


**Figure 4.44:** Endon 2D survey line 2 (Fig. 4.41 for location), showing, (a) grave locations represented by headstones with year of burial inset, (b) magnetic susceptibility plot against profile distance and, (c) apparent resistivity plot against profile distance.

GPR 225 MHz dominant frequency 2-D profile line 2 identified 14 out of the 20 graves, with the 450 MHz dominant frequency detecting 10 and the 900 MHz dominant frequency detecting 8 graves (Fig. 4.45). The summary of GPR detectability in Endon graveyard is shown in Table 4.16.

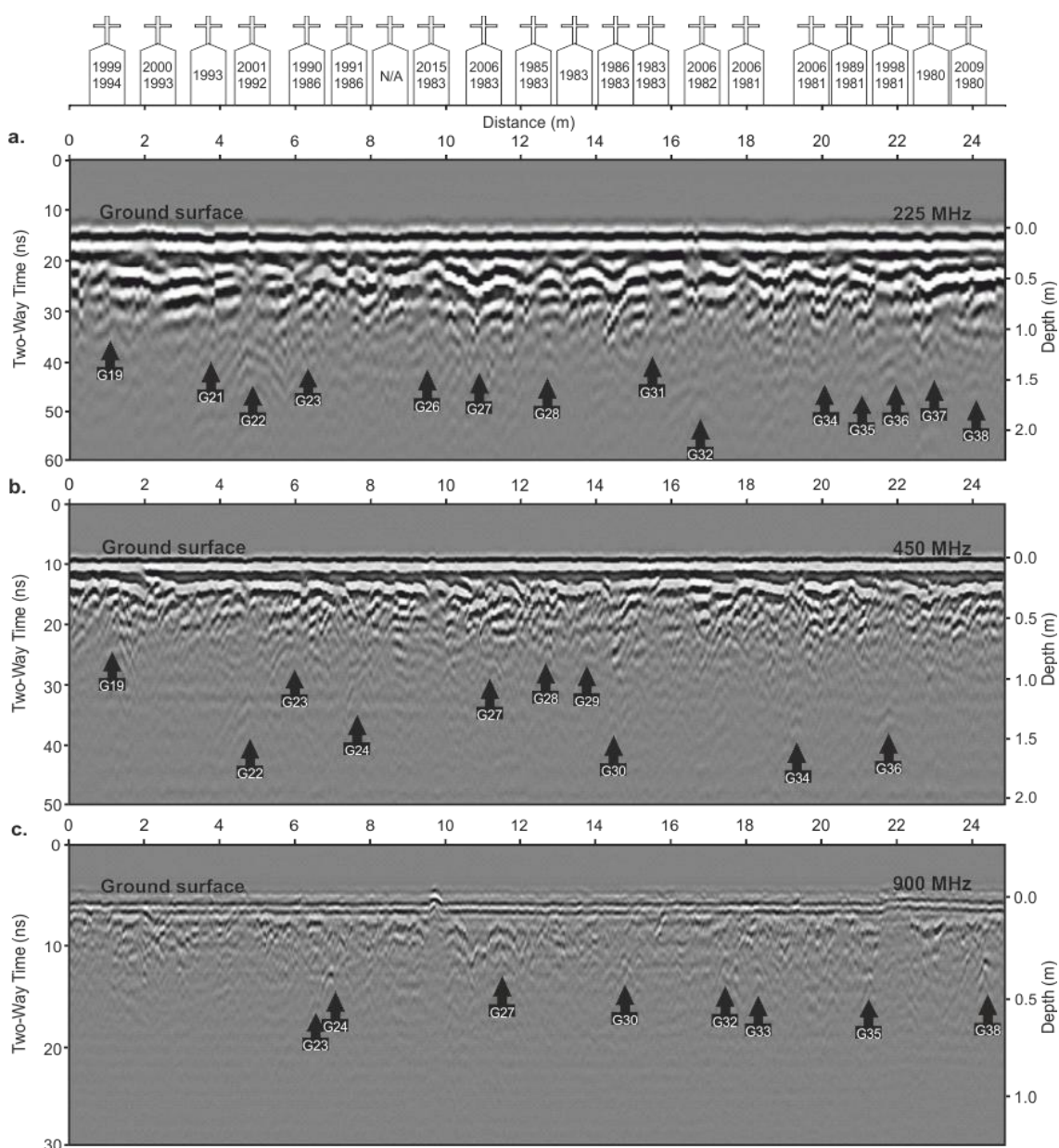


**Figure 4.45:** Endon 2D survey line 2 (Fig. 4.41 for location), showing, (a) grave locations represented by headstones with year of burial inset, (b) 225 MHz, (c) 450 MHz and, (d) 900 MHz frequency 2D GPR profiles with marked interpreted burial position.

The combined survey line cross-plots of resistivity and magnetic susceptibility data against burial age are shown in Figure 4.46 with no correlation.

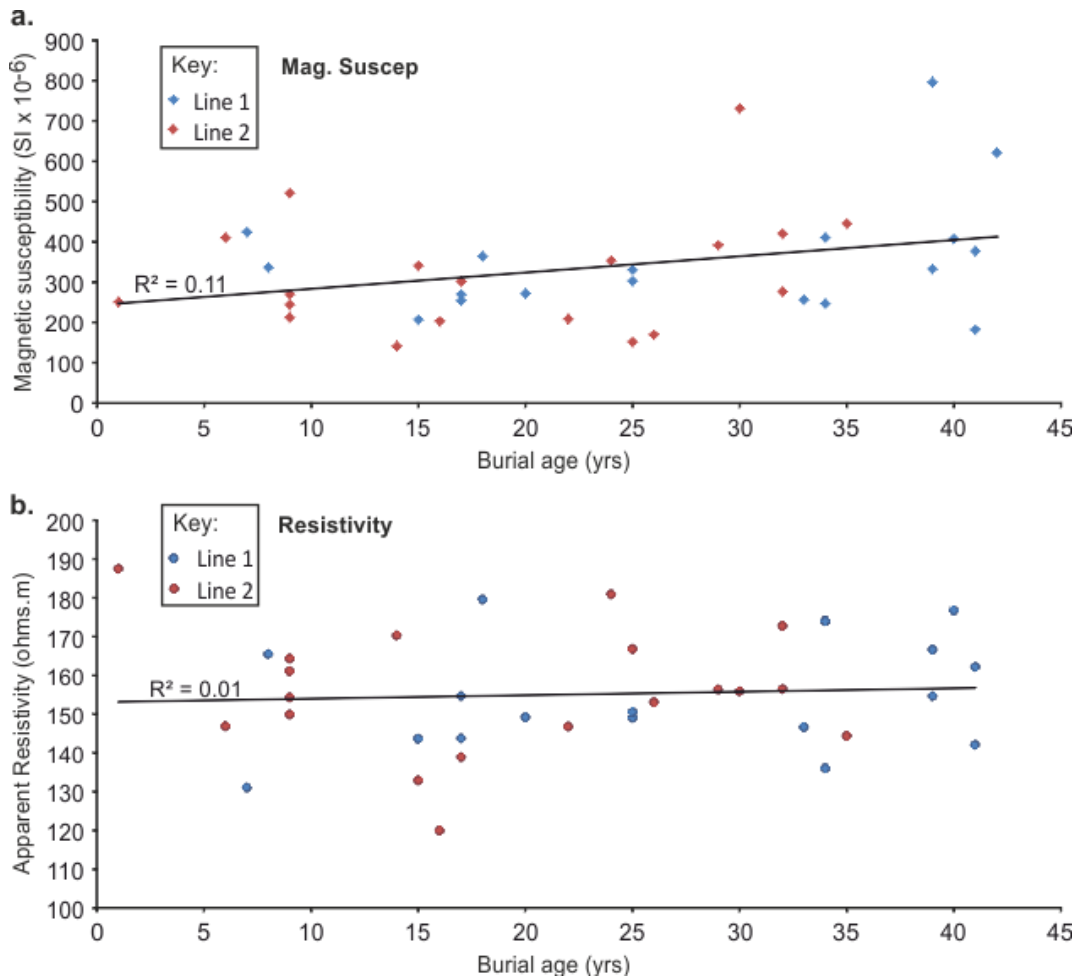


**Figure 4.46:** Combined Endon survey line cross-plot of (a) resistivity and (b) magnetic susceptibility geophysical responses against age of burial (Table 6.14) respectively.

**Table 4.16:** Summary of GPR Endon survey results (St. Luke's graveyard).

Endon Survey lines	Grave no.(burial age)	Antenna central frequency (MHz)			Occupancy
		225	450	900	
1	G1 (39)	Poor	No detection	No detection	2
	G2 (25)	Good	Poor	No detection	2
	G3 (17)	Poor	Poor	No detection	2
	G4 (41)	Poor	No detection	No detection	1
	G5 (33)	Poor	No detection	Good	2
	G6 (15)	Good	Poor	Poor	2
	G7 (34)	No detection	Good	No detection	2
	G8 (17)	Poor	Poor	Poor	2
	G9 (20)	Poor	No detection	No detection	2
	G10 (40)	Poor	Poor	No detection	2
	G11 (39)	No detection	No detection	Poor	2
	G12 (25)	Poor	Poor	Poor	2
	G13 (7)	Poor	Good	No detection	3
	G14 (18)	Good	Poor	Poor	2
	G15 (8)	Poor	Poor	Poor	3
	G16 (34)	Good	No detection	Poor	3
	G17 (41)	Poor	No detection	Poor	2
	G18 (42)	No detection	No detection	No detection	3
2	G19 (16)	Poor	Poor	No detection	2
	G20 (15)	No detection	No detection	No detection	2
	G21 (22)	Poor	No detection	No detection	1
	G22 (14)	Excellent	Good	No detection	2
	G23 (25)	Poor	Good	Poor	2
	G24 (24)	No detection	Poor	Good	2
	G25 (unknown)	No detection	No detection	No detection	Unknown
	G26 (1)	Poor	No detection	No detection	2
	G27(9)	Poor	Poor	Poor	2
	G28 (30)	Poor	Poor	No detection	2
	G29 (32)	No detection	Good	No detection	1
	G30 (29)	No detection	Poor	Poor	2
	G31 (32)	Poor	No detection	No detection	2
	G32 (9)	Poor	No detection	Poor	2
	G33 (9)	No detection	No detection	Good	2
	G34 (9)	Poor	Poor	No detection	2
	G35 (26)	Good	No detection	Poor	2
	G36 (17)	Good	Poor	No detection	2
	G37 (35)	Poor	No detection	No detection	1
	G38 (6)	Poor	No detection	Good	2
Max.detection strength (%)		32	22	18	

## 4.8 Statistical computation of techniques detectability

### 4.8.1 GPR techniques

Due to the non-quantifiable nature of GPR detected anomalies, it becomes difficult to quantify detection strength or detectability (%) of the GPR datasets. However, in this study, an attempt to quantitatively calculate the detectability of GPR at grave locations was undertaken by assigning numerical values to detected anomalies based on their hyperbolic-shaped reflection amplitudes and resolutions. Thus, anomaly scales ( $\alpha_i$ ) of 0, 1, 2 and 3 were used to represent, no-detection ( $\alpha_0$ ), poor detection ( $\alpha_1$ ), good detection ( $\alpha_2$ ) and excellent detection ( $\alpha_3$ ) respectively (see appendix 1A for detailed results) following Schultz (2012) methodology. Therefore, the maximum detection strength can then be determined statistically using equation (4.1), given as:

$$\frac{\sum \alpha_i}{3n} \times \frac{100}{1} \quad \text{eqn. (4.1)}$$

Where  $\alpha_i = 0, 1, 2$  and  $3$ ,  $n$  = total number of graves in the survey site and the coefficient  $3$  is the maximum detection scale.



#### 4.8.2 Electrical resistivity and magnetic susceptibility

Grave detection for resistivity and magnetic susceptibility techniques could be quantitatively calculated using a simple statistical ratio approach giving in equation 4.2. However, to account for the strength of detection or detectability (%) of a grave when electrical resistivity or magnetic susceptibility techniques is used, equation 4.2 is then modified into equation 4.3.

$$\frac{d}{n} \times \frac{100}{1} \quad \text{eqn. (4.2)}$$

$$\frac{\sum d_i}{3n} \times \frac{100}{1} \quad \text{eqn. (4.3)}$$

Thus,  $d$  is the detection, and  $d_i$  indicate scales of 0, 1, 2 and 3, which accounts for the degree of alignment between headstone and detection, to represent, no-alignment ( $d_0$ ), poor alignment ( $d_1$ ), good alignment ( $d_2$ ) and excellent alignment ( $d_3$ ) respectively,  $n$  is the total number of graves in the survey site and coefficient 3 is the alignment scale.

## 4.9 Discussion

This section is structured to answer and discuss the study aims and objective in sequential order.

The first aim of this study was *“to determine if geophysical responses over burial site graves, compared to background values, will decrease as the age of burial increases”*.

Looking at the survey results, geophysical response does seem to generally decrease as burial age increases, however, this variation depends mostly on the environment. This would be expected as one of the main geophysical targets in graveyard surveys, the back-filled shaft filled with disturbed soil (see Fig. 4.1) would rapidly compact over time and therefore have little geophysical contrast when compared with the undisturbed background surrounding soil. However, it does not seem to be a linear relationship as suggested in Fig 4.4; whilst relatively young burials (<30 years old) do have a statistically significant decreasing trend (*cf.* Fig. 4.26), over longer time periods the response versus burial age decrease appears to be more logarithmic (*cf.* Fig. 4.25). This would make sense as, once the grave soil is compacted and skeletonisation is complete, it would make any geophysical targets much more difficult to identify from background areas. However, this is not always the case, with results from the GPR, in particular, seem to be much more variable, even in the same study site, different age burials can result in much different detection rates (*c.f.* Tables 4.8, 4.12 and 4.16) for reasons which are, at present, unclear. Certainly the major variable of soil type also seems to mix up the results which will be discussed later.

The second aim of this study was “to *determine the optimal geophysical techniques suitable for the surveyed sites*” including old and young burials (between 1800 AD and present).

For GPR surveys, this study included 3 different commonly utilised (see Schultz, 2008; Pringle *et al.*, 2012b) GPR antenna frequencies (225, 450 and 900 MHz) with the optimal antenna frequency selection making a significant difference in anomaly detectability (see Conyers and Goodman, 1997). In Case Study 1 with clay-rich soils (Stockton graveyard), 900 MHz antenna frequency clearly identified the highest number of known burials (21 out of 27 burials), with maximum detectability of 43% (see Table 4.17). 450 MHz antenna frequency could also be used in these environments but may give less optimal results. In case study 2 with sand-rich soil (Keele graveyard), 900 MHz GPR antenna frequency was also effective, detecting 17 out of 19 known graves, with maximum detectability of 47% (Table 4.17). In case study 3 with coarse pebbly-soils (Endon graveyard), 225 MHz GPR antenna was optimal, detecting 29 out of 38 graves with detectability of 32% compared to 450 MHz (22%) and 900 MHz (18%) detectability (Table 4.17).

For the electrical resistivity surveys, Case Study 1 with clay-rich soils (Stockton graveyard) detected 15 out of 27 graves as low resistance anomalies, with maximum detectability of 56% (Table 4.18). Case study 2 with sand-rich soils (Keele graveyard) detected 14 out of 19 known graves in the site, with maximum detectability of 74% (Table 4.18). Case study 3 with pebble-rich soils (Endon graveyard) detected 29 out of 38 known graves in the site,

with maximum detectability of 76% (Table 4.18), again as relative low resistance anomalies compared to background values.

For the magnetic susceptibility technique, Case Study 1 with clay-rich soils (Stockton graveyard) detected 20 of 27 burials as relative high magnetic susceptibility anomalies compared to background values, with maximum detectability of 74% (Table 4.18). Case study 2 with sand-rich soils (Keele graveyard) detected 12 out of 19 known graves in the site as relative high magnetic susceptibility anomalies compared to background values, with maximum detectability of 63% (Table 4.18). Case study 3 with pebble-rich soils (Endon Graveyard) detected 28 out of 38 known graves in the site, with maximum detectability of 74% (Table 4.18) as relatively low resistance anomalies compared to background values. Clearly certain techniques worked very well in some environments (e.g. magnetic susceptibility in pebbly-soils) and yet were poor in another graveyard (e.g. Keele graveyard). It is interesting that in Case Study 1, despite the variations in the burial ages, 900 MHz GPR antenna frequency and magnetic susceptibility clearly distinguished both old (Line 1) and young burials (line 2). Thus, this evidenced that the major influence for detectability in Case Study 1 is not the age of burials, rather the soil type and textures which had preserved the associated properties of cadaver anomalies for a longer period (Dick *et al.*, 2015).

In addition, the dominant soil type for Endon graveyard favourably distinguished both electrical resistivity and magnetic susceptibility as optimum geophysical techniques,

detected 29 out of 38 graves for electrical resistivity and 28 out of 38 for magnetic susceptibility (Table 4.18).

**Table 4.17:** GPR grave detection summary for the 3 case studies.

Survey site	Dominant soil type	Total no. of graves	No. of detected graves/detectability (%)			Best fit antenna frequency
			225(MHz)	450 (MHz)	900(MHz)	
Stockton graveyard	Silt clay	27	6 (9)	19 (28)	21 (43)	900 (MHz) and 450 (MHz)
Keele graveyard	Sandy clay	19	10 (23)	14 (35)	17 (47)	900 (MHz)
Endon graveyard	Pebbles and sandy loam	38	29 (32)	20 (22)	17 (18)	225 (MHz)

\*Maximum detectability in brackets

**Table 4.18:** Resistivity and magnetic susceptibility grave detection summary for the 3 case studies.

Survey site	Dominant soil type	Total no. of known graves	No. of detected graves/detectability		Best fit survey technique
			Resistivity ( $\Omega.m$ )	Mag. Suscep. (SI)	
Stockton graveyard	Silt clay	27	15 (56)	20 (74)	Mag. Suscep.
Keele graveyard	Sandy clay	19	14 (74)	12 (63)	Resistivity
Endon graveyard	Pebbles and sandy loam	38	29 (76)	28 (74)	Resistivity and Mag. Suscep.

\*Detectability in brackets

The third and final aim of this study was *“to gain knowledge of the effect of different soil types and burial grave detection”*. Soil type was the most important variable to consider for the detectability and consistency of geophysical techniques in burial grave searches as others have shown (e.g. see Schultz, 2007; Fiedler *et al.*, 2009a; Hansen *et al.*, 2014). For

example, a very coarse site soil dominated with pebbles and sandy loam (Endon graveyard) had the best resistivity detectability of 76 % followed by sandy clay dominated soil type (Keele graveyard) with detectability of 74 %, whilst silty clay dominated soil type had lower detectability of 56 % as seen in Stockton graveyard (Table 4.18). In the literature electrical resistivity has commonly been used to delineate both marked and unmarked burial grave with recorded success obtained mostly in sandy dominated soil (Ruffell and Kulesa, 2009; Pringle *et al.*, 2012b). Therefore, case studies 2 (Keele graveyard) and 3 (Endon graveyard) with relatively sandy dominated soil had established resistivity as the prevailing technique for burial grave detection in such soil type scenario.

Magnetic susceptibility technique was more successful in a silty clay dominated soil (Stockton Graveyard) with target detectability of 74 %. However, the presence of pebbles in Endon site soil background had probably distinguished grave positions as areas of low magnetic susceptibility following heterogeneous nature of back-filled, thus given rise to detectability of 74 %. However in Keele graveyard which was dominated with sandy clay soil, this had the least target detectability (63 %) when compared to the other 2 case studies. Despite the popular acceptance of GPR technique in grave searches, this study suggests the use of other techniques such as resistivity or magnetic susceptibility in a clay-rich dominated soil (as others have found, see Reynolds, 2011; Gaffney *et al.*, 2015), even known graves cannot be imaged with GPR in a highly conductive soil (Bevan, 1991). In the clay-rich site soils (Stockton and Keele graveyards), GPR showed poor burial detection and low quality hyperbolic reflections, especially with 225 MHz antenna frequency due to more signal attenuation (Figs. 4.21 & 34). However, the same antenna

frequency in a clay-free dominated site (Endon graveyard) showed high burial detection with high amplitude reflections (Figs. 4.44 & 46). Figure 4.48 summarised the result of the integrated interpretation of dominant soil types and optimum techniques encountered in these case studies represented in a ternary diagram.

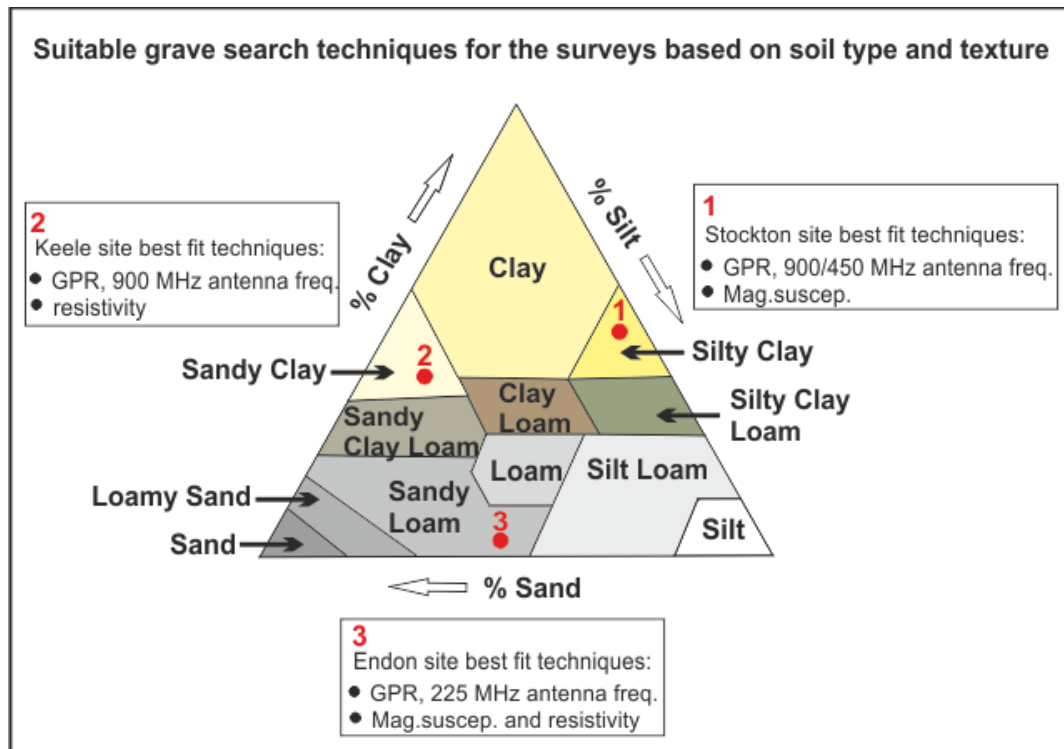


**Figure 4.47:** Ternary diagram showing optimum grave detection techniques and respective dominant soil types and textures.

#### **4.10 Limitation and further work**

Clearly a significant limitation is the number of graves that could be surveyed at the chosen study sites. Significant numbers of graves had various above-ground objects preventing geophysical data to be collected with older grave headstones having fallen over, removed or indeed leading to unmarked graves (as can be seen in the survey lines in this chapter). Clearly increasing the numbers of surveyed graves in the dataset would provide more confidence of the cross-plots of burial age versus geophysical responses.

A larger and even range of aged burials would also be optimal which wasn't possible in the survey sites here, ideally a statistically significant number (for example, 10+) would be surveyed in each decade going back 200 years would be optimal but wasn't possible here. Perhaps other graveyards with similar soil types to those surveyed may prove helpful to identify, gain permission and collect more datasets to improve results.

Whilst the major end-member soil types (sand and clay) and coarse soils were able to be surveyed, graveyards in other soil types were not surveyed, for example, peat-rich soils, coastal (saline) soils, etc. This would allow further datasets to be collected and to see what results occur in these soil types as well. Obviously other burial grounds in different climates and depositional environments would also be helpful to survey.



The graveyards studied were all Church of England; it would be beneficial to survey burials from other religious faiths to see what effect different burial styles have on target detection. For example Muslim burials are dominated by simple cloth or linen wrapping rather than a coffin. So-called green burials (Hansen and Pringle 2011) are also becoming more popular and it would be useful to see what the effect of shallow burials and wicker baskets may be on geophysical responses.

#### **4.11 Conclusions**

Selected known grave positions and burial ages in three Anglican graveyards, with varying soil types, were geophysically surveyed using multi-frequency GPR, electrical resistivity and surface magnetic susceptibility techniques. Whilst target detection did decrease as burial age increased as expected, the results here showed that soil type was a major variable. Instead of one geophysical technique being optimal for overall target detection, all three techniques were optimal in clay-rich (magnetic susceptibility), sandy (electrical resistivity) and coarse sand and pebbly (225 MHz GPR) soil types respectively when looking at geophysical anomaly quality. Relatively high frequency antenna (900 MHz) was optimal in two out of the three graveyards surveyed, with 0.5m spaced electrode probes found to be optimal for electrical resistivity surveys.

The results of this study also show that known grave marker positions may not be accurate. Clearly increasing the numbers of surveyed graves in the dataset would provide more confidence of the study results with burial age spread from 200 years to the present

day but this was not possible with the graveyards in this study due to the burial ages and above-ground materials present. More graveyards with different soil types would also prove beneficial to survey to validate and improve these study results, for example, peat-rich soils, saline coastal soils, etc. Other burial grounds in different climates and depositional environments would also be helpful to survey and compare to these data sets. It would also prove beneficial to survey burials from other religious faiths, or indeed so-called green burials to see what effect different burial styles have on target detection. The datasets and technique development for these complex environments where there are known grave contents add value to the investigations being conducted for clandestine burials.

## **CHAPTER 5: Elemental analysis of an *in situ* animal burial decomposition fluids and long term graveyard soils**

### **5.0 Overview**

This chapter presents the results from elemental analysis of decomposition fluids arising from animal/human burials in a semi-confined disposal facility (SCDF), and the characteristics of the host soil on the potential for being contaminated by inorganic elements from cadaver decomposition. This is undertaken by both the elemental analysis of decompositional fluids of an *in situ* buried pig carcass over an 18 months post-burial period and graveyard soils. The main factors that control decompositional fluid generation and concentration, and its subsequent potential to contaminate soil, are examined, with special attention on contamination impact factors to assist the search for clandestine burials. This study provides improved standard operating procedures (SOPs) to scientifically investigate potential contaminated site(s) associated with animal/human burials.

### **5.1 Chapter aims and objectives**

The aims of this chapter are; *firstly* to sample and present results from a 18 month monitoring study of a burial pig carcass, analysing the leachate and background soil water for the major inorganic chemical components; *secondly*, perform a systematic statistical analysis of the resulting element parameters to determine the contributions from

individual inorganic ions responsible; *thirdly*; determine the elevated metallic elements in long-term burial sites (three graveyards) when compared with control values, and *fourthly and finally*; using the results as a potential for detecting clandestine burials of murder victims. Thus, the objectives of this study are; (1) set up a pig grave for monthly monitoring and a corresponding control site for background soil water extraction; (2) analyse data after necessary corrections; (3) determine the relationship between electrical conductivity and inorganic elements of animal leachate and control soil water from the monitoring site and, (4) analyse and compare between soil samples from long-term burials in Church of England graveyards and corresponding off-site control soil samples.

## 5.2 Introduction

Burial, composting and incineration are among the most common methods of carcass disposal (Home Office, 2007; Williams *et al.*, 2009). Burial has been the most viable and convenient option to reduce the effect on the local environment (Amuno, 2013; Donaldson *et al.*, 2013). However, a recent comparison of disposal options in the U. S. and Canada has shown that properly composted carcasses generate little leachate (Milligan *et al.*, 2008) and have often been referred to as being more environmentally friendly than the currently favoured burial disposal method. This is because composting recycles nutrients and other potential contaminants back to the topsoil, rather than keeping them closer to groundwater (Glanville *et al.* 2009), although it is more expensive (Donaldson *et al.*, 2013). Leachate in this study can be defined as a water-based solution of compound

derived from abandoned waste and dead mammal tissue (Christensen *et al.*, 2001). Both animal/human mass burial pits and municipal solid waste (MSW) landfills are notable primary hosts for leachate generation and are very similar in operation (Fiedler *et al.*, 2012). Whilst MSW landfills contain a complex mixture of anthropogenic deposits, with wide ranges of variation in their physical and chemical properties (Meju, 2000), studies have shown that leachate generated in animal mass burial pits can be highly concentrated and be much more toxic to the environment than leachate arising from MSW landfills and other disposal methods (Bonhotal and Schwarz, 2009). Graveyards have even been described as a special kind of landfill (Fiedler *et al.*, 2012).

Landfill sites come in various shapes, sizes and depths, they may be located in purpose-built facilities, disused soft rock or hard rock quarries, opencast coal mines or other suitable holes in the ground (Meju, 2000; El-Fadel *et al.*, 2002). The availability of these suitable holes coupled with the rapid growth in human population, especially in urban areas, has resulted to an increased number of MSW landfills globally (Baderna *et al.*, 2011). Consequently, the study of landfills and its subsequent environmental hazards, has attracted more interest than in animal/human mass burials (Freedman and Fleming, 2003; Rodrigues and Pacheco, 2003). Thus, a significant amount of research has been conducted over the past several years with regards to formation of leachate in landfills, and the transport and attenuation of leachate contaminants in the environment. These studies covered both lined and unlined landfills (Al Yaqout, 2003; Al Yaqout and Hamoda, 2007; Zychowski, 2011); old and young landfills (Ettler *et al.*, 2008; Daartinen *et al.*, 2013); controlled and abandoned landfills (Meju, 2000; Kim and Kim, 2002, Melnyk *et al.*, 2014);

and closed and open landfills (Mor *et al.*, 2006; Ehirim *et al.*, 2009; Al Sabahi *et al.*, 2009; Masi *et al.*, 2014; Gibbons *et al.*, 2014).



**Figure 5.1:** Concentrated heap of solid waste near landfill, Port Harcourt, Nigeria (Ehirim *et al.*, 2009).

A study of the composition of landfill leachate and groundwater pollution conducted in the Ibb landfill in Yemen showed that abandoned landfills could be stable for a longer time, while still posing a greater risk to the environment than younger landfills (Al Sabahi *et al.*, 2009). The typical ranges of concentration of various constituents in landfill and mortality leachate are shown in Table 5.1, obtained from different authors, including the standard ranges given for the U.K. and the U.S.A. Animal/human mass burial pits could be considered as a special kind of landfill (Fiedler *et al.*, 2012), but has seen considerably lesser attention in research studies, despite being a cause for concern since the early

1950s (Van Haaren, 1951), and in relation to posing significant risks to the local and wider environment (Glanville, 2000; Freedman and Fleming, 2003). Therefore, there is a significant gap in scientific knowledge on leachate composition resulting from a decomposing carcass, and little is known about how the concentration and toxicity varies with time and the actual threat involved with a burial site (CFIA, 2006; Rodrigues and Pacheco, 2003).

**Table 5.1:** Typical measured ranges of concentration of various constituents in landfill and mortality leachates against the groundwater standards

Parameters (Units)	Landfill Leachate					Mortality Leachate		DRD (ENDWQS)* Standards (2014)	WHO Standards (2006)
	USA range (Meju, 2000)	UK range (Baun and Christensen, 2004)	Yemen range (Esmail <i>et al.</i> , 2009)	Iran range (Asadi <i>et al.</i> , 2011)	India range (Ramaiah <i>et al.</i> , 2014)	Canada range (Pratt and Fonstad, 2009)	UK range (MacArthur and Milne, 2002)		
pH	3.7-8.5	6.4-8.0	8.46	7.14	11.5	6.5-6.9	7-8	6.5 – 9.5	6.5 – 9.5
Temperature ( <sup>0</sup> C)	-	-	23.7	-	30.3			-	-
EC (µS/cm)	-	503-18400	49800	15000	18700			2500 @ 20 <sup>0</sup> C	-
Alkalinity	-	-	-	-	1050	22500-41600	11900-88200	-	-
Chloride (mg/l)	50-2400	27-3410	3905	3400	882.5	2380-2813		250	250
Sulphate (mg/l)	20-750	<5-739	336	150	198.2	2900-3970		250	400
Magnesium (mg/l)	64-410	18-470	288	39	770	17-79		-	150
Sodium (mg/l)	85-3800	12-3000	6300	800	300	1600-2000		175	200
Calcium (mg/l)	240-2400	60-1440	1840	1800	510	36-81	200-700	-	200
Potassium (mg/l)	28-1700	2.7-1480	4900	185	-	2000-2400		-	200
Ammonium (mg/l)	-	<0.25-1560	1379.16	-	-	10400-14100	3300-19200	0.5	1.5
Nitrate (mg/l)	-	-	1500	39	297	2.3-3.8	2-10	50	50
Iron (mg/l)	0.15-1640	0.1-664	46	-	1.7	18-19	52-335	0.2	0.3
Phosphate (mg/l)	0.5-130	-	-	-	2.15	1150-1927	55-476	-	-

\*ENDWQS: European and National Drinking Water Quality Standard by Department for Regional Development (DRD) Northern Ireland Environmental Agency



More recently, forensic geophysical research has focused on monitoring simulated clandestine graves containing animal cadavers as human proxies (see, e.g., Schultz, 2008; Swann *et al.*, 2010; Pringle *et al.*, 2010b). This aids the estimation of the post-burial or post-mortem interval (Forbes, 2008) and to locating the clandestine burial of a homicide victim (Pringle and Jervis, 2010). Another implication of monitoring leachate characteristics is due to the ecological risk and possible hydrogeological consequences (Dent *et al.*, 2004; Senos Matias *et al.*, 2004; Uslu *et al.*, 2009; Liu *et al.*, 2009). Substantial amount of studies have been conducted to better understand buried animal carcass decomposition in the soil (e.g., Carter and Tibbett, 2006; Pringle *et al.*, 2012b, Troutman *et al.*, 2014), the majority included temperature, moisture, soil pH, soil type and local depositional environments as the predominant factors that control the rate of decomposition and the subsequent leachate released (Carter and Tibbett, 2006; Carter *et al.*, 2008b). Note, however, that every burial site is unique in its own way based on the environmental conditions (Benninger *et al.*, 2008; Hopkins, 2009). Soil leachate that was present under decomposing or dry remains of pigs and human carcasses have been used in mapping the lateral extent of cadaver decomposition (Aitkenhead-Peterson *et al.*, 2012), and to estimate the rate of decomposition in different depths of burials (Rodriguez and Bass, 1985)

Research to monitor the seasonal variability of animal leachate conductivity *in situ* in three different environments has been made by Pringle *et al.* (2010a & 2012b), Figure 5.2 showing a constant increase in conductivity over 2 years of post-burial interval. In contrast, similar laboratory studies, without a soil matrix, found a significant difference

both in physical and chemical properties of leachate when compared with the field based experiment (Swann *et al.*, 2010). Perhaps this difference could be due to the absence of soil inhibiting micro-organisms that occur during decomposition (see Carter *et al.*, 2008b).

Monitoring of mass burials containing animal carcasses has shown elevated levels of Biochemical Oxygen Demand (BOD), Ammonium-Nitrogen ( $\text{NH}_4\text{-N}$ ), Total Dissolved Solids (TDS) and Chlorine (Cl) within or very near the burial trenches with a slow decrease in leachate concentration with depth (Young *et al.*, 1999; Freedman and Fleming, 2003). Elevated chloride and ammoniacal nitrogen levels have been generally used as the best indicators of burial-related groundwater contamination (see Freedman and Fleming, 2003; Hart, 2005). A study on average concentration of elements/ions in leachate from animal burials and groundwater shows evidence of high ammonium, sulphate, chloride and potassium concentration levels compared to background levels in groundwater (see, Fonstad, 2004).

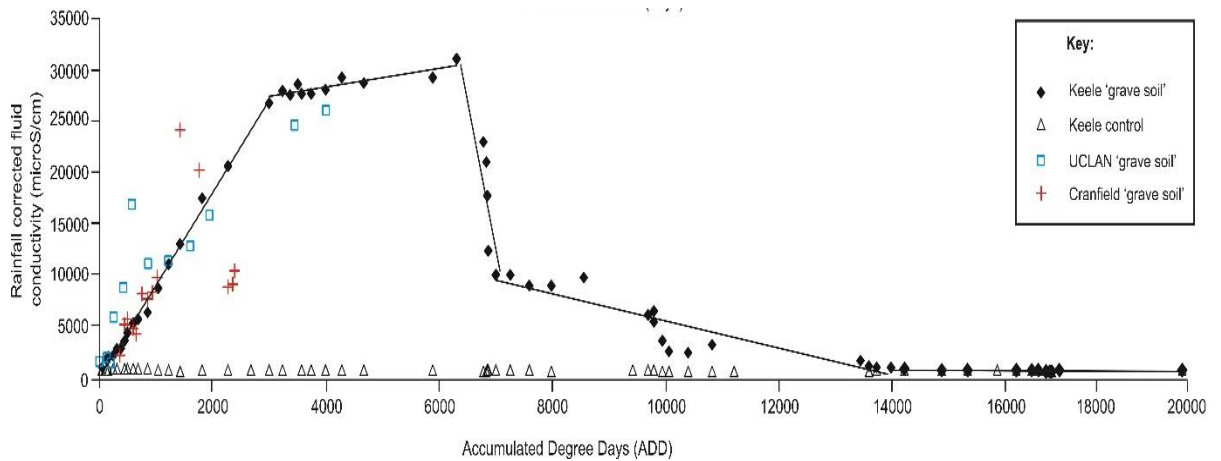


**Figure 5.2:** Measured pig leachate (solid line) sampled from three different pig grave environments and background (dashed line) soil-water conductivity values over the 3-years survey period (adapted from Pringle *et al.*, 2012b).

### 5.2.1 Animal mass burial pits

It may be very rare for a single carcass to cause major contamination. However, incidents of high mortality rates, which necessitates mass burial being a selected option, raises concern over the potential for negative impact in the local environment (Williams *et al.*, 2009). Mass burial is the loosely defined term used to refer to a burial in which significant numbers of animal or human carcass from multiple or single locations are disposed of, and which may incorporate systems and may require controls to collect, treat and/or dispose of leachate and gas. Although engineered leachate collection systems are commonly used for mass burial of animals and humans (e.g. see Fredenslund *et al.*, 2010), gradual seepage of leachate to the surrounding soil sometimes happens, especially when the site is not properly managed (Asadi *et al.*, 2011). During emergency disasters, such as the U.K.'s 2001 Foot and Mouth Diseases (FMD) outbreak (see Fig. 5.3), animal carcasses

were deposited into a semi-confined design facility, usually referred to as an Animal Mass Burial Pit (AMBP) (Schroeder and Aziz, 2003), see Figures 5.4 and 5.5 for the types of mass burial. However, on-farm disposal systems were largely allowed as burial regulations were relaxed and were considered to be crucial during the early stage to reduce the spread of the disease. The nature of such mortality disasters often prompt a rushed burial, without assessing an appropriate disposal sites or indeed to design burial pits engineered with sophisticated liners and leachate collection systems (Scudamore *et al.* 2002). The majority of the on-farm burial pits were often without liners and thereby provided animal leachate easy access to spread away from the burial position and potential into surface and/or groundwater depending on local ground conditions (MacArthur & Milne, 2002). Mostly this was where the vadose layer was very thin and/or permeable (see Szczepanska and Twardowska, 2004). When animal carcasses are disposed in burial pits, leachate contaminants may be mobilized and transported to site boundaries and the surface and/or groundwater aquifer through advection, dispersion and diffusion (Shaw *et al.*, 2011). Many approaches have been used to try and assess the contamination of underground water from animal/human mass burials. These have been commonly performed either by an experimental approach or by numerical modelling to estimate the contaminants present, their concentration and migration pathways (Senos Matias *et al.*, 2004; Swann *et al.*, 2010; Pour and Khezri, 2010; Donaldson *et al.*, 2013).

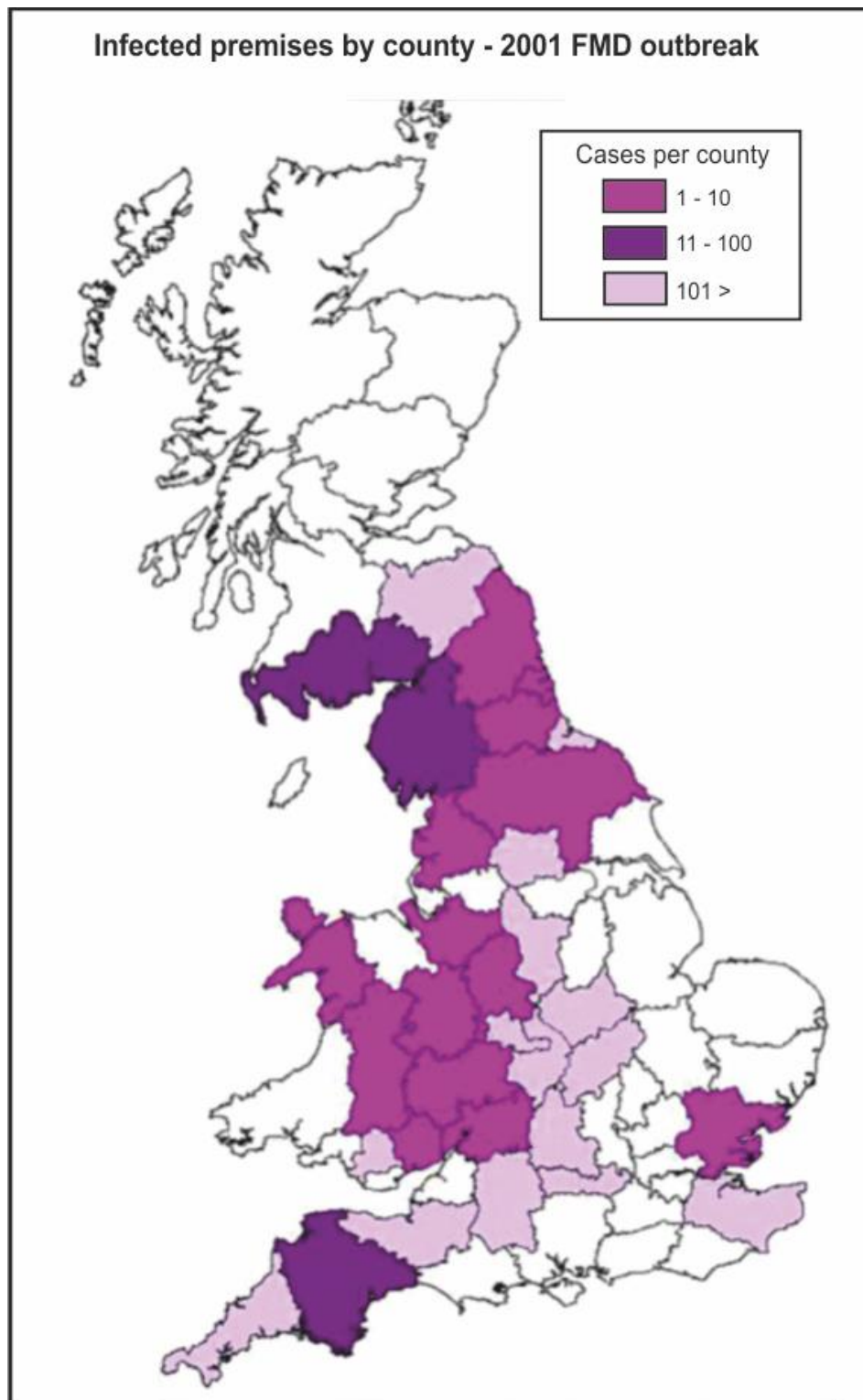


**Figure 5.3:** Map of UK 2001 FMD outbreak locations (after DEFRA, 2001).



**Figure 5.4:** Typical lined animal mass burial pit at Birkshaw Forest, Lockerbie, UK, taken in 2001 following the foot-and-mouth animal disease outbreak (Rawell, 2009).



**Figure 5.5:** Typical unlined on-farm animal mass burial pit during the UK 2001 FMD outbreak (Hickman and Hughes, 2002).

Leachates derived from human corpse are found as dissolved and gaseous organic and inorganic compounds, which are made up of essential elements such as carbon, hydrogen, oxygen and nitrogen, followed by calcium, phosphorus, sulphur, potassium, sodium, chlorine and magnesium trace elements (see Fig. 5.6, Swann *et al.*, 2010). Whilst this study includes animal (pig) and human burials, detailed discussion on the biochemical composition of pig cadavers is not required due to their accepted similarity (Carter and Tibbett, 2009; Swann *et al.*, 2010).

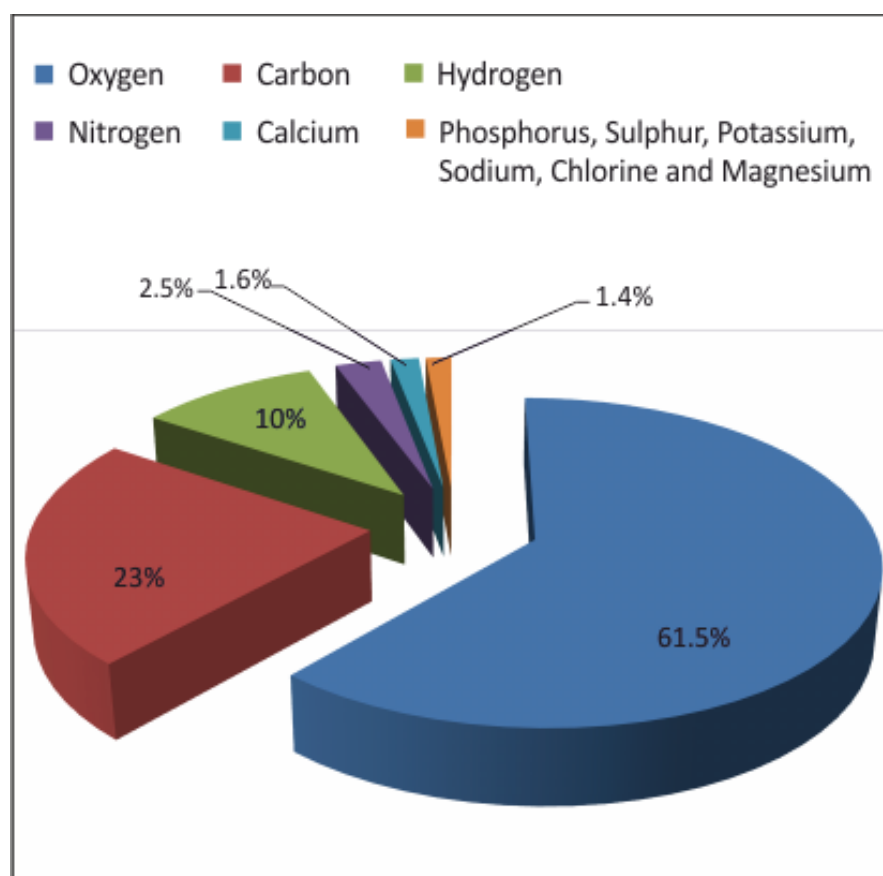


**Figure 5.6:** Composition and elemental components of a typical 70 kg human body (modified from Swann *et al.*, 2010).

### *5.2.2 Main factors that control leachate production, concentration and transport*

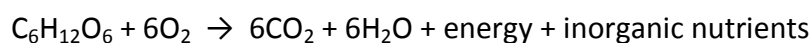
There are numerous factors that are responsible for the generation of animal leachate and the subsequent migration to the environment. These factors can be classified into two groups, based on those that contribute directly to the burial site (chiefly climatic and hydrogeological) and those that affect leachate within the site (chiefly siting, soil type and depth of burial).

Perhaps the most important aspect, with regards to animal leachate generation and composition in burial sites, is simply a biochemical reaction which is mediated by microorganisms. In general, an organic compound is oxidized (loses electrons) by an electron acceptor which in itself is reduced (gains electrons), this is known as oxidation-reduction (redox) reactions. Redox reactions can be defined as reactions in which electrons are transferred between products and reactants. Several electron acceptors have been identified, which include; oxygen ( $O_2$ ), nitrate ( $NO_3$ ), sulphate ( $SO_4$ ) or carbon dioxide. Thus the utilization of oxygen as an electron acceptor is termed aerobic decomposition and when oxygen is not present, another terminal electron acceptor, e.g.  $NO_3$ ,  $SO_4$  etc., is used but with a lower potential energy yield than oxygen, and this is known as anaerobic decomposition. If an inorganic electron acceptor is not available, glucose can act as an electron donor and acceptor during fermentation (Parkin, 1987). High concentration of organic acid compounds, dissolved hydrogen gas, and carbon (IV) oxide are generated during decomposition of cadaver material, which can significantly lower leachate pH and also quicken the rates to which inorganic waste components (free

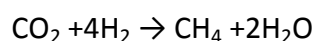
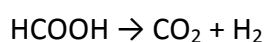
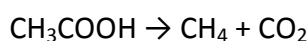
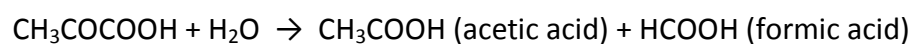


nutrients) dissolve. The decomposition of organic matter, using glucose (C<sub>6</sub>H<sub>12</sub>O<sub>6</sub>) as a generic term, is described as follows (Fetter, 1999):

*Aerobic decomposition*



*Anaerobic decomposition*



Although decomposition occurs slowly in naturally dry soil, following the activity of microorganisms unable to access water, rapid changes in moisture content can cause fluctuations in microbial activity (Hopkins, 2009)

Infiltration of precipitation into any burial site and its subsequent evapotranspiration back to the atmosphere is dominated by the local climate (Andraski, 1997). Since burial sites usually have surface depressions due to decomposition and the unconsolidated backfilled soil compacting (Dupras *et al.*, 2006), surface runoff does not occur freely. Therefore, the amount of moisture/precipitate percolation is high with subsequent gradual infiltration through the high permeable backfilled soil. However, as this water flows through buried

solid waste (animal carcasses), more leachate is produced and transported. Higher temperature, solar radiation, wind and lower humidity can generally all increase the potential decomposition rates (summarised in Table 5.2).

AMBP design and operation has been shown to affect both the quantity and quality of leachate (Schroeder and Aziz, 2003). Leachate quantity obviously increases with the size of the AMBP. In particular, coarse-gravel soils will allow greater percolation of leachate through the burial pit and into the surrounding environment if the pit is unlined. Conversely, host soils that are in a reduced state with high pH, organic matter and mineral oxides, and high acid volatile sulphides will reduce leachate migration by increasing leachate retention (Schroeder and Aziz, 2003). Thicker foundations of fine-grained soils can also provide greater retention of leachate and a reasonable amount of leachate may be attenuated through biodegradation, which is a function of the degradability of the leachate in concern, as well as the availability of electron acceptors such as oxygen, iron, sulphate (Rivett *et al.*, 2011). Aquifer location and hydrology are also important because greater spatial distance reduces the chances of leachate from entering aquifer(s). Deeper burials produce a greater concentration of leachate under similar conditions of precipitation and percolation, it requires a longer time period for soft tissue decomposition. The main factors that influence leachate formation in landfills are shown in Table 5.2.

**Table 5.2:** Main factors affecting leachate formation in landfills (after El-Fadel *et al.*, 2002).

Climatic and hydrogeological	High rainfall, Rapid snowmelt, Shallow groundwater, High temperature and Solar radiation
Site Operations and management	Refuse pre-treatment, Compaction, Baling, Vegetation, Cover design, Side walls material, Liner material, Irrigation, Leachate recirculation and Liquid waste co-disposal
Refuse characteristics	Permeability, Age, Particle size, Density and Initial moisture content
Internal processes	Refuse settlement, Waste decomposition, Moisture content change, Gas and Heat generation and transport

### **5.3 18 months monitoring study of pig burial**

#### *5.3.1 Study area*

The selected burial site was located in a restricted area on Keele University campus, approximately 200m above sea level, close to Newcastle-under-Lyme town in Staffordshire, UK (Fig. 5.7). Part of the study site was initially used for simulated clandestine graves monitoring and geophysical investigations (see Jervis *et al.*, 2009b; Pringle *et al.*, 2012b). Daily climatic records were obtained from a nearby weather observation station within Keele University, with a temperate local climate that is typical for the UK (Peel *et al.*, 2007). The study site was a small plot of land approximately 25 m by 20 m, covered with grasses and surrounded by deciduous trees on three sides. The study site scenario is a typical representative of a semi-rural environment.

Information from a nearby borehole records identified the Carboniferous (Westphalian) Butterson Sandstone bedrock geology approximately 2.6 m below ground level (bgl). The local soil is predominantly a made-ground, due to the presence of demolished greenhouses. Initial soil sampling showed a vertical site succession of a shallow (0.01 m) organic-rich, top soil (Munsel colour chart colour (mccc): 5 YR/2/2.5), with underlying 'A' Horizon (Mccc: 5 YR/3/3) comprising largely of a natural sandy loam that contained approximately 5% of isolated brick and coal fragments (Pringle *et al.*, 2012b). The natural ground 'B' Horizon was located at approximately 0.45 m bgl, consisted mainly sandstone fragments from the underlying bedrock, which suggested a shallower bedrock depth. Also further investigation on soil particle analysis shown that the typical sandy loam soil

texture, i.e. approximately 72 % sand, 26 % silt and 2 % clay, in combination with slow lateral water flow led to moderately high moistness of the soil approximately 34 %.

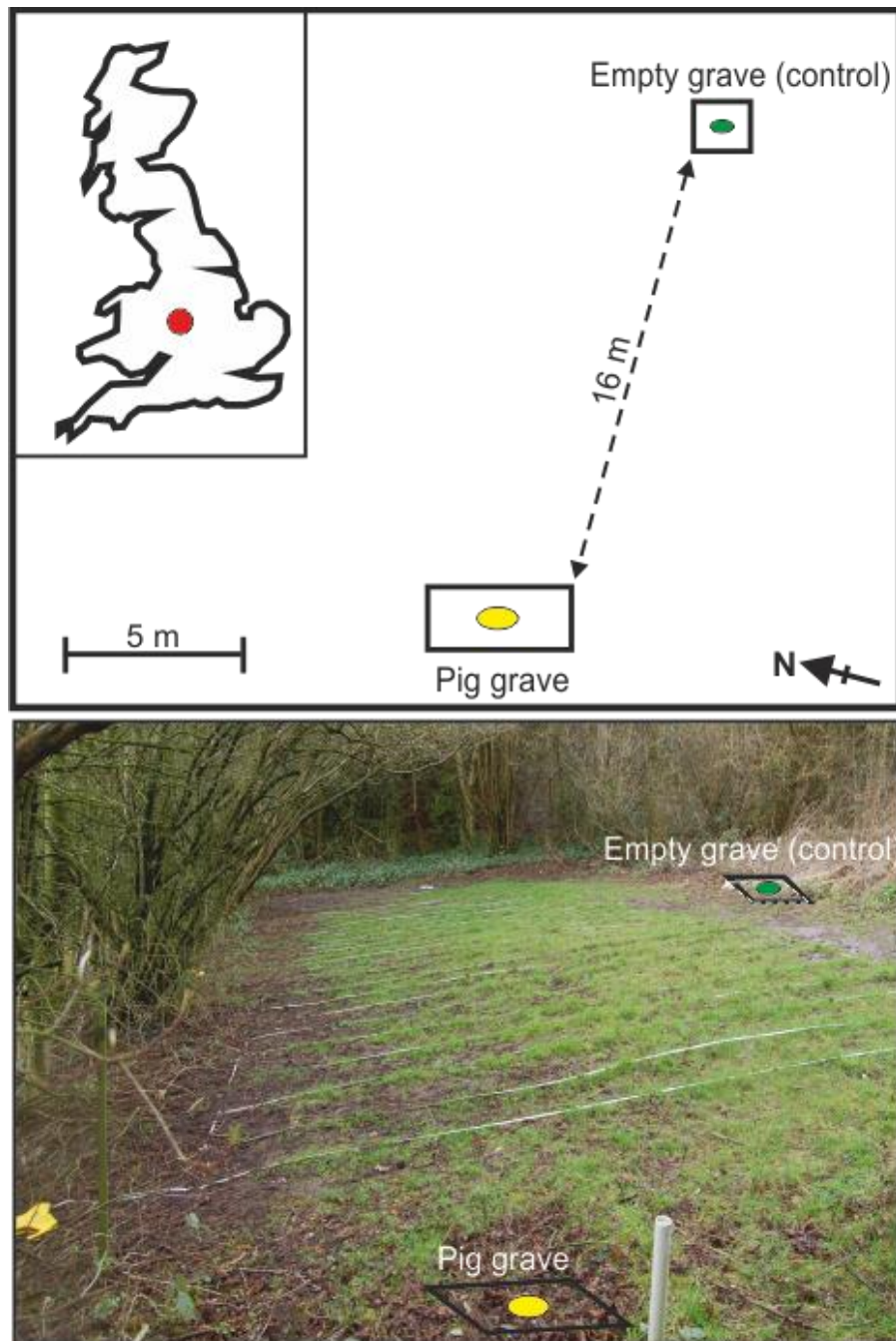


**Figure 5.7:** Schematic diagram and photograph of the study site in Keele University, showing the surveyed area with pig grave (yellow dot) and control (green dot) positions approximately indicated and location map (inset).

### 5.3.2 The Lysimeter

The availability of a recently developed device, a Lysimeter (Soilmoisture Equipment Corporation, model 2007), which can be permanently placed *in-situ* (Fig. 5.8), allows soil fluid to be extracted from the subsurface without compromising its integrity. Previously, it was difficult to monitor the temporal changes in leachate concentration without excavation of the burial cadaver to access the accumulated leachate (Jervis *et al.*, 2009a). The Lysimeter equipment consists of a stopper assembly with neoprene tubing, clamping ring, a polyvinylchloride (PVC) tube with a porous ceramic cup at one end and a removable stopper at the other end. This porous ceramic tip, with a pore space of 1.1µm, is buried at the desired sampling depth for the purpose of collecting soil-water samples, the end of the tube with the stopper is left above the ground (Fig. 5.8). It is recommended that a slurry (a mixture of the local soil and water) be prepared, poured at the base of the excavated hole and insert the lysimeter so the porous ceramic cup is completely embedded below the level of the soil slurry (Soilmoisture Equipment Corporation, model 2007). The excavated soil should then be refilled and the lysimeter emptied three times before any measurement is undertaken to remove the artificially introduced water in the slurry.

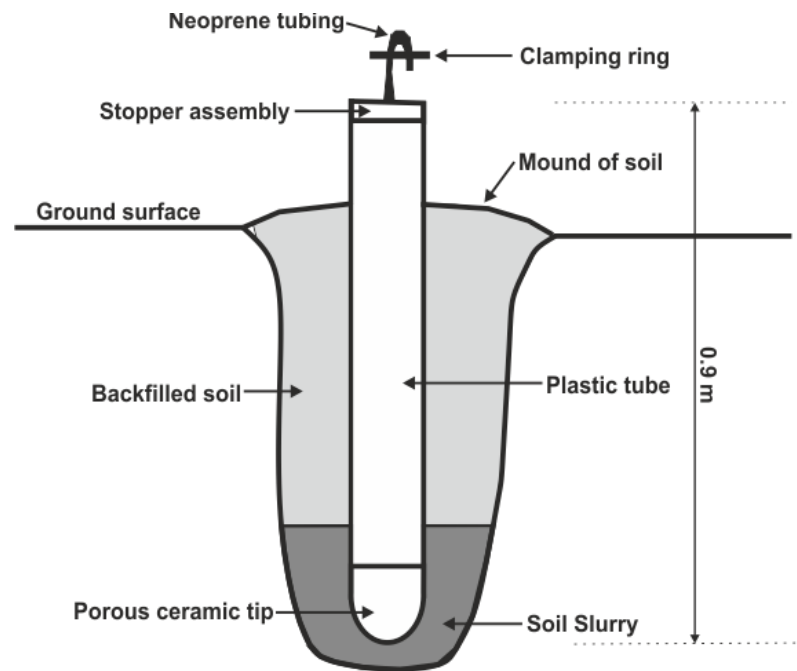


**Figure 5.8:** Annotated diagram showing how a lysimeter should be installed in the ground (after Jervis, 2010).

### 5.3.3 Methodology

#### 5.3.3.1 Simulated grave

The simulated grave was constructed at the eastern part of the site, which involved removal of the turf and then ground excavation, of a hole up to  $\sim 0.6$  m deep,  $\sim 1.5$  m length and  $\sim 0.5$  m wide. The use of human cadavers was prevented due to the ethical issues involved in the use of human cadavers for research in the UK (Human Tissue Act, 2004); however, pig cadaver of the species *Sus scrofa* could be used as proxies for human cadavers which are considered to be an acceptable substitute due to their similarity to humans in weight, fat to muscle ratio, hair coverage, biochemistry and physiology (France

*et al.*, 1992; Carter and Tibbett, 2009; Swann *et al.*, 2010). A 90kg pig of length ~1.5m, sourced from a local abattoir, was therefore killed by bolt gun; this prevented excess blood being lost as they usually despatched by electrocution and draining. The pig carcass was interred on 18th March 2014 and a lysimeter model 1900 inserted inside the made-slurry at the base of the hole between the two hind limbs and the grave wall (see Fig. 5.9). After internment of the pig carcass, the grave was backfilled with the same excavated soil, tamped firmly and leaving a slight mound to account for later settlement, before the turf was replaced. A control lysimeter was installed on the same day, approximately 16 m away from the pig grave and uphill to prevent any potential contamination (Fig. 5.9d). For this control lysimeter, a hole of ~0.3 m by ~0.3 m wide and 0.6 m deep (the same depth as the pig grave) was excavated and refilled. The lysimeters were then left in place throughout the monitoring period. Generating a suction pressure within the lysimeter causes soil water to be drawn through the ceramic cup and into the PVC tube. Leachate and soil samples can then be extracted using a plastic syringe with a narrow tube attachment inserted through the stopper assembly (Fig. 5.9e).

#### *5.3.3.2 Sample collection and on-site measurements*

Initial sample extraction was conducted two days before the sampling day, to enable a fresh accumulation of leachate fluid in the grave which should be representative during the sampling period. The lysimeter clamp ring used to fold the neoprene tubing was removed, giving access to extract any fluid present in the grave, before a vacuum hand pump was employed to generate a vacuum pressure of approximately 65 centibars (kPa)



(Fig. 5.9e). This pressure is capable of causing moisture to move from the soil through the porous ceramic cup, and into the vacuum sampler (Grossmann and Udluft, 1991). The same extraction procedure was repeated on each sampling day. Samples were extracted from both the pig grave and the control once a month for a period of 18 months, except for the first month that was sampled fortnightly, to enhance and validate the initial soil and leachate conditions. The samples were transferred to 100ml labelled plastic sample bottles (Fig. 5.9e) after a portable WTW<sup>TM</sup> Instrument Multi-line P4 conductivity meter was used on-site to measure conductivity and temperature values (Fig. 5.9e). These were automatically corrected by the conductivity meter to a reference temperature (25 °C) and are 0.1 °C accurate, thus avoiding any potential temperature variation effects when collecting samples. This procedure was repeated to check reading repeatability and reliability. Samples pH was also measured onsite in the laboratory with standards at pH 4, 7 and 10 before each use. Approximately 10ml of the collected samples were used for the ICP-OES analysis, which was conducted within 1 hour after sampling and the remaining portion kept frozen until further Dionex laboratory analysis was conducted.

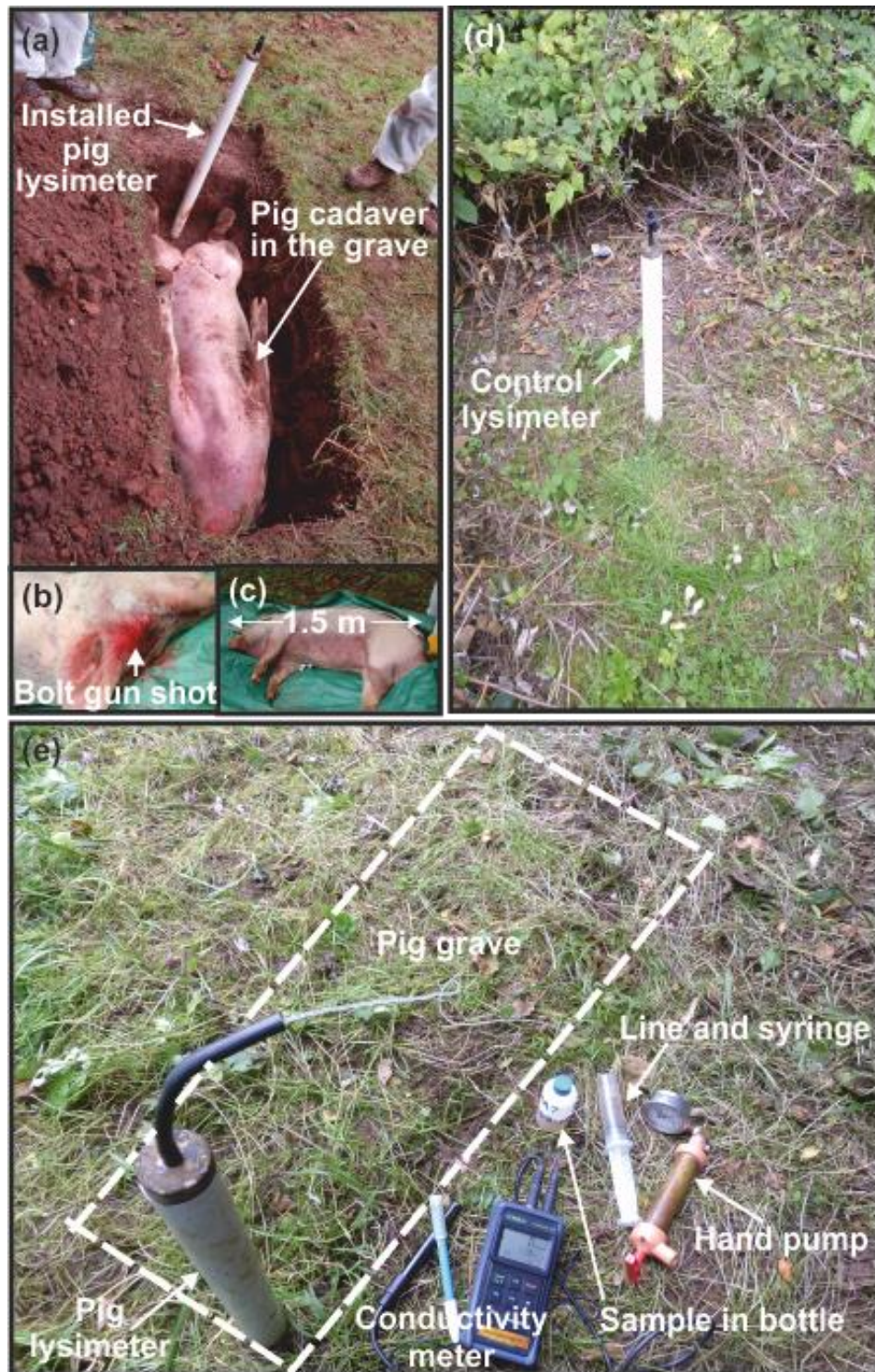


**Figure 5.9:** Study site, (a) "pig lysimeter grave," (b) and (c) "pig carcass," (d) "control site with lysimeter," and (e) soil "fluid" measurement photographs, respectively.

#### 5.3.4 Climatological data collection

Climatological information was obtained from the closest weather station, ~ 0.2 km from the test site managed by the U.K. Meteorological Office. The recorded data include average daily rainfall and air temperature reading over the corresponding monitoring periods (Table 5.3). It measured monthly minimum, maximum, and average total rainfall of 15 mm, 113 mm, and 66 mm, respectively, over the 549 day monitoring period. Calculated monthly total rainfall data of the site were used to correct measured soil water measurements for local rainfall variation, in which conductivity values were multiplied by a rainfall correction factor, generated by dividing the average monthly rainfall for England in a given year by the average monthly rainfall for the local area in the same year (see Pringle et al. 2015 for background). The reason for the correction is to adjust the rainfall value in case of relatively high rainfall rates, which could potentially dilute grave soil water and hence reduce the measured values for physicochemical parameters, and in case of relatively low rainfall rates would increase the concentration of grave soil water and hence increase values for the measured parameters.

The daily average temperature of the site was used to convert post-burial days to accumulated degree-days (ADDs) following Vass *et al.* (1992) methodologies. Accumulated degree-days provide a correction for local site temperature variations, by weighting each post-burial day and adding these per day to give a ADD value. The summarized monthly ADDs and monthly total rainfall dataset is presented in Table 5.3.

**Table 5.3:** Summary of measured monthly local average temperature and total rainfall data from the study site over the 18 months monitoring period. Stated measurements are averages with  $\pm 0.1^{\circ}\text{C}$  and 0.1 mm accuracy. Bgl – below ground level.

Sampling Date	Sample Day After Burial	Monthly ADD 0.3 m bgl	Monthly Average Temperature ( $^{\circ}\text{C}$ )			Monthly Total Rainfall (mm)
			0.3 m bgl	1.0 m bgl	Average	
18.03.14	0	0	0	0	0	0
01.04.14	14	111	7	7	7	54.8
16.04.14	29	406	10	9	9.5	50.6
15.05.14	58	818	13	11	12	96
17.06.14	91	1314	17	14	15.5	65
17.07.14	121	1878	18	16	17	67.4
15.08.14	150	2398	17	16	16.5	99.8
17.09.14	183	2870	16	15	15.5	15
16.10.14	212	3269	13	14	13.5	86.4
17.11.14	244	3566	10	12	11	98
15.12.14	272	3776	7	9	8	76.4
16.01.15	304	3930	5	7	6	62
18.02.15	337	4049	4	6	5	30.8
18.03.15	367	4228	6	6	6	71.6
18.04.15	398	4513	10	8	9	28.4
15.05.15	425	4873	12	10	11	90
18.06.15	459	5309	15	12	13.5	48.6
17.07.15	488	5819	16	15	15.5	57
18.08.15	519	6316	16	15	15.5	112.6
18.09.15	549	6742	14	14	14	44.8

### 5.3.5 Analysis techniques

#### 5.3.5.1 Ion Chromatography (IC) Dionex System

The IC is a liquid chromatography system that uses ion-exchange separations using a conductivity suppression method to determine ionic solutes, such as inorganic anions and cations (see Jackson, 2001, for background). It has relatively low detection limits for inorganic anions and cations, typically in parts per billion (ppb) range and can easily deliver simultaneous anion and cation analyses, simultaneous multi method analyses, as well as two-dimensional (2-D) methods that significantly enhance analysis sensitivity and selectivity. Figure 5.10 shows a typical chromatogram containing low mg/l levels of inorganic anions with anion exchange separation and conductivity detection obtained following standard practice (Jackson, 2001).

IC is presently the established regulatory method for the analysis of inorganic anions in environmental studies and related fields (e.g. for forensic investigation) as there are few alternative methods with the potential to determine multiple anions in a single analysis (Lopez-Ruiz, 2000). It has thus been incorporated globally by different organisational bodies as the standard method for quantifying contaminants in, for example, drinking water, wastewater, leachate, soil extracts, surface and groundwater, and other environmental sample matrixes (Jackson, 2000). Although IC provides access to information on metal speciation, not many regulatory methods for cation analysis use IC due to the possible interferences of other eluent ions which may fall in the same

timeframe with the ion of interest. However, cation analysis has many regulatory methods that rely on spectroscopic techniques (Haddad *et al.*, 2008).

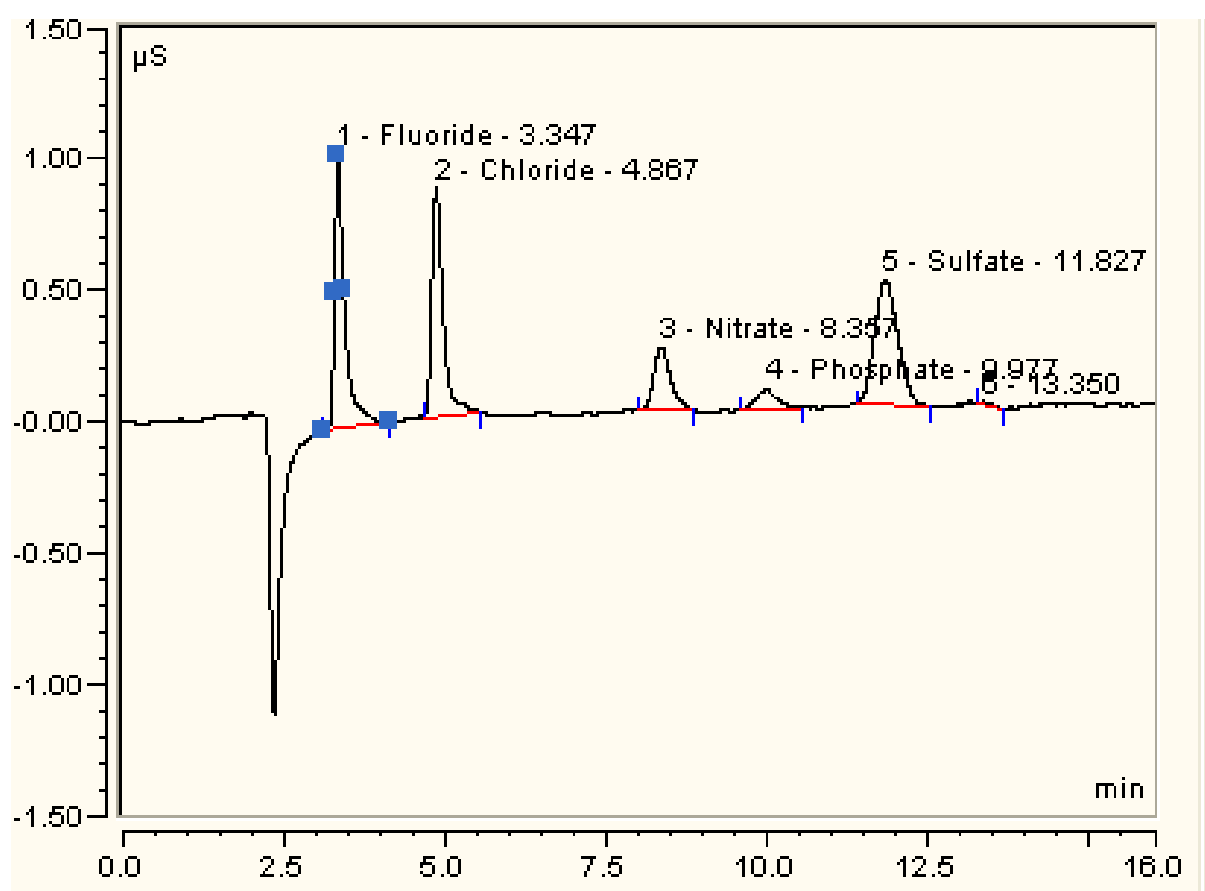


**Figure 5.10:** Screen-shot of IC separation analysis of inorganic anions in grave soilwater, showing individual anions and their respective concentration values from the test site.

#### 5.3.5.2 Inductively Coupled Plasma Optical Emission Spectroscopy (ICP-OES)

The ICP-OES is one of the most powerful and popular analytical tools that measures the light emitted by the elements in a sample aerosol introduced into an ICP source (see Boss and Fredeen, 1997). The measured emission intensities are proportional to the concentrations of analytes in the aqueous sample and are then compared to the intensities of standards of known concentration to obtain the elemental concentrations in the unknown sample (Ebdon *et al.*, 1998). The ICP allows temperature up to 10000 °K, with the sample undergoing typical temperatures between 5500 °K and 8000 °K. These high temperatures allow complete atomization of the elements in the sample, minimizing any chemical interference effects (Hou and Jones, 2000). The plasma is formed as Argon, the carrier gas for the aerosols is made conductive when exposed to an electrical discharge that creates seed electrons and ions, the representative of the processes that take place when a sample droplet is introduced into an ICP is shown in Figure 5.11. It has relatively low detection limits of less than 1 ppb for most metallic elements and easily delivers more than 30 elemental analyses at the same time. The ICP-OES instrument offers better strategies and implementation of quality assurance and control in the elemental analysis of solution samples than most other techniques. In general, the major setback of ICP-OES technique is, as the analyte concentration approaches the limit of detection, the measurement accuracy becomes poorer, however, it is recommended that for accurate quantitative analysis ( $\pm 2\%$ ), sample concentrations should be approximately 100 times greater than the LOD and for semi-quantitative ( $\pm 10\%$ ) the analyte concentration should be at least five times higher than the LOD (Hou and Jones, 2000).

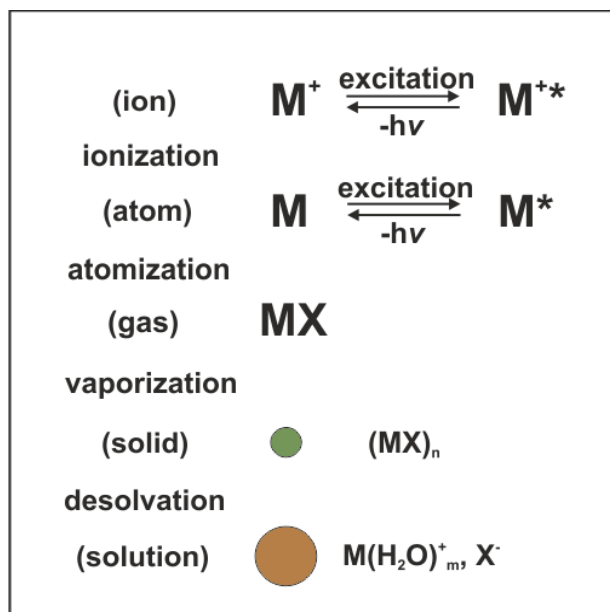


**Figure 5.11:** ICP discharge processes on a sample (adapted from Boss and Fredeen, 1997)

#### 5.3.5.3 Statistical analysis of physicochemical parameters

##### *Correlation and regression Techniques*

Both correlation and regression analysis examine the connection between dependent and independent variables. While correlation techniques measure the closeness of the relationship between chosen dependent and independent variables, regression techniques involve an implicit assumption of causality, which also attempt to establish the nature and intensity of the relationship between the variables and thereby provides extrapolation mechanism for prediction of future event or forecasting (see Seyed *et al.*, 2015; Zvizdojevic and Vukotic, 2015). In order to describe the degree of association or predictable relationship between two or more elemental variables, a preliminary descriptive technique (Pearson's correlation matrix) was utilized to estimate the



closeness of association observed between two variables. In water quality analysis, correlation technique is commonly used for the measurement of the strength and statistical significance of the relation between two or more parameters (Mehta, 2010).

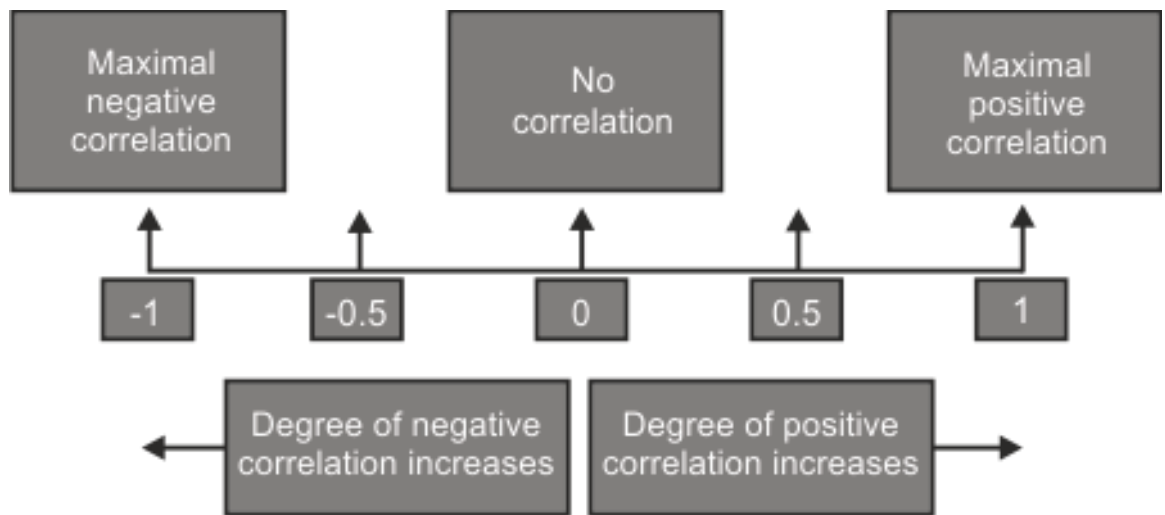


**Figure 5.12:** Degrees of positive and negative correlation.

If the correlation coefficient is nearer to +1 or -1, it shows the probability of linear relationship between the variables (x and y). The correlation between the parameters is characterised as strong, when it is in the range of +0.8 to +1 and -0.8 to -1, moderate when possessed value in the range of +0.5 to +0.8 and -0.5 to -0.8, weak when it is the range of +0.0 to +0.5 and -0.0 to -0.5 (Figure 5.12) (Zvizdojevic and Vukotic, 2015). Therefore, in this study, the relationships between parameters in soil water were determined by calculating Karl Pearson's correlation coefficient (R), using:

$$R = \frac{\sum(x-\bar{x})(y-\bar{y})}{\sqrt{\sum(x-\bar{x})^2 \sum(y-\bar{y})^2}} \quad 5.1$$

Where,  $x$  = values of  $x$  -variable,  $\bar{x}$  = average values of  $x$ , and  $y$  = values of  $y$  –variable,  $\bar{y}$  = average values of  $y$ , which represent two different inorganic ion parameters. If the values of correlation coefficient 'R' between two variables  $x$  and  $y$  are fairly large, it implies that these two variables are highly correlated.

However, the use of straight linear regression can also be adopted depending on the relationship between the parameters, thus the equation of a straight line is given as;

$$y = a + bx \quad 5.2$$

Where empirical parameters,  $a$  and  $b$  are the slope for the line and intercept on y-axis respectively, which can be calculated using the following equation:

following equation:

$$b = \frac{\Sigma xy - \bar{y}\Sigma x}{\Sigma x^2 - \bar{x}\Sigma x} \quad 5.3$$

$$a = \bar{y} - b\bar{x} \quad 5.4$$

### 5.3.6 Results

The summary of the climatological data has been presented in Table 5.3 of Section 5.3.4. Similarly, graphical representation of the data (Fig. 5.13) showed a typical sinusoidal seasonal temperature variations which also largely agrees with the monthly rainfall. However, there were notable variations between the first year monthly rainfall and their corresponding second year, and this can result to a significant variation in the concentration of grave soil water between year 1 and year 2 if not properly accounted for, as relative higher rainfall rates will reduce measured conductivities and concentrations of other element parameters.

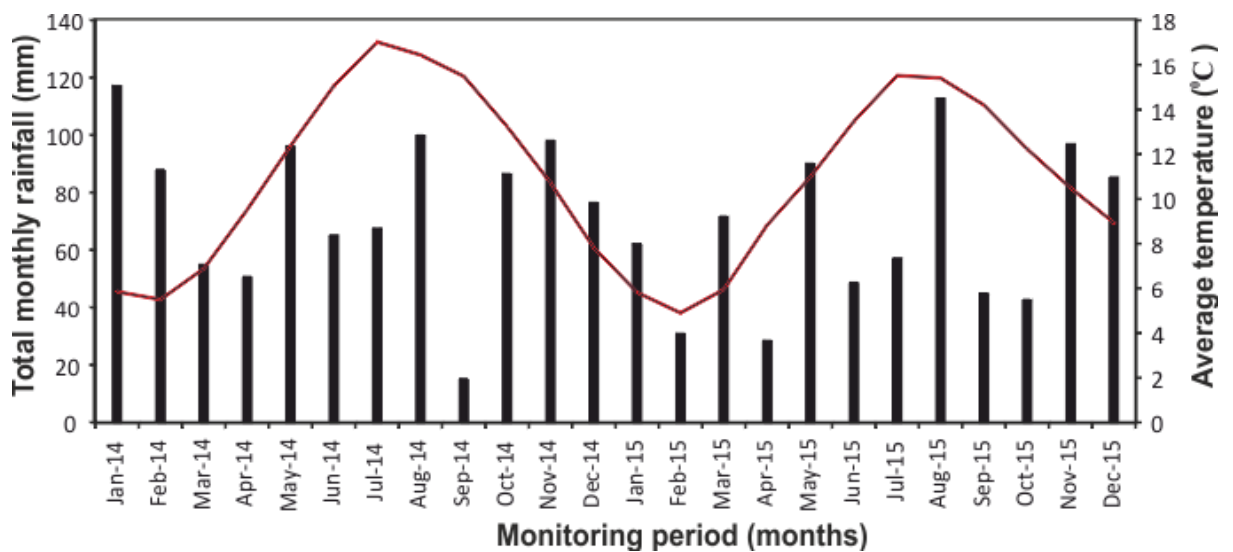


**Figure 5.13:** Graphical summary of total rainfall (bars) and average temperature (red line) data from the study site over the monitoring period.

Among the parameters measured on site were electrical conductivity (EC), temperature (T) and pH. The grave soil water (leachate) evidenced a consistent increase in conductivity value over the first nine months of monitoring, then a gradual decrease over the remaining months of monitoring (Table 5.4). Measured results from the background soil water showed consistent conductivity values over the whole monitoring period. The monthly local temperature variations which could greatly affect decomposition rates (Manhein, 1997) were removed from raw conductivity values by converting post-burial (day) interval (PBI) to ADD, as detailed in the methodology (Section 5.4.3). The maximum pH of the grave soil water (leachate) sample was recorded as 8.85 on the first month (April, 2014) of monitoring and the minimum as 6.82 on the fourth month (July, 2014) of monitoring. While the maximum pH for the background soil water was recorded as 7.83 on the fifth month of monitoring (April, 2015) and the minimum as 6.12 on the tenth month of monitoring (January, 2015).

**Table 5.4:** On-site measured physicochemical parameters in leachate and background soil water samples over the monitoring period

Sampling Date and Parameter	Grave soil water (Leachate)			Background Soil water		
	pH	T (°C)	EC (µS/cm)	pH	T (°C)	EC (µS/cm)
01.04.14	6.98	17.6	1157	7.42	17.7	195
16.04.14	8.85	17.5	816	7.51	17.7	200
15.05.14	8.40	17.8	2180	7.30	17.8	344
17.06.14	7.34	17.7	2850	7.42	17.7	228
17.07.14	6.82	17.8	15740	7.23	17.8	162
15.08.14	7.22	17.8	18520	7.83	17.6	319
17.09.14	7.36	17.6	29900	NS	NS	NS
16.10.14	7.62	17.5	35900	NS	NS	NS
17.11.14	7.54	17.5	33300	7.76	17.4	750
15.12.14	7.58	15.1	34400	7.54	12.8	396
16.01.15	6.98	15.8	21700	6.12	14.3	484
18.02.15	7.63	17.1	27400	6.64	16.6	573
18.03.15	7.44	15.8	17530	6.47	15	425
18.04.15	7.80	18.7	24900	7.39	17.5	477
15.05.15	7.66	18.2	20800	7.44	18	310
18.06.15	7.60	19.8	21100	6.45	19.9	316
17.07.15	7.71	19.4	20000	7.20	19.3	313
18.08.15	7.51	18	13830	NS	NS	NS
18.09.15	7.56	17.3	18330	6.68	15.5	384

### *Statistical analysis of elemental parameters*

The results from monthly monitoring of major inorganic chemical component in animal leachate and background soil water are presented and analysed in this section. Statistical analysis of physicochemical parameters such as; electrical conductivity (EC), pH, observed concentrations of  $K^+$ ,  $SO_4^{2-}$ ,  $Na^+$ ,  $PO_4^{3-}$ ,  $NO_3^-$ ,  $Cl^-$  and  $Ca^{2+}$  was also performed to determine contributions from individual inorganic ion to the variations in conductivity values.

Pig decomposition leachate and corresponding background soil water chemistry results are shown in Tables 5.5 and 5.6 respectively. A combined graph of elemental concentration against the post burial days (PBD) is presented in Figure 5.14a-c. The removal of soil water effect from leachate water was conducted by subtracting the corresponding concentration of elements in soil water from the values obtained in leachate water in order to obtain the concentration of a pure leachate sample used for further analysis (see Figure 5.14c).

**Table 5.5:** Summary of selected element parameters from grave soil (Leachate) sample measured during the monitoring period.

Sampling Date	Leachate Parameter (mg/l)						
	Ca <sup>2+</sup>	K <sup>+</sup>	Na <sup>+</sup>	Cl <sup>2-</sup>	SO <sub>4</sub> <sup>2-</sup>	NO <sup>3-</sup>	PO <sub>4</sub> <sup>3-</sup>
01.04.14	171	10.9	57.7	287.1	29.9	36.74	ND
16.04.14	176	30.2	78.3	119.1	35.4	26.29	ND
15.05.14	390	195	135	28.1	9.5	12.72	ND
17.06.14	440	211	127	289.0	47.7	23.38	ND
17.07.14	1390	800	307	328.4	41.3	55.08	90.8
15.08.14	1620	1000	394	591.9	55.2	50.83	184.7
17.09.14	1540	1190	513	342.2	175.0	88.14	356.1
16.10.14	1050	1230	536	379.6	153.5	151.56	627.9
17.11.14	664	882	347	286.3	158.2	132.41	563.2
15.12.14	409	797	308	175.5	139.3	9.615	469.3
16.01.15	402	559	185	198.3	70.6	2.23	267.5
18.02.15	428	652	257	405.9	92.3	28.675	341.0
18.03.15	354	380	133	235.1	46.3	3.07	183.5
18.04.15	110	623	228	159.9	56.0	2.145	297.7
15.05.15	305	463	164	176.3	35.2	2.125	206.7
18.06.15	125	498	183	156.3	33.2	1.874	225.3
17.07.15	327	453	177	118.9	19.7	3.19	165.4
18.08.15	317	297	111	194.1	0	0	105.4
18.09.15	303	338	119	121.6	14.9	4.03	206.1

**Table 5.6:** Summary of selected element parameters from background soil water sample measured during the monitoring period.

Sampling Date	Background Soil-water Parameter (mg/l)						
	Ca <sup>2+</sup>	K <sup>+</sup>	Na <sup>+</sup>	Cl <sup>2-</sup>	SO <sub>4</sub> <sup>2-</sup>	NO <sup>3-</sup>	PO <sub>4</sub> <sup>3-</sup>
01.04.14	78.3	ND	ND	3.4	4.7	4.7	2.7
16.04.14	69.6	ND	ND	3.3	3.9	2.4	1.7
15.05.14	97.8	ND	ND	3.3	3.3	2.8	2.6
17.06.14	80.6	ND	ND	2.8	3.7	4.6	3.2
17.07.14	60.5	ND	ND	2.3	3.0	2.1	2.9
15.08.14	130	ND	ND	11.1	3.7	14.8	4.7
17.09.14	NS	NS	NS	NS	NS	NS	NS
16.10.14	NS	NS	NS	NS	NS	NS	NS
17.11.14	80.1	13.7	ND	14.2	2.3	20.7	6.2
15.12.14	82.4	ND	ND	4.2	21.6	3.7	4.1
16.01.15	104	3.58	ND	13.3	24.9	1.2	6.0
18.02.15	115	ND	ND	23.4	22.89	1.2	6.2
18.03.15	86.7	ND	ND	5.7	19.3	0.8	3.8
18.04.15	56.1	ND	ND	6.1	11.8	1.4	2.7
15.05.15	69	ND	ND	1.2	10.7	0.8	3.3
18.06.15	57.6	ND	ND	1.6	9.5	0.1	3.2
17.07.15	73.2	5.54	ND	1.2	10.0	0.1	3.3
18.08.15	NS	NS	NS	NS	NS	NS	NS
18.09.15	77	ND	ND	1.2	5.0	0.5	4.1

NB: ND = Not Detected and NS = No Sample



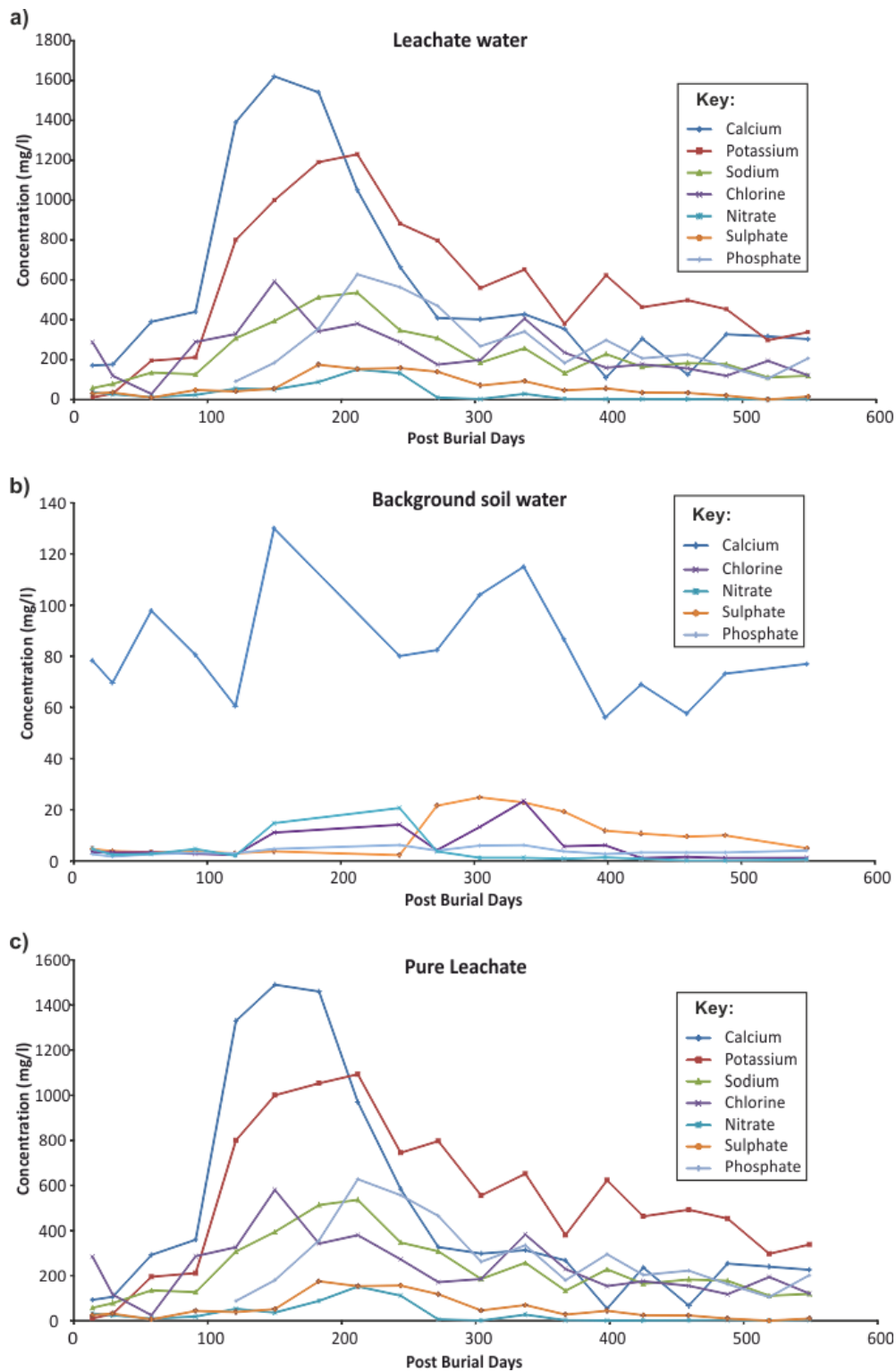


**Figure 5.14:** Combined plot of concentrations of selected element parameters against Post-Burial Days (PBD) over the monitoring period. (a) grave soil (leachate) water, (b) background soil water and (c) Pure Leachate with control values deducted from leachate.

The frequency of variability between the concentrations of inorganic element in the grave soil (Leachate) samples were variable, rapidly increasing up to 200 PBI and then more gradually reducing again (Fig. 5.14). Generally, there was a notably high correlation between the concentrations of inorganic elements and the electrical conductivity in the leachate sample (Fig. 5.15), although not in all cases. For instance, there existed an inverse relationship between conductivity and some inorganic element, e.g. calcium ranging from 150 – 212 and from 367 – 488 post burial days (PBD); and chlorine ranging from 150 – 304 PBD; and nitrate ranging from 121 – 183 PBD. Therefore, calcium, chlorine and nitrate had less influence on the conductivity trend. However, elements that had a direct relationship with conductivity showed strong influence on conductivity trend, with phosphorus showing the highest influence on conductivity trend followed by potassium, Sulphate, and Sodium respectively (*cf.* Figure 5.15).

The degree of linear association between any two of the parameters were measured by simple correlation coefficient (R) values as shown in Tables 5.7 and 5.8 for the leachate and background soil water samples respectively. Correlation is the mutual relationship between two variables. Direct correlation exists when increase or decrease in the value of one parameter is associated with a corresponding increase or decrease in the value of other parameter (Patil and Patil, 2011).

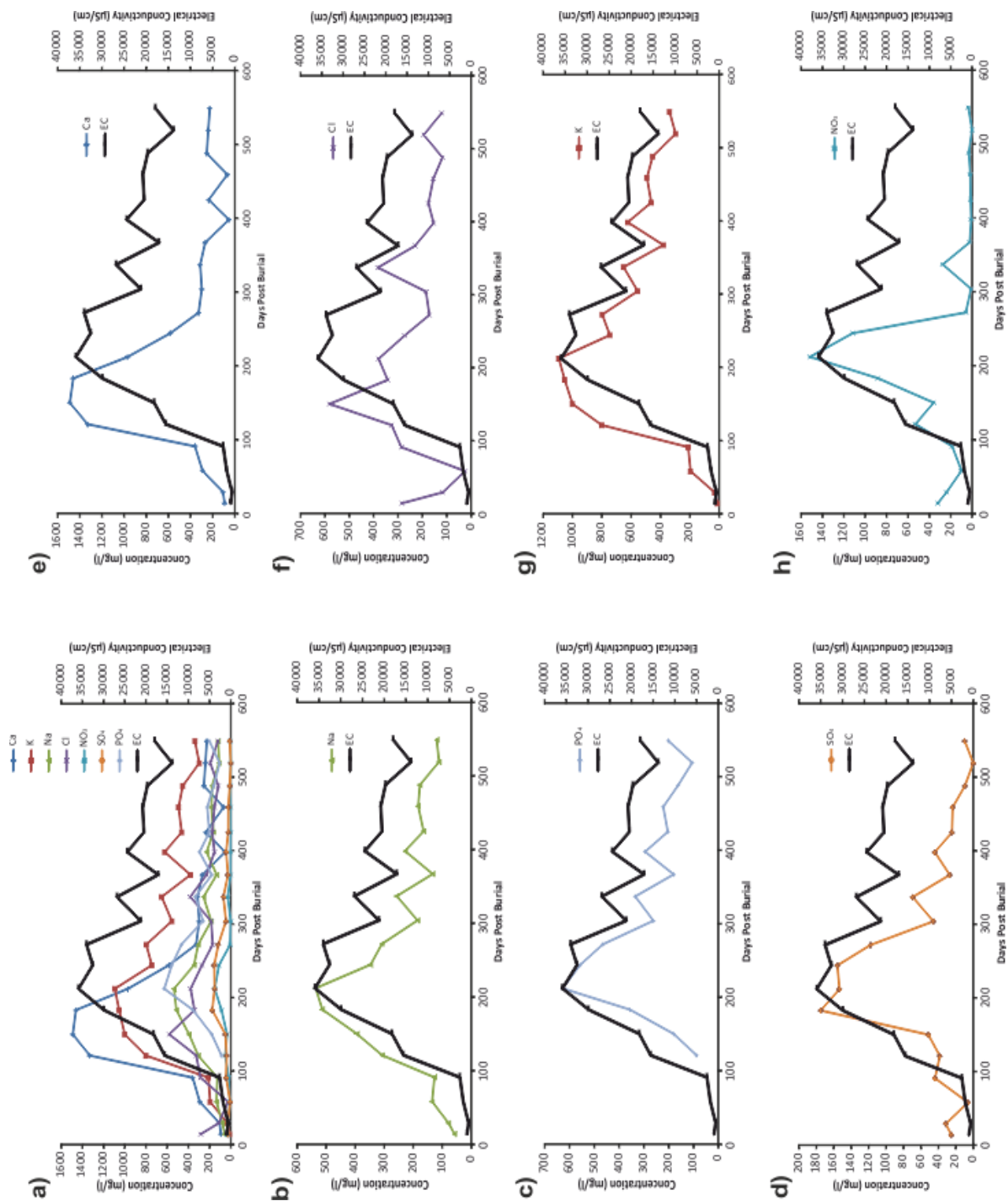


**Figure 5.15:** Comparative analysis of concentration of individual inorganic elements and electrical conductivity over the monitoring period (where Ca is Calcium, K is Potassium, Na is Sodium, Cl is Chloride, NO<sub>3</sub> is Nitrate, SO<sub>4</sub> is Sulphate, PO<sub>4</sub> is Phosphate and EC is Electrical Conductivity).

**Table 5.7:** Correlation Coefficients among different grave soil (Leachate) parameters.

	pH	Temp	EC	K	SO	Na	PO	NO3	Cl	Ca
pH	1.000									
Temp	0.180	1.000								
EC	-0.228	-0.173	1.000							
K	-0.353	-0.107	0.833	1.000						
SO	-0.128	-0.288	0.710	0.731	1.000					
Na	-0.237	-0.079	0.750	0.953	0.846	1.000				
PO	-0.119	-0.234	0.947	0.761	0.808	0.749	1.000			
NO3	-0.118	-0.025	0.452	0.597	0.807	0.775	0.613	1.000		
Cl	-0.531	-0.104	0.286	0.615	0.446	0.623	0.277	0.525	1.000	
Ca	-0.399	-0.058	0.321	0.759	0.533	0.799	0.263	0.616	0.740	1.000

NB: Except pH, Temp ( $^{\circ}$ C) and EC ( $\mu$ S/cm), all other parameters are in mg/l

Strong: 6, Moderate: 16, Weak: 7 and Negative: 16

\*Significant at 5% level,  $r > 0.525$

**Table 5.8:** Correlation Coefficients among different control soil water parameters.

parameters	pH	Temp	EC	SO <sub>4</sub> <sup>2-</sup>	PO <sub>4</sub> <sup>3-</sup>	NO <sub>3</sub> <sup>-</sup>	Cl <sup>-</sup>	Ca <sup>2+</sup>
pH	1.000							
Temp	0.294	1.000						
EC	-0.469	-0.319	1.000					
SO <sub>4</sub> <sup>2-</sup>	-0.661*	-0.627*	0.393	1.000				
PO <sub>4</sub> <sup>3-</sup>	-0.539*	-0.407	0.790*	0.468	1.000			
NO <sub>3</sub> <sup>-</sup>	0.202	0.045	0.423	-0.400	0.436	1.000		
Cl <sup>-</sup>	-0.310	-0.263	0.706*	0.447	0.823*	0.380	1.000	
Ca <sup>2+</sup>	-0.130	-0.325	0.279	0.265	0.596*	0.349	0.664*	1.000

NB: Except pH, Temp ( $^{\circ}$ C) and EC ( $\mu$ S/cm), all other parameters are in mg/l

Strong: 1, Moderate: 4, Weak: 12 and Negative: 9

\*Significant at 5% level,  $r > 0.525$

### *Test of significant of the observed correlation coefficients*

In the grave soil water samples (Table 5.7), out of the potential total of 45 correlations, 23 were found to have significant correlations at 5% ( $r > 0.525$ ), while 22 cases showed no significant correlation at 5% ( $r < 0.50$ ). Low positive correlation coefficients were observed in 7 cases between temperature and pH;  $\text{NO}_3^-$  and EC;  $\text{Cl}^-$  and EC;  $\text{Ca}^{2+}$  and EC;  $\text{Cl}^-$  and  $\text{SO}_4^{2-}$ ;  $\text{Cl}^-$  and  $\text{PO}_4^{3-}$ ; and  $\text{Ca}^{2+}$  and  $\text{PO}_4^{3-}$ . While low negative (inverse) correlation coefficient were observed in 15 cases between EC and pH;  $\text{K}^+$  and pH;  $\text{SO}_4^{2-}$  and pH;  $\text{Na}^+$  and pH;  $\text{PO}_4^{3-}$  and pH;  $\text{NO}_3^-$  and pH;  $\text{Ca}^{2+}$  and pH; EC and Temp;  $\text{K}^+$  and Temp;  $\text{SO}_4^{2-}$  and Temp;  $\text{Na}^+$  and Temp;  $\text{PO}_4^{3-}$  and Temp;  $\text{NO}_3^-$  and Temp;  $\text{Cl}^-$  and Temp and  $\text{Ca}^{2+}$  and Temp.

In the soil water samples (Table 5.8), out of the total 28 correlations found between two parameters, 8 were observed to have significant correlations at 5% ( $r > 0.539$ ), while 20 cases showed no significant correlation at 5% ( $r < 0.50$ ). Low positive correlation coefficients were observed in 11 cases between Temp and pH;  $\text{NO}_3^-$  and pH;  $\text{SO}_4^{2-}$  and EC;  $\text{NO}_3^-$  and EC;  $\text{Ca}^{2+}$  and EC;  $\text{PO}_4^{3-}$  and  $\text{SO}_4^{2-}$ ;  $\text{Cl}^-$  and  $\text{SO}_4^{2-}$ ;  $\text{Ca}^{2+}$  and  $\text{SO}_4^{2-}$ ;  $\text{NO}_3^-$  and  $\text{PO}_4^{3-}$ ;  $\text{Cl}^-$  and  $\text{NO}_3^-$ ; and  $\text{Ca}^{2+}$  and  $\text{NO}_3^-$ . While low negative correlation coefficient were seen in 8 cases between EC and pH;  $\text{Cl}^-$  and pH;  $\text{Ca}^{2+}$  and pH; EC and Temp;  $\text{PO}_4^{3-}$  and Temp;  $\text{Cl}^-$  and Temp;  $\text{Ca}^{2+}$  and Temp;  $\text{NO}_3^-$  and  $\text{SO}_4^{2-}$ .

Two variable least square approaches were used to develop a relationship between electrical conductivity as an independent variable and different leachate variables such as  $\text{K}^+$ ,  $\text{SO}_4^{2-}$ ,  $\text{Na}^+$ ,  $\text{PO}_4^{3-}$ ,  $\text{NO}_3^-$ ,  $\text{Cl}^-$  and  $\text{Ca}^{2+}$  as dependent variables. The linear regression analyses have been carried out and were found to have better and higher levels of significance in their correlation coefficient ( $R^2 > 0.5$ ). The regression equations obtained from the analysis are shown in the first column of Tables 5.9 and 5.10 for leachate and

background soil water respectively, which indicate the results of the ordinary least squares (OLS) regressions with only EC as the controlling variable and a constant. In Table 5.9, the second column shows the values of  $R^2$ , which indicates that regression results for  $K^+$ ,  $SO_4^{2-}$ ,  $Na^+$  and  $PO_4^{3-}$  equations to be significant at 1% ( $\leq 0.001$ ), while the equation of  $NO_3^-$  is significant at 10% level of confidence. However,  $Cl^-$  and  $Ca^{2+}$  equations show no significance. The significance of the relationship is also supported by F test (ratio of regression mean square and error mean square) in the fifth column, in which numerical values depict how each ion influences the variation in electrical conductivity. Thus, higher F value shows greater influence and lower F value lesser influence. However, Table 5.9, which is the regression analysis for background soil water, shows conductivity is significant at 1% level for  $PO_4^{3-}$  and  $Cl^-$ , while the rest of detected ions show no significance.

**Table 5.9:** Regression equations between elements and conductivity in leachate samples.

Regression equation	$R^2$	t Value	P Value	F Value
$K^+ = 79.834 + 0.024EC$	0.693	6.199	0.000**	38.428
$SO_4^{2-} = -9.694 + 0.003EC$	0.710	4.161	0.001**	17.315
$Na^+ = 53.130 + 0.009EC$	0.562	4.674	0.000**	21.843
$PO_4^{3-} = -72.136 + 0.016EC$	0.896	12.000	0.000**	146.412
$NO_3^- = -2.687 + 0.002EC$	0.204	2.090	0.052*	4.369
$Cl^- = 174.210 + 0.003EC$	0.082	1.230	0.235	1.514
$Ca^{2+} = 215.523 + 0.014EC$	0.103	1.396	0.181	1.950

**NB:** \* Indicates Significant at 10% level, \*\* indicates significance at 1% level

**Table 5.10:** Regression equations between elements and conductivity in soil water samples.

Regression equation	R <sup>2</sup>	t Value	P Value	F Value
$\text{SO}_4^{2-} = 2.554 + 0.020\text{EC}$	0.154	1.599	0.132	2.556
$\text{PO}_4^{3-} = 1.221 + 0.007\text{EC}$	0.624	4.817	0.000**	23.207
$\text{NO}_3^- = -1.914 + 0.016\text{EC}$	0.179	1.744	0.103	3.043
$\text{Cl}^- = -4.476 + 0.029\text{EC}$	0.499	3.726	0.002**	13.882
$\text{Ca}^{2+} = 68.621 + 0.037\text{EC}$	0.076	1.085	0.296	1.177

**NB:** \*\* indicates significance at 1% level

## 5.4 Detection of elevated metallic distribution in graveyard soils

### 5.4.1 Introduction

The contamination of cemetery soils with heavy metals has in recent times been acknowledged as a global challenge that is greatly influenced by anthropogenic activities (Pour and Khezri, 2010; Fiedler, *et al.*, 2012; Amuno and Oluwajana, 2014). According to published articles, the principal sources of elevated heavy metals were attributed to the use of embalming fluid and synthetic funeral materials (Jonker and Oliver, 2012, Uslu *et al.*, 2009), embalming fluid is the mixture of formaldehyde, glutaraldehyde, methanol and other solvents. While more attention has focused on identifying and measuring the value of these toxic trace metals against background soil values, only a handful of these studies have analysed the changes in soil chemistry due to the effect of decomposing cadavers (e.g. see Carter and Tibbett, 2009; Fiedler, *et al.*, 2012).

There is relatively little information on how empirical studies that address the problem of heavy metal contamination of cemetery soil could be used for a forensic search of clandestine burials. It is worth noting that a clandestine grave due to the nature and content of the burial contains relatively few material sources of heavy metals when compared to normal burial that contains burial accessories, and as such, soil hosting clandestine burial is expected to accommodate low concentration of available metallic elements. The rise in values of some elemental concentration in soil hosting burials had been attributed to the leachate generation from cadaver decomposition (Senos Matias *et al.*, 2004). Similarly, sampling and analysing soils around such burial site could assist in the



search for a clandestine grave, especially when there is a significant difference in physicochemical characteristics of soil matrix between the burial site and background.

The major objective of this study were to; (i) examine the differences in elemental concentrations between burial site and background soil samples; and (ii) assess the impact factors, such as; enrichment, geo-accumulation and contamination of the selected metals associated with cadaver decomposition in three selected English Church graveyards (see Chapter 4).

#### *5.4.2 Materials and Methods*

##### *5.4.2.1 Site descriptions*

Details and descriptions of the three selected graveyard sites have already been discussed in Sections 4.5.1, 4.6.1 and 4.7.1 for St. Michael's, St. John's and St. Luke's graveyards respectively in Chapter 4.

#### 5.4.2.2 Sampling and laboratory analysis

In this study, three selected English Church graveyards with different geological bedrock, soil type, vegetation, and history of land use were chosen. Field sampling for the three sites was conducted at the same season when the moisture content in the soil were reasonably low, and thus to allow site comparisons (see Carter and Tibbett, 2009; Wang *et al.*, 2015). Fifteen topsoil samples (10-20cm bgl) were collected with a Teflon-coated aluminium hand-shovel from around the vicinity of the three graveyards (Figures 5.16a, b and c). To establish the naturally occurring background soil for the sites, two offsite control soil samples were also collected from near the respective study sites between 70 m and 100 m away (Figures 5.16a, b and c). Collection of soil samples from deeper depth was not allowed during the study due to the existing law prohibiting disturbance of graveyards in UK (Home Office, 2004). These offsite (background) samples were then mixed into one sample to form a control offsite sample representing the background soil sample of the graveyard sites as shown by other studies (Jonker and Oliver, 2012; Wang *et al.* 2015). The offsite (background) soil samples were labelled SC, KC and EC for Stockton, Keele and Endon control sites respectively. While the onsite (graveyard) soil samples were labelled from S1-S15, K1-K15 and E1-E15 representing Stockton, Keele and Endon graveyard soil samples respectively.

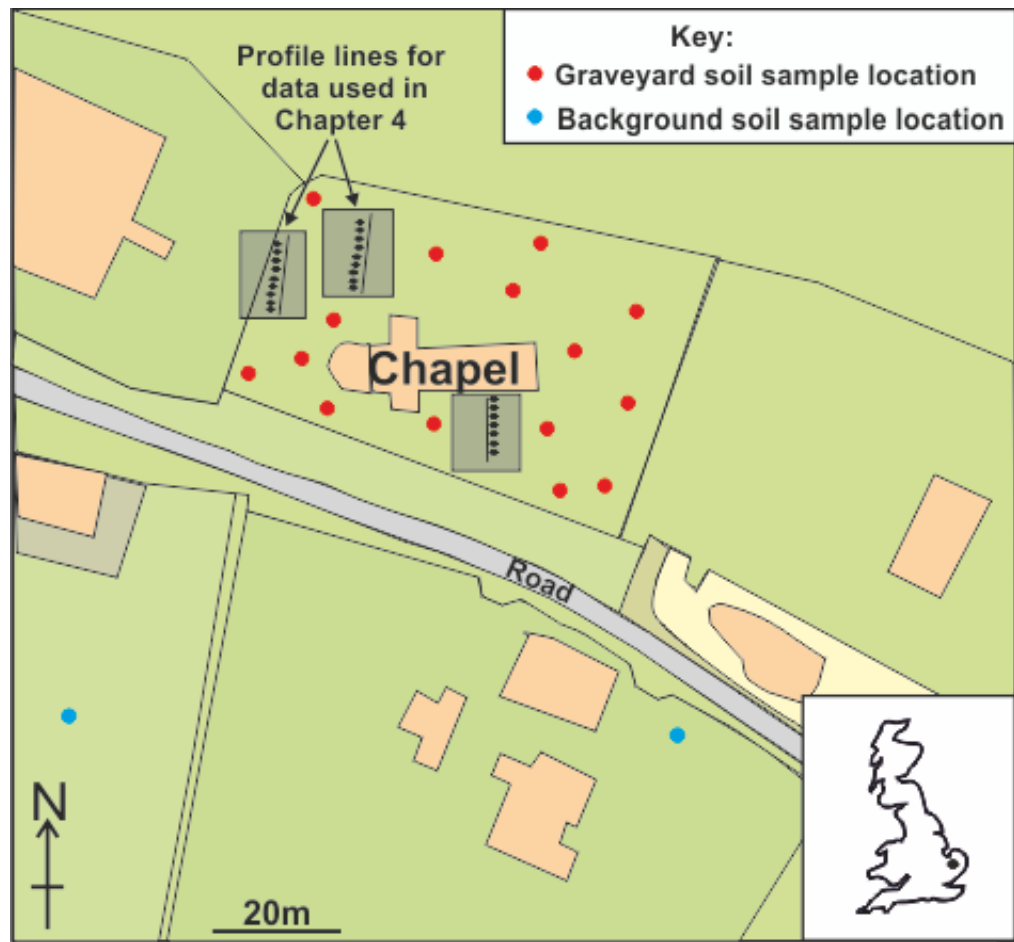


**Figure 5.16a:** Map of St. Michael's of all Angels Church graveyards Stockton, Norfolk, showing soil sample locations across the site (location map inset).

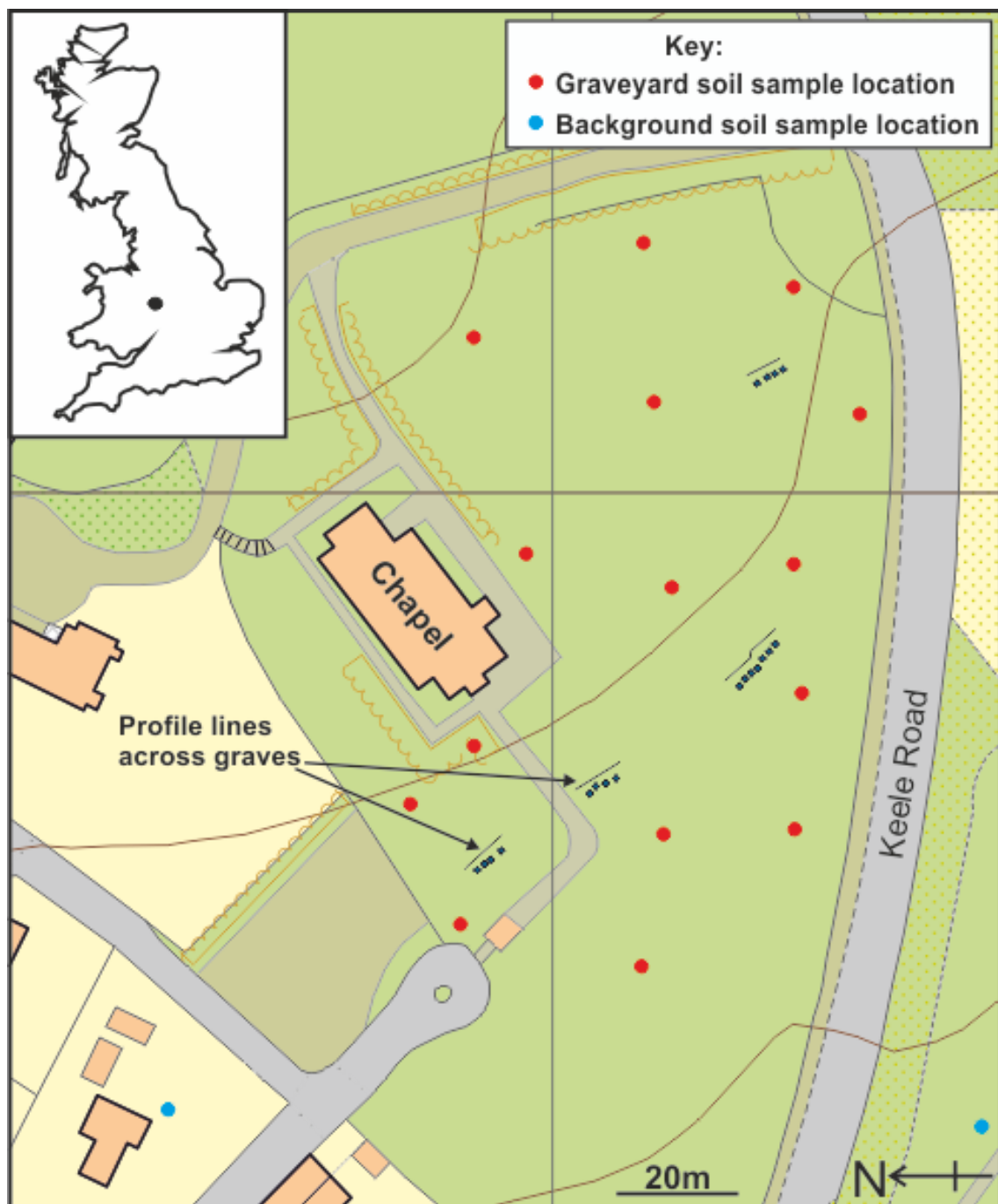


**Figure 5.16b:** Map of St. John's Church graveyards, Keele, Staffordshire, showing soil sample locations across the site (Location map inset).

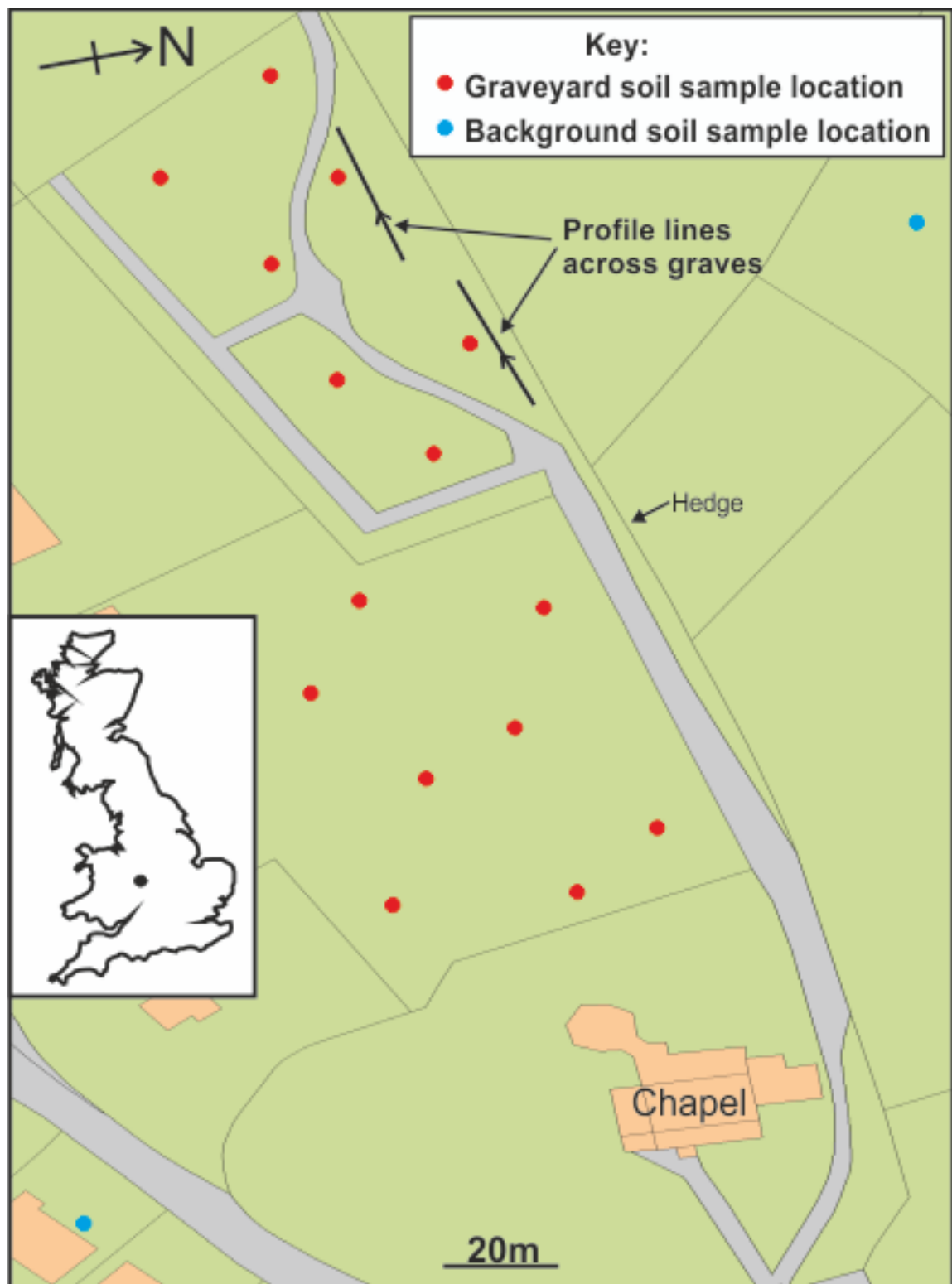


**Figure 5.16c:** Map of St. Luke's Church graveyards, Endon, Staffordshire, showing soil sample locations across the site (Location map inset).

About 250g of soil were collected from each sampling point and were put into polyethylene bags separately after the removal of organic materials and debris. All the laboratory analyses were carried out at the Chemistry and Environmental laboratory units in Keele University. The soil samples were oven-dried for about 24 hours at a temperature of 105<sup>0</sup> C to remove moisture and later sieved with nylon mesh (2 mm). The proportion <2 mm of the sample was finely grinded in an agate pestle and mortar, and passed through a 63 micro stainless steel sieve following standard practice (Environmental Agency, 2006). Prepared samples were sealed in polyethylene bags and stored at 4<sup>0</sup> C until analysed.

For estimation of metal concentrations, digestion of soil samples was carried out in a microwave digestion system. Each soil sample was accurately weighed ( $0.5 \pm 0.01$  g) and transferred to a Teflon reaction vessel and added 10 mL of 70% concentrated HNO<sub>3</sub>. The same procedure was also repeated for the background soil sample. A programmable 1200 W microwave (MAR 6, CEM Corporations. Matthews, NC, USA) with a rotor for 20 Teflon-lined vessels rated at 210<sup>0</sup>C and 350 psig (HP-500 Plus, CEM Corporations, Matthews, NC, USA) served as the closed vessel digestion system. Pressure and temperature profiles in the vessels were monitored on an external computer to better assess their effects on sample digestion. Effective digestion was achieved by setting the microwave program and power setting so that temperature was always the controlling parameter (Kulkarni *et al.*, 2007). The samples were then allowed to cool for about 15 mins to room temperature before removing from the microwave unit, and then decanted evenly distributed samples into plastic, centrifuge tubes and centrifuge for 20 mins.

The use of concentrated  $\text{HNO}_3$  is needed to avoid high background possibly obscuring the required metals; however, this could decrease ICP-AES signal intensity and may accelerate corrosion of the cones (Krachler *et al.*, 1996). Thus, samples were diluted to 1:4 with 1 %  $\text{HNO}_3$  to avoid the corrosion of cones. The determination of elemental concentration was carried out using inductively coupled plasma atomic emission spectroscopy (ICP-AES). A VARIAN VISTA-MPX simultaneous utilized ICP instrument coupled with CCD detector technology, low detection limit, high accuracy and precision, relative freedom from matrix interference and high sample throughput. Prior to analysis, the ICP-AES, located in a temperature-controlled laboratory ( $20 \pm 2^\circ\text{C}$ ), was allowed a sufficient period of time to stabilize before optimization procedures were carried out.

#### 5.5.2.3 Data Analysis

For the purpose and objective of this study, three categories of metal assessment indices were considered which include; geo-accumulation index; enrichment factor and; contamination factor.

##### *Index of Geo-accumulation ( $I_{geo}$ )*

A geo-accumulation indexing approach,  $I_{geo}$  introduced by Müller (1969), was used to assess the degree of anthropogenic activities or contamination and compare different

metals that appear in different ranges of concentration with the background values.  $I_{geo}$  is mathematically expressed as:

$$I_{geo} = \log_2 \left( \frac{C_n}{k B_n} \right) \quad 5.5$$

Where  $C_n$  is the measured average concentration of the examined soil element ( $n$ ) in  $\text{mg.kg}^{-1}$ ,  $B_n$  is the geochemical background concentration of element ( $n$ ), also in  $\text{mg.kg}^{-1}$ . The background matrix correction factor ( $k$ ) was introduced to minimize possible lithologic variation in soil ( $k$  is a constant with value 1.5). The geo-accumulation index ( $I_{geo}$ ) of the graveyard soils was established following the standard geo-accumulation classes and the corresponding pollution level (see Table 5.11) as stated by Förstner *et al.*, (1993), and Khalilova and Mammadov (2016).

**Table 5.11:** Classification of geo-accumulation index

Sediment $I_{geo}$ contamination	Geo-accumulation class level	Index, $I_{geo}$
$I_{geo} \leq 0$	0	Practically uncontaminated
$0 < I_{geo} < 1$	1	Uncontaminated to moderate
$1 < I_{geo} < 2$	2	Moderate
$2 < I_{geo} < 3$	3	Moderate to strong
$3 < I_{geo} < 4$	4	strong
$4 < I_{geo} < 5$	5	Strong to very strong
$I_{geo} > 5$	6	Extremely contaminated



### *Enrichment Factor (EF)*

To further determine the contribution of human burials to the natural levels of the elements in three graveyard soils, the enrichment factors of metals were calculated based on a comparison of concentration ratios according to equation 5.6 shown below.

$$EF = \frac{C_i/C_r}{B_i/B_r} \quad 5.6$$

Where  $C_i$  and  $C_r$  are the concentrations of the target metal and the reference metal sample respectively, while  $B_i$  and  $B_r$  are the background concentration of the target metal and the reference metal for the natural soil of the graveyards respectively. EF is calculated by normalizing the given concentration of target metals in soil to the percentage of immobile elements such as Al, Fe, Ti or Mn used as reference metal (Luoma and Rainbow, 2008; Hu *et al.*, 2013). In this study, the EFs for all the selected metals (Al, Ca, Fe, K and Mg) were calculated using Al ( $\text{mg.kg}^{-1}$ ) as the reference metal because Al is relatively immobile, occurring largely as insoluble hydroxides (Bardgett, 2005, Kulkarni *et al.*, 2007). The enrichment factor categories proposed by Sutherland (2000) were used as standard shown in Table 5.12.

**Table 5.12:** Classification of enrichment Factor

EF Indices	Degree of Enrichment
$EF < 1$	Background Concentration
$1 < EF < 2$	Depletion to minimal Enrichment
$2 < EF < 5$	Moderate Enrichment
$5 < EF < 20$	Significant Enrichment
$20 < EF < 40$	Very High Enrichment
$EF > 40$	Extremely High Enrichment

*Contamination Degree of Graveyard soil samples*

In order to assess the pollution status of the graveyards, the contamination factor ( $Cf_x$ ) for the selected metals across the graveyard sites was determined using Equation 5.7, in the suggested version by Hakanson (1980).

$$Cf_x = \frac{C_x}{C_b} \quad 5.7$$

Where  $C_x$  = metal concentration in soil sample, and  $C_b$  = unpolluted background value of metal. While enrichment factor and geo-accumulation index is only suitable for evaluating single elements, contamination degree provides a comprehensive picture of a particular site by summing the derived contamination factors ( $Cf_x$ ) of individual metal as a single

contamination index and dividing it by the total number of metals to represent the contamination degree ( $C_{deg}$ ) of the environment as expressed in Equation 5.8. It also overcomes the requirement of using a suitable location for background concentration values by using reference value-national criteria of the metal as suggested in the works of (Taylor and McLennan, 1985; Khalilova and Mammadov, 2016).

$$C_{deg} = \sum_{i=1}^N Cfx^i \quad 5.8$$

The degree of contamination ( $C_{deg}$ ) is a parameter which provides a measure of the degree of overall contamination in subsurface layers in a particular sampling site (Hakanson, 1980). The derived  $C_{deg}$  value, obtained from Equation 5.8, is assigned to a class of contamination as shown in four categories of degree of contamination (Table 5.13) by Hakanson (1980), where  $N$  is the total number of element of interest. However, equation 5.7 was used to determine the respective contamination factors ( $Cf_x$ ) for the graveyard soil samples.

**Table 5.13:** Classes of Contamination factor ( $Cf_x$ ) and Contamination degree ( $C_{deg}$ ) (Hakanson, 1980; Loska *et al.*, 2004)

$Cf_x$ classes	Contamination factor	$C_{deg}$ classes	Contamination degree
$Cf_x < 1$	Low contamination	$C_{deg} < 8$	Low degree of contamination
$1 \leq Cf_x < 3$	Moderate contamination	$8 \leq C_{deg} < 16$	Moderate degree of contamination
$3 \leq Cf_x < 6$	Considerable contamination	$16 \leq C_{deg} < 32$	Considerable contamination
$Cf_x > 6$	Very high contamination	$C_{deg} \geq 32$	Very high degree of contamination

### 5.4.3 Results

The results of analysis of metallic concentration of the three English Church graveyard soils were summarized in Tables 5.14 and 5.15 for background soil concentration ( $B_n$ ) and average site concentration ( $C_n$ ) in  $\text{mg.kg}^{-1}$  respectively. However, the details are shown in Appendix 3 as 3A, 3B and 3C for the Stockton, Keele and Endon study sites respectively. These values were used to determine the impact factor of the metals (Al, Ca, Fe, K and Mg) in the study sites. Table 5.16 presents the results of statistical analysis and mean values of  $I_{geo}$ ,  $EF$  and  $CF$  for the selected metals in the sampled sites.

**Table 5.14:** Description of sites background soil elemental concentration levels

Sampling site	Background Concentration ( $B_n$ ) $\text{mg.kg}^{-1}$				
	Al	Ca	Fe	K	Mg
Stockton	6.01	7.30	10.60	0.27	0.21
Keele	13.30	3.90	15.60	0.37	0.08
Endon	3.36	0.33	9.79	0.24	0.71

**Table 5.15:** Description of study sites average soil elemental concentration levels

Sampling site	Average site Concentration ( $C_n$ ) $\text{mg.kg}^{-1}$				
	Al	Ca	Fe	K	Mg
Stockton	13.32	13.33	12.96	0.33	0.28
	(+222%)	(+182%)	(+122%)	(+122%)	(+133%)
Keele	17.29	5.93	18.57	0.26	0.26
	(+130%)	(+152%)	(+119%)	(-142%)	(+325%)
Endon	5.47	1.23	12.65	0.32	0.90
	(+163%)	(+373%)	(+129%)	(+133%)	(+127%)

Values in bracket show the percentage increase in concentration level

The calculated values of  $I_{geo}$  in Stockton graveyard ranges from -0.21 for K to 0.39 for Al, are below unity ( $< 1$ ), indicating that the site is characterized between zero and first

classification level – practically uncontaminated to moderately contaminated. The calculated values of  $I_{geo}$  in Keele graveyard ranges from -3.65 for Mg to 0.01 for Ca, are therefore below 0, indicating that the site is characterized as practically uncontaminated. Similarly, the calculated values of  $I_{geo}$  in Endon graveyard ranges from -3.51 for Ca to 0.08 for Al, are relatively below 0, indicating that the site is characterized as practically uncontaminated. The result of geo-accumulation factor of individual element with respect to graveyards and classification is presented in Table 5.17.

The average concentrations of the selected metals in Tables 5.14 - 5.15 were used for the determination of enrichment factor (EF) using equation 4.6 for the calculation. From the results indicated in Table 5.18 below, it was observed that some soil samples show evidences of enrichment of some soil metals, particularly Ca, K, and Mg. For example, the calculated graveyard enrichment values for Calcium (Ca) across two sampled graveyard soils (Keele and Endon) exceeded unity ( $> 1$ ), thus indicating anthropogenic enrichment of these metals in the graveyard's environments (Table 5.18). The enrichment values for all target metals in Stockton sampled graveyard soil were found to be below unity ( $< 1$ ), which corresponds to background values. The result of enrichment factor of individual element with respect to graveyards and classification is presented in Table 5.18.

The result of the concentration factor of individual element, with respect to graveyards and classification, is presented in Table 5.19. It was observed from the results that the samples showed moderately high concentration factors ( $CF$ ) for all the selected metals in the three study sites. The calculated values of  $CF$  in Stockton graveyard ranges from 1.22 for Fe and K to 2.22 for Al, which is more than unity ( $> 1$ ), indicating that the site is characterized as moderately contaminated. The calculated values of  $CF$  in Keele graveyard

ranges from 0.70 for K to 3.25 for Mg, with the exception of K, Keele graveyard soil is relatively characterized as moderately to considerably contamination. The calculated values of CF in Endon graveyard ranges from 1.23 for Mg to 3.73 for Ca, with the value for individual metal greater than unity ( $> 1$ ), which corresponds to moderate to considerable contamination of the graveyard.

To complement the contamination factor, the contamination degree ( $C_{deg}$ ) which is the sum of contamination factors was used to describe the contamination of the environment by all examined metals and further defines the quality of the environment. The  $C_{deg}$  values for the three graveyard sites are 7.82, 7.97 and 9.21 for Stockton, Keele and Endon graveyards respectively. While Stockton and Keele graveyards had low degree of contamination ( $< 8$ ), Endon graveyard had moderate degree of contamination. Meanwhile, the calculated values of  $I_{geo}$ ,  $EF$  and  $CF$  for the three graveyards have been plotted against their respective metals. Considering the more suitability of contamination factor and contamination degree in evaluating or ascertaining the extent of contamination of substances in soil (Loska *et al.*, 2004; Likuku *et al.*, 2013), and its usefulness in identifying hot spots within the sampling locations, therefore, contamination factor among  $EF$  and  $I_{geo}$  was used as the determining factor for site contamination as presented in Figure 4.16a-c.

**Table 5.16:** Summary of enrichment factors, geo-accumulation factors and contamination factors for the selected metals in the three sites

Study site	Impact Factors	Al	Ca	Fe	K	Mg	$C_{deg}$
Stockton	$I_{geo}$	0.39	0.20	-0.20	-0.21	-0.12	
	$EF$	1.00	0.82	0.55	0.55	0.60	
	$CF$	2.22	1.83	1.22	1.22	1.33	7.82
Keele	$I_{geo}$	-0.14	0.01	-0.23	-0.76	-3.65	
	$EF$	1.00	1.17	0.92	0.54	2.50	
	$CF$	1.30	1.52	1.20	0.70	3.25	7.97
Endon	$I_{geo}$	0.08	-3.51	-0.15	-0.12	-0.17	
	$EF$	1.00	2.90	1.00	1.03	1.00	
	$CF$	1.63	3.73	1.29	1.33	1.23	9.21

**Table 5.17:** Geo-accumulation factor with respect to individual graveyard and classification

$I_{geo}$ Index	$I_{geo}$ factor	Target Metals		
		Stockton	Keele	Endon
$I_{geo} \leq 0$	Practically uncontaminated	Al, Ca, Fe, K and Mg	Al, Ca, Fe, K and Mg	Al, Ca, Fe, K and Mg
$0 < I_{geo} < 1$	Uncontaminated to moderate			
$1 < I_{geo} < 2$	Moderate			
$2 < I_{geo} < 3$	Moderate to strong			
$3 < I_{geo} < 4$	strong			
$4 < I_{geo} < 5$	Strong to very strong			
$I_{geo} > 5$	Extremely contaminated			

**Table 5.18:** Enrichment Factor with respect to individual graveyard and classification

EF Indices	Degree of Enrichment	Target Metals		
		Stockton	Keele	Endon
$EF < 1$	Background Concentration	Al, Ca, Fe, K and Mg	Al, Fe and K	Al, Fe and Mg
$1 < EF < 2$	Depletion to minimal Enrichment	Al	Al and Ca	Al, Fe, K and Mg
$2 < EF < 5$	Moderate Enrichment	Ca	Mg	Ca
$5 < EF < 20$	Significant Enrichment			
$20 < EF < 40$	Very High Enrichment			
$EF > 40$	Extremely High Enrichment			

**Table 5.19:** Contamination factor with respect to individual graveyard and classification

$Cf_x$ classes	Contamination factor	Target Metals		
		Stockton	Keele	Endon
$Cf_x < 1$	Low contamination		K	
$1 \leq Cf_x < 3$	Moderate contamination	Al, Ca, Fe, K and Mg	Al, Ca and Fe	Al, Fe, K and Mg
$3 \leq Cf_x < 6$	Considerable contamination		Mg	Ca
$Cf_x > 6$	Very high contamination			



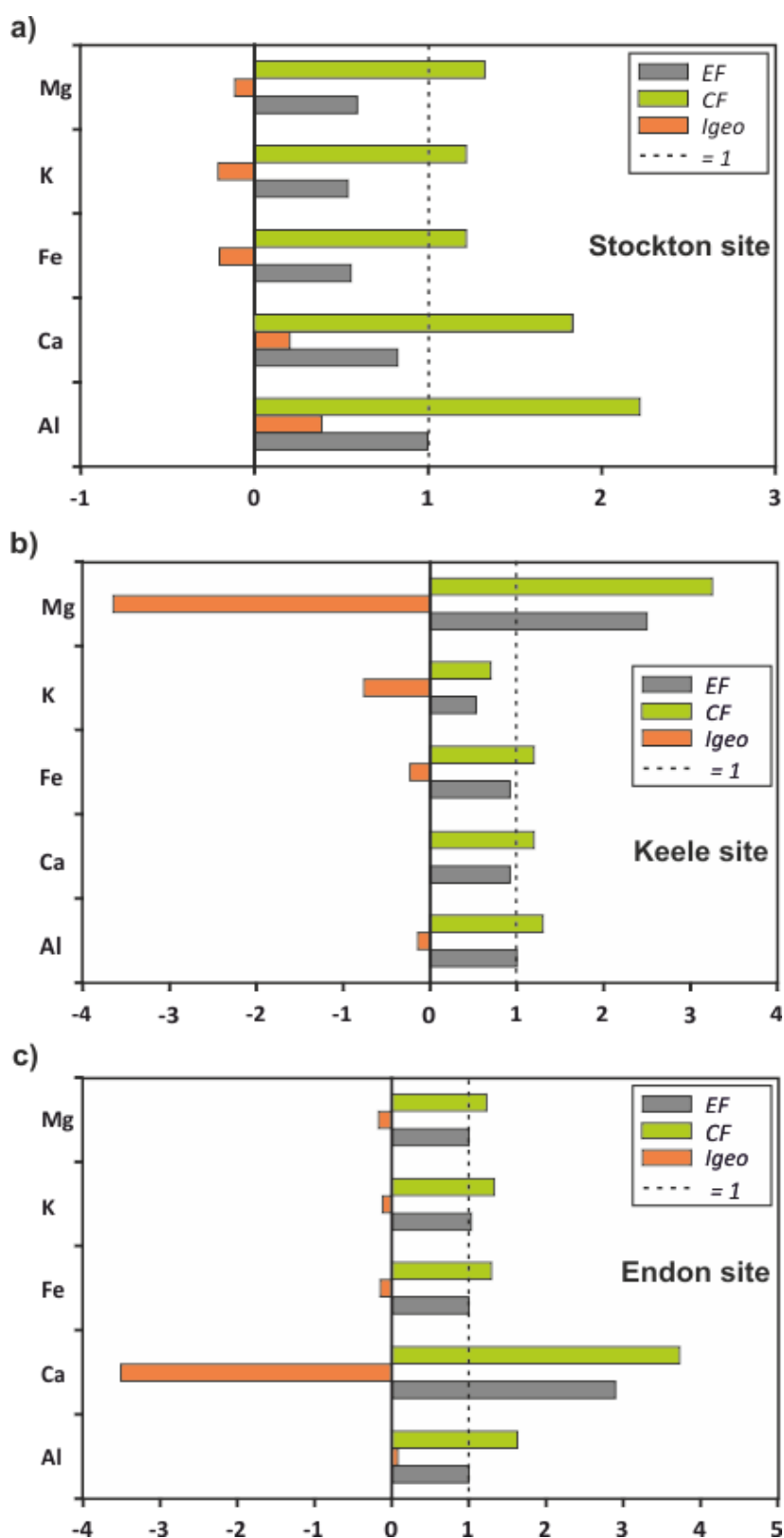


**Figure 5.17:** The enrichment factors, geo-accumulation factors and contamination factors for (a) Stockton (b) Keele and (c) Endon sites respectively. See Tables 5.17-9 for details.

## 5.5 Discussion

The burial of animal/human carcass in the soil will always lead to changes in soil composition and the accumulation of certain substances and elements in the soil (Aitkenhead-Peterson *et al.*, 2012). With the growing need for forensic taphonomic studies (Damann *et al.*, 2012), continuous monitoring of changes in elements could provide traces of evidence to the detection of clandestine burials. This section has been designed to answer and discuss the chapter aims and objectives in sequential order.

Firstly, *“to sample and present results from a 18 month monitoring study of a burial pig carcass, analysing the leachate and background soil water for the major inorganic chemical components”*.

This study has demonstrated that grave soil water (leachate) can be clearly differentiated from background soil water (control) by measuring the element of samples, which include electrical conductivity, pH and elemental concentration, and therefore, this practical approach could potentially assist the search for clandestine graves. The data shows clear soil conductivity changes over time, with significant variations in conductivity values across the monitoring period; for example, conductivity values measured from November 2014 to April 2015 showed relatively high conductivity values when compared to the other months. This is probably due to the consistent decrease in rainfall rate observed between November 2014 and April 2015 (Fig. 5.12). However, the most rapid changes occurred between ~100 and ~220 PBI which correspond with the monitoring period between June 2014 and October 2014, evidencing the summer season with low average

monthly rainfall of 66 mm over the period compared to the yearly average of 76 mm and increased temperatures. However, the changes observed in EC values during monitoring may likely be associated with contributions from individual elemental concentrations, with inorganic ions such as  $\text{PO}_4^{3-}$ ,  $\text{K}^+$ ,  $\text{SO}_4^{2-}$  and  $\text{Na}^+$  showing the most resemblance trends when compared to the electrical conductivity results (Fig. 5.14). Another interesting observation in this study was the continuous sigmoidal trend of element values immediately after values peaked (Fig. 5.13c), which other authors have reported (e.g. VanLaerhoven and Anderson, 1999; Carter *et al.*, 2008b) but these were not definitive.

This study also showed a uniform rise in concentration of inorganic ions starting from day 14 PBI up to day 220 PBI and thereafter declined to relatively low concentration at the end of the monitoring period (550 PBI) (Fig. 5.13c). Interestingly there was a very sharp decline in Nitrate values which returned to soil water background value at day 300 PBI (Fig. 4.14h), followed by Sulphate at day 520 PBI (Fig. 4.14d), however, the rest of the measured inorganic ions still showed the potential for measureable changes before returning to background value. These elements were mostly the members which showed the strongest influence on conductivity value (Fig. 5.14b, c, f and g).

The initial measured pH of grave soil water (leachate) and background soil water after two weeks of burial was neutral, with pH ~7 and 7.4 for leachate and soil background water respectively (Table 4.4), this showing the early stage of decomposition were small or no decomposition fluid had been generated, which means that the extracted fluid from grave represented the soil background water. Increasing pH was observed after the first

sampling (30 days after burial) giving rise to the peak pH values of 8.85 and 8.40 between days 30 and 60 after burial and gradually reduced up to day 120 after burial. However, the corresponding pH values of soil background water remained constant (neutral) over this period. The observed high leachate pH values between 30 and 60 days after burial may be attributed to high growth and activities of microbiological acid-consuming acetogenic and methanogenic bacterial (Barlaz *et al.*, 1989; EA, 2004), causing accumulation of ammonium (Hopkins *et al.*, 2000). The high pH values observed at the first two months of monitoring is also consistent with related results reported by Carter and Tibbett (2006) who investigated pH difference between alkaline and acid graves.

The second aim of this chapter was *“perform a systematic statistical analysis of the resulting element parameters to determine the contributions from individual inorganic ions responsible”*.

In this study, the numerical values of the correlation coefficient, R, for the measured element parameters (Table 4.7) showed a highly significant positive correlation between EC and  $K^+$ , EC and  $SO_4^{2-}$ , EC and  $Na^+$  and also EC and  $PO_4^{3-}$ ). This suggests that EC depends on dissolved salts (Shah *et al.*, 2007) such as NaCl and KCl. No significant correlation exists between EC and  $NO_3^-$ , EC and Cl, and EC and Ca. However, only  $PO_4^{3-}$  and Cl show a positive correlation with EC in background soil water (Table 4.8).

The choice of dependent and independent variables in a regression model is crucial. The dependent variable is a variable to be explained, while the independent variable is a moving force (Pindyck and Rubinfeld, 1998). Two variable least squares approach was used to develop a relationship between electrical conductivity as an independent variable

and different inorganic elements such as  $K^+$ ,  $SO_4^{2-}$ ,  $Na^+$ ,  $PO_4^{3-}$ ,  $NO_3^-$ ,  $Cl^-$  and  $Ca^{2+}$  as dependent variables in leachate sample as shown in the cross section results (Table 4.9). Different dependent characteristics of leachate sample were calculated using the regression equation and by substituting the values for the independent parameter in the equations. Regression results for  $K^+$ ,  $SO_4^{2-}$ ,  $Na^+$  and  $PO_4^{3-}$  equations showed that electrical conductivity is significant at 1% level, while the equation for  $NO_3^-$  shows significant at 10% level of confidence. Both  $Cl^-$  and  $Ca^{2+}$  show no significant correlation with EC. The significance of the relationship is also validated by F test (Table 5.9), which demonstrated that values greater than 17 have high level of confidence.

The independent variables such as  $K^+$ ,  $SO_4^{2-}$ ,  $Na^+$  and  $PO_4^{3-}$  in the leachate sample were significant in predicting changes in EC values. The multiple R value (0.880) indicates that 88% of the variability in EC could be associated to the combined effect of  $K^+$ ,  $SO_4^{2-}$ ,  $Na^+$  and  $PO_4^{3-}$ . Out of this 88%, 31.4% was due to  $PO_4^{3-}$  alone and 24.2%, 24.8% and 19.7% were due to  $K^+$ ,  $SO_4^{2-}$  and  $Na^+$  respectively (see Table 5.9). However, the variability of EC values in background soil water sample was mainly caused by the combined effect of two independent variables such as  $PO_4^{3-}$  and  $Cl^-$ . The combined multiple  $R^2$  value (0.733) indicates that 73.3% of the variability in EC of soil water could be linked to the presence of  $PO_4^{3-}$  and  $Cl^-$  with 55.6% and 44.4% contributions respectively.

Other studies have also shown that cadaver decomposition can have a significant and persistent effect on grave-soil chemistry (Juerges *et al.*, 2010; Aitkenhead-Peterson *et al.*, 2012). Therefore in an old burial scenario, where physical remains may have all decayed

and decomposition fluid no longer retained in the local soil environment, direct use of grave-fluid electrical conductivity may not be possible. However, analysing the concentration of these inorganic ions extracted from grave-soil may be used as a possible field test for clandestine grave following the strong relationship between electrical conductivity and concentration of inorganic ions.

Thirdly, *“determine the elevated metallic elements in long-term burial sites (three graveyards) when compared with control values.”*

Element results are graphically summarised in Figures 5.17, 5.18 and 5.19 for Stockton, Keele and Endon graveyards respectively.

### *Aluminium*

The Aluminium content in the soil of Stockton graveyard ranged from 6.10 – 30.5 mg/kg, with the mean concentration value of 13.3 mg/kg and background value of 6.0 mg/kg. All grave sampled locations were higher than background values. Aluminium content in the soil of Keele graveyard ranged from 9.2 – 26.1 mg/kg, with mean value of 17.3 mg/kg and background value of 13.3 mg/kg. There were reasonable difference between graveyard and control samples; however, up to 5 out of 15 sampled locations were below the background average value. The Aluminium content in the soil of Endon graveyard ranged from 3.8 – 8.1 mg/kg, with a mean value of 5.5 mg/kg and background value as 3.4

mg/kg. There were significant increases in concentration between Endon graveyard and background value, with all sampled locations having higher values than background.

### *Calcium*

The Calcium concentration in the soil of Stockton graveyard ranged from 2.1 -23.7 mg/kg, with mean value of 13.3 mg/kg and background value of 7.3 mg/kg. There were significant increase in concentration between Stockton graveyard and background value, however, 4 out of 15 sampled locations were below background value averages. Concentrations of Calcium in the Keele graveyard ranged from 0.2 – 11.6 mg/kg, with mean value of 5.9 mg/kg and background value of 3.9 mg/kg. There were significant increases in concentration between Keele graveyard and background values, however, out of 15 locations, 2 locations fell below detection limits and 4 locations were below background averages. Calcium concentrations in Endon graveyard were negligible when compared to Stockton and Keele graveyards, with ranged from 0.1 – 3.1 mg/kg, and mean values of 1.2 mg/kg.

### *Iron*

Concentration of Iron (Fe) in the Stockton graveyard ranged from 9.8 -15.2 mg/kg, with mean value of 13.0 mg/kg and background values of 10.6 mg/kg. There were increases in concentration of soil Fe between Stockton graveyard and background value, however, 1

out of 15 sampled locations was below background value averages. Concentration of Fe in the Keele graveyard ranged from 13.8 – 24.0 mg/kg, with mean value of 28.6 mg/kg and background value as 15.6 mg/kg. There were significant increases in concentration of soil Fe between Keele graveyard and background value, however, 5 out of 15 locations were background level averages. Concentration of Fe in the soil of Endon graveyard ranged from 9.8 – 18.7 mg/kg, with mean value of 12.6 mg/kg. Changes in levels of soil Fe occurred throughout the sampled locations when compared with background values.

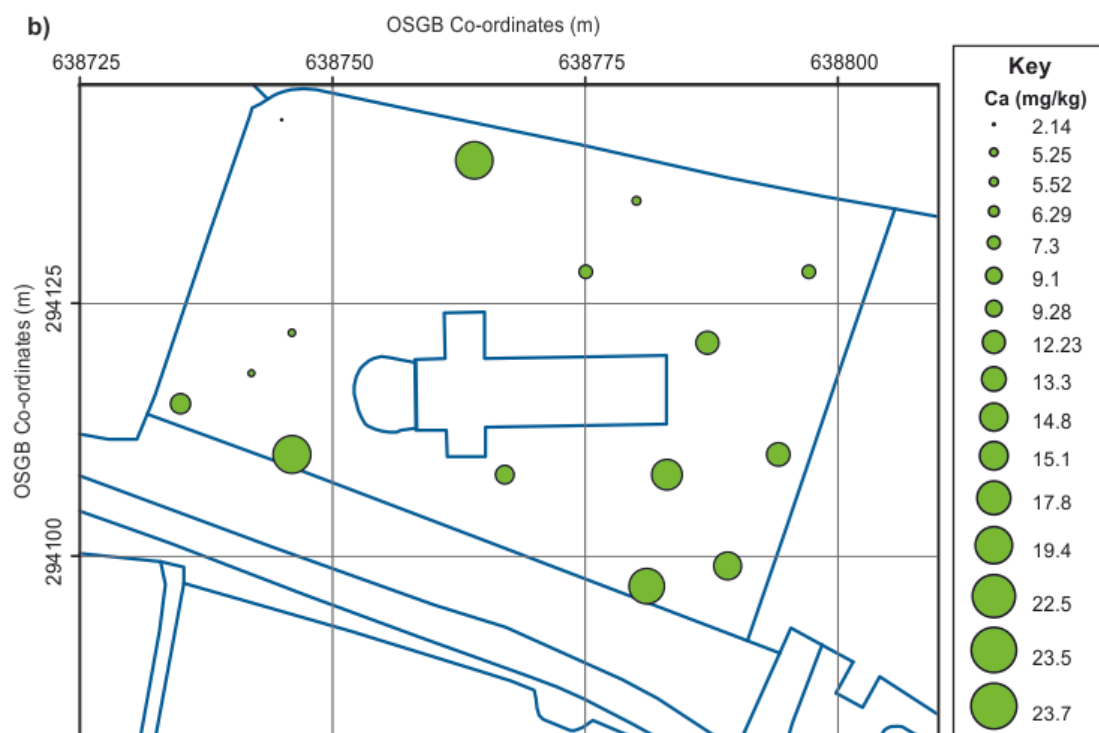
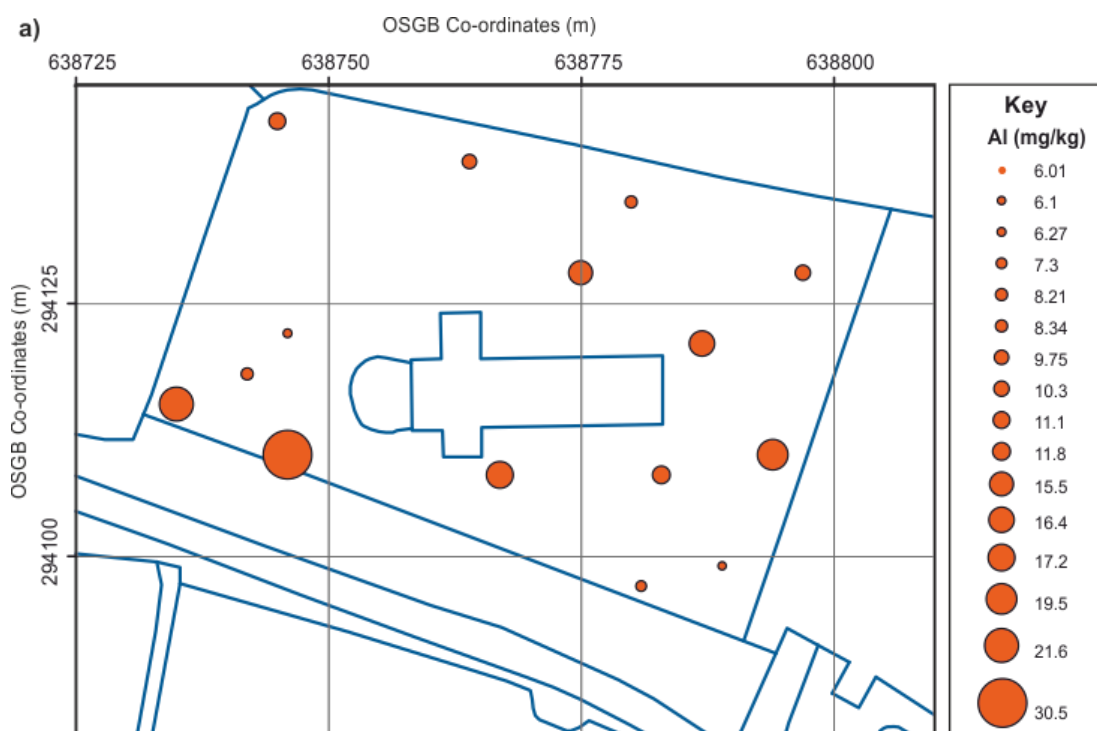
#### *Potassium and magnesium*

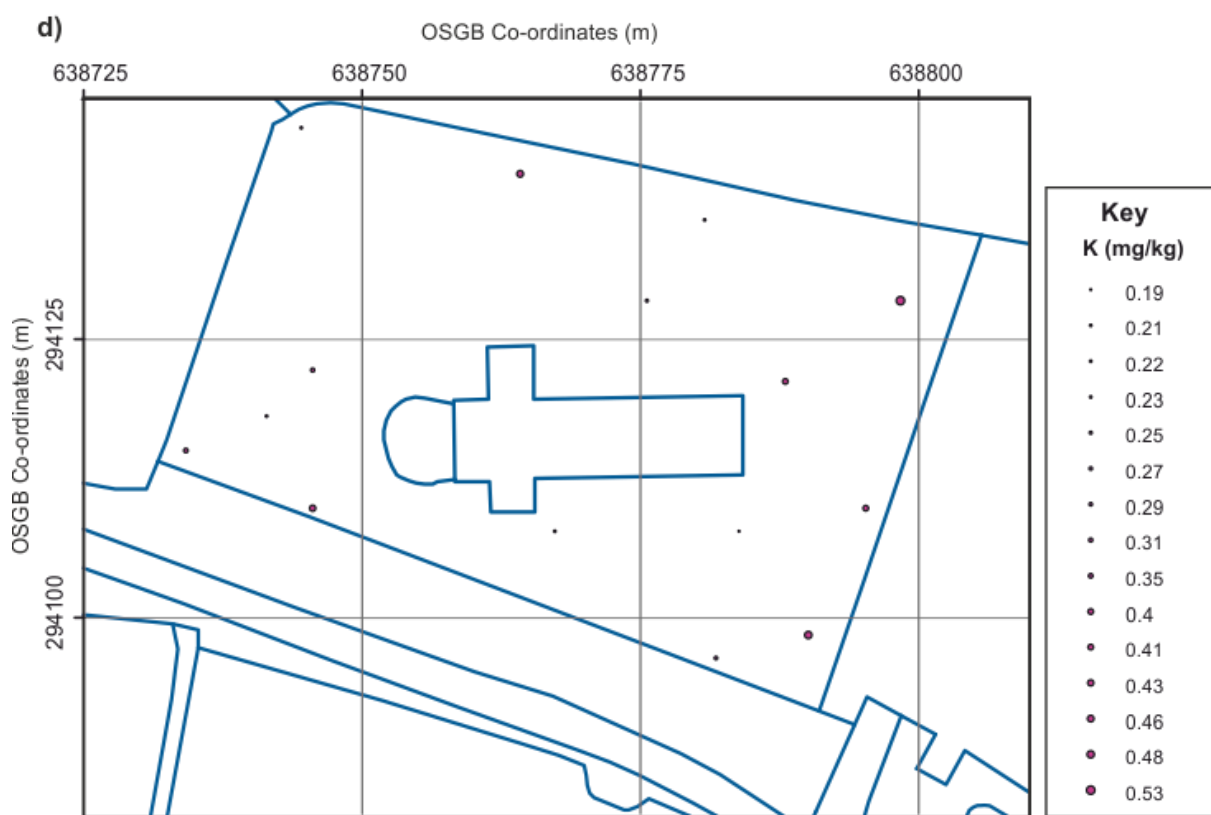
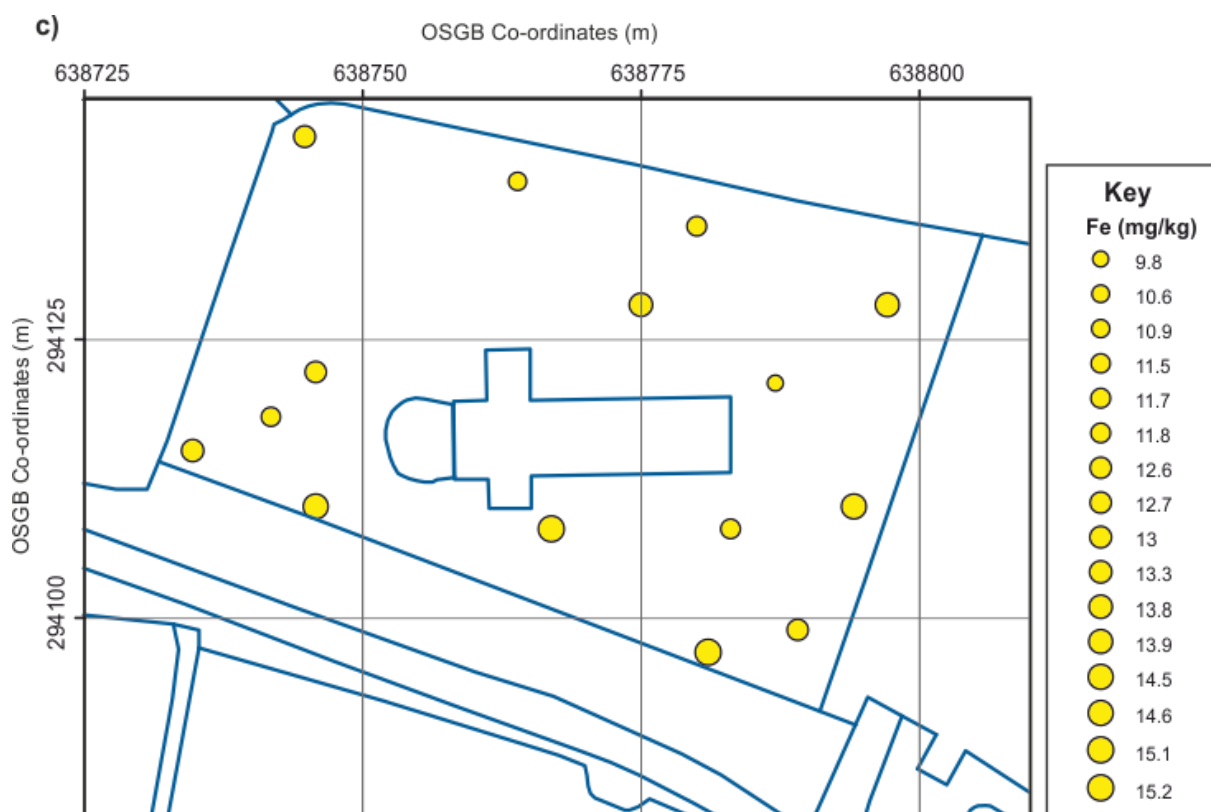
Potassium and magnesium concentration in the three graveyard soils were negligible when compared to other measured elements in the three sampled sites. In Stockton graveyard, potassium ranged from 0.2 - 0.5 mg/kg, with mean values of 0.3 mg/kg and background values of 0.3 mg/kg, while magnesium ranged from 0.15 to 0.4 mg/kg, mean values of 0.2 mg/kg and background of 0.3 mg/kg, with mean values of 0.3 mg/kg and background of 0.3 mg/kg.

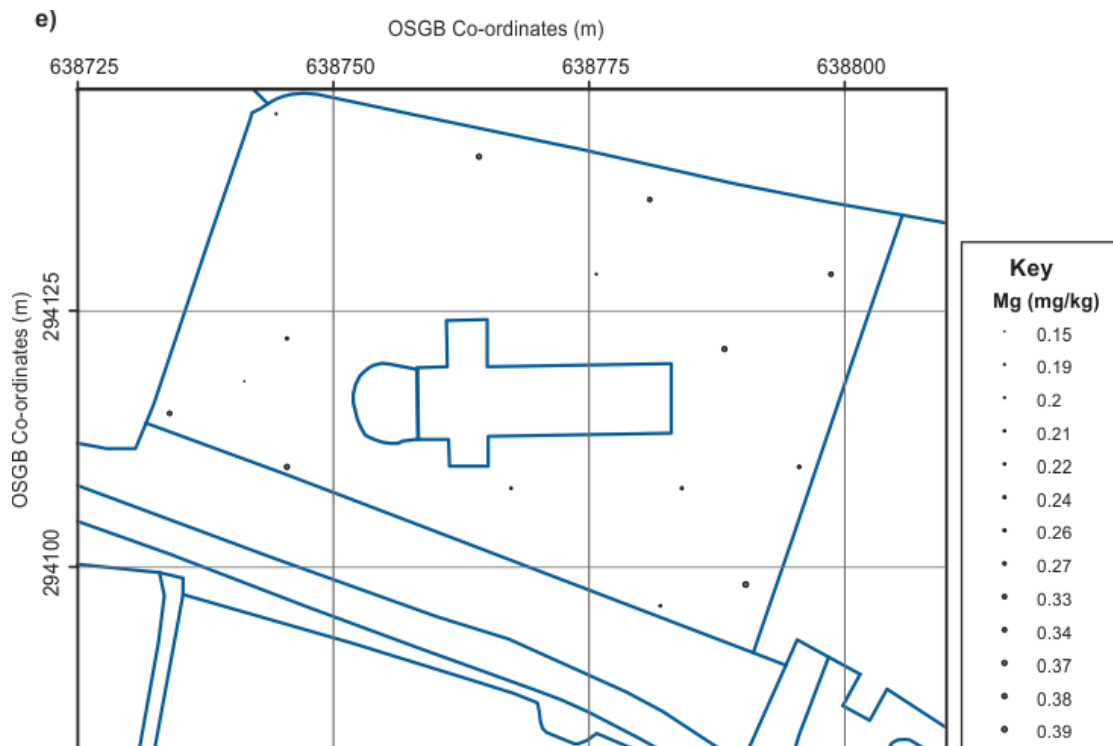
Although the low concentrations of magnesium in the sites is understandable, as would be expected of a burial site due to the low input of magnesium from cadaver decomposition, but it is not clear why the concentration of potassium was low in the study sites, following the evidence of high concentration of potassium that was generated during cadaver decomposition (see Section 4.3). However, it is a very mobile element, which could suggest input of potassium from cadavers into soil may have been leached rapidly and remains poorly detected. This is further evidenced by the downslope



topography of Keele and Endon graveyards as shown by Aitkenhead-Peterson *et al.* (2012). Concentrations of K and Mg in Keele graveyard ranged from 0.06 – 0.4 mg/kg and 0.03 – 0.06 mg/kg respectively, the mean concentration of K (0.3 mg/kg) obtained in Keele graveyard was observed to be lower than background values (0.4 mg/kg), with the mean Mg concentration value (0.26 mg/kg) was significantly higher than background values (0.08 mg/kg). Concentration of K and Mg in Endon graveyard ranged from 0.15 – 0.5 mg/kg and 0.6 – 1.3 mg/kg respectively, with mean values of 0.3 mg/kg and 0.9 mg/kg for K and Mg respectively and background values of 0.2 mg/kg and 0.7 mg/kg for K and Mg respectively. Site plots of elemental concentration of the sites are shown in Figures 5.18a-e – 5.20a for Stockton, Keele and Endon graveyards respectively.

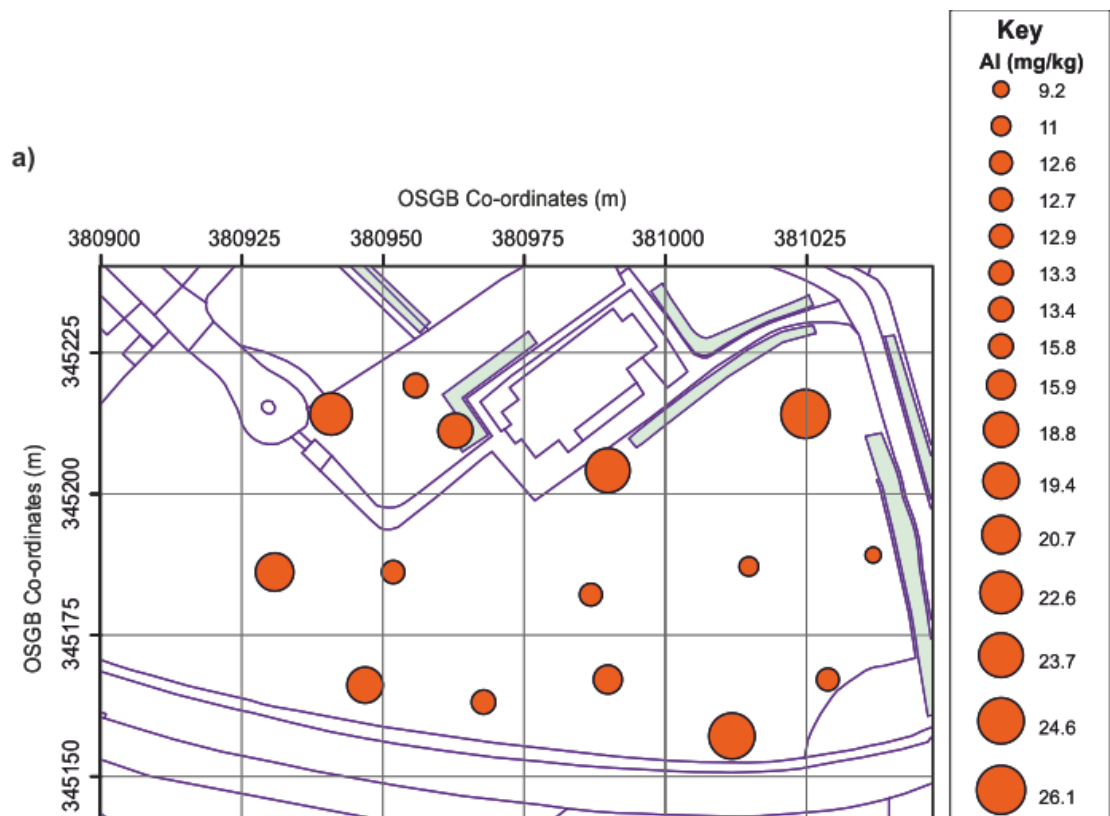


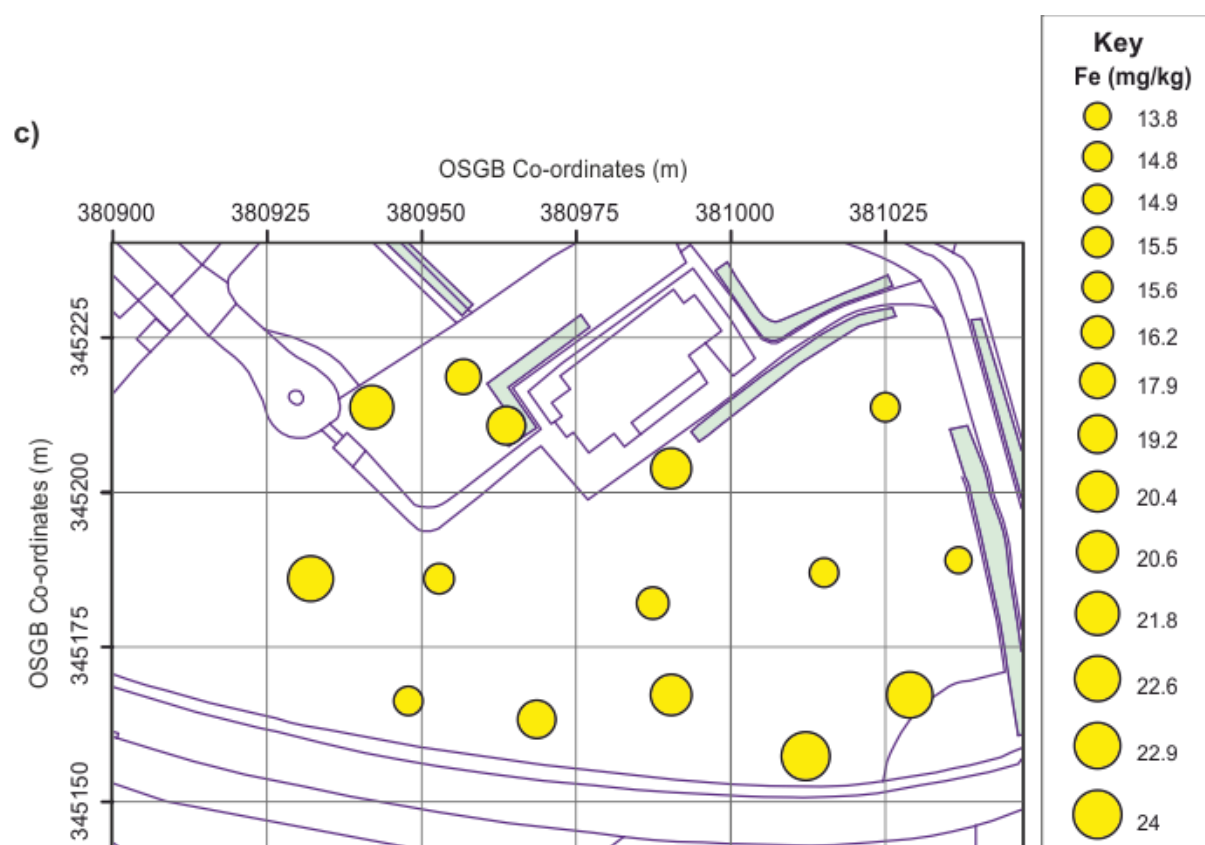
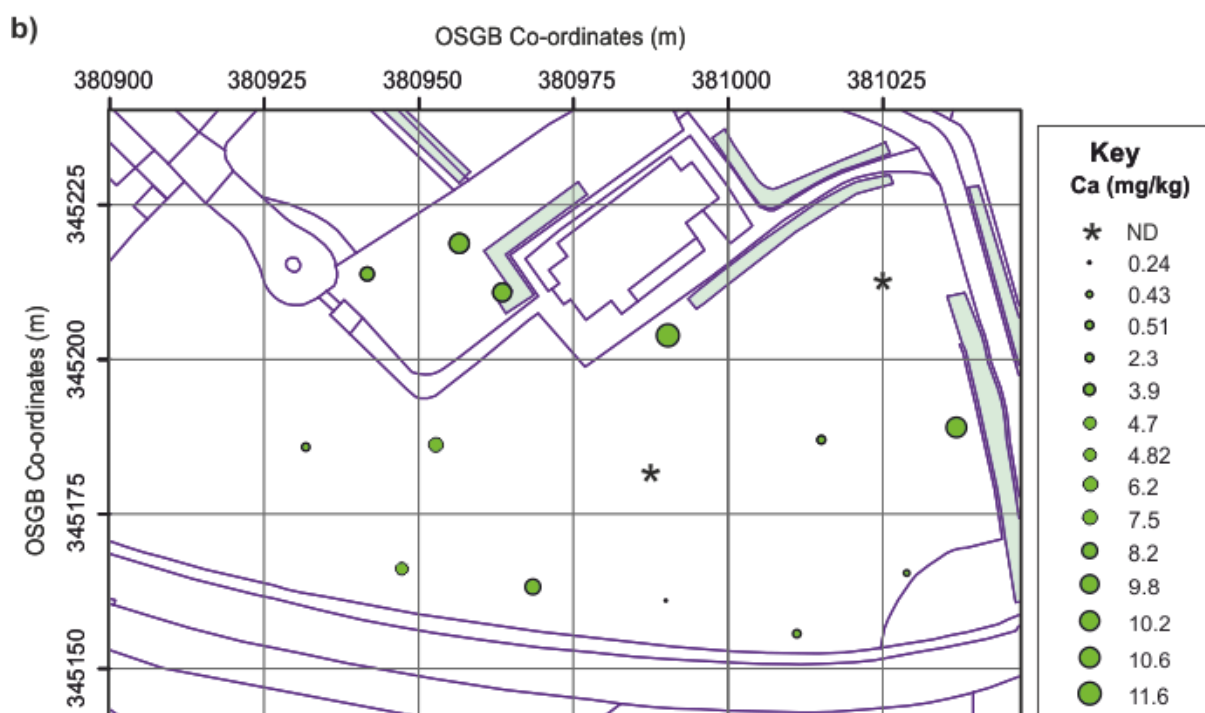


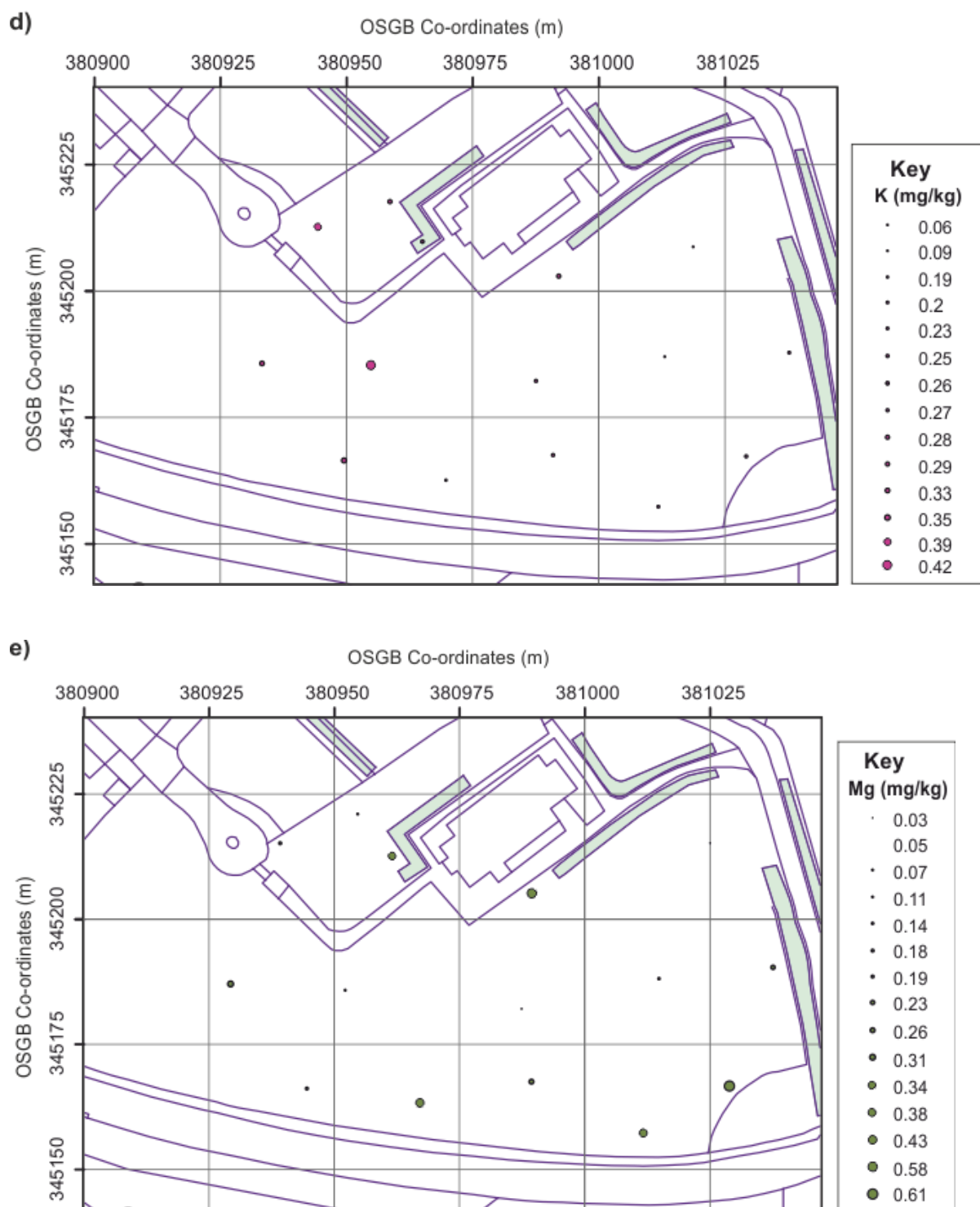


**Figure 5.18a-e:** Stockton site map with element concentration levels at sampled locations

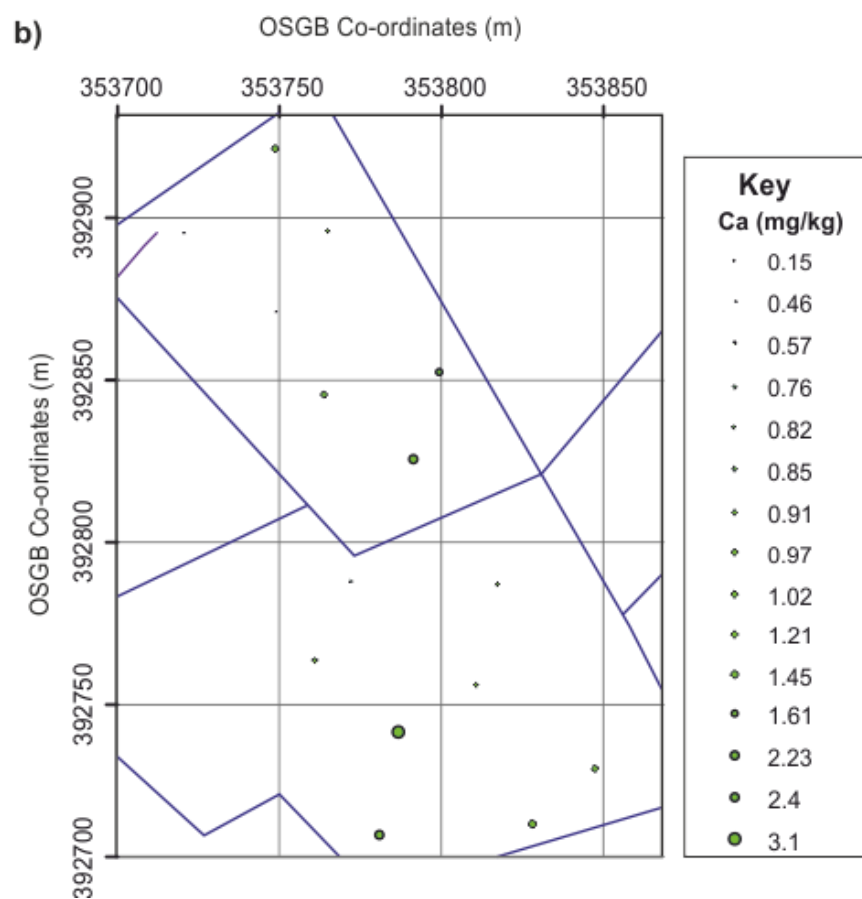
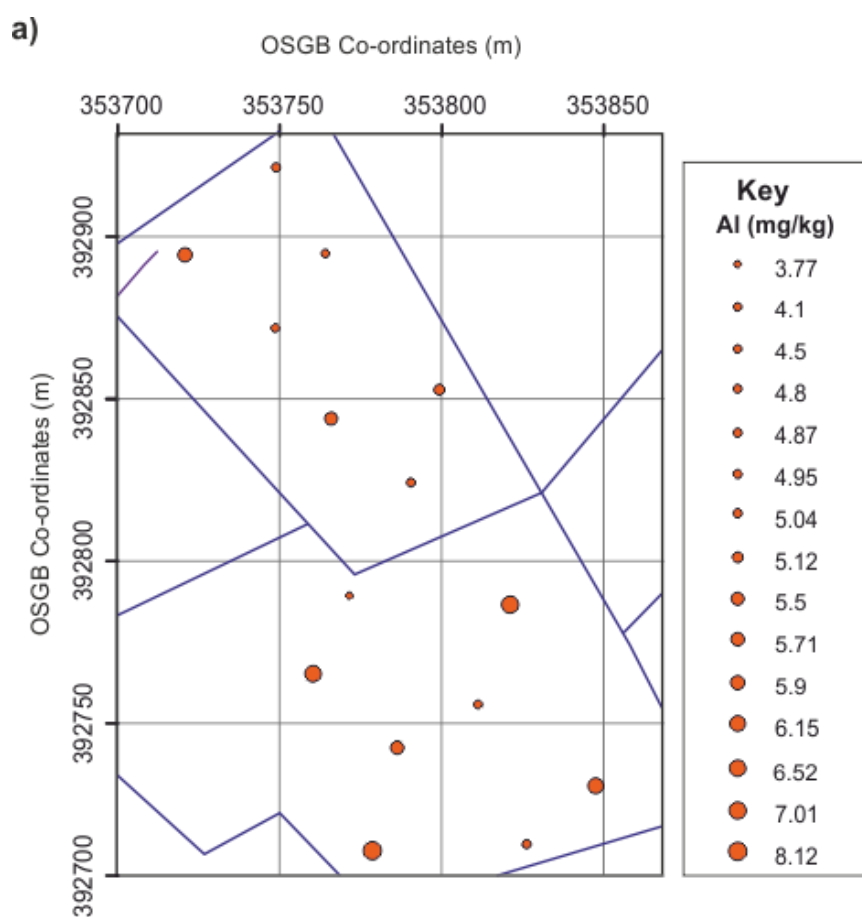
a) aluminium (Al), b) calcium (Ca), c) iron (Fe), potassium (K) and magnesium (Mg).

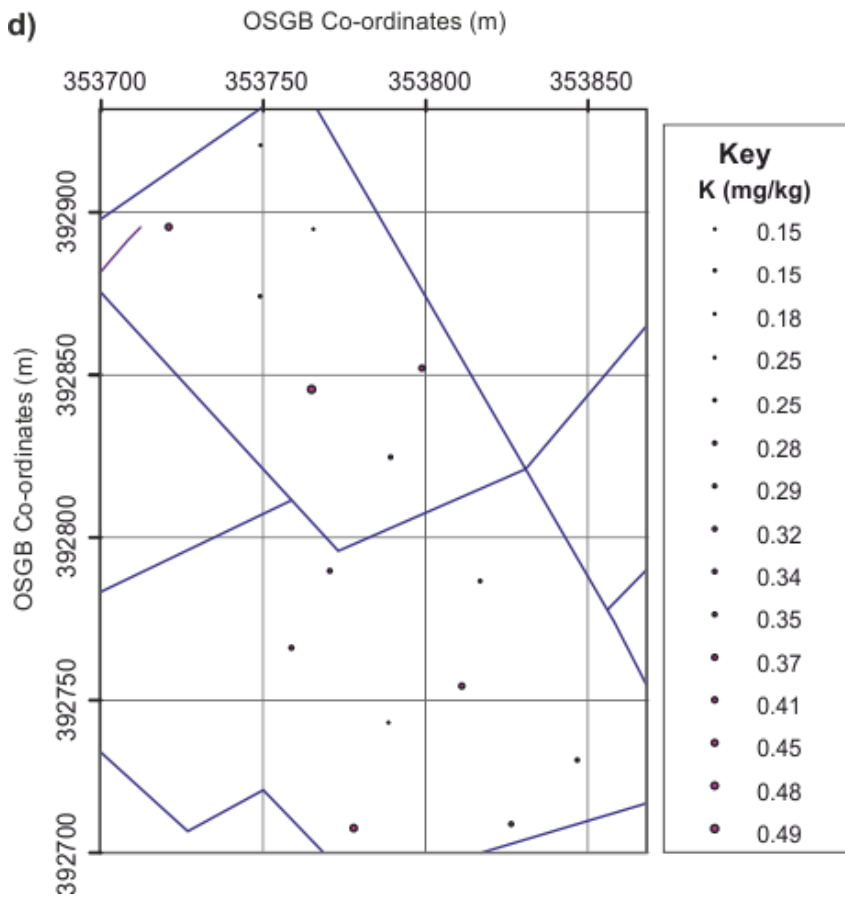
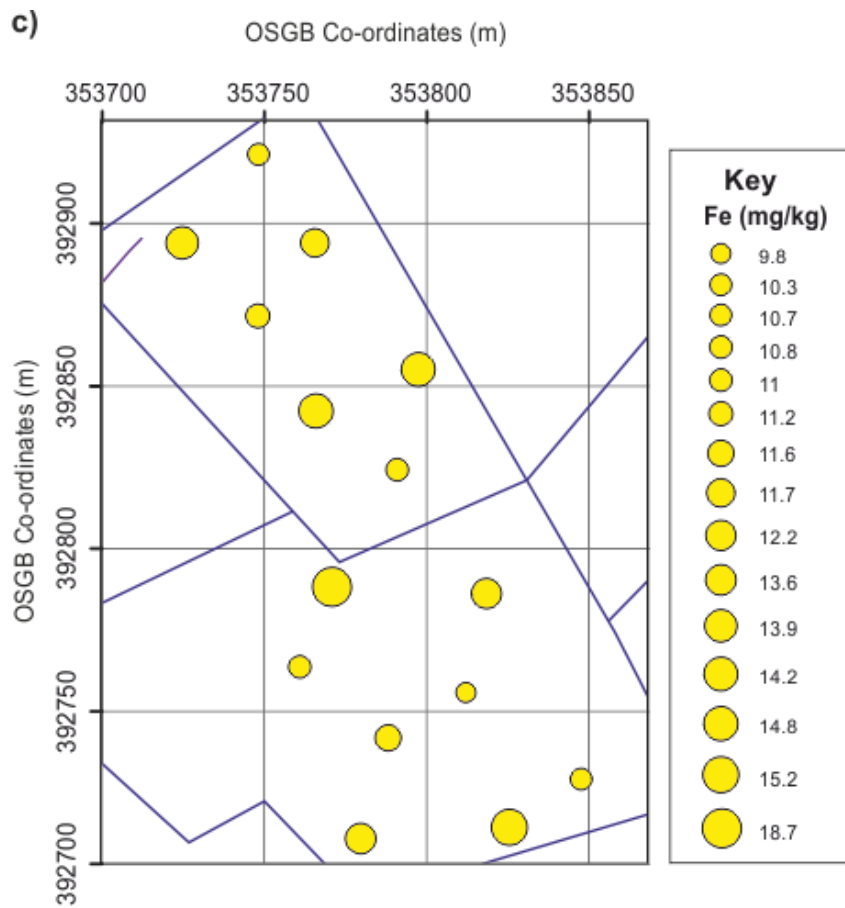






**Figure 5.19a-e:** Keele site map with element concentration levels at sampled locations a) aluminium (Al), b) calcium (Ca), c) iron (Fe), potassium (K) and magnesium (Mg).







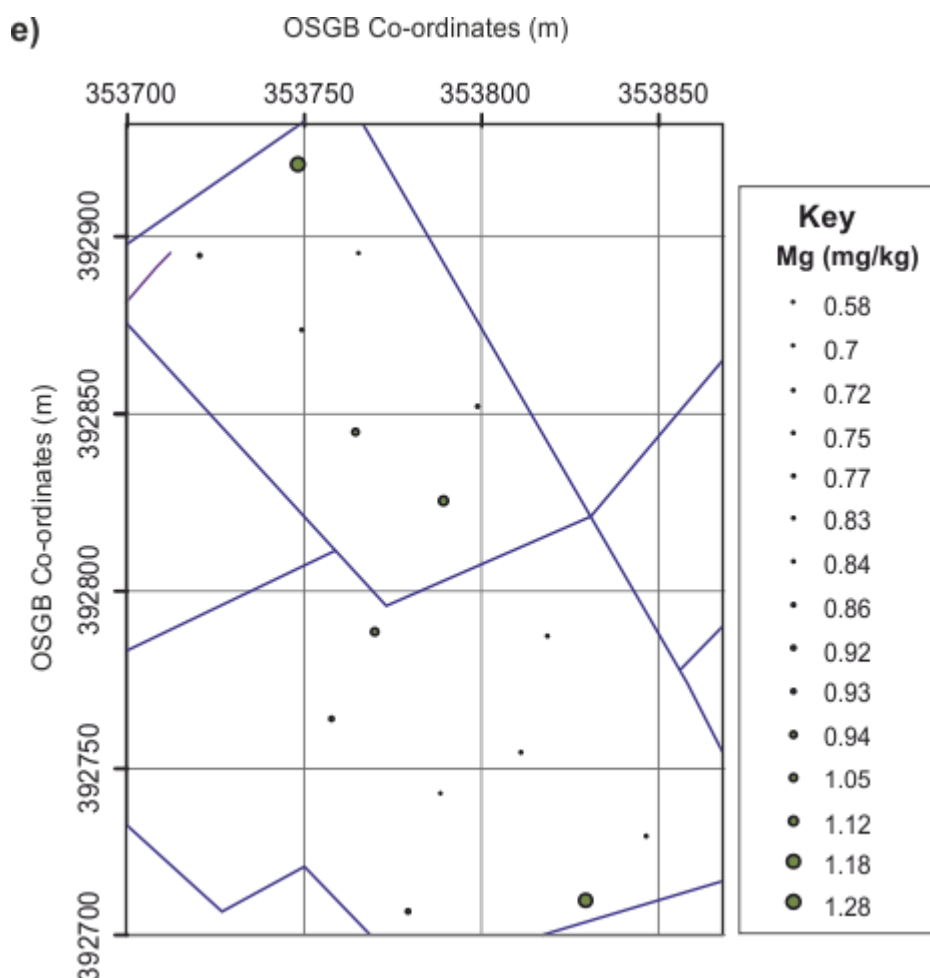


**Figure 5.20a-e:** Endon site map with element concentration levels at sampled locations a) aluminium (Al), b) calcium (Ca), c) iron (Fe), potassium (K) and magnesium (Mg). See Figure 15.16c for profile lines across grave locations

#### *Contribution of particular metals to the contamination of soil in three graveyards*

Assessment of the overall contamination of graveyard soils was based on the degree of contamination ( $C_{deg}$ ). On the basis of the contamination factor ( $C_f$ ), the Stockton graveyard soil was classified as moderately contaminated with Ca, Fe, K, Mg and Al (Table 4.16). Keele graveyard soil was classified as uncontaminated with K, moderately contaminated with Al, Ca and Fe, considerably contaminated with Mg (Table 5.16).

However, it was found that ~41% of the degree of contamination index of the graveyard was contributed by Mg, followed by Ca, Al, Fe and K as contributing 19%, 16%, 15% and 9% respectively. This observation was also in agreement with the value obtained by enrichment index; however, geoaccumulation index was not able to reveal this. Endon graveyard soil was classified as moderately contaminated with Al, Fe, K and Mg, considerably contaminated with Ca (Table 5.16). It was found that ~40% of the degree of contamination index of the graveyard was contributed by only Ca, followed by 18%, 14%, 14% and 13% for Al, Fe, K and Mg respectively. Enrichment index also show a correlation with contamination factor in predicting the degree of contamination in Endon graveyard. In general, the  $C_{deg}$  for the mean metal contents in the three graveyard soils shows that Stockton and Keele graveyards had low degree of selected metal contamination of 7.8 and 8.0 respectively, while Endon graveyard soil had a moderately degree of contamination as 9.2.

Figure 5.17 showed the graphical representation of the relationship between the three contamination impact factors, which indicated that contamination factor was significantly higher and more robust than the other factors, thus was used as the basis for the estimation of site contamination. Meanwhile the negative values obtained in most of the metallic indexes of geo-accumulation were a result of deficient to minimal enrichment. The nature of the  $I_{geo}$  calculation, which involves the logarithmic function and a background multiplication factor of 1.5, is somewhat different from the other pollution calculation methods used in this study. Locations where contamination indices are equal to 1 is indicated by a dotted line.

*Fourthly, and finally, the results as a potential for detecting clandestine burials of murder victims.*

Combined analysis of soil water and grave soil (leachate) water samples were used to successfully established the presence of human graves in three case studies of selected English graveyards. Whilst leachate conductivity has been used to determine the presence of cadaver burial, this study has determined the major inorganic ions that control the variability in conductivity of leachate, with phosphorus having the strongest influence on conductivity followed by potassium, sulphate and sodium. In this chapter, an attempt has been made through the application of geostatistical techniques such as geo-accumulation index, enrichment factors and contamination factors to examine the elevated contents of selected inorganic ions and metals in the graveyards (onsite) and surrounding (offsite) as control. The information presented in this study is significant in that a quantitative assessment of the contamination status of graveyard soils have been determined. It was found that the elemental composition of soils within the graveyards was moderately contaminated with most of the investigated elements. However, Keele and Endon graveyards were considerable contaminated with Mg and Ca respectively.

It is what noting that this research precludes the analysis of pathogenic or organic ions from leachate and graveyard soils due to highly unstable and complex nature of organic ions. However, the study is dependent on estimations of the concentration of inorganic ions in the leachate and metals that are already introduced into the graveyards. It also reflects metal contamination arising from metal deposits that have been accumulated over time hence the graves were not interred in a fixed pattern or at the same time. The

fact that Keele and Endon graveyards are located on the slopes may cause leaching of minerals into the groundwater and result to potential health hazards.

## **5.6 Conclusions, study limitations and further work**

This study has shown the potential to assist geophysical techniques in detecting and characterising a clandestine burial using soil water inorganic element analysis through both a modern and ancient burials study. This may, perhaps, promise a more realistic approach to grave searches as it relies on a ground truth investigation of soil and grave fluid to determine concentration of selected elements. Certainly conductivity measurements of soil water can be easily undertaken in the field and could provide a rapid test to identify suspect area(s). Inorganic element analysis is also a standard laboratory analytical technique and thus should be easily transferred to the forensic domain. It is obvious that electrical conductivity of leachate is controlled by metallic ion concentration of the leachate; however, following the second aim of this study, which is to determine the contributions from individual inorganic ions responsible for conductivity variations, hence, the need to calculate the percentage of individual contribution to changes in electrical conductivity. The elevated element may serve as a pointer to assist the location of a potential clandestine burial in the site. Therefore, instead of relying only on the conductivity measurement which cannot be easily obtained especially when there is no leachate fluid remaining in the grave, on-site measurement of multi-elemental concentration in soil using equipment such as X-ray spectrometer can be conducted in the site for a quick search of a potential clandestine burial site.

However, this experimental methodology only used a single modern simulated study and three English graveyards, it should be repeated in others with different burial patterns and contrasting soil types, possibly, in a mass burial scenario in which the interment occurred at the same period to actually monitor how grave-soil elemental concentration changes with time when compared with offsite values, in order to establish whether this approach could be effectively employed for forensic search for clandestine burials.

## **CHAPTER 6    Discussion**

As stated in Chapter 1, the overall aim of this study was to provide more realistic information and to support the forensic search of burials using a combined multi geophysics and soil sampling analysis investigation approach. Although some geophysical techniques have shown successful detection of graves, however, there is still no single published study that distinguishes between geophysical technique(s) that are most optimal for grave detection. Current research has not even evidenced the optimal identification of burials in contrasting soil types and depositional environments.

However, GPR has been commonly adopted as the tool of choice for grave detection by forensic geophysicists. Electrical resistivity techniques have also been used and show promise as recent published studies have evidenced (see, for example, Jervis, 2010; Pringle and Jervis, 2010). It has been suggested that electrical resistivity can be an all-round successful tool in non-invasively detecting buried forensic targets that includes human burials but is not exclusively so. This chapter now sequentially discusses the main thesis results and directly links back to the thesis aims.

## **6.1 The rate of detection of modern and potential ancient mass burial**

*Aim 1: To determine if non-invasive geophysical methods could both detect and characterise a potential ancient mass burial;*

As shown in Chapter 3, non-invasive, near-surface geophysical surveys can both detect and characterise an ancient mass burial site, as evidenced here in the Charter house cemetery in central London. Historical records have suggested that this so-called Black Death mass burial pit was sited here and the near-surface, geophysical surveys have confirmed this, which reinforces other researchers' findings, for example (Reynolds, 2011; Ruffell and McKinley, 2014).

From this study it was shown that a phased investigation approach was crucial to successfully achieving the study aims, sequentially going through the phased approach of desk study, historical accounts, maps, soil/geology, trial reconnaissance surveys to quantify optimum search technique(s) and equipment configuration(s) as per best practice suggestions (see Harrison & Donnelly, 2009; Larson *et al.* 2011; Pringle *et al.* 2012a). Importantly combining different geophysical techniques in this case study has also provided extra information on the specific site. For example, the eastern boundary position was identified on ERT 2D profiles, but the GPR 2D profile on the same survey line had much better resolution of the boundary, imaging an interpreted ditch and bank as historical records had indicated. Some near-surface buried items, for example, the WW2 water tanks in the north-west of Charter house square, were successfully identified and

characterised by the three trialled techniques (EM, CST electrical resistivity and GPR); however, possible foundations of a demolished 15<sup>th</sup> century building was only detected by one (EM) technique. it is therefore recommended that multi-technique surveys be undertaken over such sites, in order to maximize the detection rates of buried target(s), such as others have found, e.g. Witten *et al.* (2001) account of locating 1920s riot mass graves in Tulsa, USA.

This study has shown that human remains can be geophysically detected even after 650+ years of burial, however, the success may be attributed to both the local soil type and depositional environments. Note that other sites may not have such optimum ground conditions, as other studies have evidenced the importance of soil type and local depositional environments on target detection (e.g. Brown, 2006; Ruffell *et al.* 2009; Pringle *et al.* 2012c).

GPR analysis could assist any subsequent intrusive investigations by quantifying both burial orientations and burial depths. For example, analysis of the ~200 anomalies in the 2D GPR profile data showed over 80% of burials were located between 1 m and 2 m bgl. However, geophysical investigations could not definitively identify burial styles, this could only be confirmed by archaeological intrusive excavations.

The geophysical and archaeological intrusive investigations have evidenced that contemporary historical accounts (discussed in Sloane, 2009) were inaccurate, i.e. human



remains were not deposited in mass burial pits, but were instead buried in orderly, evenly-spaced, and similarly-orientated individual graves during this time, in contrast to the Black Death commingled victim remains found in French graveyards of similar age (see, for example, Kacki *et al.* 2011).

As shown in Chapter 4, old and young burials (between 1800 A.D. to the present day) were not only detected using non-invasive, near-surface geophysical techniques, which included GPR, ER and MS, but they also were used to establish the optimal geophysical techniques and survey configuration in each of the surveyed sites. However, survey results indicated the importance of the dominate survey soil type for geophysical surveys. Other researchers (for example, Ruffell *et al.*, 2009; Hansen *et al.*, 2014), have found optimal geophysical techniques to be highly dependent on soil type.

In the first case study site with clay-rich soils (Stockton), GPR 900 MHz antenna frequency showed the maximum grave detectability of 43%, followed by 450 MHz antenna frequency of 28% grave detectability and finally 225 MHz antenna frequency had a 9% grave detectability. This may mean that lower frequencies, for example the 225 MHz, with wider EM wavelengths would be more susceptible to the clay-rich soils effects of EM wave attenuation, thereby, causing a significant penetration strength reduction of the radar signal. Because the performance of GPR in soils strongly depends on soil electrical conductivity, soils having high electrical conductivity, such as salts in solution and clay-rich content, rapidly attenuate radar energy, which restricts penetration depths and severely limits the effectiveness of GPR. Magnetic susceptibility showed a higher

detectability than resistivity in this case study. This therefore suggests that in a site dominated by a clay-rich soil, the optimum techniques with potential for maximum detectability may be 900 MHz antenna frequency GPR and magnetic susceptibility.

In the second case study site with sandy clay soil (Keele), 900 MHz GPR antenna frequency was also most effective, given a maximum grave detectability of 47%, whilst 450 MHz and 225 MHz GPR antenna frequency showed 35% and 23% grave detectability respectively. This is similar to the results obtained in Case Study 1. However, electrical resistivity performed better than magnetic susceptibility, with grave detectability of 74 % compared to grave detectability of 63% with magnetic susceptibility.

In the last case study site with coarse pebbly-soils (Endon), 225 MHz GPR antenna was optimal, with grave detectability of 32% compared to 450 MHz with a grave detectability of 22% and finally 900 MHz with a grave detectability of 18%. The absence of clay-rich soil in the Endon graveyard may likely be why 225 MHz frequency antenna had the maximum detectability. However, both resistivity and magnetic susceptibility techniques were optimal in the coarse pebbly-soil of this last case study site.

## 6.2 Geophysical responses against age of burials

*Aim 2: To determine if geophysical responses over modern burial site graves, compared to background values, will decrease as the age of burial increases;*

Other authors (e.g. Nobes, 1999; Hansen *et al.*, 2014) have shown variable success to detect graves in graveyards and cemeteries; however this study is the first to show data from graves of known ages, by geophysically surveying graves with best possible aligned headstones. This has allowed the comparison of geophysical anomalies to be assessed against their respective burial ages.

Some geophysical methods can be easily assessed quantitatively for anomaly responses (e.g. comparison of resistivity values), others (e.g. GPR), have had to be assessed more qualitatively with an *Excellent* to *None* rating (following published methodologies by Schultz *et al.*, 2016). It is highly likely that most geophysical surveys are measuring the 'grave soil' within the grave shaft rather than the grave itself, due to the depths of burials (unlike clandestine graves), but grave soil still seems to be an effective detection target.

From this study, it has been difficult to classify which technique or GPR antenna frequency is the optimal for grave detection in all sites, as each site is unique with burial ages, relative spatial positions and most importantly, dominant soil type. Soil type has

been determined to be the major variable on determining optimum geophysical grave detection technique in this thesis.

For GPR, 900 MHz GPR antenna frequency was optimal in a sand-to clay-rich soil graveyard, whereas 225 MHz GPR antenna frequency was optimal in a coarse pebbly-soil graveyard. Other studies (e.g. Hansen *et al.*, 2014) have found low to medium frequency antennae to be optimal in an organic-rich black earth soil and mid-range frequency antennae to be optimal in glacial-till soils (Ruffell *et al.* 2009).

For electrical resistivity, 0.5m probe spacings on equipment and 0.1 m sample spacings on survey lines were evidenced to be optimal, again, most probably picking up the grave soil rather than the target itself. This agrees with other authors (e.g. Nobes, 1999; Hansen *et al.* 2014). For magnetic susceptibility, 0.1 m sample spacings on survey lines were evidenced to be optimal, and with a stated 6 cm penetration depth, grave soil was again the target with this technique, as others have shown (see, Pringle *et al.*, 2015a). A combination of both electrical resistivity and GPR surveys are advised to locate unmarked graves in burial sites (Hansen *et al.*, 2014).

Based on the data collected from the three graveyards in this study, the relationship between geophysical response and age of burials does not appear to be linear (see Figure 6.1). However, relatively young burials (<30 years old) do show a high geophysical response when compared to background values, whilst relatively older burials do not. It

is observed that geophysical response decreases with increase age of burial in young burials, however, this relationship seems to be reasonably constant as the burial age becomes very old (e.g. above 150 years) as shown in Stockton graveyard survey.

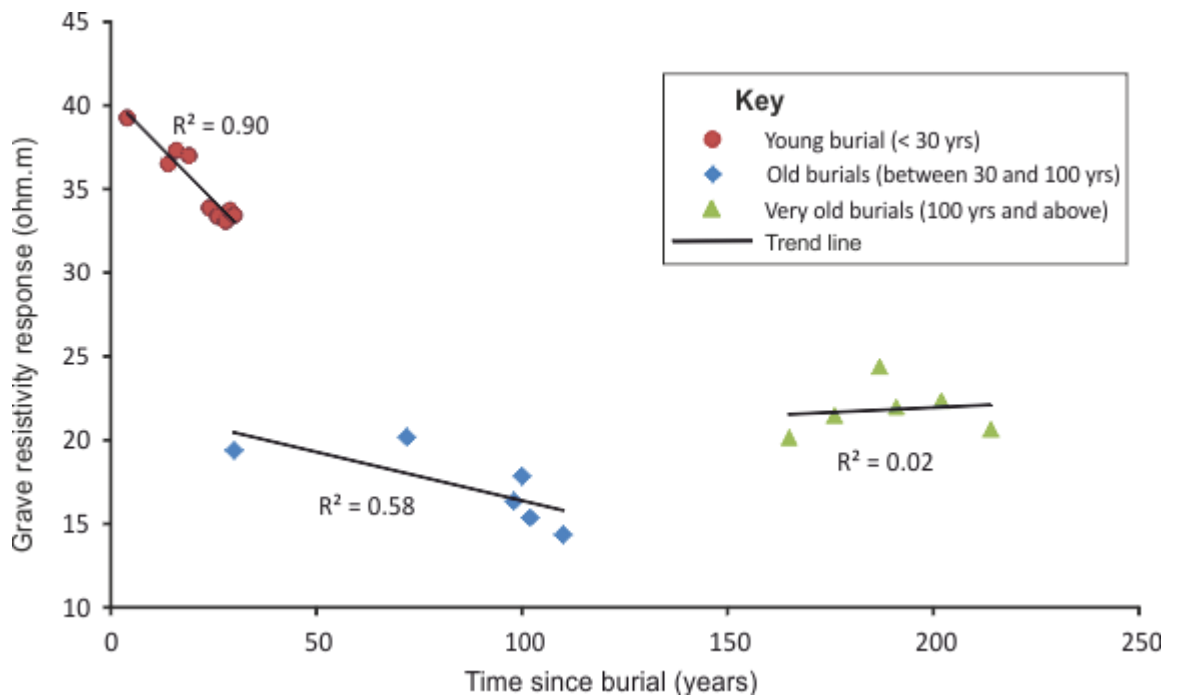


**Figure 6.1:** Combined Stockton graveyard survey line cross-plots showing different linear trends (youngest being statistically significant) for the three burial age divisions.

### 6.3 Grave soil water conductivity dependant

*Aims 3: Perform a systematic statistical analysis of parameters to determine the contributions from individual inorganic ions responsible for the variations in pig cadaver 'soil water' conductivity;*

Whilst background control soil water conductivities were observed to stay relatively constant throughout the 18 months survey period, grave soil water 'leachate' rapidly increased up to 220 PBI before declining, potentially giving a target grave burial detection method as other authors have evidenced (for example, see Pringle *et al.*, 2015b). Whilst grave soil water 'leachate' conductivity has been used to determine the presence of cadaver burial, this study has determined the major inorganic ions that control the variability in conductivity of leachate, here being phosphorus having the strongest influence, followed by potassium, sulphate and sodium. It is also noted that calcium, chlorine and nitrogen have less influence on the conductivity values.

There was also observed to be a statistically significant difference in elemental concentration between grave soil water (leachate) and background soil water, and as such, this could potentially assist with the search of clandestine graves, should a specific programme of targeted soil sampling, centrifuging, water extraction and subsequent analysis be undertaken.

Correlation coefficients (R) for the measured element parameters showed a highly significant positive correlation between EC and  $K^+$ , EC and  $SO_4^{2-}$ , EC and  $Na^+$  and also EC and  $PO_4^{3-}$ . This suggests that EC depends on dissolved salts (Shah *et al.*, 2007) such as NaCl and KCl. No significant correlation exists between EC and  $NO_3^-$ , EC and Cl, and EC and Ca. However, only  $PO_4^{3-}$  and Cl show a positive correlation with EC in background soil water. Regression equations for  $K^+$ ,  $SO_4^{2-}$ ,  $Na^+$  and  $PO_4^{3-}$  in the leachate samples evidenced that electrical conductivity is significant at 1% level of confidence, while the equation for  $NO_3^-$  shows significant at 10% level of confidence (see Table 5.9). However,  $Cl^-$  and  $Ca^{2+}$  showed no significant correlation with EC. Finally, the significance of the relationship was also validated by F test (Table 5.9), which demonstrated that values greater than 17 had high levels of confidence.

## 6.4 Graveyards contamination impact factors

*Aim 4: Determine the elevated metallic elements in long-term burial sites (graveyards) when compared with control values, using contamination impact factors as a potential for detecting clandestine burials.*

Two of the three graveyards studied (Stockton and Keele) had statistically a low degree of selected metal soil contamination. However, the third (Endon) graveyard had a moderately degree of soil contamination. Stockton graveyard soil was classified as moderately contaminated with Ca, Fe, K, Mg and Al. Keele graveyard soil was classified as uncontaminated with K, moderately contaminated with Al, Ca and Fe, and considerably contaminated with Mg. However, it was found that ~41% of the degree of contamination of the graveyard was contributed by Mg, followed by Ca, Al, Fe and K as contributing 19%, 16%, 15% and 9% respectively. This observation was also in agreement with the value obtained by enrichment index; however, geo-accumulation index was not able to reveal this. Endon graveyard soil was classified as moderately contaminated with Al, Fe, K and Mg, considerably contaminated with Ca. Approximately 40% of degree of contamination of the graveyard was contributed only by Ca, followed by 18%, 14%, 14% and 13% for Al, Fe, K and Mg respectively. The enrichment index also showed a correlation with contamination in predicting the degree of contamination in Endon graveyard. In general, the  $C_{deg}$  for the mean metal contents in the three graveyard soils shows that Stockton and Keele graveyards had low metal contaminations of 7.8 and 8.0 respectively, whilst Endon graveyard soil had a moderately degree of contamination of 9.2.































































Statistical and graphical representation of the relationship between the three contamination impact factors, indicated that contamination factor was significantly higher and more robust than the other factors (geo-accumulation index and enrichment index), thus this was used as the basis for the estimation of site contamination, as evidenced by other authors (see for examples, Remy *et al.*, 2003; Likuku *et al.*, 2013; Amuno and Oluwajana, 2014; Sahraoui *et al.*, 2016).

A generalised table has been generated (Table 6.1) to indicate the potential of search technique(s) success for burial targets, assuming optimum equipment configuration(s). Soil type and burial age are, however, important to consider, when searching for burials in forensic searches (as Chapters 3-5 documents). It is generally known that soil types, especially clay-rich soils, result in poor GPR penetration depths (see, for example, Reynolds, 2011). Also the success rate of elemental analysis detection and rates of decomposition, with generation of fluid plumes, are higher in sandy and coarser grain-sized soils compared to clay-rich soils (see Chapter 5). However, this study showed the potential of using high frequency antenna GPR (e.g. 900 MHz frequency) to successfully identify the location of burials in clay-rich soils; however, this is contrary to usual lower frequency antenna used in clay soil for better detection. Table 6.1 also shows the success rate variability in common depositional environments, such as; woodland, rural, urban and coastal environments. Rural depositional environment commonly shows the highest rate of burial detectability, possibly due to less potential difficulties for search teams to use specialist equipment, for example, no metal fencing/objects to hinder the use of

conductivity survey in the site. Similarly, this particular depositional environment has been the most investigated site scenario, or at least the most documented successes.

**Table 6.1.** Generalised table to indicate potential of geophysical techniques and soil sampling analysis success for grave(s) location assuming optimum equipment configurations. Note this table does not differentiate between target size, burial depth/age and other important specific factors (see text). The dominant sand | clay soil end-types are detailed where appropriate for simplicity, therefore not including peat, cobbles etc. types. Modified from Pringle *et al.*, (2012b).

Target(s)  Soil type: sand  clay	Near-Surface Geophysics/ Soil sampling						
	Conductivity	Resistivity	GPR	Magnetics	Metal detector	Magnetic susceptibility	Soil sample analysis
Unmarked grave(s) 0-50 yrs							
Unmarked grave(s) 50-100 yrs							
Unmarked grave(s) 100+ yrs							
Clandestine grave(s)							
<b>Common depositional environment</b>							
Woods							
Rural							
Urban							
Coastal							
Key:  Good;  Medium;  Poor chances of success							

## **6.5 Analysis of graveyard and mass grave leachate plume**

### *6.5.1 Geophysical analysis of graveyard*

Leachate from graveyards or mass burials can potentially accumulate into a plume, and may change the groundwater conductivity of the subsurface (Senos Matias, *et al.*, 2004). Leachate quality is generally saline and as such produces high electrical conductivity or low resistivity due to dissolved ionic elements (Pratt and Fonstad, 2009). To correctly characterise and analyse the extent of leachate, geophysical techniques, such as electrical resistivity, electromagnetic induction and GPR surveys have successfully been employed in such case scenarios, with additional benefit of leaving the integrity of subsurface intact.

This study analysed the applicability of geophysical techniques to detect changes in physical parameters of the subsurface due to the presence of leachate and as such assist to determine the location of buried carcass(es). A bulk ground conductivity meter (Geonics™ EM31D-MkII) was used to carry out graveyard site surveys. It is expected that leachate plume zone would show high conductivity values (as shown by Senos Matias, *et al.*, 2004). Based on the EM results, GPR profiles may also be acquired over the zones of high conductivity to provide a detailed geological structure and locate potential human burial(s) as discrete half hyperbola reflection events. Electrical resistivity techniques are well known to identifying leachate plume in the subsurface (Reynolds, 2011). The underground resistivity depends mainly on soil porosity, water saturation, salinity and clay content (Telford *et al.*, 1990), as the ionic concentration of elements increases due to generated leachate from decomposing carcass(es), there is a corresponding increase in electrical conductivity which reduces the electrical resistivity of subsurface. 2D resistivity

pseudo-sections in Figs 3.14 and 3.15 show a very high conductivity or low resistivity zone near the Medieval mass burial boundary in Charterhouse square Central London.

#### 6.5.2 Geochemical analysis of grave fluid

In graveyards or mass graves, the high organic and inorganic ion loads in leachate originating from decomposition of buried human carcasses may cause sharp changes in the geochemistry of soil and grave fluid (Perrault and Forbes, 2016). And as such, conducting a geochemical analysis of inorganic ion concentration of grave soil or fluid can assist in determining the elevated inorganic ions that could be used as detection markers to potential burial location(s). A successful analysis of both the vertical and horizontal extent of leachate plume concentration has been conducted by monitoring wells around a graveyard (Senos Matias *et al.*, 2004). In this study, the identification and analysis of the effects of elevated elemental composition of graveyard soil water was carried out thus:

- Soil samples collected from fifteen different positions in each graveyard studied (3) at depths between 10-20 cm bgl with a Teflon-coated aluminium hand-shovel;
- Samples digested in concentrated HNO<sub>3</sub> using a programmable microwave and centrifuged after standard laboratory sampling preparation techniques;
- ICP-AES and Dionex instruments used to quantify the concentration of dominant inorganic elements in the samples. The results are shown in Tables 5.14 - 5.15.

## 6.6 Study limitations

Despite following common practice procedures throughout the investigations, there is still need to mention the major limitations in data acquisition and processing in Chapters 3 - 5. This is necessary in order to effectively evaluate and properly relate the relevance of this study to what it was meant to achieve.

For example, in Chapter 3, there was significant survey space restrictions outside the Charter House Square, due to surrounding building structures and other fixed infrastructure, and therefore, the surveys could not acquire more background values or identify the possible north, south and west boundaries of the emergency cemetery. There was also a restriction on collecting soil samples from Charter House Square, which precluded the possible ground-truth information that would have been gathered from soil samples to effectively validate the causative anomalies. Contrary to the archaeological site excavation, which evidenced two different orientations (NE-SW and N-S) for the encountered human skeleton remains, the GPR dataset gathered with 225 MHz frequency antenna could not reveal any further information about the orientation and alignment of the buried anomalies in Charter House Square.

In Chapter 4, due to the specific graveyards surveyed, there were gaps in burial ages in which little or no information was gathered. For example, there was almost no surveyed graves with burial age between 30 years and 50 years before present, or indeed between 120 years and 165 years; however, the major reason for this was because the few graves

within these ranges were covered with above-ground objects such as shown in Figure 4.7, or perhaps have had their headstone removed (unknown burials) leaving no inscription of when the burials were interred, thereby preventing geophysical data collection from them. Another notable limitation encountered in this study is the significant variation in the site background geophysical responses in a given site. This was clearly evident as geophysical responses (e.g. resistivity and magnetic susceptibility) plotted against survey distance (see Figure 4.45). However, grave locations were still clearly distinguished even as the background value varies, for example, see Figure 4.45c. However, this variation may have obscured further information about the cross-plot trend between geophysical response and burial age, thereby resulting to a very poor regression values of 0.11 and 0.01 for magnetic susceptibility and resistivity respectively (see Figure 4.47). This can be further evidenced by observing the difference between grave numbers G24-G26 and G28-G30 in Figure 4.45c.

It was not clear whether some older burials (e.g. older than 200 years) in Stockton graveyard were initially buried elsewhere in the graveyard and the headstones moved to their present location, following anecdotal information obtained from one of the church member present in the site during survey. If this was true, the implication is that the ages of such burials have been compromised and therefore could not be properly matched with the corresponding geophysical responses.

In Chapter 5, only a single simulated clandestine burial of a domestic pig cadaver was used for monitoring and collection of grave soil water fluid in this study. There should be both more replicates and more burial scenarios interred at the same period, possibly, in a contrasting soil types to be able to draw a better conclusion of the results.

Another issue common to GPR investigations is the presence of anomalies or signals related to non-target features. For example, the three graveyards were surrounded with several deciduous trees which made acquisition of data difficult and uneven topography caused by their roots at the ground surface. Tree roots could create false positive GPR anomalies to be recorded that could disguise signals relating to target bodies in the data. Thus, it becomes important to understand target properties and data manipulation during processing to discard these from the identified targets. One of the ways to verify this is to determine what depth is the anomaly, because non-target hyperbolae may not appear at the depth which would be expected for a normal grave (see Figure 3.12).

## **CHAPTER 7    Conclusions**

In this thesis, many geophysical search techniques were considered for locating grave burials, with an additional support approach of soil sampling analysis to provide ground truth information of some burial sites. In line with best practice, the suggested employed phased approach will not only guide search teams in the choice of geophysical techniques and configurations in a variety of forensic and archaeological investigations, but it will also assist in the generation of statistical quantification of detection success rate (detectability) and to predict the possible age of burial through geophysical responses. In this concluding chapter, the main results of the work discussed in this thesis are summarised. Subsequently, some suggestions for future research in the detection of forensic and archaeological burials are provided.

### **7.1    Key Outcomes**

The general contrasting nature of the selected study sites in this research has shown that there is no single geophysical technique for successful detection of burials on every site. Whereas the GPR technique has gained popularity in grave searches, however, the dominant clay-rich nature of UK soils has evidenced that GPR has an intrinsic limitation depending on the local soil environment. In order to provide an efficient and successful detection, there are several considerations to be made in terms of the best technique(s) for search scenarios, equipment configuration(s), optimum profile line distance from



target(s), geophysical responses in variable age of burials and statistical estimation of soil contamination arising from burials.

It is important to know that geophysical techniques hold great potential in locating unmarked graves. Techniques such as GPR, magnetic susceptibility, electrical resistivity and electromagnetic induction have been utilised throughout this study and have demonstrated success at detecting burials. Preliminary results into optimum equipment configurations found that the optimum probe spacing for electrical resistivity survey (fixed off-set) is 0.5 m, as opposed to 0.25 m and 1 m probe spacing. This study also suggested positioning survey profile lines at 1 m away from headstones for adult-sized burials, the reason because this location will usually image the buried cadaver, compared to the other 0.5 m and 1.5 m distance survey lines away from headstones respectively.

Another consideration which should support effective forensic burial detection is the choice of GPR antennae frequency. Despite the fact that GPR generally suffers significant signal attenuation in clay-rich soil and other conductive materials, this study has shown that with higher frequency antenna such as 900 MHz, data results can be mixed, with this frequency being capable of delineating graves in high conductive soils. However, the higher the frequency of antenna, the significant time required to complete the survey and relatively poor penetration depths, and detection of numerous non-target anomalies could become problematic for forensic investigations.

There has been a lack of information on predicting the age of burial using geophysical responses to-date (Hansen *et al.* 2014). In this study, it is observed that geophysical response decreases with increased age of burials; however, geophysical responses gradually become constant as the burial age goes above 150 years. This perhaps provides information on a potentially significant variable which may assist forensic teams in locating the position of potential burials, when the need to exhume and re-interred is called for. This outcome may also assist to identify young burial which may have been interred over same location with known old burial with visible presence of marked headstone (multiple burials), hence produces an unexpectedly high geophysical response. It also demonstrates the benefits of using non-invasive geophysical surveys to other regions and countries where there is a lack of burial space in graveyards and cemeteries. In certain countries, for example, Germany, where burials over 25 years are to be exhumed to give space for new burials, this will also be of much use. Finally, the study also evidenced poor documentation on burial space positions in graveyards that were not captured in the respective church burial register or known to church members.

Aside from GPR, there is no significant difference in response from both electrical resistivity and magnetic susceptibility, in respect to being able to delineate the number of occupants in a single grave. However, with the GPR technique, grave occupancy can be distinguished in some cases, especially where they are either slightly off-set (as evidenced in one grave in Keele graveyard (Figure 3.13.)).

Graveyard burials are expected to cause changes in the local soil composition and the accumulation of certain elements in the soil, due to the number of burials in a restricted space over time. In this study, all the measured elemental values, obtained from soil samples in the three graveyards, were significantly greater than their corresponding control sample values. This study also revealed that a graveyard soil can be considered as contaminated by the influx of these elements from cadaver decomposition, more especially if the cadavers were embalmed or caskets treated with chemicals. The study showed that Endon graveyard had a moderately degree of selected metal contamination, while Stockton and Keele graveyards had low degree of selected metal contamination. It also evidenced that the buried cadavers were not embalmed with substances containing heavy metals such as mercury, lead and arsenic, otherwise such metals would have been detected in the elemental analysis. Therefore, temporal and spatial monitoring of element changes in soils could assist as an indicator to the presence of clandestine burials.

## **7.2 Recommendations for future research**

### **7.2.1 *Clandestine grave monitoring***

It is recommended that more simulated clandestine graves be created at the same time, but with different local soil types and depositional environments. Contemporary grave soil-water should also be extracted from all sites, in order to provide a better understanding of how and what elements are responsible for the grave fluid electrical conductivity changes, and to also determine whether such changes are site specific. The grave soilwater 'leachate' study should be extended over a longer time period, for at least 10 years, in order to determine when the elemental concentrations reduce to background soil-water values (Pringle *et al.*, 2015b). The implication is that from the internment period to when elemental concentration of grave soil-water equilibrates with that of background soil-water, this can be regarded as the cadaver decomposition period. However, in many literatures, the approximate duration for buried cadaver decomposition is still uncertain, as different articles provide different ranges. Similarly, geophysical surveys should also be collected and compared with grave soil-water ionic concentrations over such long time periods to determine whether there is a significant correlation in their changes. Ideally human cadavers should also be used rather than animal cadavers in future control experiments if permitted, as these will be more realistic for clandestine burial research.

### 7.2.2 *Graveyards*

Further studies from other graveyards and cemeteries of different faiths (e.g., Muslims, Jewish, Hindus, etc.), in different local depositional environments and soil types should also be undertaken to also provide additional information on age of burial, burial styles, contents and the subsequent effect it may have on the respective geophysical response recorded from using electrical resistivity (fixed off-set), GPR and magnetic susceptibility geophysical techniques. Importantly, it would also be useful to determine which equipment configurations (e.g., resistivity electrode spacing and GPR antenna frequency) would provide optimal surveys in such scenarios. Such research can contribute to the increasing source of knowledge which informs forensic and archaeological search teams to choose appropriate geophysical tools for particular search scenarios. Soil samples should also be conducted to provide ground truth information whether or not such burial ground(s) are contaminated following the decomposition of buried remains as was carried out in this research.

### 7.2.3 *Soil sampling*

Seasonal and regular soil sample collection and analysis in selected burial grounds should be conducted throughout activity calendar year, in order to determine the most appropriate season for optimal soil sampling and to also inform search investigators on how soil elemental concentration varies both temporally and spatially. The studies should also indicate how factors such as local rainfall, temperature, soil moisture content and

downslope topography can influence the concentration of element, especially mobile elements such as potassium and aluminium.

### **7.3 Concluding remarks**

Integration of multi-geophysical techniques and soil sample analysis has the potential to be a useful approach for the detection of both forensic and archaeological burials. Perhaps among the most important benefits of this research is the possible prediction of time since burial from geophysical responses, which would contribute significantly to forensic and archaeological searches. Understanding the soil types and texture of a survey site is a vital factor for successful detection of graves, even in contrasting depositional soil environments; there is usually a suitable geophysical technique and configuration for optimal detection. This study has attempted to fill this gap in forensic geophysical literature and has highlighted that there is a need for more research into the recorded geophysical response obtained from varying burial ages for other religious denominations and corresponding soil sampling analysis.

## References

- Aitkenhead-Peterson, J. A., Owings, C. S., Alexander, M. B., Larison, N. and Bytheway, J. A. (2012). Mapping the lateral extent of human cadaver decomposition with soil chemistry. *Forensic Science International*, 216(1-3):127-134
- Al Sabahi, E., Rahim, S. A., Zuhairi, W. Y., Al Nozaily, F. and Alshaebe, F. (2009). The characteristics of leachate and groundwater pollution at municipal solid waste landfill of Ibb City, Yemen. *American Journal of Environmental Sciences*, 5(3):256-266.
- Al Yaqout, A. F. (2003). Assessment and analysis of industrial liquid waste and sludge disposal at unlined landfill sites in arid climate. *Waste Management*, 23:817-824.
- Al Yaqout, A. F. and Hamoda, M. F. (2007). Movement of unlined landfill under preloading surcharge. *Waste Management*, 27:448-458.
- Amendt, J., Campobasso, C.P., Gaudry, E., Reiter, C., LeBlanc, H.N. and Hall, M.J.R. (2007). Best practice in forensic entomology: standards and guidelines. *International Journal of Legal Medicine*, 121:90-104.
- Amuno, S. A. (2013). Environmental Legacy of the Genocide: An Exploration into the contamination potential of mass grave soils in Post- Genocide Rwanda. Unpublished PhD thesis submitted in Global Studies, Academic Faculty, university of Saint Joseph, Macau, China. 240 pages.



- Amuno, S. A. and Oluwajana, A. (2014). Comparative assessment of trace metals in soils associated with casket burials: Towards implementing green burials. *Eurasian Journal of Soil Science*, 3:65-76.
- Andraski, B. J. (1997). Soil-water movement under natural-site conditions: A multiple-year field study in the Mojave Desert, Nevada. *Water Resources Resources*, 33(8):1901-1916.
- Annan, A. P. (2003). Ground penetrating radar: Principles, procedures and applications. Sensor & Software Inc. Mississauga, Canada.
- Aquila, I., Ausania, F., Di Nunzio, C., Serra, A., Boca, S. and Capelli, A. (2014). The role of forensic botany in crime scene investigation: case report and review of literature. *Journal of Forensic Sciences*, 1111:1556-4029.
- Archie, G. E. (1942). The electrical resistivity log as an aid in determining some reservoir characteristics. *Transactions of the American Institute of Mining, Metallurgical and Petroleum engineers*, 146:54–62.
- Aries, P. (1982). The hour of our death. New York, *Vintage Books*, page 54.
- Asadi, A., Shariatmadari, N., Moayedi, H. and Huat, B. K. (2011). Effect of MSW leachate on soil consistency under influence of electrochemical forces induced by soil particles. *International Journal of Electrochemical Science*, 6:2344-2351.
- Baderna, D., Maggioni, S., Boriani, E., Gemma, S., Molteni, M., Lombardo, A., Colombo, A., Bordonali, S., Rotella, G., Lodi, M. and Benfenati, E. (2011). A combined approach to

investigate the toxicity of an industrial landfill's leachate: Chemical analyses, risk assessment and *in vitro* assays. *Environmental Research*, 111:603-613.

Banham, S. G. and Pringle, J. K. (2011). Geophysical and intrusive site investigations to detect an abandoned coal-mine access shaft, Apedale, Staffordshire, UK. *Near Surface Geophysics*, 9: 483-496.

Barber, B. and Thomas, C. (2002). The London Charterhouse. *Museum of London Archaeology Service*, 10:73-74.

Bardgett, R. D. (2005). The biology of soil: a community and ecosystem approach. Oxford University Press, pp. 4

Barker, R. D. (1979). Signal contribution sections and their use in resistivity studies. *Geophysical Journal of the Royal Astronomical Society*, 59:123–129.

Barlaz, M. A., Schaefer, D. M. and Ham, R. K. (1989). Bacterial population development and chemical characteristics of refuse decomposition in a simulated sanitary landfill. *Applied Environmental Microbiology*, 55: 55-65.

Bass, W. M. (1963). The use of heavy power equipment in the excavation of human skeleton material. *Plains Anthropologist*, 8(20):122-123.

Batayneh, A. T., Abueladas, A. A. and Moumani, K. A. (2002). Use of Ground Penetrating radar for assessment of potential sinkhole conditions: An example from Ghor al Haditha area, Jordan. *Environmental Geology*, 41(8):977-983.

- Baun, D. L. and Christensen, T. H. (2004). Speciation of heavy metals in landfill leachate: a review. *Waste Management Resources*, 22:3-23.
- Benninger, L. A., Carter, D. O. and Forbes, S. L. (2008). The biochemical alteration of soil beneath a decomposing carcass, *Forensic Science International*, 180:70-75.
- Bergslien, E. (2012). An introduction to forensic geoscience. Wiley-Blackwell Publications. United Kingdom.
- Bevan, B. W. (1991). The search for graves. *Geophysics*, 56:1310–1319.
- Bigman, D.P. (2012). The use of electromagnetic induction in locating graves and mapping cemeteries: an example from Native North America. *Archaeological Prospecting*, 19:31-39.
- Bloemenkamp, R. and Slob, E. (2003). The effect of the elevation of GPR antennas on data quality. Proceedings of the Second International Workshop on Advanced GPR, Delft, Netherlands, pp. 201-206.
- Bonhotal, J. and Schwarz, M. (2009). Environmental effects of mortality disposal. 3rd international symposium: Management of animal carcasses, tissue and related by-products, University of California, 10 pages.
- Boss, C. B. and Fredeen, K. J. (1997). Concepts, instrumentation and techniques in inductively coupled plasma optical emission spectrometry. The Perkin-Elmer Corporation, USA, 125 pages.

- Brilis G.M., Gerlach C.L. and van Waasbergen R.J. (2000a). Remote sensing tools assist in environmental forensics. Part I. Digital tools-traditional methods. *Environmental Forensics*, 1:63–67.
- Brilis G.M., van Waasbergen R.J., Stokely P.M. and Gerlach C.L. (2000b). Remote sensing tools assist in environmental forensics. Part II. Digital tools. *Environmental Forensics*, 1:1–7.
- Brown, A.G. (2006). The use of forensic botany and geology in war crimes investigations in N-E Bosnia. *Forensic Science International*, 163:204-210.
- Buck, S. C. (2003). Searching for graves using geophysical technology: Field tests with ground penetrating radar, magnetometry, and electrical resistivity. *Journal of Forensic Sciences*, 48(1):5–11.
- Calkin, S. F., Allen, R. P., and Harriman, M. P. (1995). Buried in the basement – geophysics role in a forensic investigation. In *Proceedings of the Symposium on the Application of Geophysics to Engineering and Environmental Problems (SAGEEP)*, pages 397–403.
- Calkosinski, I., Ploneczka-Janeczko, K., Ostapska, M., Dudek, K., Gamian, A. and Rypula, M. (2015). Microbiological analysis of necrosols collected from urban cemeteries in Poland. *BioMed Research International*, Article ID 169573, pp. 1-7.  
<http://dx.doi.org/10.1155/2015/169573>

- Canadian Food Inspection Agency (CFIA). (2006). Burial procedural plan draft 1: Disease Control Programs Branch, Animal Production and Health Division.
- Carcione, J. M. (1998). Radiation patterns for 2-D GPR forward modelling. *Geophysics*, 63(2):424-430.
- Carpenter, P. J., Ding, A. and Cheng, L. (2012). Identifying groundwater contamination using resistivity surveys at a landfill near Maoming, China, *Nature Education Knowledge*, 39(7):20-26.
- Carter, D. O. and Tibbett, M. (2006). Microbial decomposition of skeletal muscle tissue (*Ovis aries*) in a sandy loam soil at different temperatures. *Soil Biology and Biochemistry*, 38(5):1139-1145.
- Carter, D. O. and Tibbett, M. (2009). Cadaver decomposition and soil: processes. In Tibbett, M. and Carter, D. O., editors, *Soil Analysis in Forensic Taphonomy: Chemical and Biological Effects of Burial Human Remains*. Boca Raton: CRC Press, pages 29-52.
- Carter, D. O., Yellowlees, D. and Tibbett, M. (2007). Cadaver decomposition in terrestrial ecosystems. *Naturwissenschaften*, 94:12-24.
- Carter, D.O., Yellowlees, D. and Tibbett, M. (2008a). Using ninhydrin to detect gravesoil. *Journal of Forensic Sciences*, 53:397–400.

- Carter, O. D., Yellowlees, D. and Tibbett, M. (2008b). Temperature affects microbial decomposition of cadavers (*Rattus rattus*) in contrasting soil. *Applied Soil Ecology*. 40(1):129-137.
- Cassidy, N. J. (2009). Ground Penetrating Radar data processing, modelling and analysis. In Jol, H. M., editor, *Ground Penetrating Radar: theory and applications*, pages 141-176. Elsevier Press.
- Cassidy, N. J., Eddies, R. and Dods, S. (2011). Void detection beneath reinforced concrete sections: the practical application of ground-penetrating radar and ultrasonic techniques. *Journal of Applied Geophysics*, 74:263-276.
- Castex, D., Reveillas, H. (2007). Investigation sur une crise de mortalité à Boulogne-sur-Mer (Pas-de-Calais, XVIIIe s.). Hypothèses d'interprétation. *Bulletins et Mémoires de la Société d'Anthropologie de Paris*, 19(1-2):21-37.
- Chambers, J. E., Kuras, O., Meldrum, P. I., Ogilvy, R. D., and Hollands, J. (2006). Electrical resistivity tomography applied to geologic, hydrogeologic, and engineering investigations at a former waste-disposal site. *Geophysics*, 71:B231–B239.
- Chanteau, S., Rahalison, L., Ralafiarisoa, L., Foulon, J., Ratsitorahina, M., Ratsifasomanana, L., Carniel, E., Nato, F., (2003). Development and testing of a rapid diagnostic test for bubonic and pneumonic plague. *The Lancet*, 361:211–216.
- Chapman, P.J. (2005). Soil and the Environment. In: Holden, J. (Ed.), *An Introduction to Physical Geography and the Environment*. Pearson.

- Cheetham, P. (2005). Forensic Geophysical Survey. In Hunter, J. and Cox, M. (eds.), *Forensic Archaeology: Advances in theory and practice*, Routledge, London, pp. 62-95.
- Chisum, W., Turvey, B., 2000. Evidence dynamics: Locard's exchange principle and crime reconstruction. *Journal of Behavioral Profiling*, 1:1-15.
- Christensen, A. M., Lowe, W. M. and Reinecke, G. W. (2009). The forensic bulldozer as a clandestine grave search tool. In: *Forensic Science Communications, Back Issues*, Technical note, vol. 11, number 4.
- Christensen, T. H., Kjeldsen, P., Bjerg, P. L., Christensen, J. B., Baun, A., Albrechtsen, H. J. and Heron, G. (2001). Biogeochemistry of landfill leachate plumes. *Applied Geochemistry*, 16:659-718.
- Conyers, L. B. (2004a). *Ground-Penetrating Radar for Archaeology*. AltaMira, Press, Walnut Creek, CA.
- Conyers, L. B. (2004b). Moisture and soil differences as related to the spatial accuracy of amplitude maps at two archaeological tests sites. *Proceedings of the Tenth International Conference on Ground-penetrating Radar, Delft, The Netherlands*; 435–438.
- Conyers, L. B. (2006a). Ground penetrating radar. In *Remote sensing in archaeology: An explicitly North American perspective*. Edited by Jay K. J., The University of Alabama Press, Tuscaloosa, Alabama, USA.

- Conyers, L. B. (2006b). Ground penetrating radar techniques to discover and map historic graves. *Historical Archaeology*, 40(3):64-73.
- Conyers, L. B., & Goodman, D. (1997). Ground-penetrating radar: An Introduction for Archaeologists. Walnut Creek, CA: AltaMira Press. Pg. 149-194
- Conyers, L. B., Ernewein, E. G., Grealy, M. and Lowe, K. M. (2008). Electromagnetic conductivity mapping for site prediction in meandering river floodplains. *Archaeological Prospection*, 15:81–91.
- Coyle, H. M. (2005). Forensic botany: principles and applications to criminal casework. Boca Raton, FL: CRC Press.
- Crossrail Project Report (2013). Archaeological targeted watching brief: Charterhouse Square Grout Shaft (XTE12) Interim Statement. *Crossrail Central Section Project*, Doc. No. C257-MLA-X-RGN-M123-50003.
- Crowther, J, and Barker, P., 1995. Magnetic susceptibility: distinguishing anthropogenic effects from the natural. *Archaeological Prospection*, 2:207-216.
- Crowther, J. (2003). Potential magnetic susceptibility and fractional conversion studies of archaeological soils and sediments, *Archaeometry*, 45:685–701.
- Daartinen, T., Sormunen, K. and Rintala, J. (2013). Case study on sampling, processing and characterization of landfilled municipal solid waste in the view of landfill mining. *Journal of Cleaner Production*, 55:56-66.



- Dalan, R. A. (2006). A geophysical approach to buried site detection using down-hole susceptibility and soil magnetic techniques. *Archaeological Prospection*, 13(3):182–206.
- Dalan, R. A. and Goodman, D. (2007). Imaging buried landforms using down-hole susceptibility data and three-dimensional GPR visualization software. *Archaeological Prospection*, 14(4):273–280.
- Dalan, R. A., De Vore, S. L. and Clay, R. B. (2010). Geophysical identification of unmarked historic graves. *Geoarchaeology*, 25(5):572-601.
- Damann, F. E., Tanittaisong, A. and Carter, D. O. (2012). Potential carcass enrichment of the University of Tennessee Anthropology Research Facility: a baseline survey of edaphic features. *Forensic Science International*, 222:4-10.
- Damiata, B. N., Steinberg, J. M., Bolender, D. J. and Zoëga, G. (2013). Imaging skeletal remains with ground-penetrating radar: comparative results over two graves from Viking Age and Medieval churchyards on the Stóra-Seyla farm, northern Iceland. *Journal of Archaeological Science*, 40:268-278.
- Daniels, D. J. (2004). Ground penetrating radar. IEEE Radar, Sonar, Navigation and Avionics Series 15, 2nd edition, 723pp.
- Davenport, G. C. (2001). Remote sensing applications in forensic investigation. *Historical Archaeology*, 35:87–100.

- Davis, J. L., Heginbottom, J. A., Annan, A. P., Daniels, R. S., Berdal, B. P., Bergan, T., Duncan, K. E., Lewin, P. K., Oxford, J. S., Roberts, N., Skehel, J. J., and Smith, C. R. (2000). Ground penetrating radar surveys to locate 1918 Spanish flu victims in permafrost. *Journal of Forensic Sciences*, 45:68–76.
- Dearing, J. A., Hay, K. L., Baban, S. M. J., Huddleston, A. S., Wellington, E. M. H. and Loveland, P. J. (1996). Magnetic susceptibility of soil: an evaluation of conflicting theories using a national dataset. *Geophysics Journal International*, 127:729-734.
- DEFRA (2001). Comparison with the 1967 Foot and Mouth Disease outbreak. Accessible online at: <http://archive.defra.gov.uk/foodfarm/farmanimal/diseases/atoz/fmd/documents/fmd-comparisons-1967.pdf> Accessed on 20th August, 2014
- Dekeirsschieter, J., Verheggen, F.J., Gohy, M. Hubrecht, F., Bourguignon, L., and Lognay, G. (2009). Cadaveric volatile organic compounds released by decaying pig carcasses (*Sus domesticus*) in different biotopes. *Forensic Science International*, 189:46–53.
- Dent, B. B., Forbes, S. L. and Stuart, B. H. (2004). Review of human decomposition processes in soil. *Environmental Geology*, 45:576-585.
- DeWitte, S. N. (2010). Age patterns of mortality during the Black Death in London, A.D. 1349-1350. *Journal of Archaeological Sciences*, 37:3394-3400.
- DeWitte, S.N. (2014). Mortality risk and survival in the aftermath of the Medieval Black Death. *PLOS ONE*, 9(5):e96513. DOI:10.1371/journal.pone.0096513

- DeWitte, S. N. and Hughes-Morey, G. (2012). Stature and frailty during the Black Death: the effect of stature on risks of epidemic mortality in London, A.D.1348-1350 *Journal of Archaeological Sciences*, 39:1412-1419.
- Dick, H. C., Pringle, J. K., Sloane, B., Carver, J., Wisniewski, K. D., Haffenden, A., Porter, S., Roberts, D. and Cassidy, N. J. (2015). Detecting and characterising of Black Death burials by multi-proxy geophysical methods. *Journal of Archaeological Science*, 59:132-141.
- Djuric, M., Dunjic, D., Djonic, D. and Skinner, M. (2007). Identification of victims from two mass-graves in Serbia: a critical evaluation of classical markers of identity. *Forensic Science International*, 172:125-129.
- Donaldson, B. M., Smith, G. P., Kweon, Y. and Sriranganathan, N. (2013). An analysis of leachate constituents and pathogen destruction in deer mortality static windrow composting. *Water Air Soil Pollution*, 224:1431.
- Donnelly, L. (2009). The Investigator: Essential reading for today's investigators. Published July/August 2009, pg. 41-49.
- Donnelly, L. (2011). The renaissance in forensic geology. *Teaching Earth Sciences*, 36(1): 46-52.
- Donnelly, L. (2013). The design and implementation of a high-assurance forensic geology and police search following the discovery of the Staffordshire (Anglo Saxon) Gold

Hoard: In Pirrie, D, Ruffell, A. and Dawson, L. A. edition, Geological Society, London, *Special Publications*, 384(1): 195-208.

Donnelly, L. J. (2009). The geological search for a homicide grave. *The investigator*, July/August, pp. 42-29.

Doolittle, J.A. and Bellantoni, N.F. (2010). The search for graves with ground-penetrating radar in Connecticut, *Journal of Archaeological Sciences*, 37:941–949.

DRD (2014). European and national drinking water quality standards. Accessible online at: <http://www.doeni.gov.uk/niea> Accessed on 13th March, 2015

Duday, H. (2007). Archaeological proof of an abrupt mortality crisis: simultaneous deposit of cadavers, simultaneous deaths? In: Raoult, D. and Drancourt, M. (Eds.), *Paleomicrobiology: Past Human Infections*. Springer-Verlag, Berlin, Heidelberg, pp. 49-54.

Dupras, T., Schultz, J. J., Wheeler, S. M. and Williams, L. J. (2006). Forensic recovery of human remains: archaeological approaches. Taylor and Francis Publications, London.

Ebdon, L., Evans, E. H., Fisher, A. and Hill, S. J. (1998). An introduction to analytical atomic spectrometry. In Evans, E. H., editor, pages 73-136, John Wiley & Sons Press.

Ehirim, C. N., Ebeniro, J. O. and Olanegan, O. P. (2009). A geophysical investigation of solid waste landfill using 2-D resistivity imaging and vertical electrical sounding methods

in Port Harcourt municipality, Rivers, Nigeria. *The journal of Science and Technology*, 10(2):604-613.

El-Fadel, M., Bou-Zeid, E. and Chahine, W. (2002). Long-term simulations of leachate generation and transport from solid waste disposal at a former quarry site. *Journal of solid waste technology and management*, 28(2):60-70.

Ellwood, B.B., Owsley, D.W., Ellwood, S.H., Mercado-Allinger, P.A. (1994). Search for the grave of the hanged Texas gunfighter, William Preston Longley. *Historical Archaeology*, 28:94–112.

Environment Agency (2004). Science project: potential groundwater pollutants from cemeteries. Available online: <http://publications.environmentagency.gov.uk/pdf/SCHO1204BIKS-e-e.pdf>. Last accessed 07th August 2014.

Environmental Agency (2006). The determination of metals in solid environmental samples: methods for examination of waters and associated materials. [https://www.gov.uk/government/uploads/system/uploads/attachment\\_data/file/316812/Book\\_204.pdf](https://www.gov.uk/government/uploads/system/uploads/attachment_data/file/316812/Book_204.pdf). (Accessed on April 20th, 2016)

Esmail, A. S., Abdul Rahim, S. Wan Zuhairi, W. Y., Fadhl, A. N. and Fares, A. (2009). The characteristics of leachate and groundwater pollution at municipal solid waste landfill of Ibb city, Yemen. *American Journal of Environmental Sciences*, 5(3):256-266.

- Ettler, V., Mihaljevic, M., Matura, M., Skalova, M. and Sebek, O. (2008). Temporal variation of trace elements in waters polluted by municipal solid waste landfill leachate. *Bulletin of Environmental Contamination and Toxicology*, 80(30):274-279.
- Fenning, P. J. and Donnelly, L. J. (2004). Geophysical techniques for forensic investigations. In: Pye, K., Croft, D. J. (eds), *Forensic Geoscience: Principles, Techniques and Applications*. Geological Society, London, Special Publications, 232, 11-20.
- Fetter, C. W. (1999). *Contaminant Hydrogeology*. Upper Saddle River, NJ, Prentice-Hall.
- Fiedler, S., Berger, J., Stahr, K. and Graw, M. (2009b). Localisation of a mass grave from the Nazi era—a case study. in Ritz, K., Dawson, and L., Miller, D., editors, pages 303–314. Springer Publication.
- Fiedler, S., Breuer, J., Pusch, C. M., Holley, S., Wahl, J., Ingwersen, J. and Graw, M. (2012). Graveyards – Special landfills. *Science of the Total Environment*, 419:90-97.
- Fiedler, S., Illich, B., Berger, J. and Graw, M. (2009a). The effectiveness of ground-penetrating radar surveys in the location of unmarked burial sites in modern cemeteries. *Journal of Applied Geophysics*, 68:380–385.
- Fitzpatrick, R. W. (2008). Nature, distribution, and origin of soil materials in the forensic comparison of soils. In: Tibbett, M. and Carter, D. O., editors, *Soil analysis in forensic taphonomy: chemical and biological effects of buried human remains*, pages 1-28. CRC Press.

- Fonstad, T. A. (2004). Transport and Fate of Nitrogen from Earthen Manure Storage Effluent Seepage. Unpublished PhD Thesis, University of Saskatchewan, Saskatoon, SK.
- Fontoura, J. M., Moura, M. R. and Dias, G. A. (2011). Combining geophysical, geochemical and geostatistical methods to detect contamination anomalies in a controlled Dump in Oporto, North Portugal. *12<sup>th</sup> International Congress of the Brazilian Geophysical Society*, pages 1-4.
- Forbes, L. S. (2008). Potential determinants of post-mortem and post-burial interval of burial remains. In: Tibbett, M. and Carter, D. O., editors, *Soil analysis in forensic taphonomy: chemical and biological effects of buried human remains*, pages 225-246. CRC Press.
- Forbes, S. L., Keegan, J., Stuart, B. H. and Dent, B. B. (2003). A gas chromatography-mass spectrometry method for the detection of adipocere in grave soils. *European Journal of Lipid Science and Technology*, 105(12):761-768.
- Forbes, S. L., Stuart, B. H. and Dent, B. B. (2002). The identification of adipocere in grave soils. *Forensic Science International*, 127:225-230.
- Forbes, S. L., Stuart, B. H. and Dent, B. B. (2005). The effect of the burial environment on adipocere formation. *Forensic Science International*, 154:24-34.
- Förstner, U., Ahlf, W. and Calmano, W. (1993). Sediment quality objectives and criteria development in Germany. *Water Science and Technology*, 28(8-9): 307-316.

- France, D. L., Griffin, T. J., Swanburg, J. G., Lindemann, J. W., Davenport, G. C., Trammell, V., Armbrust, C. T., Kondratieff, B., Nelson, A., Castellano, K. and Hopkins, D. (1992). A multi-disciplinary approach to the detection of clandestine graves. *Journal of Forensic Sciences*, 37:1445–1458.
- France, D. L., Griffin, T. J., Swanburg, J. G., Lindemann, J.W., Davenport, G. C., Trammell, V., Travis, C. T., Kondratieff, B., Nelson, A., Castellano, K., Hopkins, D., and Adair, T. (1997). Necrosearch revisited: further multidisciplinary approaches to the detection of clandestine graves. In Haglund, W. D. and Sorg, M. H., editors, *Forensic taphonomy: the postmortem fate of human remains*, pages 497–509. CRC Press.
- Fredenslund, A. M., Scheutz, C. and Kjeldsen, P. (2010). Tracer method to measure landfill gas emissions from leachate collection systems. *Waste Management*, 30:2146-2152.
- Freedman, R. and Fleming, R. (2003). Water Quality Impacts of Burying Livestock Mortalities. *Ridgetown College Publication*.
- Friedman, S. P. (2005). Soil properties influencing apparent electrical conductivity: a review. *Computers and Electronics in Agriculture*, 46:45–70.
- Frohlich, B. and Lancaster, W.J. (1986). Electromagnetic surveying in current Middle Eastern archaeology – application and evaluation. *Geophysics*, 51:1414-1425.



- Gaffney, C., Harris, C., Pope-Carter, F., Bonsall, B. Fry R. and Parkyn, A. (2015). Still searching for graves: an analytical strategy for interpreting geophysical data used in the search for “unmarked” graves. *Near Surface Geophysics*, 13:557-569.
- Gelonch-Sole, J. (2013). Mass graves from the Civil War and the Franco Era in Spain: once forgotten, now at the heart of the public debate. *European Review*, 21(4):507-522.
- Gennard, D. (2012). Forensic entomology: an introduction. 2nd edition, *Wiley-Blackwell*.
- Gibbons, R. D., Morris, J. W., Prucha, C. P., Caldwell, M. D. and Staley, B. F. (2014). Longitudinal data analysis in support of functional stability concepts for leachate management at closed municipal landfills. *Waste Management*, 34:1674-1682.
- Glanville, T. (2000). Impact of Livestock Burial on Shallow Groundwater Quality. *American Society of Agricultural Engineers*, Mid Central Meeting, April 28-29.
- Glanville, T. D., Ahn, H. K., Richard, T. L., Shiers, L. E. and harmon, J. D. (2009). Soil contamination caused by emergency bio-reduction of catastrophic livestock mortalities. *Water Air Soil Pollution*, 198:285-295.
- Grant, I. S. and Phillips, W. R. (1990). Electromagnetism. John Wiley and Sons, second edition.
- Grant, F. S. and West, G. F. (1965). Interpretation theory in applied geophysics. New York, McGraw-Hill.

- Grossmann, J. and Udluft, P. (1991). The extraction of soil water by the suction-cup method: a review. *Journal of Soil Science*, 42:83-93.
- Haddad, P. R., Nesterenko, P. N. and Buchberger, W. (2008). Recent developments and emerging directions in ion chromatography. *Journal of Chromatography A*, 1184:456-473.
- Haensch, S., Bianucci, R., Sgnoli, M., Rajerison, M., Schultz, M., Kacki, S., Vermunt, M., Weston, D. A., Hurst, D., Achtman, M., Carniel, E. and Bramanti, B. (2010). Distinct clones of *Yersinia pestis* caused the Black Death. *PLoS Pathogens*, 6(10):e1001134. Doi:10.1371/journal.ppat.1001134.
- Hakanson, L. (1980). An ecological risk index for aquatic pollution control. A sedimentological approach, *Water Research*, 14: 975-1001.
- Hammon, W.S. III, McMechan, G.A. and Zeng, X., (2000). Forensic GPR: finite-difference simulations of responses from buried human remains. *Journal of Applied Geophysics*, 115:191-204.
- Hansen, J. D. and Pringle, J. K. (2011). Geophysical investigations in UK graveyards: re-use of existing burial grounds. *Extended abstract for a presentation at the 16th European Meeting of Environmental and Engineering Geophysics of the Near Surface Geoscience Division of the EAGE, Leicester, 12th-14th September*.
- Hansen, J.D. and Pringle, J.K. (2013). Comparison of magnetic, electrical and GPR surveys to detect buried forensic objects in semi-urban and domestic patio environments,

in: Pirrie, D., Ruffell, A. and Dawson, L.A. (eds.), *Environmental and Criminal Geoforensics*, Geological Society of London Special Publication, 384:229-251.

Hansen, J.D., Pringle, J.K. and Goodwin, J., (2014). GPR and bulk ground resistivity surveys in graveyards: locating unmarked burials in contrasting soil types. *Forensic Science International*, 237:e14-e29.

Harrison, M. and Donnelly, L.J. (2009). Locating concealed homicide victims: developing the role of geoforensics. in Ritz, K., Dawson, L., Miller, D., editors, *Criminal and Environmental soil forensics*, pages 197–219. Springer.

Hart, A. (2005). Ammonia shadow of my former self: a review of potential groundwater chemical pollution from cemeteries. *Land Contamination Reclamation*, 13(3):239-245.

Hautot, S., Tarits, P., Perrier, F., Tarits, C. and Trique, M. (2002). Groundwater electromagnetic imaging in complex geological and topographical regions: A case study of a tectonic boundary in the French Alps. *Geophysics*, 67(4):1048–1060.

Hawley, D. A., Harruff, R. C., Pless, J. E., and Clark, M. A. (1994). Disinterment from paving materials: Use of heavy equipment for exhumation and examination of bodies. *Journal of Forensic Sciences*, 39:100–106.

Hickman, G. and Hughes, N. (2002). Carcass disposal: a major problem of the 2001 FMD outbreak. *State Veterinary Journal*, 12:27-32.

- Hildebrand, J. A., Wiggins, S. M., Driver, J. L. and Waters, M. R. (2007). Rapid seismic reflection imaging at the Clovis Period Gault Site in Central Texas. *Archaeological Prospection*, 14:245–260.
- Hildebrand, J. A., Wiggins, S. M., Henkart, P. C., and Conyers, L. B. (2002). Comparison of seismic reflection and ground-penetrating radar imaging at the controlled archaeological test site, Champaign, Illinois. *Archaeological Prospection*, 9:9–21.
- Hillel, D. (2004). Introduction to environmental soil physics. Elsevier Academic Press, USA.
- Hirschfield, A., Bowers, K. (2001). Mapping and Analysing Crime Data: Lessons from Research and Practice. Taylor and Francis, London. 312 pp.
- Home Office (2004). Burial law and policy in the 21<sup>st</sup> century: the need for a sensitive and sustainable approach.  
[http://webarchive.nationalarchives.gov.uk/+/http://www.dca.gov.uk/consult/buriallaw/buriallaw\\_cp.pdf](http://webarchive.nationalarchives.gov.uk/+/http://www.dca.gov.uk/consult/buriallaw/buriallaw_cp.pdf) (Accessed on April 29th, 2016)
- Home Office (2007). Planning for a possible Influenza Pandemic: A Framework for Planners Preparing to Manage Deaths. *Crime Reduction and Community Safety Group*, London, UK.
- Hope, W. J (1925). The History of the London Charterhouse. *Society of Promoting Christian Knowledge Publication*, pages 7-8.

- Hopkins, D. W. (2009). The role of soil organisms in terrestrial decomposition. In Tibbett, M. and Carter, D. O., editors, *Soil Analysis in Forensic Taphonomy: Chemical and Biological Effects of Burial Human Remains*. Boca Raton: CRC Press, pages 53-66.
- Hopkins, D. W., Wiltshire, P. E. J. and Turner, B. D. (2000). Microbial characteristics of soils from graves: an investigation at the interface of soil microbiology and forensic science. *Applied Soil Ecology*, 14(3):283-288.
- Hou, X. and Jones, B. T. (2000). Inductively couple plasma/optical emission spectrometry: In Meyers, R. A. editor, *Encyclopedia of Analytical Chemistry*, John Wiley & Sons Ltd, Chichester, pages 9468-9485.
- Hu, Y., Liu, X., Bai, J. Shih, K., Zeng, E. Y. and Cheng, H. (2013). Assessing heavy metal pollution in the surfave soils of a region that had undergone three decades in intense industrializa and urbanization. *Environmental Science and Pollution Research International*, 20(9):6150-6159.
- Hunter, J. and Cox, M. (2005). *Forensic archaeology: advances in theory and practice*. Routledge.
- Independent Commission for the Location of Victims Remains. Accessible online at: <http://www.iclvr.ie/> Last Accessed: 26th April 2014.
- Instanes, A., Lønne, I., and Sandaker, K. (2004). Location of avalanche victims with ground penetrating radar. *Cold regions science and technology*, 38:55–61.

- Ivashov, S. I., Sablin, V. N., Sheyko, A. P., Vasiliev, I. A., Isaenko, V. N., Konstantinov, V. F. (1998). GPR for detection and measurement of filled up excavations for forensic applications. Proceedings, 7th International Conference on Ground Penetrating Radar, University of Kansas. pp. 87–89.
- Jackson, P. E. (2000). Ion chromatography in environmental analysis: In Meyers, R. A. editor, *Encyclopedia of Analytical Chemistry*, John Wiley & Sons Ltd, Chichester, pages 2779-2801.
- Jackson, P.E. (2001). Determination of inorganic ions in drinking water by ion chromatography. *Trends in Analytical Chemistry*, 20(6+7):320-329.
- Jervis, J. (2010). The detection of clandestine graves using electrical resistivity surveys: results from controlled experiments and a case study. Unpublished PhD Thesis, Keele University, Staffordshire, UK. 346 pages.
- Jervis, J. R., Pringle, J. K., Cassella, J.P. and Tuckwell, G.T. (2009a). Using soil and groundwater to understand resistivity surveys over a simulated clandestine grave. In: Ritz, K., Dawson, L. and Miller, D. (Eds.), *Criminal and Environmental Soil Forensics*, Dordrecht: Springer Press, 271-284.
- Jervis, J. R., Pringle, J. K., and Tuckwell, G. (2009b). Time-lapse resistivity surveys over simulated clandestine graves. *Forensic Science International*, 192:7–13.

- Jervis, J. R. and Pringle J. K. (2014). A study of the effect of seasonal climatic factors on the electrical resistivity response of three experimental graves, *Journal of Applied Geophysics*, 108:53-60.
- Jones, G. (2008). Geophysical mapping of historical cemeteries. *Technical Briefs in Historical Archaeology*, 3:25-38.
- Jones, G.M., Cassidy, N.J., Thomas, P.A., Plante, S. and Pringle, J.K. (2009). Imaging and monitoring tree-induced subsidence using electrical resistivity tomography, *Near Surface Geophysics*, 7:191-206.
- Jonker, C. and Oliver, J. (2012). Mineral contamination from cemetery soils: case study of Zandfontein cemetery, South Africa. *International Journal of Environmental Research and Public Health*, 9(2):511-520.
- Juerges, A., Pringle, J. K., Jervis, J. R. and Masters, P. (2010). Comparisons of magnetic and electrical resistivity surveys over simulated clandestine graves in contrasting burial environment. *Near Surface Geophysics*, 8:529-539.
- Kacki, S., Rahalison, L., Rajerison, M., Ferroglio, E. and Bianucci, R. (2011). Black Death in the rural cemetery of Saint-Paurent-de-la-Cabrerisse Aude-Languedoc, southern France, 14<sup>th</sup> century: immunological evidence. *Journal of Archaeological Sciences*, 38:581-587.

- Kalacska, M., Bell, L.S., Sanchez-Azofeifa, G.A. and Caelli, T. (2009). The application of remote sensing for detecting mass graves: an experimental animal case study from Costa Rica. *Journal of Forensic Sciences*, 54:159-166.
- Kearey, P., Brooks, M. and Hill, I. (2002). An introduction to geophysical exploration. Blackwell Publishing.
- Khalilova, H. and Mammadov, V. (2016). Assessing the anthropogenic impact on heavy metal pollution of soils and sediments in urban areas of Azerbaijan's oil industrial region. *Polish Journal of Environmental Studies*, 25(1):159-166.
- Kiernan, B. (2003). The demography of genocide in Southeast Asia. *Critical Asian Studies*, 35:585-597.
- Killam, E. W. (2004). The detection of human remains. Second edition, Thomas, C. C. Publication, Illinois, USA. Pg. 93-94.
- Kim, K. and Kim, M. (2002). Mercury emissions as landfill gas from a large-scale abandoned landfill site in Seoul. *Atmospheric Environmental*, 36:4919-4928.
- Knight, R. J. and Endres, A. L. (2005). An introduction to rock physics principles for near-surface geophysics, In: Near-Surface Geophysics, Investigations in Geophysics, No. 13, *Society of Exploration Geophysics*, Butler, D. K., pp.357-438, ISBN 1-56080-130-1, Tulsa, OK.



- Krachler, M., Radner, H. and Irgolic, K. J. (1996). Microwave digestion methods for the determination of trace-elements in brain and liver samples by inductively-coupled plasma mass spectrometry. *Fresenius Journal of Analytical Chemistry*, 355:120-128.
- Kulkarni, P., Chellam, S., Flanagan, J. B. and Jayanty, R. K. M. (2007). Microwave digestion – ICP-MS elemental analysis in ambient airborne fine particulate matter: Rare earth elements and validation using a filter borne fine particle certified reference material. *Analytica Chimica Acta*, 599:170-176.
- Kvamme, K. L., and Ahler, S. A. (2007). Integrated remote sensing and excavation at the Double Ditch State Historic Site, North Dakota. *American Antiquity*, 72:539–561.
- Larson, D. O., Vass, A. A. and Wise, M. (2011). Advanced scientific methods and procedures in the forensic investigation of clandestine graves. *Journal of Contemporary Criminal Justices*, 27:149–182.
- Lasseter, A. E., Jacobi, K. P., Farley, R., and Hensel, L. (2003). Cadaver dog and handler team capabilities in the recovery of human remains in the South-Eastern United States. *Journal of Forensic Sciences*, 48:617–621.
- Likuku, A. S., Mmolawa, K. B. and Gaboutloeloe, G. K. (2013). Assessment of heavy metal enrichment and degree of contamination around the copper-nickel mine in the Selebi Phikwe Region, Eastern Botswana. *Environment and Ecology Research*, 1(2):32-40.

- Linford, N. (2014). Rapid processing of GPR time slices for data visualisation during field acquisition. 15<sup>th</sup> International Conference on Ground Penetrating Radar (GPR), pg. 702-706, doi:10.1109/ICGPR.2014.6970517. (Accessed on 21/05/2015) <http://ieeexplore.ieee.org/stamp/stamp.jsp?tp=&arnumber=6970517&isnumber=6970371>
- Linford, N. T. (2004). Magnetic ghosts: mineral magnetic measurements on Roman and Anglo-Saxon graves. *Archaeological Prospection*, 11:167-180.
- Liu, J., Li, Y., Zhang, B., Cao, J., Cao, Z. and Domagalski, J. (2009). Ecological risk of heavy metals in sediments of the Luan River source water. *Ecotoxicology*, 18:748-758.
- London Planning Advisory Committee (1997). Planning for Burial Space in London: Policies for Sustainable Cemeteries in the New Millennium, London: LPAC, CBA, IBCA, Corporation of London.
- Lopez-Luiz, B. (2000). Advances in the determination of inorganic anions by ion chromatography. *Journal of Chromatography A*, 881:607-627.
- Loska, K., Wiechula, D. and Korus, I. (2004). Metal contamination of farming soils affected by industry. *Environmental International*, 30:159-165.
- Luoma, S. N. and Rainbow, P. S. (2008). Metal contamination in aquatic environments: science and lateral management. Cambridge University Press, New York, USA, xiv +573 pp.

- Lynam, J. T. (1970). Techniques of geophysical prospection as applied to near surface structure determination. PhD thesis, University of Bradford.
- MacArthur, A. J. and Milne, J. C. (2002). Leachate characteristics and management requirements arising from Foot and Mouth operations in Scotland. In: *Proceedings Waste 2002 Integrated Waste Management and Pollution Control: Research, Policy and Practice*: 305-314.
- Manhein, M. H. (1997). Decomposition rates of deliberate burials: a case study of preservation. In: *Forensic Taphonomy: The Post-mortem fate of human remains*, edited by W. D. Haglund and M. H. Sorg. Boca Raton, FL: CRC, pp. 469-482.
- Marchetti, M. and Settini, A. (2011). Integrated geophysical measurements on a test site for detection of buried steel drums. *Annals of Geophysics*, **54**(1):105-114.
- Martinho, E. and Dionisio, A. (2014). Main geophysical techniques used for non-destructive evaluation in cultural built heritage: a review. *Journal of Geophysics and Engineering*, **11**: 1-15. doi:10.1088/1742-2132/11/5/053001.
- Masi, S., Caniani, D., Grieco, E., Lioi, D. S. and Mancini, I. M. (2014). Assessment of the possible reuse of MSW coming from landfill mining of old open dumpsites. *Waste Management*, **34**:702-710.
- Mehta, K. V. (2010). Physicochemical characteristics and statistical study of groundwater of some places of Vadgam taluka in Banaskantha district of Gujarat State (India). *Journal of Chemical Pharmaceutical Research*, **2**(4): 663-670.

- Meju, A. M. (2000). Geoelectrical investigation of old/abandoned, covered landfill sites in urban areas: model development with a genetic diagnosis approach. *Journal of Applied Geophysics*, 44:115-150.
- Mellet, J. S. (1992). Location of human remains with ground-penetrating radar. In *Proceedings of the fourth international conference on ground penetrating radar*, pages 359–365.
- Mellet, J. S. (1996). GPR in forensic and archaeological work: hits and misses. Symposium on the Application of Geophysics to Engineering and Environmental Problems, SAGEEP, *Environmental and Engineering Geophysical Society*, pp. 487-491.
- Melnyk, A., Kuklinska, K., Wolska, L. and Namiesnik, J. (2014). Chemical pollution and toxicity of water samples from stream receiving leachate from controlled municipal solid waste (MSW) landfill. *Environmental Research*, 135:253-261.
- Miller, P.S. (1996). Disturbance in the soil: finding buried bodies and other evidence using ground penetrating radar. *Journal of Forensic Sciences*, 41:648-652.
- Milligan, E. E., Bomke, A. A. and Temple W. D. (2008). Compost layering effects on poultry litter leaching: a column study. *Compost Science and Utilization*, 16(2):171-182.
- Milsom, J. and Eriksen, A. (2011). Field Geophysics. 4<sup>th</sup> review edition, *Wiley Publishers*, Chichester.
- Ministry of Justice (2006). Burial Law and Policy in the 21st Century: The Need for a Sensitive and Sustainable Approach. Available online:

[https://www.gov.uk/government/uploads/system/uploads/attachment\\_data/file/162865/burial\\_grounds\\_web\\_whole\\_plus\\_bookmarks.pdf](https://www.gov.uk/government/uploads/system/uploads/attachment_data/file/162865/burial_grounds_web_whole_plus_bookmarks.pdf). Last accessed: 07th August 2014.

Molina, C. M., Pringle, J. K., Saumett, M. and Evans, G. T. (2016). Geophysical monitoring of simulated graves with resistivity, magnetic susceptibility, conductivity and GPR in Colombia, South America. *Forensic Science International*, 261:106-115.

Moorman, B. J. (2001). Ground Penetrating Radar Applications in Paleo-limnology. In: Last, W. M. and Smol, J. P. (eds.), *Tracking Environmental Change Using Lake Sediments: Physical and Chemical Techniques*. Kluwer Academic Publishers, Dordrecht, Netherlands, pp. 23-48.

Mor, S., Ravindra, D., Dahiya, R. P. and Chandra A. (2006). Leachate characterization and assessment of groundwater pollution near municipal solid waste landfill site. *Environmental Monitoring Assessment*, 118(1-3):435-456.

Morgan, R. M. and Bull, P. A. (2007). Forensic geoscience and crime detection: Identification, interpretation and presentation in forensic geoscience. *Minerva Med Leg*, 127: 73-89.

Mualem, Y. and Friedman, S. P. (1991). Theoretical prediction of electrical conductivity in saturated and unsaturated soils. *Water Resources Research*, 27:2771–2777.

Müller, G. (1969). Index of geo-accumulation in sediments of Rhine River. *Geojournal*, 2:108-118.

- Murray, R. C. (2004). Evidence from the earth: forensic geology and criminal investigation. Missoula, MT, Mountain Press Publishing.
- Murray, R.C. and Tedrow, J.C.F. (1975). Forensic geology: earth sciences and criminal investigation. Rutgers University Press, NJ, USA.
- Museum of London Archaeology (MoLA). (2013). A Black Death Cemetery at Charterhouse Square. London EC1, pp. 364-370.
- Nobes, D. C. (1999). Geophysical surveys of burial sites: a case study of the Oaro urupa. *Geophysics*, 64(2):357-367.
- Nobes, D. C. (2000). The search for "Yvonne": a case example of the delineation of a grave using near-surface geophysical methods. *Journal of Forensic Science*, 45(3):715-721.
- Norfolk Coast Partnership (2011). Geological Landscapes of the Norfolk Coast: Introducing five areas of striking geodiversity in the Norfolk Coast Area of outstanding natural beauty. [www.norfolkcoastanb.org.uk](http://www.norfolkcoastanb.org.uk), 43 pages.
- Novo, A., Lorenzo, H., Ria, F., and Solla, M. (2011). 3D GPR in forensics: finding a clandestine grave in a mountainous environment. *Forensic Science International*, 204:134-138.
- Oesterhelweg, L., Kröber, S., Rottman, K., Willhöft, J., Braun, C., Thies, N., Puschel, K., Silkenath, J., and Gehl, A. (2008). Cadaver dogs - a study on the detection of contaminated carpet squares. *Forensic Science International*, 174:35–39.

- Ossowski, A., Kuś, M., Brzeziński, P., Prüffer, J., Piatek, J. and Zielińska, G. (2013). Example of human individual identification from World War II gravesite. *Forensic Science International*, 233:179-192.
- Owsley, D.W. (1995). Techniques for locating burials, with emphasis on the probe. *Journal of Forensic Sciences*, 40:735–740.
- Pacheco, A., Mendes, J. M. B., Martins, T., Hassuda, S. and Kimmelman, A. A. (1991). Cemeteries: A potential risk to groundwater. *Water Science and Technology*, 24(11):97-104.
- Park, S., Yi, M., Kim, J. and Shin, S. (2016). Electrical resistivity imaging (ERI) monitoring for groundwater contamination in an uncontrolled landfill, South Korea. *Journal of Applied Geophysics*. doi:10.1016/j.jappgeo.2016.07.004 <http://www.sciencedirect.com/science/article/pii/S0926985116301793>
- Parker, R., Ruffell, A., Hughes, D., and Pringle, J. (2010). Geophysics and the search of freshwater bodies: a review. *Science and Justice*, 50:141–149.
- Parkin, T. B. (1987). Soil microsites as a source of denitrification variability. *Soil Science Society of America Journal*, 51(5):1194-1199.
- Patil, K. V. and Patil, P. R. (2011). Groundwater quality of open wells and tube wells around Amalner town of Jalgaon district, Maharashtra, India. *Electronic Journal of Chemistry*, 8:53-58.

- Peel, M. C., Finlayson, B. L. and McMahon, T. A. (2007). Updated world map of the Koppen-Geiger climate classification. *Hydrological Earth System Science*, 11:1633-1644.
- Perrault, K. A. and Forbes, S. L. (2016). Elemental analysis of soil and vegetation surrounding decomposing human analogues. *Canadian Society of Forensic Science Journal*, pg. 1-14.  
<http://www.tandfonline.com/doi/pdf/10.1080/00085030.2016.1184840>. (Accessed on June 27th, 2016)
- Pindyk, R. S. and Rubinfeld, D. L. (1998). *Econometric models and economic forecasts*, 4<sup>th</sup> edition Irwin McGraw-Hill Coy USA.
- Porter, S. (2009). *The London Charterhouse*, Amberley Publications, page 107.
- Pour, S. J. and Khezri, S. M. (2010). Assessing the groundwater resources pollution potential by Beheshte Zahra Cemetery. *International Conference on Chemistry and Chemical Engineering (ICCCE)*, pp. 414-418.
- Powell, K. (2004). Detecting human remains using near-surface geophysical instruments. *Exploration Geophysics*, 35:88–92.
- Pratt, D. L. and Fonstad, T. A. (2009). Livestock mortalities burial leachate chemistry after two years of decomposition. In: *3rd International symposium on management of animal carcasses, tissue, and related by-products*, Davis, California, USA.



- Pringle, J. K. and Jervis, J. R. (2010). Electrical resistivity survey to search for a recent clandestine burial of a homicide victim. *Forensic Science International*, 202:e1–e7.
- Pringle, J. K., Cassella, J. P. and Jervis, J. R. (2010a). Preliminary soil water conductivity analysis to date clandestine burials of homicide victims. *Forensic Science International*. 189:126-133.
- Pringle, J. K., Cassella, J. P., Jervis, J. R., William, A., Cross, P. and Cassidy, N. J. (2015b). Soilwater conductivity analysis to date and locate clandestine graves of homicide victims. *Journal of Forensic Sciences*, 60(4):1052-1060.
- Pringle, J. K., Cassidy, N. J., Styles, P., Stimpson, I. G. and Toon, S. M. (2010b). Training text generation of near-surface geophysicists: team-based, student-led, problem-solving field exercise, Cumbria, UK. *Near Surface Geophysics*, 8:503-517.
- Pringle, J. K., Giubertoni, M., Cassidy, N. J., Wisniewski, K. D., Hansen, J. D., Linford, N. T. and Daniels, R. M. (2015a). The use of magnetic susceptibility as a forensic search tool. *Forensic Science International*, 246:31-42.
- Pringle, J. K., Holland, C., Szkornik, K. and Harrison, M. (2012c). Establishing forensic search methodologies and geophysical surveying for the detection of clandestine graves in coastal beach environments. *Forensic Science International*, 219:e29-e36.
- Pringle, J. K., Jervis, J. R., Cassella, J. P., and Cassidy, N. J. (2008). Time-lapse geophysical investigations over a simulated urban clandestine grave. *Journal of Forensic Sciences*, 53:1405–1416.

- Pringle, J. K., Jervis, J. R., Hansen, D. D., Jones, G. M., Cassidy, N. J., and Cassella, J. P. (2012b). Geophysical Monitoring of Simulated Clandestine Graves Using Electrical and Ground-Penetrating Radar Methods: 0-3 Years after Burial. *Journal of Forensic Sciences*, 57(6):1467-1486.
- Pringle, J. K., Jervis, J. R., Roberts, D., Dick, C. H., Wisniewski, K. D., Cassidy, N. J. and Cassella, J. P. (2016). Longterm geophysical monitoring of simulated clandestine graves using electrical and ground penetrating radar methods: 4-6 years. *Journal of Forensic Sciences*, 61(2):309-321.
- Pringle, J. K. Lenham, J. W. and Reynolds, J. M. (2009). GPR investigations to characterise Medieval and Roman foundations under existing shop premises: case study from Chester, Cheshire, UK. *Near Surface Geophysics*. 7(2):93-100.
- Pringle, J. K., Ruffell, A., Jervis, J. R., Donnelly, L., McKinley, J., Hansen, J., Morgan, R., Pirrie, D. and Harrison, M. (2012a). The use of geoscience methods for terrestrial forensic searches. *Earth Science Reviews*, 114:108-123.
- Pye, K. and Croft, D. J. (2004). Forensic geoscience: introduction and overview. In Pye, K. and Croft, D. J., editors, *Forensic Geoscience: principles, techniques and applications*, pages 1–5. Geological Society, Special Publication 232.
- Ramaiah G. V., Krishnaiah, S., Naik, M. and Shankara, A. (2014). Leachate characterization and assessment of ground water pollution near MSW dumpsite of Mavallipura, Bangalore. *Int. Journal of Engineering Research and Applications*, 4(1):267-271.

Rawell (2009) 'Waterproofing Environmental Protection', Rawell Environmental Ltd,  
[https://secure1.namesco.net/rawell.co.uk/environmental\\_protection/case\\_history\\_sheets.hp](https://secure1.namesco.net/rawell.co.uk/environmental_protection/case_history_sheets.hp), accessed 24th March 2014.

Rebmann, A. J., Koenig, M., David, E. and Sorg, M. H. (2000). Cadaver Dog Handbook: Forensic Training and Tactics for the Recovery of Human Remains. Boca Raton, FL: CRC Press.

Rehman, F., Abuelnaga, H. S. O., Harbi, H. M., Cheema, T. and Atef, A. H. (2016). Using a combined electrical resistivity imaging and induced polarization techniques with the chemical analysis in determining of groundwater pollution at Al Misk Lake, Eastern Jeddah, Saudi Arabia. *Arabian Journal of Geosciences*, 9(4):286-296.

Remy, S., Prudent, P., Hissler, C., Probst, J. L. and Kremp, G. (2003). Total mercury concentrations in an industrialized catchment, the Thur River basin (north-eastern France): geochemical background level and contamination factors. *Chemosphere*, 53:635-644.

Renfrew, C. and Bahn, P. (2000). Archaeology: theories, methods and practice, Thames and Hudson, New York.

Reynolds, J. M. (1997). An introduction to applied and environmental geophysics. First Edition, *John Wiley and Sons*.

Reynolds, J. M. (2011). An introduction to applied and environmental geophysics. Second Edition, *John Wiley and Sons*.

- Rezos, M. M., Schultz, J. J., Murdock, II R. A. and Smith, S. A. (2010). Controlled research utilizing a basic all metal detector in the search for buried firearms and miscellaneous weapons. *Forensic Science International*, 195:121-127.
- Ríos, L., García-Rubio, A., Martínez, B., Alonso, A., Puente, J. (2012). Identification process in mass graves from the Spanish Civil War II. *Forensic Science International*, 219:e4-e9.
- Ríos, L., Overjero, J.I.C., Prieto, J.P. (2010). Identification process in mass graves from the Spanish Civil War I. *Forensic Science International*, 199:e27-e36.
- Rivett, M. O., Wealthall, G. P. Dearden, R. A. and McAlary, T. A. (2011). Review of unsaturated-zone transport and attenuation of volatile organic compound (VOC) plumes leached from shallow source zones. *Journal of Contaminant Hydrology*, 123(3-4):130-156.
- Rodrigues, L. and Pacheco, A. (2003). Groundwater contamination from cemeteries cases of study. International symposium Environment 2010 Situation and Perspectives for the European Union, Porto 6-10 May, Portugal.
- Rodriguez, W. C. (1997). Decomposition of buried and submerged bodies. In *Forensic Taphonomy: The Postmortem Fate of Human Remains* (Haglund, W. D. and Sorg, M. H., eds). Boca Raton, FL, CRC Press, 459-468.
- Rodriguez, W. C. and Bass, W. M. (1985). Decomposition of buried bodies and methods that may aid in their location. *Journal of Forensic Science*, 30(3):836-852

- Ruffell, A. (2005a). Burial location using cheap and reliable quantitative probe measurements. *Forensic Science International*, 151:207–211.
- Ruffell, A. (2005b). Searching for the IRA “disappeared”: ground penetrating radar investigation of a churchyard burial site. *Journal of Forensic Sciences*, 50:1430–1435.
- Ruffell, A. (2010). Forensic pedology, forensic geology, forensic geoscience, geoforensics and soil forensics. *Forensic Science International*, 202:9-12.
- Ruffell, A. and Kulesa, B. (2009). Application of geophysical techniques in identifying illegally buried toxic waste. *Environmental Forensics*, 10:196–207.
- Ruffell, A. and McKinley, J. (2005). Forensic Geosciences: applications of geology, geomorphology and geophysics to criminal investigations. *Earth Science Reviews*, 69(3-4):235-247.
- Ruffell, A. and McKinley, J. (2008). *Geoforensics. John Wiley and Sons*, Chichester, UK.
- Ruffell, A. and McKinley, J. (2014). Forensic geomorphology, *Geomorphology*, 206: 14-22.
- Ruffell, A., McCabe, A., Donnelly, C. and Sloan, B. (2009). Location and assessment of an historic (150–160 years old) mass grave using geographic and ground penetrating radar investigation, NW Ireland. *Journal of Forensic Sciences*, 54:382–394.
- Ruffell, A., Pringle, J.K., Forbes, S. (2014). Search protocols for hidden forensic objects beneath floors and within walls. *Forensic Science International*, 237:137-145.

- Sahraoui, H., Attia, R., Hamrouni, H. and Hachicha, M. (2016). Assessment of trace elements contamination of agriculture topsoil around Lakhouat mine area, Tunisia. *Walailak Journal of Science and Technology*, 13(11):965-976.
- Sarris, A., Dunn, R. K., Rife, J. L., Papadopoulos, N., Kokkinou, E and Mundigler, C. (2007). Geological and geophysical investigations in the Roman Cemetery at Kenchreai (Korinthia), Greece. *Archaeological Prospection*, 14:1-23.
- Schroeder, P. R. and Aziz, N. M. (2003). Effects of confined disposal facility and vadose zone characteristics on leachate quality. DOER Technical Notes Collection (ERDC TN-DOER-C31), U.S. Army Engineer Research and Development Centre, Vicksburg, MS. Accessible online at: [http://acwc.sdp.sirsi.net/client/en\\_US/search/asset/1003927;jsessionid=E2512AB52A680EB3377AF338DB94416E.enterprise-15000](http://acwc.sdp.sirsi.net/client/en_US/search/asset/1003927;jsessionid=E2512AB52A680EB3377AF338DB94416E.enterprise-15000). Accessed on 12th February, 2015.
- Schultz, J. J. (2007). Using ground-penetrating radar to locate clandestine graves of homicide victims: forming forensic archaeology partnerships with law enforcement. *Homicide Studies*, 11:15-29.
- Schultz, J. J. (2008). Sequential monitoring of burials containing small pig cadavers using ground-penetrating radar. *Journal of Forensic Sciences*, 53:279–287.
- Schultz, J. J. (2012). The application of ground penetrating radar for forensic grave detection. In: Dirkmaat, D. C. (Eds.), *A companion to forensic anthropology*. Wiley-Blackwell Publication, pages 85-100.

- Schultz, J. J., Collins, M. E. and Falsetti, A. B. (2006). Sequential monitoring of burials containing large pig cadavers using ground penetrating radar. *Journal of Forensic Science*, 51(3):606-616.
- Schultz, J. J., Martin, M. M. (2011). Controlled GPR grave research: comparison of reflection profiles between 500-MHz and 250-MHz antennae. *Forensic Science International*, 209:64–69.
- Schultz, J. J., Walter, B. S. and Healy, C. (2016). Long-term sequential monitoring of controlled graves representing common burial scenarios with ground penetrating radar: Years 2 and 3. *Journal of Applied Geophysics*, 132:60-74.
- Scott, J. and Hunter, J. R. (2004). Environmental influences on resistivity mapping for the location of clandestine graves. In Pye, K. and Croft, D. J., editors, *Forensic Geoscience: principles, techniques and applications*, pages 33–38. Geological Society, Special Publication 232.
- Scudamore, J. M., Trevelyan, G. M., Tas, M. V., Varley, E. M., Hickman, G. A. W. (2002). Carcass disposal: lessons from Great Britain following the foot and mouth disease outbreaks of 2001. *Rev. Sci. Tech. Off. Int. Epiz.*, 21(3):775-787.
- Sen, P. N., Goode, P. A., and Sibbit, A. (1988). Electrical conduction in clay bearing sandstones at high and low salinities. *Journal of Applied Physics*, 63: 4832–4840.
- Senos Matias, M. J., Marques da Silva, M. Goncalves, L. Peralta, C., Grangeia, C. and Martinho, E. (2004). An investigation into the use of geophysical methods in the

study of aquifer contamination by graveyards. *European Association of Geoscientist and Engineers, Near Surface Geophysics*, 3:131-136

Seyed, h. t., Parisa, R. R. and Ahmad, R. M. (2015). Prdicting potential mineralization using surface geochemical data and multiple linear regression model in the Kuh Panj Porphyry Cu mineralization (Iran). *Arabian Journal for Science and Engineering*, 40:163-170.

Shah, M. C., Shilpkar, P. and Sharma, S. (2007). Correlation, regression study on physico-chemical parameters and water quality assessment of ground water of Mansa Taluka in Gujarat. *Asian Journal of Chemistry*, 19(5):3449-3454.

Shaw, E. M., Beven, K. J., Chappell, N. A. and Lamb, R. (2011). *Hydrology in Practice*. 4<sup>th</sup> edition, Spon press publication, London and New York.

Sloane, B. (2011). The Black Death in London. *The History Press*, Stroud, UK.

Smith, W. F. and Wessel, P. (1990). Gridding with continuous curvature splines in tension. *Geophysics*, 55:293:305.

Speake, R. (1974). The Old Road to Endon. Department of Adult Education Publication, Keele University, Staffordshire, UK.

Spennemann, D. H. R., Franke, B. (1994). On the dark stains observed in some Tongan burials. *New Zealand Journal of Archaeology*, 37(1):35–43.



St John's Church News. (2015). A very warm welcome. Available:  
<http://www.stjohnsnews.co.uk/>. Last accessed 10th Aug 2015.

Stanger, R. and Roe, D. (2007). Geophysical surveys at the West End Cemetery, Townsville: an application of three techniques. *Australian Archaeometry*, 65:44–50.

Strongman, K.B. (1992). Forensic applications of ground penetrating radar. In *Proceedings of the second international conference on ground penetrating radar*, pages 203–211.

Styles, P. (2012). Environmental Geophysics: Everything you ever wanted (needed) to know but were afraid to ask. Education Tour Series, *EAGE Publications*, pp. 38-56.

Sutherland, R. A. (2000). Bed sediment-associated trace metals in an urban stream, Oahu, Hawaii. *Environmental Geology*, 39:611-627.

Sutton, M.J. and Conyers, L.B. (2013). Understanding cultural history using ground penetrating radar mapping of unmarked graves in the Mapoon Mission Cemetery, Western Cape York, Queensland, Australia. *International Journal of Historical Archaeology*, 17:782-805.

Swann, L., Forbes, S. and Lewis, S. W. (2010). Observations of the temporal variation in chemical content of decomposition fluid: A preliminary study using pigs as a model system. *Australian Journal of Forensic Sciences*, 42(3):199-210.

Syrian Observatory for Human Rights (SOHR). Available online at [www.syriahr.com/en/](http://www.syriahr.com/en/),  
Last accessed: 24th May 2014.

- Szalai, S. and Szarka, L. (2008). On the classification of surface geoelectrical arrays. *Geophysical Prospecting*, 56:159-175.
- Szczepanska, J. and Twardowska, I. (2004). IV.5 Principles of vadose and saturated zones monitoring in mining waste dumps. *Waste Management Series*, 4:551-575.
- Szleszkowski, L., Thannhäuser, A., Szwagrzyk, K., Konczewski, P., Kawecki, J., Świątek, B. (2014). Exhumation research concerning the victims of political repressions in 1945-1956 in Poland: a new direction in forensic medicine. *Forensic Science International*, 235:e1-e6.
- Takahashi, N., Morishita, M., Miyagi, D. and Nakano, M. (2011). Comparison of magnetic properties of magnetic materials at high temperature. *IEEE Transactions on Magnetics*, 47(10):3452-3455.
- Taylor, S. R. and McLennan, S. M. (1985). The continental crust: its composition and evolution. Blackwell scientific Publication, Carlton, 312 pp.
- Telford, W. M., Geldart, L. P. and Sheriff, R. E. (1990). *Applied geophysics*. Cambridge University Press, second edition.
- Temple, P. (2010). *The Charterhouse*, Survey of London Monograph 18. Yale University Press for English Heritage, page 30.
- Thabit, J. M. and Khalid, F. H. (2016). Resistivity imaging survey to delineate subsurface seepage of hydrocarbon contaminated water at Karbala Governorate, Iraq. *Environmental Earth Sciences*, 75(1):1-7, DOI: 10.1007/s12665-015-4880-y.

- Thacker, P. T., Ellwood, B. B. and Pereira, C. M. (2002). Detecting Palaeolithic activity areas through electrical resistivity survey: an assessment from Vale de Obidos, Portugal. *Journal of Archaeological Science*, 29:563-570.
- Tibbett, M. and Carter, D. O. (2009). Research in forensic taphonomy: a soil-based perspective. In Ritz, K., Dawson, L., and Miller, D., editors, *Criminal and environmental soil forensics*, pp. 317–331. Springer.
- Tringham, N. J. (1996). Endon. In: Greenslade, M. W. (ed.) *A history of the county of Stafford: Leek and the Moorlands*. Oxford University Press: *Institute of Historical Research*, 7:176-186.
- Troutman, L., Moffatt, C. and Simmons, T. (2014). A preliminary examination of differential decomposition patterns in mass graves. *Journal of Forensic Sciences*, 59(3):621-626.
- Tsokas, G. N., Diamanti, N., Tsourlos, P. I., Vargemezis, G., Stampolidis, A. and Raptis, K. T. (2013). Geophysical Prospection at the HamzaBey (Alkazar) Monument Thessaloniki, Greece. *Mediterranean Archaeology and Archaeometry*, 13(1):9-20.
- Tsourlos, P., and Tsokas, G.N. (2011). Non-destructive electrical resistivity tomography survey at the South walls of the Acropolis of Athens, *Archaeological Prospection*, 18:173-186.
- Ubelaker, D. H. (1989). Human Skeletal Remains: Excavation, Analysis, Interpretation. 2nd ed., Taraxacum, Washington, D.C., pg. 9.

- Ulriksen, C. P. F. (1982). Application of impulse radar to civil engineering. Ph.D. thesis, Lund University of Technology, Lund, Sweden.
- Uslu, A., Baris, E. and Erdogan, E. (2009). Ecological concerns over cemeteries. *African Journal of Agricultural Research*, 4(13):1505-1511.
- Van Belle, L. E., Carter, D. O. and Forbes, S. L. (2009). Measurement of ninhydrin reactive nitrogen influx into gravesoil during aboveground and belowground carcass (*Sus domesticus*) decomposition. *Forensic Science International*, 193:37-41.
- Van der Kruk, J., Klotzsche, A., Mester, A., Busch, S., Meles, G. A., Blkowski, J. and Vereecken, H. (2012). High resolution electromagnetic hydrogeophysical imaging. *International Water Technology Journal*, 2(4):261-267.
- Van Haaren, F. W. J. (1951). Cemeteries as sources of groundwater contamination. *Water*, 35(16):167-172.
- VanlearHoven, S. L. and Anderson, G. S. (1999). Insect succession on buried carrion in two biogeoclimatic zones of British Columbia. *Journal of Forensic Science*, 44:32-43.
- Vargemezis, G., Diamanti, N., Fikos, I. Stampolidis, A., Makedon, T. and Chatzigogos, N. (2013). Ground penetrating radar and electrical resistivity tomography for locating buried building foundations: a case study in the city centre of Thessaloniki, Greece. *Bulletin of the Geological Society of Greece*, vol. XLVII, 11 pages.

- Vass, A. A., Bass, W. M., Wolt, J. D., Foss, J. E. and Ammons, J. T. (1992). Time since death determinations of human cadavers using soil solution. *Journal of Forensic Sciences*, 37:1236-1253.
- Vass, A.A., Smith, R.R., Thompson, C.V., Burnett, M.N., Dulgerian, N. and Eckenrode, B.A. (2008). Odor analysis of decomposing human remains. *Journal of Forensic Sciences*, 53(2):384–391.
- Viberg, A., Berntsson, B. and Liden, K. (2013). Archaeological prospection of a high altitude Neolithic site in the Arctic mountain tundra region of northern Sweden, *Journal of Archaeological Science*. 40:2579–2588.
- Walkington, H. (2010). Soil science applications in archaeological contexts: a review of key challenges, *Earth Science Reviews*, 103:122–134.
- Wang, Y., Ao, L., Lei, B. and Zhang, S. (2015). Assessment of heavy contamination from sediment and soil in the Riparian zone China's Three Gorges Reservoir. *Polish Journal of Environmental Studies*, 24(5):2253-2259.
- Watters, M. and Hunter, J. R. (2004). Geophysics and burials: field experience and software development. In: Pye, K., Crofts, D. J. (Eds.), *Forensic Geoscience: Principles, Techniques and Applications*. Geological Society of London Special Publication, 232:21–31.
- Williams, A., Temple, T., Pollard, J. S., Jones, A. R. and Ritz, K. (2009). Environmental considerations for common Burial Site Selection after pandemic events. In: Ritz, K.,

Dawson, L. and Miller, D. (eds.), *Criminal and Environmental Soil Forensics*, Springer, Berlin, pp. 87-101.

Wilson, A. S., Janaway, R. C., Holland, A. D., Dodson, H. I., Baran, E., Pollard, A. M., and Tobin, D. J. (2007). Modelling the buried human body environment in upland climes using three contrasting field sites. *Forensic Science International*, 169:6–18.

Witten, A. J. (2006). Handbook of geophysics and archaeology. Equinox Publishing Ltd: London.

Witten, A. J., Calvert, G, Witten, B and Levy T. (2003). Magnetic and electromagnetic induction studies at archaeological sites in southwestern Jordan. *Journal of Environmental and Engineering Geophysics*, 8:209–215.

Witten, A., Brooks, R. and Fenner, T. (2000). The Tulsa race riot of 1921: a geophysical study to locate a mass grave. *Leading Edge*, 20:655–660.

Witten, A., Brooks, R. and Fenner, T. (2001). The Tulsa Race Riot of 1921: a geophysical study to locate a mass grave. *Leading Edge*, 20:655–660.

World Health Organisation (2006). WHO Guidelines for the safe use of wastewater, excreta and greywater: Volume II wastewater use on agriculture. Geneva, Switzerland. 196 pages.

Wynn, J. C. and Sherwood, S. I. (1984). The self-potential (SP) method: an inexpensive reconnaissance and archaeological mapping tool. *Journal of Field Archaeology*, 11(2):195-204.

- Young, C. P., Blackmore, P. J., Reynolds, P. J. and Leavens, A. (1999). Pollution potential of cemeteries, draft guidance. *R & D Technical Report P223, Environmental Agency*, Bristol, England.
- Yuan, Q., Snow, D. D. and Bartelt-Hunt, S. L. (2013). Potential water quality impacts originating from land burial of cattle carcasses. *Science of The Total Environment*, 456:246-253.
- Zume, J. T., Tarhule, A., and Christenson, S. (2006). Subsurface imaging of an abandoned solid waste landfill site in Norman, Oklahoma. *Groundwater Monitoring and Remediation*, 26:62-69.
- Zvizdojevic, J. and Vukotic, M. (2015). Application of Statistical methods in analysis of agriculture – correlation and regression analysis. *Agriculture and Forestry*, 61(1):309-324.
- Zychowski, J. (2011). Geological aspects of decomposition of corpses in mass graves from WW1 and 2, located in SE Poland. *Environmental Earth Science*, 64:437-448.
- Zychowski, J. (2012). Impact of cemeteries on groundwater chemistry: A review. *Catena*, 93:29-37.

## Appendices

1. **Dick, C. H.**, Pringle, J. K., Sloane, B., Carver, J., Wisniewski, K. D., Haffenden, A., Porter, S., Robert, D. and Cassidy, N. J. (2015). Detecting and characterising of Black Death burials by multi-proxy geophysical methods. *Journal of Archaeological Science*, 59: 132-141.
2. Pringle, J. K. and **Dick, C. H.** (2016). Forensic geophysics: assisting law enforcement agencies in clandestine grave detection. *FastTIMES*, June edition, pages 20-27.
3. **Dick et al.** (In review). Determining geophysical responses from graves. *Journal of Geophysics*.





## Detection and characterisation of Black Death burials by multi-proxy geophysical methods



Henry C. Dick<sup>a, b</sup>, Jamie K. Pringle<sup>a, \*</sup>, Barney Sloane<sup>c</sup>, Jay Carver<sup>d</sup>,  
Kristopher D. Wisniewski<sup>a</sup>, Austin Haffenden<sup>a</sup>, Stephen Porter<sup>e</sup>, Daniel Roberts<sup>a</sup>,  
Nigel J. Cassidy<sup>a</sup>

<sup>a</sup> School of Physical Sciences & Geography, Keele University, Keele, ST4 6DA, UK

<sup>b</sup> Applied Geophysics Group, Physics Dept., University of Port Harcourt, Nigeria

<sup>c</sup> Historic England, Swindon, SN2 2GZ, UK

<sup>d</sup> Crossrail Ltd, 25 Canada Square, Canary Wharf, London, E14 5LQ, UK

<sup>e</sup> Sutton's Hospital in Charterhouse, London, UK

### ARTICLE INFO

#### Article history:

Received 3 September 2014

Received in revised form

22 April 2015

Accepted 23 April 2015

Available online 5 May 2015

#### Keywords:

Burials

Plague

Black Death

London

Geophysics

### ABSTRACT

The construction of the new Crossrail railway discovered 25 well preserved skeletons shallowly buried in Central London in 2013. Subsequent carbon dating and aDNA analysis confirmed the archaeological age and presence of the *Yersinia pestis* "Black Death" plague epidemic strain. Here we present the non-invasive multi-proxy geophysical survey of the adjacent Charterhouse Square, rapidly undertaken to detect any further burials and characterise the site. Historical records suggested the area was a burial ground for Black Death plague victims, before subsequent cemetery and urban land use. Following initial trial surveys, surveys imaged ~200 isolated and similar-sized burials in the south-west of the site. There were also two contrasting burial orientations present at various depths which suggested a series of controlled phased burials. A well-defined eastern burial boundary, taking the form of a ditch and bank, was also discovered. Geophysical surveys also identified a subsequent complex site history with multiple-aged features. This study revises knowledge of Black Death aged-burials and provides important implications for successful geophysical burial detection with significant time- and space-limited site constraints.

© 2015 Elsevier Ltd. All rights reserved.

### 1. Introduction

In 2013 Europe's biggest construction project, the construction of the new Crossrail railway, discovered 25 well preserved skeletons, shallowly buried in close proximity to each other, in Charterhouse Square in Central London. Historical records suggested that the site was an emergency burial ground for Black Death victims during the 1348–1349 AD plague epidemic (Porter, 2009; Sloane, 2011). A non-invasive archaeological geophysical survey of Charterhouse Square with a limited time scale was commissioned because of active construction deadlines.

There are generally accepted to be three plague pandemics in recorded human history, Justinian's Plague (541–542 AD) that was mostly contained within Mediterranean countries, the much wider European so-called Black Death plague (1345–1750 AD) and the 19th Century Chinese plague epidemic which spread globally in 1894 AD (Haensch et al., 2010). The Black Death was the first widespread outbreak of medieval plague in Europe, with recent historical research estimating that it reduced London's population by 30%–50% between 1347 and 1351 AD (Sloane, 2011). Contemporary accounts detail the sheer numbers of dead prevented Christian burials from being undertaken "so great a multitude eventually died that all the cemeteries of the aforesaid city were insufficient for the burial of the dead. For this reason, many were compelled to bury their dead in places unseemly, not hallowed or blessed; some, it was said, cast the corpses into the river" (Sloane, 2011).

Recent scientific advancements in dating skeletal remains have allowed research into age of mortality in London during this period (DeWitte, 2010; DeWitte and Hughes-Morey, 2012), subsequent

\* Corresponding author. Keele University, School of Physical Sciences & Geography, William Smith Building, Keele, ST5 5BG, UK. Tel.: +44 (0)1782 733163.

E-mail addresses: [h.c.dick@keele.ac.uk](mailto:h.c.dick@keele.ac.uk) (H.C. Dick), [j.k.pringle@keele.ac.uk](mailto:j.k.pringle@keele.ac.uk) (J.K. Pringle), [barneysloane@historicengland.org.uk](mailto:barneysloane@historicengland.org.uk) (B. Sloane), [jaycarver@crossrail.co.uk](mailto:jaycarver@crossrail.co.uk) (J. Carver), [k.d.wisniewski@keele.ac.uk](mailto:k.d.wisniewski@keele.ac.uk) (K.D. Wisniewski), [a.haffenden@keele.ac.uk](mailto:a.haffenden@keele.ac.uk) (A. Haffenden), [s.c.porter@tiscali.co.uk](mailto:s.c.porter@tiscali.co.uk) (S. Porter), [dan.roberts35@gmail.com](mailto:dan.roberts35@gmail.com) (D. Roberts), [n.j.cassidy@keele.ac.uk](mailto:n.j.cassidy@keele.ac.uk) (N.J. Cassidy).

# FORENSIC GEOPHYSICS: ASSISTING LAW ENFORCEMENT AGENCIES IN CLANDESTINE GRAVE DETECTION

Jamie K. Pringle, Senior Lecturer  
School of Physical and Geographical Sciences  
Keele University  
Keele, Staffordshire, United Kingdom  
email: [j.k.pringle@keele.ac.uk](mailto:j.k.pringle@keele.ac.uk)

Henry C. Dick, PhD Student  
School of Physical and Geographical Sciences  
Keele University  
Keele, Staffordshire, United Kingdom  
email: [h.c.dick@keele.ac.uk](mailto:h.c.dick@keele.ac.uk)

## Introduction

Thousands of people are reported missing in the world every year to their respective Police Services, 250,000 annually in the United Kingdom alone (UK Home Office, 2010). In other countries, with larger populations, these figures will be considerably more, for example, the US National Crime Information Center lists 84,136 missing persons cases as of 2013, with ~57,000 currently missing in Colombia (Molina and others, 2016). Where the missing have sadly become homicide victims, their bodies are commonly hidden inside structures (see Ruffell and others, 2014), deposited in water (see Parker and others, 2010) or buried in terrestrial environments (see Pringle and others, 2012). Where these cases are unsolved, they are commonly referred to as 'cold cases' which periodically get revisited every decade or so, where new case information may come to light and/or forensic techniques have been recently developed which may assist with the investigation.

There are various methods used for detection of these victims, with best practice suggesting a phased approach, moving from large-scale remote sensing methods to suggest likely areas, down to ground reconnaissance and control studies of suspect area(s) before full site searches are initiated (see Larsen and others, 2011, Pringle and others, 2012). Full site searches can include a variety of techniques, including forensic geomorphology, scent-trained 'cadaver' victim recovery dogs, chemical analysis of soil/water samples and near-surface forensic geophysics. Near-surface geophysical methods are being increasingly used by forensic search teams to assist them with detecting a variety of forensic-related items of interest.

## Forensic Geophysical Methods

Forensic geophysics has been defined as 'the study of locating and mapping hidden objects or features that are underground or underwater' (Dupras and others, 2011) for both civil and criminal court purposes. Geophysical methods should be able to non-invasively, rapidly survey extensive suspected areas; subsequent targeted anomalies can then be investigated using conventional and forensically careful, intrusive methods. Forensic geophysical targets are many, the highest profile of which are both isolated and mass clandestine graves of homicide victims, but other targets, for

**Keywords:** Forensic Geophysics, Clandestine/Cemetery Burials, Search Program Workflow.